Universidade de Lisboa

Faculdade de Farmácia

Synthesis, Characterization and Evaluation of Bioactive Cyclodextrin Derivatives for Bimodal Applications in Drug Delivery

António Ricardo Lopes Marouvo Gonçalves

Doutoramento em Farmácia

Tecnologia Farmacêutica

2014

Universidade de Lisboa

Faculdade de Farmácia

Synthesis, Characterization and Evaluation of Bioactive Cyclodextrin Derivatives for Bimodal Applications in Drug Delivery

António Ricardo Lopes Marouvo Gonçalves

Tese orientada pela Doutora Konstantina Yannakopoulou (NSCR "Demokritos", Atenas, Grécia) e pela Prof.ª Doutora Helena Cabral Marques (FFUL, Lisboa, Portugal). Elaborada para a obtenção do grau de doutor no ramo de Farmácia e especialidade em Tecnologia Farmacêutica.

I dedicate this work to my girlfriend Cátia, to my parents António and Helena, to my sisters Joana and Cátia, to my nephew Tiago and to my bother-in-law Augusto.

Abstract

Photodynamic therapy (PDT) is an alternative cancer treatment, which works through the synergy of three components: a photosensitizer (PS), molecular oxygen (O_2) and light of a specific wavelength (λ) to activate the PS and generate reactive oxygen species (ROS), primarily singlet oxygen ($^1O_2$). ROS are then responsible for the therapeutic action of PDT through the localized destruction of cancer tissues at the area of light irradiation. Therefore, PDT can be seen as photoinduced "drug delivery" processes. Porphyrins are PSs known for their lack of water solubility and strong aggregation tendency in aqueous solvents, characteristics that affect their photophysical properties and limit their application to biological systems. Modifications on porphyrins structures are desired to achieve PSs that are easy to prepare, well-characterized and that possess improved photophysical properties and enhanced aqueous solubility. 5,10,15,20-tetrakis(*m*-hydroxyphenyl)-21,23*H*-porphyrin (*m*THPP), is the porphyrin analogue of the clinically approved chlorin temoporphin (*m*THPC, Foscan®), prescribed for the palliative treatment of patients with advanced head and neck squamous cell carcinomas.

Both *m*THPP and *m*THPC have proven to be 25-30 times as potent as the clinically used hematoporphyrin derivatives, *e.g.* photofrin in vivo; however, like other porphyrin compounds, *m*THPP and *m*THPC suffer from poor water solubility, forming non-fluorescent aggregates in a wide pH range in aqueous solution. Foscan® is adminstered in injectable form as an ethanol and propylene glycol mixture. Thus, there is a clear need to improve the water solubility, to promote deaggregation, without affecting the photochemistry of the porphyrin core of these PSs. Cyclodextrins (CDs) are cyclic oligosaccharides composed of α-D-glucopyranose units (α-, β- and γ-CDs), that in aqueous media are able to encapsulate hydrophobic molecules in their cavities, usually resulting in increase of aqueous solubility, stability, and bioavailability of the molecule (drug). Therefore, several types of CDs are approved pharmaceutical excipients and are extensively used in drug formulations. The covalent attachment of a CD moiety to a porphyrin is a strategy that is meant to combine the drug encapsulation / solubilization capabilities of a CD macrocycle, with the photosensitizing / fluorescence and imaging properties of the porphyrin, thus creating a multimodal drug carrier. In this sense, a CD-porphyrin conjugate could have increased aqueous solubility and enhanced photophysical properties of the porphyrin moiety and moreover, possesses the ability to encapsulate suitable drug molecules for cancer treatment. In general, there is an interest in developing potential useful drug candidates relying on already approved molecules, namely an approved safety profile for human use.

In this dissertation preparation, characterization and photophysiscal properties of a cyclodextrin-porphyrin conjugate (CD-*m*THPP) are described. Specifically, *m*THPP was successfully attached to βCD to form a 1:1 conjugate (CD-*m*THPP). This was prepared in pure form in 40 % yield in an optimized up-scalable procedure. Additionally, its structure was fully characterized by NMR, MALDI-TOF MS and elemental analysis. Moreover, its photophysical properties were investigated by UV-Vis and fluorescence spectroscopy. CD-*m*THPP revealed more than 1.7-fold improved absorbance and more than 20-fold increased fluorescence emission in phosphate buffer saline and improved solubility in water, when compared to *m*THPP. The latter, although limited to μM range of concentration due to formation of small-sized aggregates was enough to conduct cell experiments. The use of *m*THPP alone was impossible, under the same conditions due to massive aggregation. Consequently, the low aqueous solubility of CD-*m*THPP was drastically improved to the mM range of concentration by the addition of *per*-methylated-βCD (pMβCD) that acts as solubilizer, through the formation of water-soluble inclusion complexes with CD-*m*THPP (pMβCD/CD-*m*THPP). The inclusion complexation was extensively studied regarding structure with NMR spectroscopy and regarding stoichiometry with UV-Vis experiments and these results were compared with the corresponding complexation of pMBCD with *m*THPP (pMβCD/*m*THPP). Moreover, the binding constants for pMβCD/CD-*m*THPP 1:1 complex and for the pMβCD/ *m*THPP 2:1 complex were found from titration experiments to be extremely high, $K_{(1:1)} \approx 3.8 \times 10^{6}$ M^{-1} and $K_{(2:1)} \approx 4.9 \times 10^{12}$ M^{-2}, respectively. Although the stoichiometry of complexation of pMβCD/CD-*m*THPP (1:1) is different from pMβCD/*m*THPP (2:1), CD-*m*THPP preserved the properties of *m*THPP but with noticeable improvements in phosphate buffer saline (PBS): decreased aggregation to practically monomer form, increased up to 8-fold fluorescence emission intensity, good cell internalization with preferred localization into lysosomes (or endosomes) and the additional ability to carry suitable drug molecules, through inclusion in its cavity, as shown by NMR experiments. These results offer a robust methodology for preparing bimodal CD-porphyrin conjugates with improved properties, potentially useful for overcoming crucial limitations attributed to PSs used in PDT treatments. The methodology used to prepare CD-*m*THPP can eventually be expanded to the preparation of other conjugates and even extended to other PSs.

In the second part of this dissertation, positively charged cyclodextrin-based polymers were studied, with the focus in the capture and delivery of negatively charged drugs (*e.g.* nucleotides). Cyclodextrin-based polymeric materials (CD-polymers) are interesting as potential DDS because they are easily prepared in larger scales, their properties can be modified and offer potential advantages when compared to single CD derivatives *i.e.* keeping the same complexation ability for specific guest molecules, improving the solubility of drugs and acting as bioavailability modifiers. Amino-CDs derivatives are positively charged CDs studied as

biomimetic molecules. *Per*(6-aminoalkylamino-6-deoxy)-CDs are a family of amino-CDs, that have previously revealed good cell penetrating properties (CPCDs) and moderated interaction with DNA. Additionally, *per*(6-guanidino-6-deoxy)-CDs showed strong interactions through cavity inclusion with model nucleotides. To explore this new and interesting field of delivery of anionic drugs (nucleotides), two strategies have been employed to prepare cationic CD-polymers, based on *per*(6-aminoalkylamino-6-deoxy)-βCD (βpen). Two different strategies have been used to prepare and characterize CD-polymers that involved: i) the reaction of βpen with preformed polymeric material namely poly-L-lysine (pLys) and ii) the preparation of a polymer from a monomeric material, followed by reaction with CD derivatives precursors of βpen. Several batches of βpen-polymers have been prepared and characterized, resulting in βpen-rich polymeric materials. These were shown able to complex suitable negatively charged molecules as shown by 2D NMR spectroscopy experiments. Moreover, they acted as release modifiers of nucleotides, as demonstrated using Franz cell experiments. Although the polymeric systems were not fully optimized, in the preliminary trails performed they showed the ability to regulate the release of adenosine 5'-monophosphate (5'-AMP) and of the anticancer drug gemcitabine (GEM).

Keywords

Bimodal System; Cancer; Cyclodextrin; Conjugates of Cyclodextrin-Porphyrin; Drug Delivery System; Porphyrin; Photodynamic Therapy; Polymers; Photosensitizer

Resumo

A terapia fotodinâmica (TF) é um tratamento para o cancro baseada em três componentes que trabalham em conjunto: um fotossensibilizador (FS), o oxigénio (O_2) e luz de um comprimento de onda específico (λ) que activam o FS e geram espécies reactivas de oxigénio, principalmente o oxigénio singuleto ($^1O_2$). Estas espécies reactivas são responsáveis pela acção terapêutica que envolve a destruição localizada das células cancerígenas na área de irradiação. Portanto, a TF pode ser entendida como um modo de administração de fármacos foto-induzida. As porfirinas são conhecidas pela sua reduzida solubilidade e forte tendência para formar agregados que afectam as suas propriedades foto-físicas e limitam a sua aplicação biológica. Modificações na estrutura das porfirinas são desejadas para obter FS, fáceis de preparar, caracterizar e que possuam propriedades melhoradas como uma melhor solubilidade. 5,10,15,20-tetrakis(*m*-hydroxyphenyl)-21,23*H*-porphyrin (*m*THPP) é uma molécula análoga de uma clorina (*m*THPC, temoporphin) aprovada como Foscan®, prescrita para o tratamento paliativo de doentes com carcinoma avançado das células escamosas na cabeça e no pescoço. *m*THPP e *m*THPC mostraram ser 25 - 30 vezes mais potentes que os derivados da hematoporfirina clinicamente aprovados, mas apresentam problemas de solubilidade que conduzem à formação de agregados que não fluorescem em soluções aquosas. Foscan® é administrado como injecção numa mistura de etanol e propileno glicol. Existe portanto, a necessidade de melhorar a solubilidade dos FS e evitar a formação de agregados em água, sem comprometer a propriedades fotofísicas / fotoquímicas características das porfirinas. As ciclodextrinas (CDs) são oligo-sacarídeos cíclicos compostos por unidades de α-D-glucopyranose (α-, β- e γ-CDs), que em água são capazes de encapsular moléculas hidrofóbicas na sua cavidade resultando em melhorias na solubilidade, estabilidade e biodisponibilidade de fármacos. Alguns derivados de CDs já se encontram aprovados como excipientes e são usados actualmente em diversas formulações disponíveis no mercado. A ligação covalente de CDs a porfirinas é uma estratégia que promove a conjugação das propriedades como a melhoria de solubilidade, encapsulamento e solubilização de moléculas atribuído às CDs, e com as propriedades de visualização e características fotofísicas das porfirinas, criando potenciais conjugados entre CD-porfirinas úteis como sistemas de libertação de fármacos (SLF) multimodais. Neste sentido, os conjugados entre CD-porfirinas podem apresentar melhor solubilidade e propriedades fotofísicas, oferecendo ainda a habilidade de poder transportar, na cavidade da CD, fármacos para o tratamento do cancro. O interesse no desenvolvimento de fármacos baseados em moléculas já aprovadas pelas entidades para o uso em humanos foi igualmente reconhecido.

Nesta dissertação será descrita a preparação, caracterização e propriedades de um conjugado CD-porfirina (CD-*m*THPP). Especificamente, *m*THPP foi ligada a βCD, formando o

conjugado CD-*m*THPP, com a estequiometria 1:1. CD-*m*THPP foi preparado com um rendimento de 40 % e através de um método que pode ser melhorado para uma estala superior (scale-up). CD-*m*THPP foi caracterizado por ressonância magnética nuclear (RMN), espectrometria de massa (EM) e análise elementar. As suas propriedades fotofísicas foram investigadas por espectrofotometria de UV-Vis e fluorescência. Comparativamente com *m*THPP, o conjugado CD-*m*THPP revelou melhor absorbância (1.7 x superior), fluorescência (20 x superior) e melhor solubilidade em água. Contudo, a solubilidade é limitada a concentrações (μM) devido à formação de agregados, mas suficiente para realizar experiências em células. Não foi possível a utilização de *m*THPP em condições semelhantes. A baixa solubilidade de CD-*m*THPP é limitada a concentrações μM mas foi melhorada até mM, pela adição de βCD-*per*-metilada (pMβCD) usada como solubilizante, através da formação de complexos de inclusão com CD-*m*THPP (pMβCD/CD-*m*THPP). Os complexos de inclusão pMβCD/CD-*m*THPP foram estudados quanto à estrutura por RMN e quanto à estequiometria por espectrofotometria de UV-Vis e os resultados foram comparados com complexos (pMβCD/*m*THPP). As constantes de complexação para pMβCD/CD-*m*THPP (1:1) e para pMβCD/*m*THPP (2:1) foram determinadas por ensaios de titulação e são $K_{(1:1)} \approx 3.8 \times 10^{6}\ M^{-1}$ and $K_{(2:1)} \approx 4.9 \times 10^{12}\ M^{-2}$, respectivamente. Apesar da estequiometria de complexação de pMβCD/CD-*m*THPP (1:1) ser diferente da estequiometria apresentada por pMβCD/*m*THPP (2:1), CD-*m*THPP preservou as propriedades de *m*THPP com melhoramentos em solução aquosa (tampão fosfato salino): menor agregação, aumento da fluorescência, boa internalização nas células localizando-se preferencial nos lisossomas e a capacidade de transportar fármacos por inclusão na cavidade da βCD. Estes resultados são importantes porque oferecem a possibilidade de ultrapassar algumas das limitações dos PSs usadas na PDT. A metodologia usada para preparar CD-*m*THPP pode ser expandida a outros conjugados e outros PS.

Na segunda parte desta dissertação, pretendemos estudar polímeros baseados em CD com carga positiva potencialmente úteis na complexação e transporte de fármacos com carga negativa como nucleótidos. Polímeros baseados em CDs são interessantes pois podem ser preparados em grande escala, as propriedades podem ser modificadas e apresentam melhorias comparativamente com CDs, tais como: a melhoria na solubilidade de fármacos e acção como potenciais modificadores de biodisponibilidade. Amino-CDs são exemplos de CDs com carga positiva estudadas como moléculas biomiméticas. *Per*-amino-alquil-amino-CDs são uma família de amino-CDs, que dependendo do pH da solução podem apresentar aminas ($-NH_2$) e catiões amónio ($-NH_4^+$) que revelaram boa capacidade de internalização em células e interacção moderado com o ADN. Finalmente, *per*-(6-guanidino-CDs) revelaram forte interacção com nucleótidos levando à sua inclusão.

Para explorar este novo e interessante campo de pesquisa envolvendo o transporte de fármacos aniónicos (nucleótidos), duas estratégias foram desenvolvidas para preparar polímeros baseados em *per*-6-amino-etil-amino-βCD (βpen). A primeira estratégia envolveu a reacção de βpen com polímeros preformados baseados em poli-L-lisina (pLys) e a segunda, envolveu a preparação de um polímero com base em monómeros, seguida de reacção destes com derivados de CDs precursores da βpen. Alguns polímeros contendo βpen foram preparados e caracterizados, revelando-se úteis na complexação de moléculas carregadas negativamente, como demonstrado por experiências de espectroscopia de RMN em duas dimensões (2D RMN). Além disso, foi mostrado que estes polímeros actuam como modificadores de libertação de nucleotídeos, através de experiências com células de Franz modificadas. Embora os sistemas poliméricos não tenham sidos optimizados, os resultados obtidos revelaram a capacidade de regular a libertação de adenosina 5'-monofosfato (5'-AMP) e o fármaco anticancerígeno, gemcitabina 5'-monofosfato (GEM).

Palavras - chave

Cancro; Ciclodextrina; Conjugados de Ciclodextrinas-Porfírinas; Fotossensibilizador; Porfirina; Polímeros; Sistemas Bimodais; Sistemas de Libertação de Fármacos; Terapia Fotodinâmica

Acknowledgements

I would like to acknowledge to my coordinator, scientific advisor and mentor Dr. Konstantina Yannakopoulou (NCSR "Demokritos" Greece) for all her support in conducting this extraordinary research project. Even in moments where I felt I was struggling, you were always there pushing me forward and showing me the way.

To my professor, coordinator and dear friend Prof. Dr. Helena Maria Cabral Marques, (Faculty of Pharmacy of the University of Lisbon, Portugal), because if it was not for her perhaps this life-changing opportunity would not be there for me.

To my dear colleague Dr. Theodossis A. Theodossiou for all the fruitful scientific discussions, the cell internalization and confocal microscopy experiments through a vivid collaboration.

To Milo Malanga and Dr. Eva Fenyvesi from Cyclolab (Budapest, Hungary); to Zoltan Fulop and Dr. Prof. Thorsteinn Loftsoon from Faculty of Pharmaceutical Sciences (Reykjavik, Iceland); to Dr. Aurore Fraix and Dr. Salvatore Sortino from the Laboratory of Photochemistry Department of Drug Sciences, Catania University (Catania, Italy) and to Dr. Vladimir Kirejev and Dr. Marica Ericson from Biomedical Photonics Group, Department of Chemistry and Molecular Biology, University of Gothenburg (Gothenburg, Sweden) for the fruitful collaborations in the joint research project.

To James Birtley, Alberto Manfrim, Linda Piras, Toula Manouilidou, Mariza Lampropoulou, Chrysa Aggelidou, Manolis Saridakis and Dr. Irene M. Mavridris and all of my dear colleagues in NCSR "Demokritos", Greece for all of your help and support in this long journey.

To European Union and to Marie Curie Program # 237962 CYCLON (FP7-PEOPLE-ITN-2008) for the scientific training, vivid interactions with world leading scientific experts, for the ability to travel and improve my academic as well as interpersonal skills and for all the financial support.

To National Centre of Scientific Research NCSR "Demokritos" (Aghia Paraskevi, Athens) for the additional financial support, for hosting me in laboratory and for granting me assess to all infrastructures, which enabled the success of my research project. To Faculty of Pharmacy of University of Lisbon (FFUL) for accepting me as a PhD student.

Abbreviations

AcOH – Acetic acid

ADA-NH_3Cl – 1-Adamantanamine hydrochloride

ADA-COOH – 1-Adamantanecarboxylic acid

5'-AMP – Adenosine 5'-monophosphate

ATR – Attenuated total reflexion

βmTs – 6-*O*-monotosyl-β-cyclodextrin

βpBr – Heptakis(6-bromo-6-deoxy)-β-cyclodextrin

βpI – Heptakis(6-iodo-6-deoxy)-β-cyclodextrin

βpen - Heptakis(6-aminoethylamino-6-deoxy)-β-cyclodextrin

CD(s) – Cyclodextrin(s)

CECF – 1-Chloroethylchloroformate

$CHCl_3$ – Chloroform

COSY – Homonuclear correlation spectroscopy

DAE – 1,2-Diaminoethane

DDS – Drug delivery system

DHB – 4-Hydroxy-2,5-dihydroxybezoic acid

DIPEA – *N,N'*-diisopropylethylamine

DLS – Dynamic light scattering

DMF – Dimethylformamide

DMSO - Dimethylsulfoxide

DNA – Deoxyribonucleic acid

ΔG – Gibbs energy change

ΔH – Enthalpy change

ΔS – Entropy

EG – Ethylene glycol

EPI - Epichlorohydrin

EtOAc – Ethyl acetate

EtOEt – Diethyl ether

EtOH – Ethanol

FITC – Fluorescein isothiocyanate isomer I

FTIR - Fourier transform infrared spectroscopy

FWHM – Full width at half-maximum

GEM – Gemcitabine

HATU - 1-[bis(dimethylamino) methylene]-1*H*-1,2,3-triazolo[4,5-b]pyridinium 3-oxid hexafluorophosphate

H_2SO_4 – Sulphuric acid

HCCA – α-cyano-4-hydroxycinamic acid

HCl – Hydrochloric acid

HMBC – Heteronuclear multiple-bond correlation

HOMO – Highest occupied molecular orbital

Hp – Hematoporphyrin

HP-βCD – Hydroxylpropyl-β-cyclodextrin

HPLC – High performance liquid chromatography

HSQC – Heteronuclear single-quantum correlation spectroscopy

*i*PrOH – Isopropanol

IR - Infrared

IUPAC – International Union of Pure and Applied Chemistry

J – Coupling constant

K – Equilibrium constant

KOH – Potassium hydroxide

LUMO – Lowest unoccupied molecular orbital

MALDI-TOF – Matrix assisted laser desorption ionization – time-of-flight defection

MeOH / MeOD-d_4 – Methanol / deuterated methanol

*m*THPP – 5,10,15,20-Tetrakis(*m*-hydroxyphenyl)-21,23*H*-porphyrin

NaCl – Sodium chloride

NaOH – Sodium hydroxide

NBS – *N*-bromosuccinimide

NDTAM.HCl – *N*-desmethyltamoxifen

NH_3 / NH_4^+ - Ammonia / ammonium cation

NMR – Nuclear magnetic resonance

NOE(SY) – Nuclear Overhauser effect spectroscopy

$^1O_2$ – Singlet oxygen

$^3O_2$ – Triplet oxygen

OETPP – Octaethylphenylporphyrin

OTs – Tosylate

PCI - Photochemical internalization

PDT – Photodynamic therapy

PEI – Poly-ethylenimine

Ph – Phenyl

pLys.HBr – Poly-L-lysine hydrobromide salt

pLys - Poly-L-lysine

PPh_3 – Triphenylphosphine

PS – Photosensitizer

PVA – Poly-(vinyl alcohol)

Py – Pyrrole

R_F – Retention coefficient

RM-βCD – Randomly methylated βCD

RNA – Ribonucleic acid

ROESY – Rotating frame nuclear Overhauser effect spectroscopy

SBE-βCD – Sulfobutyl ether β-cyclodextrin

SEM – Scanning electron microscopy

siRNA – Small interfering ribonucleic acid

SLS – Static light scattering

TAM – Tamoxifen

TLC – Thin layer chromatography

TOCSY – Total correlation spectroscopy

TPP – 5,10,15,20-tetra(phenyl)-porphyrin

TsCl – 4-toluenesulfonic chloride

UV-Vis – Ultraviolet – visible

XRD – X-ray powder

Table of contents

INTRODUCTION

1. Cyclodextrins (CDs)

1.1 Structural features

Carbohydrates (saccharides) are chemical compounds of carbon, oxygen and hydrogen described by the empirical formula $C_x(H_2O)_y$. These are involved in many important biological processes that include:

i) the energy storage in plants (starch) and in animals (glycogen)

ii) they are structural elements in cell walls of bacteria, plants (cellulose) and in the exoskeleton of arthropods (chitin)

iii) they are linked to many lipids, proteins, make the structural framework of ribonucleic acid (RNA) and deoxyribonucleic acid (DNA)

iv) they are involved in cell recognition processes [1,2]

Carbohydrates are categorized as mono-, di-, oligo- and polysaccharides. These are also designated as aldoses or ketoses depending on their structure *i.e.* if they are derived, respectively from an aldehyde or a ketone group. D-glucose in its open structure is a six-carbon atom monosaccharide aldose (Figure 1 A) and is one of the most abundant carbohydrates in nature. Carbohydrates display a diversity of biological functions, which are related to their chemical structure and in turn determine their reactivity.

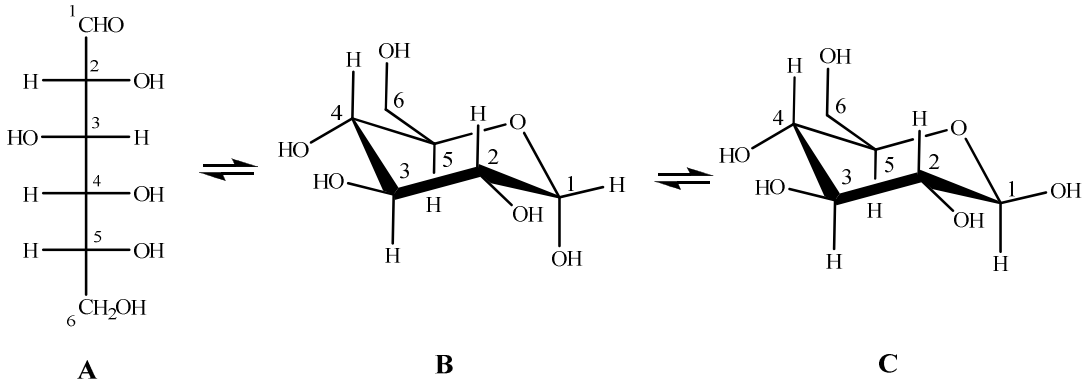

Figure 1. Structures of D-glucose (an aldose): A) its Fischer projection, B) α-D-glucopyranose and C) β-D-glucopyranose. There are three forms in aqueous solution, together with negligible amounts of the furanose forms.

A characteristic reaction of carbohydrates is the endocyclic or intramolecular hemiacetal formation, characterized by a nucleophilic attack of the terminal secondary hydroxyl

group (OH) to the carbonyl group of the ketone (R_1-CO-R_2) or aldehyde (R_1-COH). In D-glucose, for an intramolecular hemiacetal formation between the hydroxyl group on C_5 and the aldehyde group at C_1 (Figure 1 A), a cyclization reaction has to occur leading to the formation of D-glucopyranose. Depending on the stereochemistry of the OH group attached to C_1, two different stereoisomers or anomeric forms are possible: α-D-glucopyranose (Figure 1 B) – a *trans* isomer, with the hydroxyl group on C_1 in axial position relative to C_6-OH; and, β-D-glucopyranose (Figure 1 C) – a *cis* isomer, with the hydroxyl on C_1 in an equatorial position with respect to C_6-OH position. All other OH groups at C_2, C_3, C_4 and C_6-OH are in the equatorial position. In aqueous solutions, α-D-glucopyranose interconverts into β-D-glucopyranose isomer via open form in an equilibrium that involves changes in optical rotation ($[\alpha]^{20}_D$) of both isomers called mutarotation, manifested through changes in the overall $[\alpha]^{20}_D$ of the substance (Figure 2) [3].

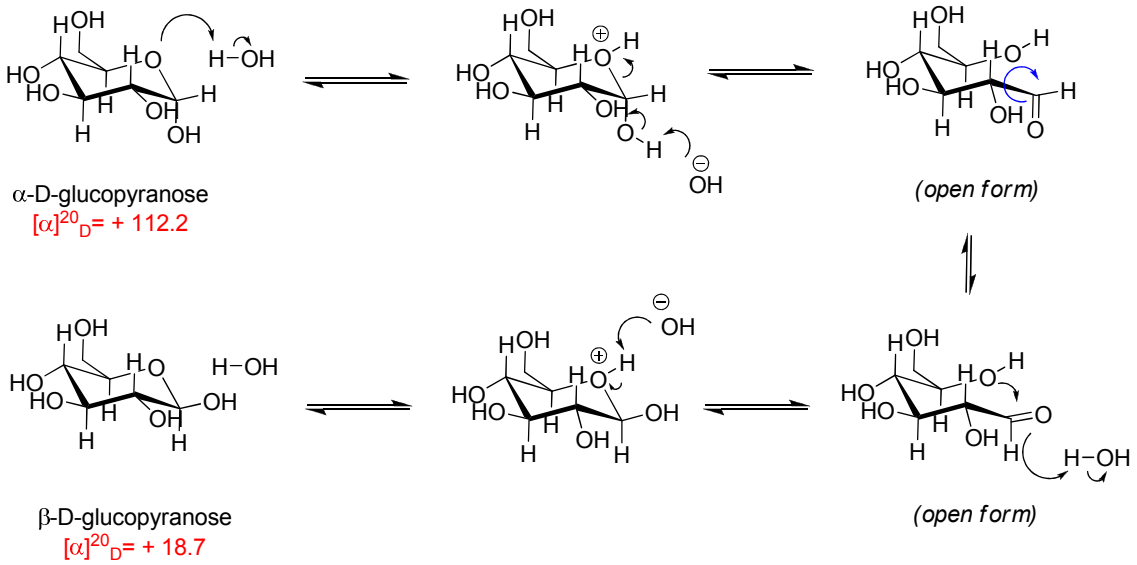

Figure 2. In an equilibrated aqueous solution of D-glucose the observed optical rotation ($[\alpha]^{20}_D$ = 52.7) due to mutarotation, resulting from 36 % of α-D-glucopyranose and 64 % of β-D-glucopyranose.

In D-glucose, each anomeric form can be involved in an intermolecular acetal formation reaction. The resulting chemical bond is a "glycosidic bond" and is responsible for the connectivity between many carbohydrates giving rise to disaccharides, oligosaccharides and polysaccharides. They are often named as α- or β-, depending on the stereochemistry of the initial anomeric carbon, followed by the numbering of the two positions involved in the connection between brackets (Figure 3).

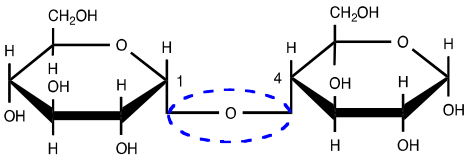

Figure 3. Connectivity between two α-D-glucopyranose units, through α-(1, 4)-*O*-glycosidic linkage (bond).

According to the IUPAC recommendations [4], other types of glycosides can be formed when the anomeric oxygen is substituted by other elements namely: thioglycosides (sulphur, -SR); selenoglycosides (selenium, -SeR); *N*-glycosides (nitrogen, $-NR_1R_2$) or *C*-glycosides (carbon, $-CR_1R_2R_3$).

Naturally occurring cyclodextrins (CDs) are cyclic oligosaccharides resulting from sequential α-(1,4)-*O*-glycosidic linking of 6-, 7- and 8 α-D-glucopyranose units, represented as αCD, βCD and γCD, respectively (Figure 4) [5]. These macrocycles are industrially produced by enzymatic conversion of starch and other α-(1,4)-glucans, through the action of glucosyltransferase (CGTase, EC 2.4.1.19) [6] in an intramolecular transglycosylation reaction [7].

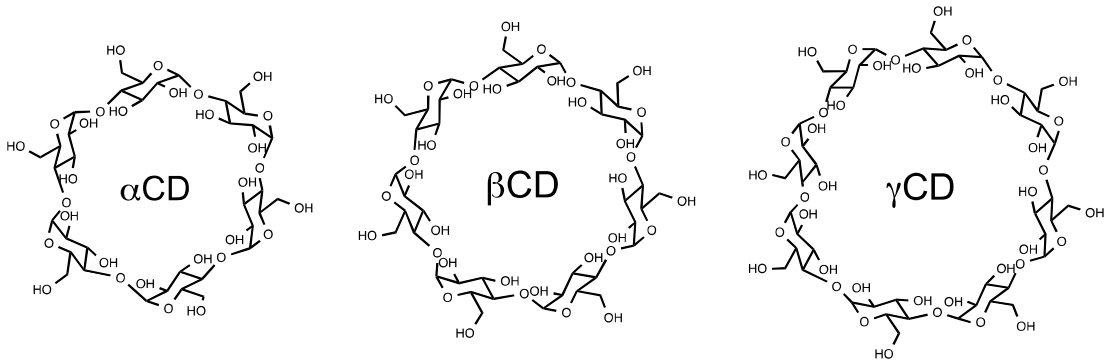

Figure 4. Structures of the three native cyclodextrins: αCD, βCD and γCD.

The structure of CDs was found and assigned to a cyclic geometry after a series of findings and discoveries classified by Szejtli [8] as the "discovery stage" in CD chemistry [9, 10]. The α-(1,4)-*O*-glycosidic linkage, between two consecutive α-D-glucose units and the hydrogen bonding network on the secondary side between adjacent hydroxyl groups, in positions 2 and 3 of the n glucopyranose units, explain its doughnut-shaped structure. The inner lining comprises the hydrogen atoms at positions 3 and 5 of glucopyranose (n-1) and the glucopyranose oxygen bridging atoms that render the cavity its lipophilic character, in opposition to its outer hydrophilic rims lined with hydroxyl groups [11] (Figure 5).

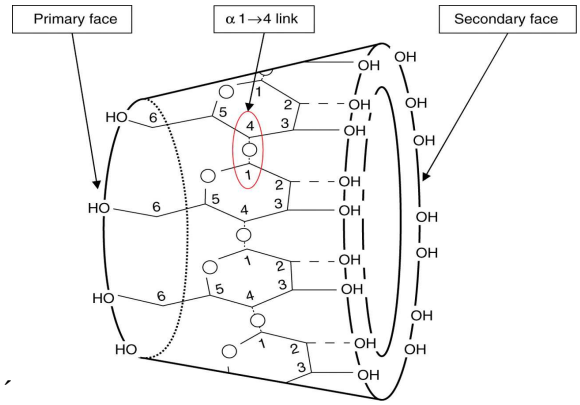

Figure 5. Structural arrangement of glucopyranose units in γ-cyclodextrin connected through α-(1, 4)-*O*-glycosidic linkages with the hydroxyl groups at the rims creating the primary and secondary faces [12].

X-ray and neutron diffraction studies in the crystalline state revealed that [13]: i) each glucose unit adopts a $^4C_1$ chair conformation; ii) there is freedom of rotation about the C(6) – C(5) bond, resulting in OH(6) rotated either away (*gauche-gauche*) or towards (*gauche-trans*) the centre of the CD; iii) the secondary hydroxyls groups of adjacent glucose units are connected by intramolecular hydrogen bonding and, as a consequence iv) in native CDs rotation about C_1-O-C_4 is not possible.

Native CDs are water-soluble compounds and their glycosidic bonds are stable in alkaline solution [14], whereas in strong acids they are prone to acid hydrolysis to give linear oligosaccharides (pH < 3.5; T > 60 ºC) [15]; however, the hydrolysis is considerably slower, compared to that observed for linear oligomers (maltohexaose, -heptaose, -octaose).

The number of glucose units in the macrocycle determines the dimensions of the cavity namely: the annular diameter and the volume of α, β, and γCD. Additionally, the dimensions of the macrocycle determine the properties of CDs (Table 1) [13, 16] namely its water solubility and ability to complex different guest molecules. For example, the solubility of native CDs in water (γCD > αCD > βCD, Table 1) has been related to the number of glucopyranose units in each macrocycle: βCD is poorly soluble because is has the appropriate number of glucose units and has a complete hydrogen bonding network, comprising all seven glucopyranose units; the intermediate solubility of αCD is associated with the incomplete hydrogen bond in network between the six glucopyranose units, because one of the six glucopyranose units is distorted relative to all of the others; finally, γCD is larger and possesses a more flexible structure and thus an even better solubility [9].

Table 1 – Some physico-chemical properties of native CDs, adapted from Easton & Lincoln [13].

CD Feature	αCD	βCD	γCD
Number of glucose units	6	7	8
Molecular weight (g/mol)	972.9	1135.0	1297.1
Annular diameter (Å)	4.7 – 5.2	6.0 – 6.4	7.5 – 8.3
Annular depth (Å)	7.9 – 8.0	7.9 – 8.0	7.9 – 8.0
Volume cavity (10^6 pm^3)	174	262	427
Optical rotation, $[\alpha]_D$ (25 ºC)	150.0 ± 0.5	162.5 ± 0.5	177.4 ± 0.5
Water molecules cavity	6	11	17
Solubility (g/L, 25 ºC)	145	18.5	232

1.2 Formation of inclusion complexes

The most remarkable characteristic of native CDs is their ability to accommodate poorly water-soluble guest molecules of appropriate size and geometry that are able to fit into the CD hydrophobic cavity in aqueous solutions [9]. Inclusion is explained by the simplest complexation equilibrium, between one guest molecule (G, drug) and one host molecule (H, CD) (Figure 6). However, there is the possibility of multiple equilibria and involving various stoichiometries, between h molecules of H and g molecules of G (Figure 6, Eq. 1) resulting in an overall equilibrium constant (Figure 6, Eq. 2).

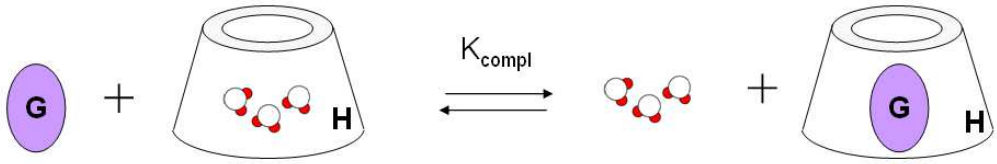

A)

$$hH + gG \underset{}{\overset{K_{compl}}{\rightleftharpoons}} H_hG_g \qquad (Eq.\ 1)$$

$$K_{compl} = \frac{[HG]}{([H]^h \times [G]^g)} \qquad (Eq.\ 2)$$

B)

Figure 6. A) Complexation equilibrium between a CD unit (H) and a guest molecule (G), with the corresponding release of high energy water molecules; B) Chemical equation describing the inclusion complex formation, between *h* moles of host (H) and *g* moles of guest (G) to form a *hg* moles of the complex (HG): general equilibrium equation (Eq. 1) and overall equilibrium constant K_{compl} (Eq. 2).

The magnitude of the binding constant (K_{compl}) determines the stability of the complex and it is related to the chemical structure of both guest and host molecules. The driving force for the inclusion is the hydrophobic effect and stabilization of the complex was explained by a

series of H-G intermolecular interactions: van der Waals forces, dipole-dipole and hydrogen bonding interactions. In this respect, it was recognised that van der Waals forces justify the inclusion phenomena, whereas electrostatic interactions and hydrogen bonding usually dictate the spacial conformation of a given inclusion complex [17]. The magnitude of K_{compl} can be improved through drug ionization, salt formation, use of co/solvents, metal complexation, polymer complexation and acid-base ternary complexes [8]. The binding process involves a combination of factors, comprising: i) the insertion of the hydrophobic part of the G molecule into the H cavity; ii) the dehydration of the organic guest and iii) the release of high-energy water molecules, located inside the CD cavity to the aqueous medium [18].The thermodynamic parameters ruling inclusion of G molecules by CDs have been studied and inclusion is usually characterized by: negative Gibbs energy change ($\Delta G^o < 0$) and enthalpy ($\Delta H^o < 0$) whereas the entropy (ΔS) is small negative or positive.

The determination of the binding constants (K_{compl}) and of the stoichiometric coefficients can be achieved by measuring the changes in the analytical response of an experimental technique such as UV-Vis, fluorescence emission or NMR spectroscopy. A typical experiment involves the continuous addition of H molecule to a G solution or vice-versa, followed by recording of the changes observed. These values are then plotted and fitted to suitable equations, describing binding experimental models to determine the proper stoichiometry of complexation and the binding constant (K_{compl}) for that specific stoichiometry [19]. The method of continuous variations (or Job´s plot) is a graphical representation of any property (UV-Vis / NMR) that changes as a function of the molar ratio of H and G in a solution, keeping the concentration of [H + G] constant, that enables the determination of stoichiometry of the complex formed [20, 21].

1.3 Structure of inclusion complexes in solution

Complexation / inclusion equilibrium involving CDs in aqueous media can be assessed by NMR spectroscopy. A common feature of all CD inclusion complexes is that the ^1H NMR signals corresponding to the internal protons of the cavity (H_3/H_5) of a CD are affected after complexation with a suitable guest. Usually, H_3 and H_5 are shielded by the electrons of the incoming guest and the respective resonances move to lower frequencies (smaller ppm), when compared the initial host solution.

In addition, NMR spectroscopy is useful to study the mode of complexation through 2D NMR experiments based on nuclear Overhauser effect (NOE), because the observed

correlations enable the detection of protons spatially close to one another in a distance up to ≈ 5 Å. NOE arises from cross relaxation mechanism, explained by the mutual interactions of two spins through space acting as two magnetic dipoles (dipolar coupling). Dipolar interactions affect the spin population that are close in space, generate NOE and can be detected by two major NOE experiments, which are independently used, depending on the size of the molecules being analysed: i) Rotating frame nuclear Overhauser Effect SpectroscopY (ROESY) is used for molecules with molecular weight ≈ 1000 Da and ii) Nuclear Overhauser Effect SpectroscopY (NOESY) which is negative for larger molecules (molecular weight > 1000 Da) and positive for small molecules. A consequence of NOE effect and a successful 2D NMR experiment is that the geometry of the complex and the mode of complexation can be determined.

Furthermore, one important aspect to be considered in NMR complexation studies is the exchange rate regime between two different states, which might involve a complex (A) and free guest molecule (B). In the fast exchange regime, the overall rate of the complexation (K_{ex}) is much higher than the chemical shift differences ($\Delta\nu$) between A and B and the signals are not distinguishable, but appear at an intermediate frequency, which is the weighted average between frequencies ν_A and ν_B, multiplied by the respective spin populations, P_A and P_B, so that the $\nu_{obs} = P_A\nu_A + P_B\nu_B$. However, in slow exchange regime where $\Delta\nu > K_{ex}$, clear signals for both A and B are observed and these species can be independently detected during a NMR experiment (Figure 7) [22].

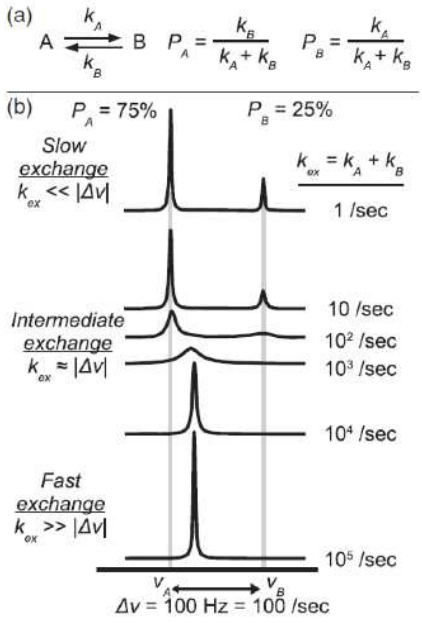

Figure 7. Chemical exchange processes [22]: (a) exchange between two states A and B, with different equilibrium constants (k_A, k_B), chemical shifts (ν_A, ν_B) and populations fractions (P_A, P_B) of each state, (b) variation of k_{ex} on NMR spectra with P_A = 75 % and $\Delta\nu$ = 100Hz.

The crystal structure of CDs has been studied by X-ray crystallography, which in combination with other techniques such as NMR spectroscopy revealed the structure of cyclodextrin complexes in the solid state. The structure of several drug complexes has been investigated in the presence of CDs such as: i) non- steroidal anti-inflammatory drug (NSAID), acemetacin [23] and β-naphthyloxyacetic acid (NOA) [24] in solution, to mention just a few examples from our laboratory. Almost invariably, in solution, all possible intermolecular complexes are observed, while in the crystal state the most populated (or most stable) complex eventually crystallizes out.

1.4 Chemical modifications

Chemical modification is a way of introducing various substituents on a CD macrocycle, resulting in CD derivatives with different properties. The conversion of a CD molecule into a new derivative, both efficiently and selectively, has always been challenging due to the large number of OH groups in each CD macrocycle: 18 in αCD, 21 in βCD and 24 OH in γCD and extensive heterofunctionalization has only recently been achieved [25]. Chemical modification could, nevertheless result in: i) improvements on the solubility of the CD derivative and its complexes; ii) a better fitting between the CD and the guest molecule with stabilization of the guest; iii) attachment of specific catalytic groups to the binding site (e.g., in enzyme modelling); or even lead to iv) the formation of insoluble or surface-immobilized CD polymers for different applications [9]. Most of the times, the type of CD derivative and selection of synthetic strategies to be applied are strongly dependent on the purpose of application.

In 1978 Lenh and co-workers [26], while preparing and characterizing a series of substituted αCD derivatives, realized that the order of substitution is affected by the difference in hydroxyl group reactivity, namely between the primary side (6-OH) and the secondary side (2-OH / 3-OH). Primary side 6-OH are more nucleophilic and less sterically hindered than the secondary side (2-OH / 3-OH); which results in easier reactivity of 6-OH [27]. By 1998, Kahn *et. al.* [27] suggested a classification for CD modification, which could comprise three categories: i) the “clever way”, achieved by the shortest route possible involved less synthetic steps; ii) the “long way”, followed a series of protection and de-protection steps and finally, iii) the “sledgehammer way”, where the reaction is left to react to give a mixture of products latter separated through extensive and time-consuming separation techniques.

Relevant findings regarding specific CD modification include but are not limited to: i) the preparation of mono-substituted CD derivatives described by Melton *et. al.* [28]; ii) modification of the original macrocycle configuration (from a natural $^4C_1$ to an 'induced' $^1C_4$ configuration, through conversion into their *mono*- or *per*-3,6-anhydro CDs derivatives (Figure 8) described by Ashton *et. al.* [29]; and, iii) *per*-6-halogenation of CDs was described by Defaye *et. al.* during trials to find alternatives to directly sulfonate the primary side of the CDs [30].

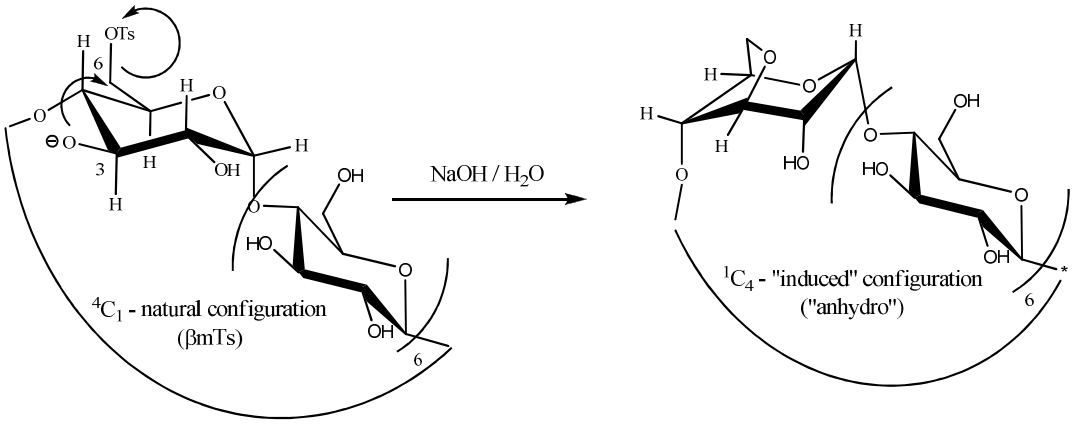

Figure 8. Formation of by-product mono-3,6-anhydro-βCD ("anhydro") from βCD in strong alkaline conditions ($NaOH/H_2O$), involving a nucleophilic attack of 3-OH to 6-OH leading to the inversion of configuration from a natural $^4C_1$ to an induced $^1C_4$. OTs = Tosylate.

Mono-tosylation (tosyl group, Ts) of a βCD [31] (Figure 9 i) is a versatile methodology that offers the possibility of further mono-modifications. This reaction can be performed in aqueous alkaline conditions and takes advantage of the inclusion ability of CDs, that is explored through the insertion of the Ts moiety into the CD cavity. This is the reason often suggested for the high purity of the mono-substituted product (βmTs), obtained in low yields but easily purified by precipitation from the reaction mixture [32]. Alternatively, mono-tosylation can proceed in pyridine where, by changing the relative ratio of reactants used, higher yields and other substitution products can be obtained at the expense of time spent in a tedious isolation/purification procedure based on column chromatography. The preparation of *per*-6-halogenated-CDs is another common modification reported by Defaye *et. al.* [30, 33] that proceeds through the *in situ* formation of the Vilsmeier-Haack reagent in dry dimethylformamide (DMF), in the presence of a halogen atom donor [bromine (Br_2), *N*-bromosuccinimide (NBS) or iodine (I_2) and triphenylphosphine (PPh_3)] (Figure 9 ii). Per-alkylation and per-acylation is also possible. Furthermore, selective 2,6-modification can be achieved (*e.g.* 2,6-di-*O*-methyl-βCD) as well as 2- or 3-modifications [27].

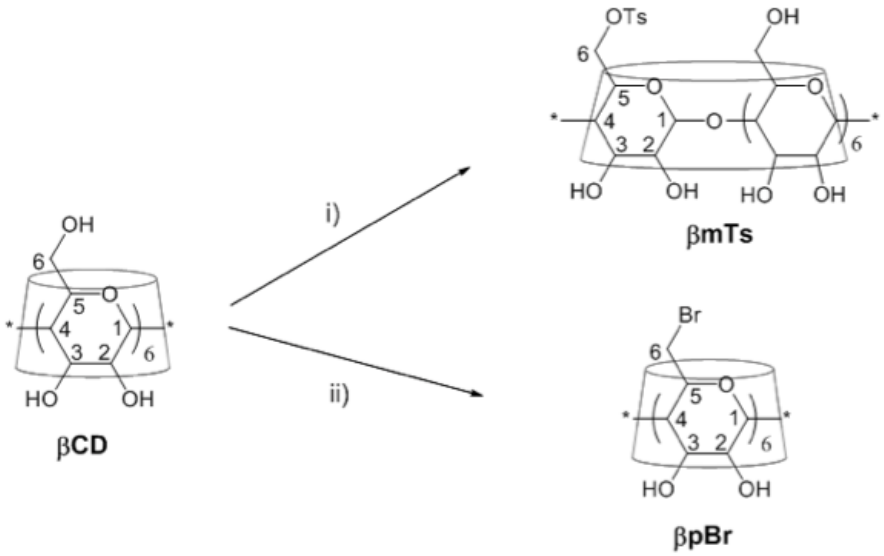

Figure 9. Different methodologies to convert CDs into: i) βmTs, a monosubtituted CD (conditions: TsCl, NaOH, H_2O) and ii) βpBr, a *per*-substituted CD (conditions: DMF, Br_2, PPh_3).

1.5 Derivatives as approved excipients

The flexibility in chemical modifications of CDs, their established safety profile [34] and their extensive range of application as encapsulation / complexation agents of several active pharmaceutical ingredients (API) makes CD derivatives especially attractive from the pharmaceutical industry perspective. In fact, most of the derivatives studied are derived from βCD that possesses the appropriate dimensions of the cavity better suited for complexation of phenyl groups, a common group in the structure of many drug molecules already approved for human use (Table 2). This is in contrast with the small cavity size of αCD derivatives and the expensive γCD derivatives [35]. Some examples of typical host CD derivatives already marketed involve: i) βCD; ii) randomly methylated βCD (RM-β-CD); iii) hydroxypropyl-βCD (HP-β-CD) and iv) sulfobutyl ethers (SBE-β-CD) (Table 2) [36].

Table 2. Some selected examples [37] of drugs molecules used in drug formulations containing CDs derivatives.

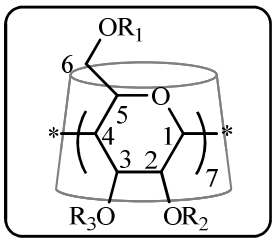

Derivative	R_1	R_2	R_3
βCD	-H	-H	-H
SBE-βCD	$-(CH_2)_4SO_2H$ (or *Na*)	$-(CH_2)_4SO_2H$ (or *Na*)	$-(CH_2)_4SO_2H$ (or *Na*)
HP-βCD	$-CH_2CHOHCH_3$	-H	-H
RM-βCD	$-CH_3$ or -H	$-CH_3$ or -H	$-CH_3$ or -H

Derivative	Brand Name	Route Administration	Drug (label)	Year	Company
SBE-βCD	Vfend	Intravenous	Vorizonazole (A)	2002	Pfizer
SBE-βCD	Geodon	Intra muscular	Ziprazidone (B)	2002	Pfizer
SBE-βCD	Abilify	Intra muscular	Aripiprazole (C)	2006	BMS/Otsuka
HP-βCD	Sporanox	Intravenous	Itraconazole (D)	1997	Janssen
HP-βCD	Vibativ	Intravenous	Telavancin	2009	Astellas Pharma / Therevance
RM-βCD	Aerodiol	Nasal spray	Ostradiol (E)	2001	Servier
βCD	Brexin	Rectal	Piroxicam	-	Chiesi
αCD	Rigidur	Intravenous	Alprostadil (PGE_1)	-	Ferring / Denmark

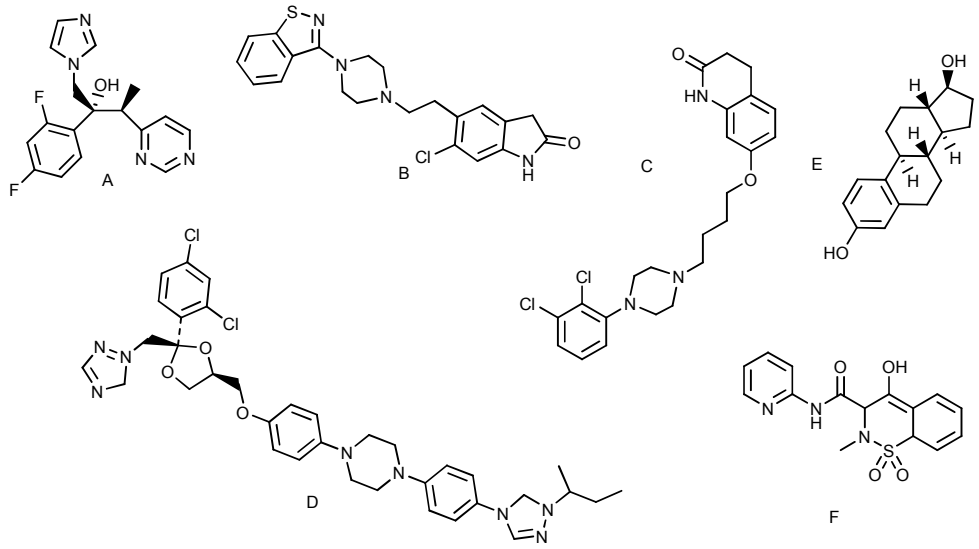

2. Porphyrins

2.1 Structure and properties

Porphyrins are naturally occurring compounds constituted by four pyrrole (Py) units, connected by methine bridges (=CH-) in a cyclic structure (Figure 10 A) [38]. This conjugated macrocycle has 22 π electrons, of which only 18 are effectively delocalized and contribute to its aromatic character, following Hückel's law of aromaticity: [4 n + 2] π electrons, with n = 4 [39]. Due to their tetravalent centre, porphyrins are able to form coordination complexes called metalloporphyrins with nearly any metal in nature, where they reveal biological activity as prosthetic groups (active site) [40]. Examples of several porphyrin-based prosthetic groups are iron (Fe^{2+}) complexes present in: i) the cytochromes responsible for electron transfer processes; ii) the cytochrome P_{450} oxidases involved in the oxidation of organic substrates; iii) the *heme* group suited for oxygen transport (Figure 10 B) and in myoglobin, used in oxygen storage. Magnesium (Mg^{2+}) complexes are common in the chlorophyll c1 green pigment (Figure 10 C) relevant in light harvesting processes during photosynthesis and cobalt complexes (Co^{2+}) of porphyrins like in vitamin B_{12} (Figure 10 D) are important in biocatalysis processes.

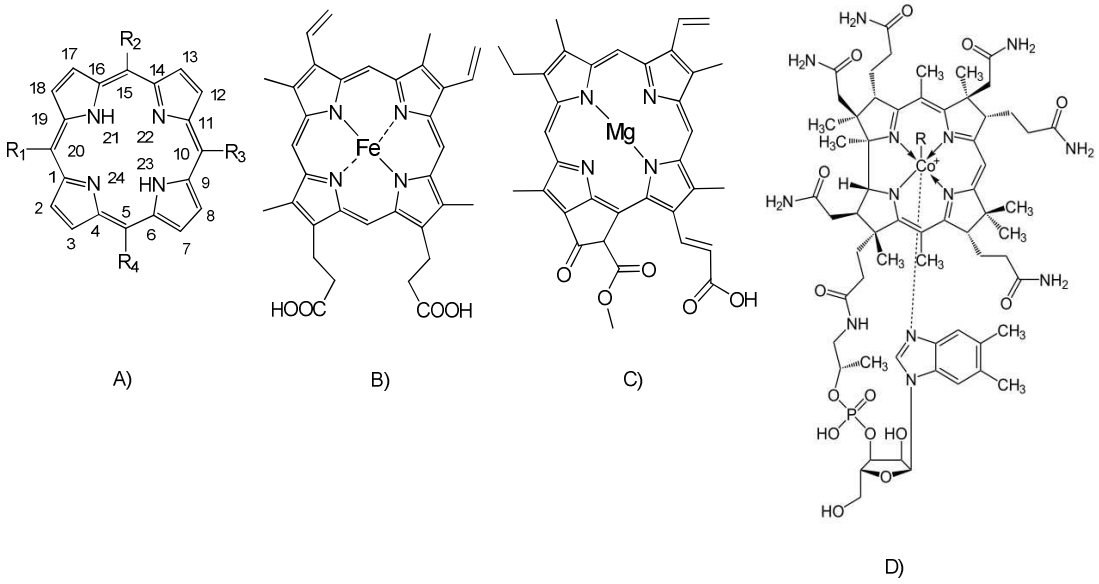

Figure 10. Examples of porphyrin macrocycle core structures: A) porphyrin numbering according to IUPAC [38]; B) *heme B*, an iron binding porphyrin located at the oxygen binding site of myoglobin; C) chlorophyll c1; D) vitamin B12.

Their abundance in nature, the diversity of their structural features and the importance of the biological processes mediated by them has boosted the research regarding porphyrins,

which is mainly focused on medical applications of these macrocycles. An example is given by derivatives of hematoporphyrin (Hp), which were first studied and revealed interesting features like good tumour localization and photosensitization properties [41,42]. However, Hp derivative first isolated, were a mixture of compounds, which motivated studies on its purification [43] and was latter extended to the synthesis of new porphyrins with improved properties.

Synthetic porphyrin derivatives enriched with different chemical functional groups, can be prepared through a diversity of methods [44], which involve the condensation reaction between pyrroles and aldehydes [45] (Figure 11).

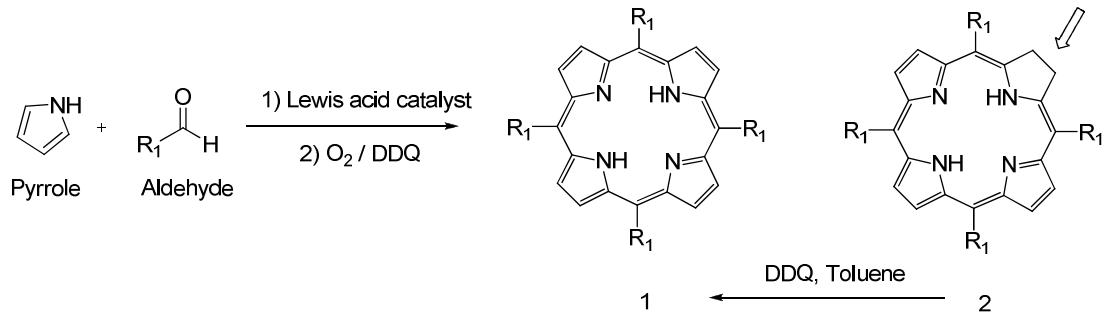

Figure 11. Synthesis of porphyrins according to Alder and co-workers [46], involving the condensation reaction of pyrrole with a substituted aldehyde in aerobic conditions, in the presence of a Lewis acid catalyst to obtain porphyrin (1) and the chlorin (2). The chlorin (2) can be oxidized back to porphyrin (1), with 2,3-dichloro-5,6-dicyanobenzoquinone (DDQ) in toluene.

Taking a freebase porphyrin as a reference structure shown in Figure 10 A, several modifications can be successful achieved, as explained in the full issue dedicated just to porphyrin nomenclature by the IUPAC [38] and more recent publications [47]. These modifications comprise: i) peripheral groups attachment to the pyrrole unit (β positions: 2, 3, 7, 8, 12, 13, 17, 18); or to ii) the *meso* positions (5, 10, 15, 20 – R_1, R_2, R_3, R_4); iii) the reduction of one or more double bounds in the macrocycle resulting in chlorins like chlorophyll a (Figure 12 A) and chlorophyll b (Figure 12 B); iv) the fusion of other ring systems to the porphyrin core structure (phthalocyanins) and also by v) substituting a carbon atom of the ring by another atom like nitrogen (N) or sulphur (S), are examples of the diversity of structures currently available.

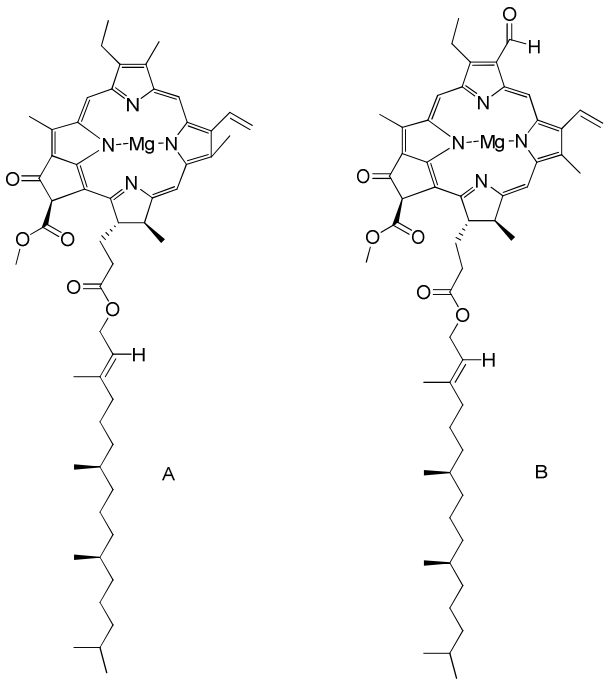

Figure 12. Structure of two chlorins: A) chlorophyll a and B) chlorophyll b.

2.1.1 **Photophysical properties**

One consequence of interaction of light with matter is the appearance of colour. The absorption of a quantized amount of energy (A) can promote the transition of one or more electrons in a molecule, from their electronic ground state (S_0) to an electronic excited state (S_1).

The study of the excited state properties is important because using light, a new type of reactivity can be achieved. Excited states can be characterized based on their lifetime (τ, lifetime) and on the yield of the transition of interest, measured by quantum yield (ϕ) [48]. Following light excitation of S_0 a molecule by absorption of light, the energy of the S_1 can be dissipated by radiative and non-radiative relaxation mechanisms and these transitions can be easily understood following the Jablonski diagram – Figure 13 [49].

Two important radiative decay pathways are fluorescence and phosphorescence. In fluorescence, the transition from a singlet excited state (S_1) to the singlet ground state (S_0) ($S_1 \rightarrow S_0$) is an allowed transition and occurs very rapidly, with very short fluorescence lifetimes ($\tau_F \approx 10^{-9} - 10^{-6}$ s) and high quantum yield of fluorescence (ϕ_F). In phosphorescence, the transition from the singlet-excited state (S_1) to the triplet state (T_2) ($S_1 \rightarrow T_2$) is "forbidden", resulting in a slower relaxation rate, and longer phosphorescence lifetimes ($\tau_P \approx 10^{-3} - 1$ s) and lower quantum yield.

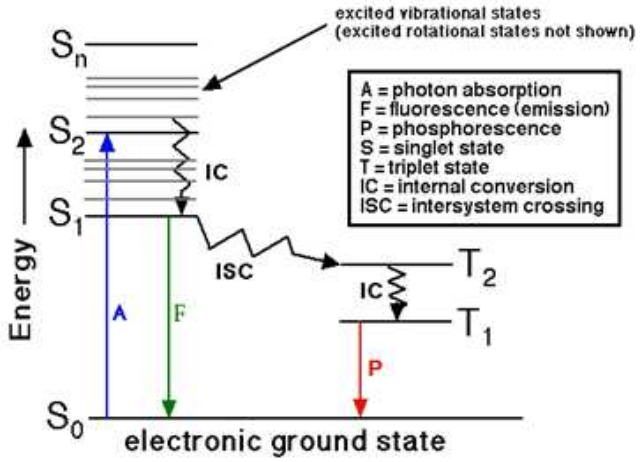

Figure 13. Jablonski diagram with electronic transitions and corresponding relaxation processes [49].

Due to their conjugated system of double and single bounds, porphyrins are coloured and present a characteristic UV-Vis absorption spectrum. A typical porphyrin (freebase) shows a strong absorption band (Soret band, 400 – 450 nm) and a group of small intense bands (Q bands I, II, III, IV, 500 – 700 nm) – Figure 14 [50, 51].

An absorption band is characterized by its intensity (Abs, AU), a wavelength (λ, nm) and a molar extension coefficient (ε, $M^{-1}.cm^{-1}$) characteristic of the chromophore. For the porphyrins, ε values are typically greater than 10^5 $M^{-1}cm^{-1}$. The origin of each spectral band is related to the electronic transitions between the highest occupied molecular orbital (HOMO) and the lowest unoccupied molecular orbital (LUMO). The "four-orbital model" proposed by Gouterman and then extended to other porphyrin derivative structures explained the spectrum of one of the simplest synthetic porphyrin (5,10,15,20-tetrakis(tetraphenyl)-porphyrin, TPP) [52].

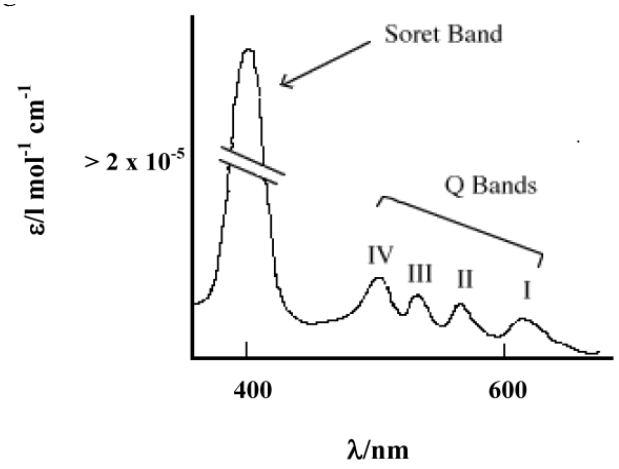

Figure 14. Typical UV-Vis absorption spectrum of a porphyrin, with typical Soret and Q-bands [50].

The bands in a freebase tetraphenylporphyrin (TPP) spectrum were attributed to π-π electronic transitions between HOMO and LUMO orbitals. Taking into account the differences in the polarity of the electronic transitions and the symmetry group of a starting porphyrin, the interpretation of several spectral changes was possible. A simple example is illustrated in Figure 15, where a TPP complexed with a metal (M) and their spectral changes were evaluated [53]. Upon metallation there is a symmetry group change, from a D_{2h} in porphyrin (TPP) to a D_{4h} in the metalloporphyrin (M-TPP) associated with HOMO-LUMO energy changes. This results in a simplified spectrum of a metalloporphyrin with less absorption bands as opposed to the spectrum of TPP (freebase).

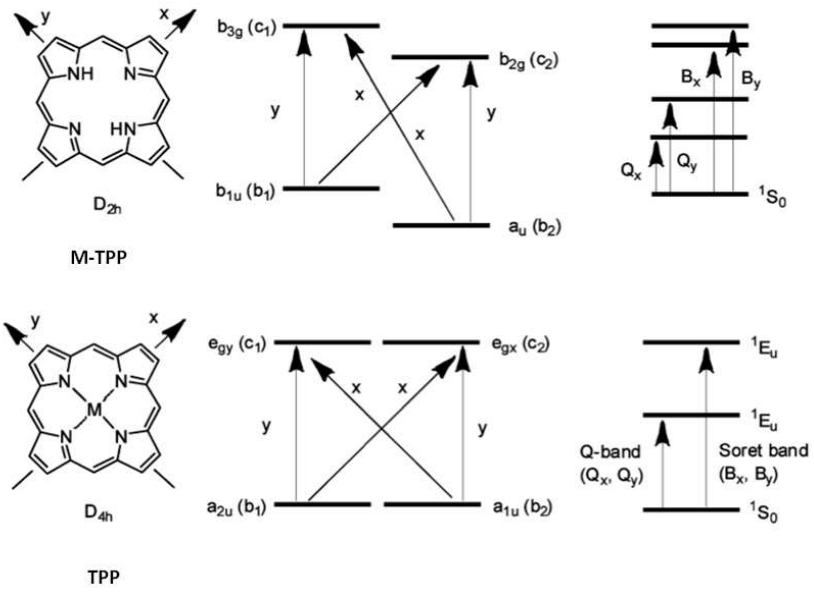

Figure 15. Simplified Gouterman model for the transitions between a TPP (freebase) and the corresponding metalloporpyrin (M-TPP) [53].

A porphyrin spectrum can be classified according to the relative intensity of its four Q bands (I, II, III, IV), as suggested and interpreted by Dolphin [40] through the following classification system: i) etio-type (IV > III > II > I); ii) rhodo-type (III > IV > II > I); iii) oxo-rhodo-type (III > II > IV > I) and iv) the phyllo-type (IV > II > III > I). In addition to structural changes in the porphyrin structure, the UV-Vis spectrum of porphyrins can be affected by factors as diverse as: the solvent [54], the temperature [59], the pH of the solution [55] and the concentration of the porphyrin [56].

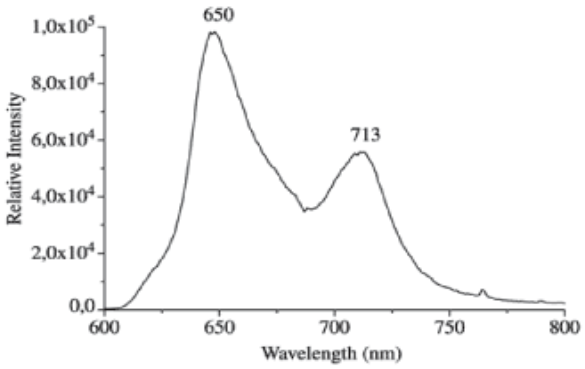

Figure 16. Typical emission spectrum of a porphyrin derivative: 5,10,15,20-tetrakis(2-hydroxy-5-nitrophenyl)-porphyrin ($T_2H_5NPPH_2$) [57].

Porphyrins are also characterized by their typical fluorescence properties (Figure 16 [57]), which enable their detection with higher sensitivity than the one achieved by UV-Vis spectroscopy. This is advantageous because from an analytical perspective, a smaller amount of material has to be used to obtain an equivalent analytical response. Porphyrins have a low energy gap between the lowest singlet (S_1) and triplet (T_2) states and a good intersystem crossing efficiency [40]. Consequently, they are considered good donors of triplet excitation, enabling excited molecules to relax to their triplet state. This is a property intimately related to their ability to generate singlet oxygen ($^1O_2$) and explains why porphyrins are so widely used as photosensitizers (PS) (section 2.2.4).

2.1.2 Metal coordination ability

One of the most remarkable characteristics of porphyrins is their ability to coordinate metals in their core, which has an approximate diameter of 3.7 Å [58]. A study on the complexation reaction of synthetically modified tetraphenylporphyrin (TPP) with zinc ion (Zn^{2+}) revealed that metallation is a very slow process (kinetically unfavourable) and is thermodynamically very stable ($K \approx 1 \times 10^{29}$) [58]. The stoichiometry of complexation with most metals is 1:1, although Na^+, K^+, Li^+ showed to form 2:1 complexes with one metal atom located below and the other one above the porphyrin macrocycle plane [58]. Formation of metal-oxo compounds is a type of connectivity characteristic of transition metals and oxygen commonly found in many metalloporphyrins. Metal-oxo connectivity showed to be responsible for: i) dimerization of protoferriheme and deuteroferriheme [59]; or ii) connectivity of an extra ligand to chelates of Mg^{2+}, Cd^{2+} and Zn^{2+}, to form penta-coordinated complexes with square-pyramidal structure [58]. The affinity of porphyrins to metals was also illustrated by the experimental determination of molar absorption coefficients of porphyrin esters, based on copper titration [60].

2.1.3 Aggregation of porphyrins

The possibility of having different porphyrin derivatives possessing useful photophysical properties and complexation ability, made the interest in the research grow even more. However, despite the reported advantages, in certain circumstances porphyrins can present undesired properties such as poor water-solubility and high tendency to aggregate especially in aqueous solvents [61], thus impairing their photophysical properties and hampering their effective delivery.

The great similarity between porphyrin structure and that of chlorophyll has been recognised, following studies to understand light harvesting processes in plants [62, 63]. It has been shown that chlorophyll is part of large protein complexes responsible for photosynthesis called photosystems I and II. Therefore, it is important not only to evaluate the properties of porphyrins as a single molecule, but also to assess them when a porphyrin is part of large molecular structures such as dimers, trimers or larger porphyrin aggregates.

Brown and co-workers [59] described the aggregation behaviour of protoporphyrin IX, deuteroporphyrin IX, hematoporphyrin IX and coproporphyrin in a comparative study using diluted buffer solutions and they have shown that: aggregation was promoted by an increase in concentration and was attributed to Fe-oxo-complexation, stabilized by additional bonding from the side chain groups of the macrocycles. Even synthetically modified porphyrins, often described as "water-soluble" porphyrins, motivated studies due to their high tendency for aggregation in aqueous media [64]. The extent of aggregation of porphyrin solutions in aqueous media is dependent of factors like: the concentration of the active species in solution [65]; the ionic strength of the solvent [65]; the temperature [66] and the pH of the solution.

The driving forces responsible for the aggregation phenomenon arise from a combination of factors. These include the cooperative formation of hydrogen bonds, van-der-Waals, dipole-dipole interactions, the hydrophobic effect and any other change that modifies the porphyrin core structure, like formation of a metalloporphyrin, for example [67]. Studies on the nucleation of water-soluble porphyrins in aqueous environment revealed different aggregation mechanisms [68] and kinetic studies [59] on naturally occurring porphyrins performed in aqueous solvents, revealed formation of micelles prior to extensive aggregation.

Important considerations that support dimerization/aggregation have been derived from UV-Vis spectroscopy. It is widely accepted that: i) the effect of aggregation is manifested by a decrease in intensity and shape broadening of the Soret band; ii) the Soret band splitting might occur, if the orientation of an aggregate of two porphyrins held together by hydrogen bonds changes [67] and during a dilution experiment performed on a solution porphyrin keeping constant the number of monomer units in the light path, the appearance of one isobestic point is usually attributed to dimerization phenomena [69, 70].

Two modes of interaction have been proposed resulting in two modes of aggregation [71] that differ on the geometry of the spatial arrangement between the porphyrin macrocycles – Figure 17 [72, 66]:

- H-type aggregate, characterized by a plane-to-plane stacking associated with a hypsochromic shift (blue shift, low λ) and Soret broadening

- J-type aggregate, characterized by an edge-to-edge interaction resulting in a bathrochromic shift (red shift, high λ) and a Soret splitting

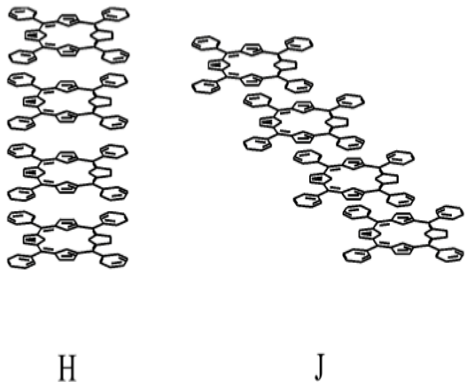

Figure 17. Two different modes of aggregation found in porphyrins [72]: plane-to-plane interactions (H – aggregate) and edge-to-edge interaction (J-aggregate).

A different study suggested at least six modes of interactions between protoporphyrins and 5,10,15,20-tetrakis(tetraphenylporhyrin) (TPP) in aqueous media, leading to fibres, tubules, helical ribbons and sheets with different photophysical / photochemical properties [67]. Micali *et. al*. described how the geometry of aggregation changes, from fractal to rod like arrangements, by tuning the concentration and ionic strength of water-soluble porphyrin [5,10,15,20-tetrakis(4-sulfonatophenyl)-porphyrin ($TPPS_4$)] [65]. The so-called "molecular wires" were prepared exploring the complexation ability of cyclodextrins, by independently connecting the same TPP derivative to two different molecules namely an adamantane moiety and a cyclodextrin derivative [73]. TPP / OETPP derivatives were modified with a bicyclic compound (bicycle [2.2.2] octene) to rigidify and maintain a planar conformation of the tetrapyrrolic macrocyles in solution [74]. Ordered monolayers, nanoparticles [75] and even nanoporous solid materials based on porphyrins have been proposed [65].

2.2 Applications in photodynamic therapy (PDT)

Porphyrins are well-known for their extended field of application, largely because of the easiness in preparation/modification and due to their interesting photophysical properties. Their metal complexes can act as catalysts in many organic relevant reactions like epoxidation of olefins [76] and selective functionalization of inactivated C-H bonds by hydroxylation [77]. They have been utilized as sensors for nitrous oxide [78], oxygen [79] or in electrochemical sensors for determination of inorganic anions [58]. Methods for water treatment were developed based on porphyrins as well as hydrogen fuel cells designed based on cobalt porphyrins [80].

In medicine, porphyrins can be used both as imaging agents based on their fluorescence properties [81] or as photosensitizers in photodynamic therapy (PDT) [82]. PDT is of major importance to the current work.

2.2.1 **Principles of PDT**

PDT is comprised of three independent elements: a light source (λ), a photosensitizer (PS) and molecular oxygen (O_2). The individually inert components act in combination to trigger type II photochemical reactions, with the corresponding production of singlet oxygen ($^1O_2$) leading to cell death by apoptosis or by necrosis [83]. PDT is an alternative treatment to radiotherapy and chemotherapy presenting many advantages. In comparison to conventional methods, PDT is a non-evasive method, reveals good cosmetic results (Figure 18), can be repeated without fear of overdosing or developing resistance and, through the use of an optical fiber, the desired therapeutic effects can be localized only to the irradiation site [82, 84].

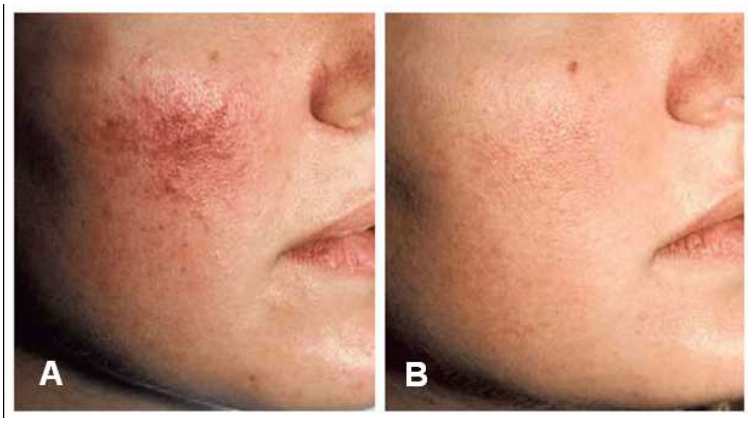

Figure 18. Cosmetic effect achieved after PDT treatment: before (A) and after (B) PDT treatment [85].

2.2.2 **Molecular oxygen (O_2)**

One key element in PDT is molecular oxygen (O_2). Usually, the valence electrons of most organic molecules that occur in nature, in their ground state, have their electrons in a singlet state configuration. However, O_2 is a particular molecule because the valence electrons in its ground state, occupy a two degenerate orbitals, with low energy corresponding to a more stable triplet state ($^3O_2$) (Figure 19).

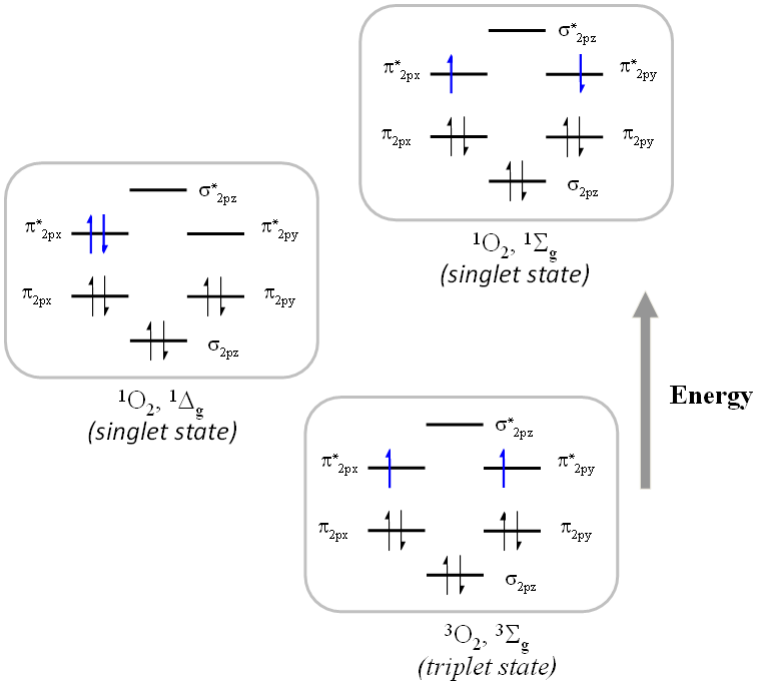

Figure 19. Molecular orbital diagram of molecular oxygen (O_2).

Singlet oxygen ($^1O_2$) is an important reactive oxygen species (ROS) and has great impact in biological processes like cell migration, circadian rhythms, stem cell proliferation and neurogenesis [86]. Once generated $^1O_2$ is very reactive with common substrates and, if its action is not controlled, it can have potentially harmful effects in biological systems and lead to photooxidative damage, with potential DNA damage [87]. Nature has evolved to control all of these processes: in plants during photosynthesis, any excess of $^1O_2$ produced is blocked by the action of carotenoids [88, 62]; whereas in animal cells, polyphenol antioxidants can protect and scavenge harmful $^1O_2$ and avoid its uncontrolled reactivity and undesired effects.

Reactions that involve electronic transitions with change in electron spin multiplicity are quantum mechanically "forbidden" or "not allowed transitions" and have very small probability of occurrence [89]. The conversion of $^3O_2$ to $^1O_2$ (singlet oxygen) is mediated by the

photosensitizer (PS) molecule and through the controlled use of light (wavelength λ; irradiation time) the cytotoxic action of $^1O_2$ can be achieved. This action is fast because $^1O_2$ is a short-lived species (10^{-10}-10^{-9} s) [90] and is limited to a short distance (0.05 μm).

2.2.3 **Photosensitizers (PS)**

A substance that is able to absorb energy and transfer part of its energy to another molecule, enabling a physical or chemical modification in this molecule is a photosensitizer (PS). The first PS for the treatment of early-stage lung cancer and bladder cancer was a mixture of porphyrins derivatives based on hematoporphyrin (Hp, Protofrin®, 1993) [91]. Nearly a decade later an improved PS was approved and was based on a pure reduced porphyrin derivative: a chlorin, namely 5,10,15,20-tetrakis(*m*-hydroxyphenyl)-chlorin (*m*THPC, 2003, temoporfin, Foscan®) [92]. In addition to Foscan® and Protofrin only four other PSs have been approved for clinical PDT: i) 5-aminolevulinic acid (ALA, Levulan®); ii) its methyl ester ,MAL (Metvix®); iii) verteporfin (Visudyne®) and iv) talaporfin (Laserphyrin®; only in Japan) [93] (Figure 20). Moreover, hexyl levulinate (hexvix, Cysview®, USA) has been marketed for *in situ* imaging of bladder cancer. The aminolevulinic acid derivatives are endogenously converted by natural biosynthetic pathways to protoporphyrin IX and thus express their PS properties.

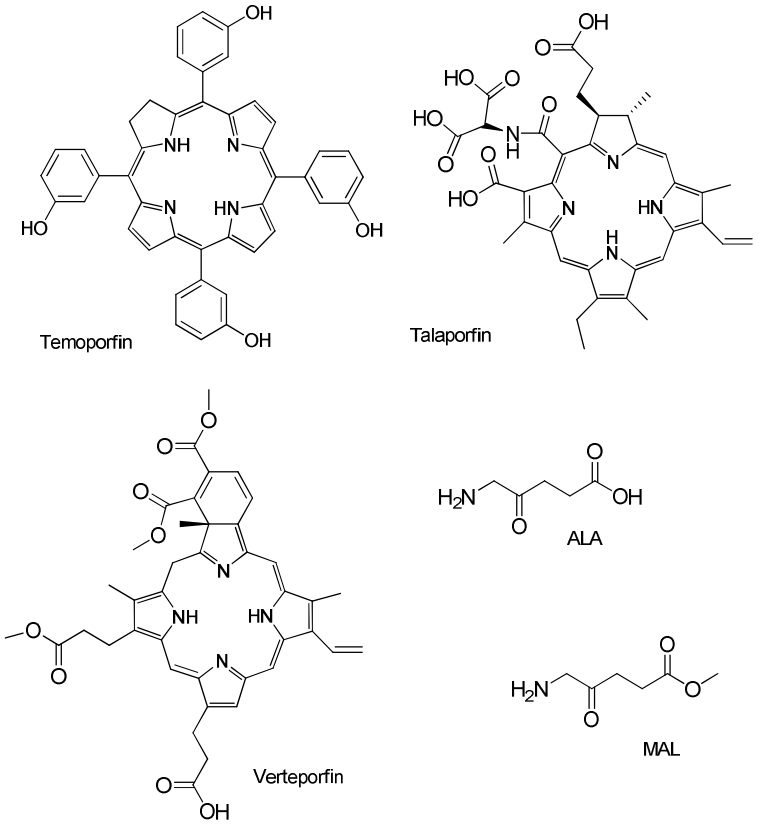

Figure 20. Chemical structure of some clinically approved photosensitizers.

Foscan® used in a typical PDT treatment comprises a two-step process: i) first, PS (Foscan®) is injected in a single shot, lasting at least six minutes and using an indwelling intravenous cannula; then and only four days later ii), the entire surface of the tumour is irradiated with laser light (specific λ) using a fibre-optic cable to induce the desired therapeutic effects. Extreme care is taken not to illuminate other areas of the body, because the light sensitization is still not selective. Therefore, as a precaution, the patient should avoid exposure to bright light for 6 months after the treatment [94].

2.2.4 **Porphyrin as a PS**

An example of the PS action on a molecule results in the generation of $^1O_2$ and porpyrins can act as efficient PS: first, the PS in its ground state PS(S_0) is promoted to an excited singlet state PS(S_1), by absorption of light (λ) of a specific wavelength; then, through an efficient intersystem crossing (ISC), it relaxes and traps part of its energy in its triplet state PS(T_1); finally, because the lifetime (τ_P) of a triplet state of the PS(T_1) is longer than that of a singlet state PS(S_1), there is more time to react efficiently with other substrates, namely with molecular oxygen ($^3O_2$) trapped in tissues. Two important mechanisms are often proposed to explain the reactivity of excited species PS(T_1) and these are described as follows [95]:

i) In type I – PS(T_1) transfer an electron or abstracts hydrogen atoms from the substrate (S), generating species (cations / radicals) that then react with $^3O_2$ yielding oxidized products;

$$PS(T_1) + RH \rightarrow PS(T_1)H^+ + R^- \rightarrow PS(T_1)H^+ + {}^3O_2 - \textit{type I}$$

$$PS(T_1) + RH \rightarrow PS(T_1)H^\bullet + R^\bullet \rightarrow PS(T_1)H^\bullet + {}^3O_2$$

ii) In type II – follow from a collision of the excited sensitizer PS(T_1) with molecular oxygen (triplet state, $^3O_2$), singlet oxygen is generated and can then react with biological substrates (S) leading to photodegradation products;

$$PS(T_1) + {}^3O_2 \rightarrow PS(S_0) + {}^1O_2 \rightarrow {}^1O_2 + S - \textit{type II}$$

The exact mechanism by which $^1O_2$ is produced has been a matter of debate. Although now it is accepted that a type II photochemical reaction is involved in $^1O_2$ generation [96, 97], it cannot be excluded that the overall PDT effect might result from a combination of type I / type II mechanisms. The overall yield of type II photochemical reaction might be affected by

photobleaching and quenching of fluorescence. Photobleaching occurs due to PS exposure to light, which can lead to irreversible changes in PS structure due to photon-induced chemical damage and covalent modification. A practical consequence is that PS absorbance and fluorescence intensity are lost. The number of times a PS can absorb and become excited before it starts photobleaching depends on the local environment and on the structure of PS [98]. Quenching results in fluorescence loss and involves a non-radiative energy loss that occurs because of oxidizing agents, the presence of salts, heavy metals or halogenated compounds [98].

2.2.5 Other photosensitizers

The photosensitizer (PS) property is not limited to porphyrin structures and many other molecules proved successful in generating singlet oxygen ($^1O_2$). Some examples are perylenequinones (PQs), hypericin (HC), quinones and rhodamines Figure 21) [99].

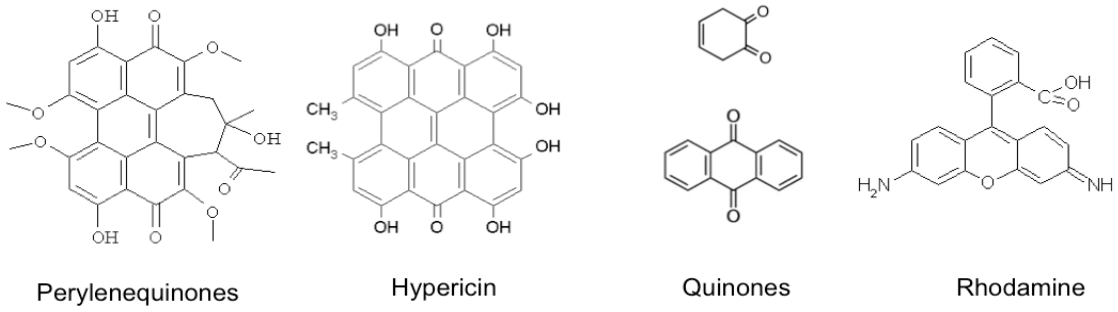

Figure 21. Structures of some PSs based on different chemical entities: quinones, perylenequinones, hypericin and rhodamines.

Although all of these molecules can potentially be useful as PSs, none of them was so successful as the porphyrins or any of their derivatives. In the past few decades, the ultimate goal has been to develop an "ideal photosensitizer molecule" that would display a set of unique characteristics which define the "ideal PS": a good chemical purity / stability; high quantum yield of singlet oxygen production; significant absorption in the long wavelength region (700 nm – 800 nm); preferential tumor localization (targeting); minimal dark toxicity; delayed phototoxicity and display good water solubility suitable for injectable solvents used in formulation [100, 92].

In a quest to find the best PS molecule, three generations of PS have been considered: the first refers to PSs based on hematoporphyrin derivative (HpD) and Photofrin®; the second

generation, intended to chemically modify porphyrin structure into its derivatives and iii) the third generation comprises the attachment of tags to existing PS molecules to increase their selectivity [93]. A matter of recent focused research has been to provide bimodal cancer treatments, combining photo- and chemotoxicity capability in a singular system.

2.2.6 **Photochemical internalization (PCI)**

Photochemical Internalization (PCI) is a recently proposed technology based on the same principles as PDT but with an important difference: the PS has to be localized intracellularly in endocytic vesicles, together with a therapeutic agent. Therefore, after irradiation of light (specific λ), there is the generation of $^1O_2$ which leads to the local burst of membranes of endosomes with the release of the drug into the cell - PCI mechanism of action (Figure 22) [101]. PCI acts as a precise photocontrolled drug delivery system of large macromolecules therapeutics, that otherwise would be degraded in the lysosome and excreted / eliminated from the cell.

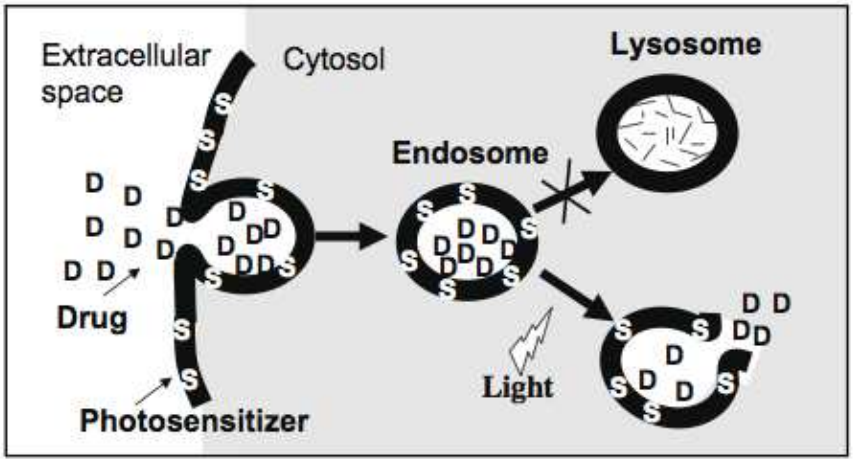

Figure 22. Photochemical internalization (PCI) mechanism of action, showing light induced release of drug (D) and photosensitizer (PS) into the cytosol after burst of the endosome [101].

Amphinex-based PCI of bleomycin (Figure 23) uses 5,10,15,20-tetraphenylchlorin substituted by two adjacent sulfonated groups (TPCS2a) as PS, to treat patients with local recurrence or advanced/metastatic, cutaneous or sub-cutaneous malignancies [102].

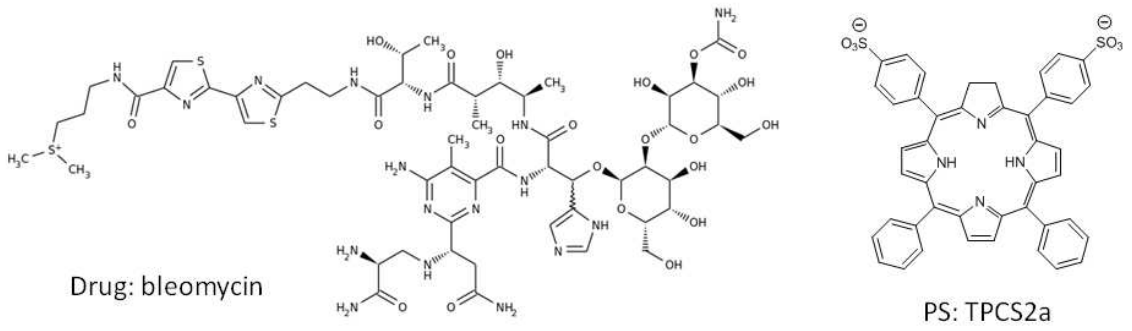

Figure 23. Components of amphinex medicine: a photosensitizer (TPCS2a) and the drug (bleomycin).

3. Multifunctional drug delivery systems (DDS) based on CDs

3.1 DDS purpose

In opposition to the systemic administration of medicines, it is expected that a drug delivery system (DDS) can deliver the desired agent (medicine), in the right amount, specifically to the affected tissue resulting in the therapeutic treatment leaving the host tissue undamaged following the *magic bullet* concept, as suggested by Ehrich [103]. Examples of extensively studied and established DDS include liposomes, polymers, micelles, nanoparticles and antibodies and have been extensively studied (Figure 24) [104].

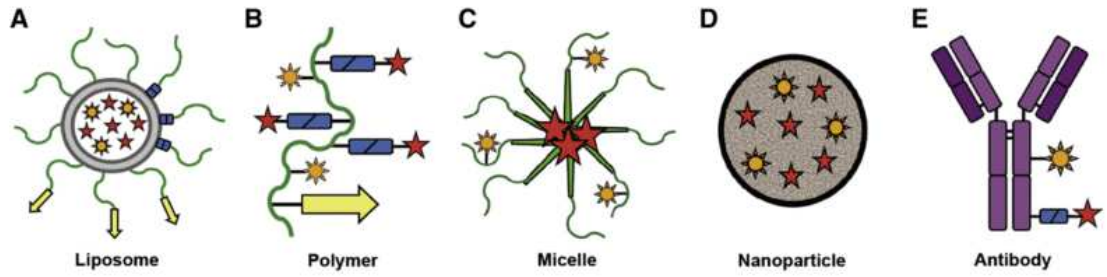

Figure 24. DDS examples: A) Liposome; B) polymer; C) micelle; D) nanoparticle and E) antibody [104].

3.1.1 **Passive *vs* active targeting**

The type and mode of administration of the DDS is dependent on the desired effect and on the specific targeting strategies, which are divided into “active” or “passive” drug targeting strategies. These have been reviewed by Sinko and co-workers [105]:

Active targeting involves the attachment of a specific chemical group (or tag) to the DDS, in order to attach the DDS directly to the specific site of action. Examples are: i) tumour specific antigens or receptors; ii) antibody-directed enzyme prodrug therapy (ADEPT); iii) gene-directed enzyme prodrug therapy (GDEPT) / virus-directed enzyme prodrug therapy (VDEPT); antibody-targeted, triggered, electrically modified prodrug type strategy (ATTEMPTS) and membrane transporters. On the other hand, passive drug targeting strategies [106] take advantage of the enhanced permeability and retention effect (EPR) of large DDS [107], which due to their prolonged blood circulation time can effectively penetrate into cancer cells possessing irregular morphology, density and high vasculature of these tissues, as opposed to healthy tissues. Some examples comprise i) polymer-directed enzyme prodrug therapy (PDEPT) and ii) polymer-directed enzyme liposome therapy (PELT).

Figure 25 shows a schematic representation between active and passive targeting approaches, comparing an ideal case with a realistic scenario. Clearly, active and passive targeting strategies to treat cancer still face many limitations that impair their extended and successful application [104]. These can be summarized as follows:

i) variable EPR effect or extravasation of DDS to the tumour

ii) variable degree of penetration of DDS into tumours

iii) active targeting faces many physical barriers due to high cell density in tumour cells, that lead to blockage or loss of the tag attached to the DDS

iv) inadequate formulation of the DDS with a systematic failure to show significant therapeutic benefit

v) difficulty to reach good correspondence between animal models and humans

vi) difficulties in achieving personalised healthcare treatments

The safety profile of these materials and their performance cannot be assessed relying on the same principles, as those used for single drug molecules due to the complexity and big number of components in a DDS. Therefore, the characterization of these DDS, regarding physico-chemical properties, is often limited to a distribution or average value. There is a lack of reproducibility in its preparation and although, in the majority of cases nanomedicines (DDS) applied in cancer treatment managed to reduce toxicity, they have failed to improve efficacy (response rates / survival times) which decreases their commercial attractiveness [104].

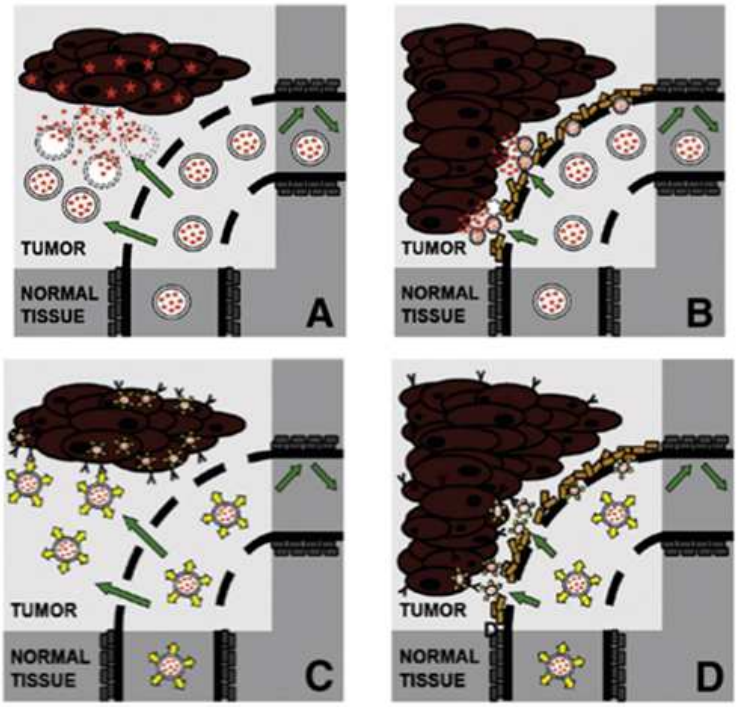

Figure 25. Comparison between a conceptual and realistic DDS targeting strategies: passive drug targeting (conceptual (A) *vs* realistic (B)) and active targeting (conceptual (C) *vs* realistic (D)) [104].

3.1.2 **Polymeric DDS**

The use of synthetic polymeric DDS as carriers has been recognised and a good polymeric drug carrier should be decorated with chemical functional groups to enable, simultaneously: i) polymer-drug conjugates solubilisation; ii) attachment of the drug to the polymer matrix and iii) attachment of the carrier to the binding site [108].

The structural features and properties of CDs make them suitable building blocks to be used in polymeric reactions. CDs can be grafted to many natural and synthetic polymers through a variety of methods [109] resulting in different polymer architectures (Figure 26) [110]. Additionally, CDs being generally recognised as safe substances (GRAS) do not pose as many concerns regarding toxicity, as other non-GRAS compounds and the possibility of combining them with other biocompatible materials has been recognised. Examples of polymers combined with CD include dextrans [111, 112], hyper-branched [113] as well as linear poly-ethylenimine (PEI) [114], poly-(ε-lysine) [115] or poly(vinylalcohol) (PVA) [116]. Some CD-based polymers are suitable for gel formation [117], DNA transfection [118] and can act as carriers of various drugs.

In polymeric materials, a CD can modulate the release profile of drugs [119] and it has been proposed that this action was due to the combined action of several CD units acting cooperatively to solubilise and stabilize drugs in a polymeric matrix [109]. Examples include: i) the increase in the complexation efficiency and drug bioavailability by addition of water-soluble polymers to simple CD solution of the drug [120]; ii) increased of the dissolution rate of poorly soluble drugs like indomethacin [121] and iii) improved mechanical properties of tablets [122].

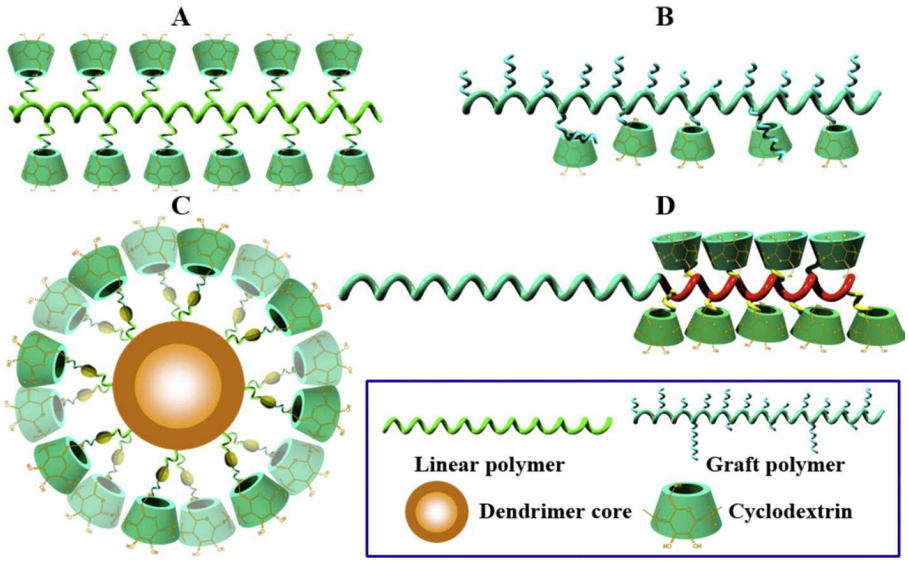

Figure 26. Examples of CD-pendent polymers: A) CD-grafted linear polymer; B) CD-pendant graft copolymer; C) CD-conjugated dendrimer and D) CD-flanking block copolymer [110].

Interestingly, CD-polymers can also have an opposite effect as CDs can hold the drug more tightly in the polymer matrix, thus delaying its release or even blocking the active molecule inside the polymer [123]. This has been attributed to a reduction of diffusivity of the guest in the polymer matrix, especially after complexation of the guest because there is: i) an increase in the molecular weight of the complex (CDPs/drug); ii) possible formation of poorly soluble complexes, in which the host (drug) is covalently bonded to the polymer backbone; and also iii) a reduction of the pore size in the polymer matrix when CD acts as a crosslinking agent.

Moya-Ortega *et. al.* [124] proposed that the preparation of polymeric CDs can be achieved, using three different strategies: i) the key-lock assembly, where two constituents are mixed together and are allowed to spontaneous assemble in aqueous solutions, one having CD units and the other possessing suitable guest molecules to enable complexation equilibrium; ii) the covalent cross-linking of CDs through the use of proper monomeric units like epoxides and isocyanates; and, iii) through polymerization of CDs monomers, previously modified with reactive acrylic or vinyl moieties.

3.1.3 CD and small interfering RNA (siRNA) delivery

RNA silencing is a control mechanism for gene expression that enables the detection and avoids transcription of non-endogenous cell RNA. Small interfering RNA (siRNA) is involved in RNA silencing and it mediates the suppression of genes corresponding to double stranded RNA, through targeted RNA degradation [125]. The research and development of strategies to deliver siRNA into cells have been widely explored, mainly due to the high specificity in the inhibition of the target of interest [126].

The first targeted delivery of siRNA in humans with cancer was a CD polymer construct called CALAA-01®. This molecular assembly (Figure 27) was developed based on two different difunctional monomers: a βCD derivative (A) and a difunctional charged spacer (B), arranged in a linear fashion where the βCD is part of the polymer backbone. Another interesting feature is the appendage of an adamantylamine (AD) moiety, modified with a steric stabilization agent (poly-ethylene glycol (PEG) moiety) and a specific transferrin receptor (Tf) (Figure 27) [127]. This system was used to deliver a siRNA against the ribonucleotide redutase subunit 2 (RRM2) gene products, which is an established cancer target.

CALAA-01 tolerability, safety profile and maximum tolerated dose (MTD) proved to be successful in the treatment of patients with relapsed or refractory cancer, when intravenous administrated [128]. Additionally, polycationic amphiphilic cyclodextrins (paCDs) were used as gene-delivery systems, combining properties of both lipids and cationic polymers in a nonviral gene vector [118].

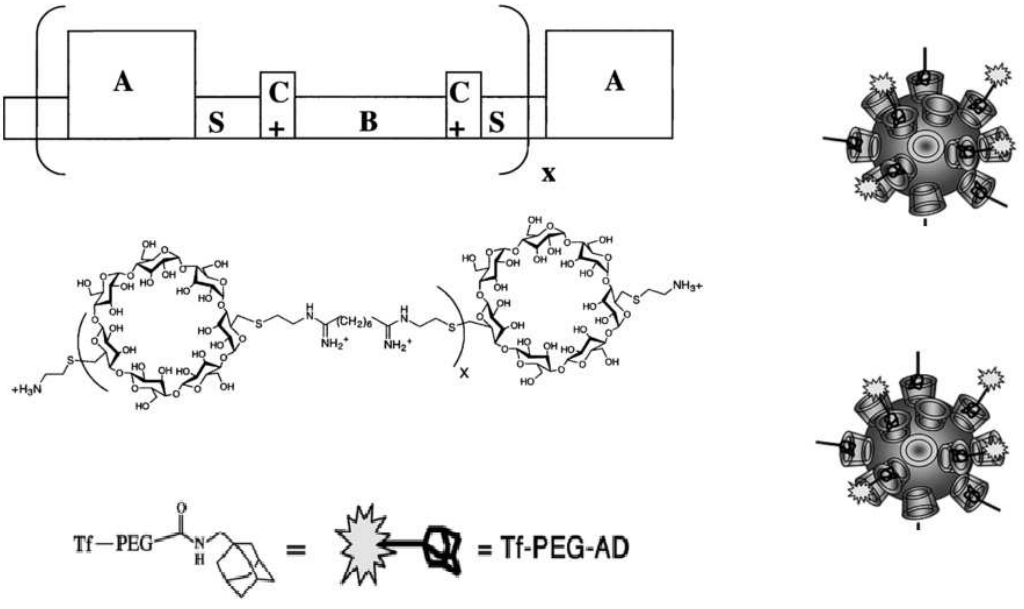

Figure 27. CALAA-01® a βCD polymer DDS construct able to deliver siDNA into humans [127].

3.1.4 **Camptothecin (CPT) – CD-based polymer**

Camptothecin (CPT) is a molecule initially isolated from the tree *Camptotheca acuminate* that revealed anticancer activity in animal models. CPT can display two different pH dependent forms: i) an active and poorly water-soluble lactone and ii) an inactive, carboxylate form favoured at physiological pH. Therefore, once administered CPT is rapidly converted into its carboxylate form though a lactone-ring opening and losses its potential antitumor function [129]. Two chemically modified CPT based drugs (topotecan and irinotecan) are currently approved for use in humans.

A CPT conjugated to a linear polymer CD-based polymer (CRLX101) revealed good safety profile and has been approved for intravenous administration in humans, for the treatment of advanced solid tumours [130]. CRLX101 consists of a β-CD, difunctionalized with the natural amino acid cysteine (CDDCys) and polyethylene glycol (PEG). Small drug molecules such as CPT can be attached to each polymer unit via a linker (Figure 28).

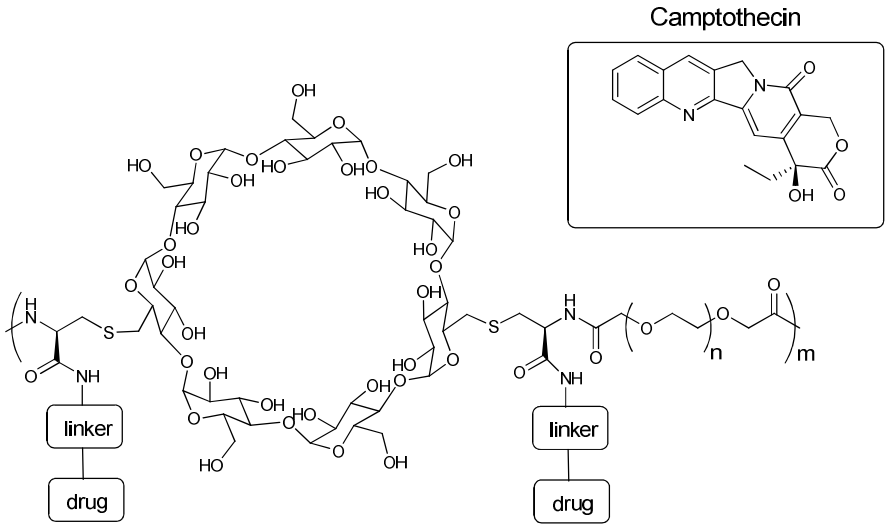

Figure 28. Structure of CRLX101 polymer and camptothecin (CPT).

3.1.5 **CD-Porphyrin DDS**

Light can trigger photochemical reactions and in the case of photoactivated compounds, three of the most important criteria to judge a good a carrier system comprising a PS are: i) its biocompatibility; ii) the ability to cross biological membranes to reach the active site and iii) the ability to preserve the PDT properties of the PS [131].

One possibility to increase PS selectivity to cancer tissues is through attachment of site-specific tags directly to the PS. Some examples include:

i) Attachment of porphyrins derivatives to peptides conjugates that revealed good DNA binding properties [132]

ii) Modification of porphyrin derivatives with cationic groups, showed good mitochondria-targeting capabilities and minor dark toxicity [133]

iii) Modification of porphyrin with specific groups over-expressed in cancer cells like: folate or arginyl glycyl aspartic peptide (RGD) revealing good targeting properties and cellular uptake by cancer cells [134]

The focus on bimodal systems based on CD-porphyrins conjugates, that is, systems that are able to display simultaneously the properties of porphyrins (photophysical, localization) and CDs (water solubility; inclusion/complexation ability) is a recent area of research with a promising future.

3.2 Aims of the dissertation

The goals of this thesis can be divided into two main parts.

The first part involves:

- The efficient preparation, purification and characterization of a new bimodal system (CD-*m*THPP), consisting of a βCD covalently bound a porphyrin (5,10,15,20-tetrakis(*m*-hydroxyphenyl)-21,23*H*-porphyrin, *m*THPP), which is a chemical analogue of an already approved commercial PS (Foscan®). CD-*m*THPP is expected to possess improved aqueous solubility and preserve all photophysical *m*THPP properties, with the advantage of having an extra CD cavity to complex suitable guest molecules, to enable biological studies on CD-*m*THPP system.
- The drastic improvement of solubility of CD-*m*THPP in aqueous solutions and the complete recovery of UV-Vis and fluorescence properties to achieve concentrations that could enable complete characterization of CD-*m*THPP its use in parenteral formulations.
- The chemical modification of selected anticancer drugs to be tested as guest molecules, using the above mentioned bimodal carrier in aqueous environment.

The second part involves:

- the preparation of positively-charged CDs, namely *per*(6-aminoethylamino-6-deoxy)-βCD (βpen) and its incorporation in polymeric materials to be tested for the inclusion of specific anionic guest molecules and to study them as release modifiers of nucleotides or nucleotide drugs, through semi-permeable dialysis membranes.

RESULTS AND DISCUSSION

4. A CD-porphyrin conjugate (CD-*m*THPP) as a water soluble bimodal DDS

4.1 Introduction

The development of a pure and well-characterized CD-pophyrin conjugate that desirably, would combine the distinct properties of both porphyrin and CD macrocycles in a single nanosized molecular system has been a matter of relevant research, concerning primarily water-soluble photoactive systems and, to a much lesser extent, water-soluble bimodal drug delivery systems. These CD-pophyrin conjugates could display: i) the imaging, photoactive and electroactive properties attributed to the porphyrin moiety ii) the capacity to generate efficiently $^1O_2$ from $^3O_2$ by the action of light iii) improved aqueous solubility and ability to carry, solubilise and stabilize desired drug molecules ascribed to CDs [135].

Great effort has been devoted to the characterization of CD-porphyrin conjugate photophysical properties given its extensive application as model systems in binding studies, catalytic, photocatalytic and photo-induced processes [136]. For example, a conjugate between βCD unit and 5,10,15,20-tetrakis(pentafluorophenyl)-porphyrin was prepared and its characterization revealed that their photophysical properties were not affected by connection of the porphyrin to the CD macrocycle. Additionally, a 5,10,15,20-tetrakis(*p*-hydroxyphenyl)-porphyrin (*p*THPP) was connected to a βCD unit and, when studied in aqueous solvents, revealed self-aggregation that was attributed to porphyrin-to-porphyrin interactions with participation of the CD cavity. The addition of a guest solution of 1-adamantol to this solution, promoted the spatial rearrangement of the aggregates but the photophysical properties of the conjugate were preserved [135].

The covalent attachment of a 5,10,15,20-tetrakis(pentafluorphenyl)-porphyrin to βCD and γCD has been described and the CD-porphyrin conjugates isolated (monomers, dimers, trimers and tetramers) have been studied as potential DDS, taking advantage of CD ability to include in its cavity relevant cytotoxic drugs, suitable for cancer treatment [137].

One the other hand, considering the preparation of porphyrin-cyclodextrin conjugates, the efficiency of the reaction and the purity of the product can be really challenging. Thus, one of the first examples of a CD-porphyrin conjugates described in the literature was prepared from the reaction of a βCD-iodide with 5,10,15,20-tetrakis[4-(methylsulfoxyl)phenyl]-porphyrin, in 25 % yield. The same authors also reported the preparation of a CD-porphyrin dimer (30 % yield), from the reaction of 5,15-bis(methylsulfoxyphenyl)-10,20-diphenylporphyrin with the same βCD derivative, carried out in DMF, at 60 ºC, during 24 h [138]. More recently, a CD-porphyrin monomer was obtained in 30 % yield, prepared from reaction of 6-*O*-monotosyl-

βCD (βmTs) with 5,10,15,20-tetrakis(*p*-hydroxyphenyl)-21,23*H*-porphyrin (*p*THPP) in a reaction conducted at 140 ºC, for 24 h, in DMF [135]. The conjugation of a 5,10,15,20-tetrakis(pentafluorophenyl)-chlorin bearing a *N*-benzylisoazolidine ring (FC) with four β-cyclodextrin unit, resulted in a water soluble tetramer prepared in DMF at room temperature and obtained in 24 % yield [139]. In most of the examples described above, there is poor literature evidence of chemical purity (*e.g.* in the form of elemental analysis, TLC (R_F), mass spectrometry data).

Thus, most CD-porphyrin conjugates show important limitations such as the small yields obtained, the time-consuming purification methods and incomplete characterization. CD-porphyrin conjugates, also lack of sufficient water solubility that often results in extensive aggregation and in the loss of their photophysical properties in aqueous medium. Additionally, there is also a strong desire in developing potential useful drug candidates, based on already marketed or approved molecules with a well-characterized safety profile [140].

In the light of the current the limitations of commercially available PSs and taking into account the approved status of CDs, the purpose of this chapter is to describe the efficient preparation, complete purification and characterization of a water-soluble CD-porphyrin conjugate. This bimodal conjugate will be composed by: i) one porphyrin unit (5,10,15,20-tetrakis(*m*-hydroxyphenyl)-21,23*H*-porphyrin, *m*THPP), used because it is the porphyrin precursor to an already marketed chlorin (*m*THPC), *i.e.* having one pyrrole double bond reduced, the drug Temoporfin, commercial available as Foscan®. According to European Medicine Agency, 2005 "Foscan® is indicated for the palliative treatment of patients with head and neck squamous cell carcinoma failing prior therapies and unsuitable for radiotherapy, surgery or systemic chemotherapy" [94].

4.2 Results and discussion

4.2.1 **Preparation / purification of CD-*m*THPP**

Previous literature precedents exist describing the covalent connection of porphyrins to cyclodextrins in order to obtained supramolecular systems with catalytic potential or redox properties; or, to study the photophysical properties of the resulting CD-porphyrin conjugates. In our group, the preparation of CD–porphyrin conjugates was explored through: i) the connectivity of one βCD unit to a protoporphyrin IX (PpIX) moiety [141] and ii) by the attachment of a mono-substituted βCD derivative and *m*THPP in alkaline conditions [142]. The original purification strategy for the purification of the latter comjugate (CD-*m*THPP) was

based on a methodology involving: i) dialysis of the crude mixture; ii) extensive washings with methanol; followed by iii) size exclusion chromatography on Sephadex G-25. This lead to the desired conjugate (CD-*m*THPP) isolated with an excess (30 % *m/m*) of mono-3,6-anhydro-βCD as an impurity, revealed by MALDI-TOF mass spectrometry. The isolated product (CD-*m*THPP) revealed good water solubility and enabled cell inclusion studies with encouraging results, but failed to show reproducible phototoxicity results, owing to the lack of reproducibility in the preparation / purification of CD-*m*THPP. Thus, there was an urgent need for the development of a more efficient purification strategy to improve the purity of CD-*m*THPP, its yield and to scale-up the reaction with reproducible results.

CD-*m*THPP was prepared from the reaction of 6-*O*-monotosyl-βCD (βmTs), with a commercially available porphyrin namely, 5,10,15,20-tetrakis(*m*-hydroxyphenyl)-21,23*H*-porphyrin (*m*THPP). The reaction was performed under anhydrous conditions, in dry dimethylsulfoxide (DMSO), at 40 ºC under constant magnetic stirring for a total of 72 h (Figure 29).

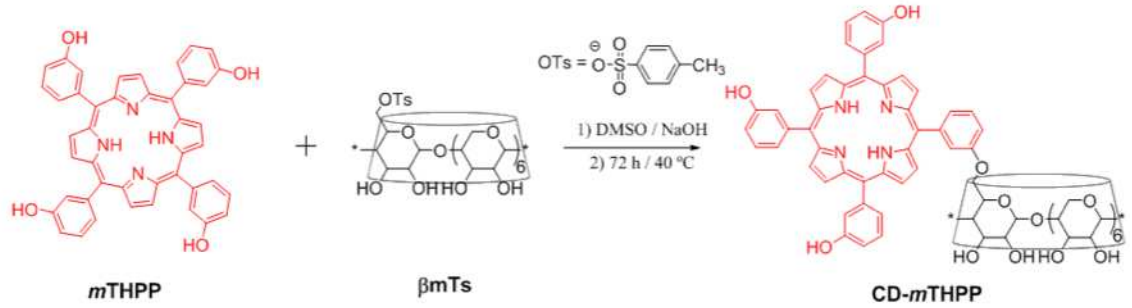

Figure 29. Preparation of the conjugate (CD-*m*THPP) from reaction of βmTs with *m*THPP in DMSO.

Initially, *m*THPP was dissolved in alkaline DMSO, to generate the appropriate allyloxide species (Ph-O^-), expected to displace the good leaving tosyl group (-OTs) present in βmTs to generate of the desired CD-*m*THPP conjugate, comprised by one *m*THPP and one βCD connected through a non-hydrolysable ether bond. TLC (silica gel 60, *i*PrOH / EtOAc / H_2O / NH_3 (5:3:3:1, *v/v*)) was used to monitor the reaction progress. CD-*m*THPP was eluted as a red/brown spot (R_F = 0.61), revealed red fluorescence when irradiated at UV light (λ = 254 nm) and turned green upon revealing/burning with a 4 % H_2SO_4 ethanolic solution. The pure CD-*m*THPP molecule was isolated from the reaction crude in four steps:

1. The crude product mixture was solubilised in water and dialysed through a benzoylated dialysis tubing (MW_{CO} = 2000 Da), at neutral (pH ≈ 7) against water to remove dimethylsulfoxide (DMSO), traces of NaOH, tosic acid and water soluble βCD related by-products

2. Liquid-liquid extraction was performed on the dialysed mixture, using ethyl acetate / water to wash away and recover from the dialysed crude, unreacted *m*THPP and some of its salts
3. Column chromatography (silica gel 60, *i*PrOH / EtOAc / H_2O / NH_3 (5:3:3:1, *v/v*)) was employed to isolate the desired product (CD-*m*THPP) from unreacted porphyrin (*m*THPP) and other reaction by-products, not removed in the previous steps
4. A second dialysis at acidic pH ≈ 5 was required, to remove from the reaction mixture any excess of ammonia used in the mobile phase, in its ammonium chloride salt form
5. Freeze-drying was performed to remove the excess of water and obtain a black powder (CD-mTHPP)

Under optimised conditions, pure CD-*m*THPP was achieved in 40 % yield, calculated with respect to the amount of reacted porphyrin (*m*THPP). Additionally, following the purification strategy developed, nearly one-third (30 %) of the whole amount of porphyrin (*m*THPP) was efficiently recovered and can be reused.

The strongly alkaline conditions used to promote the formation of *m*THPP alkoxide species, also favour undesired reactions that help to explain the moderate obtained yield. These are: i) the hydrolysis of the sulfonic ester in βmTs, with the consequent formation of βCD and ii) the formation of mono-3,6-anhydro-βCD (Figure 8) via the deprotonation of the βCD–OH_3 and nucleophilic attach to C_6, leading to glucopyranose ring inversion and displacement of the tosyl (OTs) moiety. Moreover, the tetravalency of *m*THPP, could possible result in *cis*-dimer (CD-*m*THPP (2:1), *trans*-dimer (CD-*m*THPP (2:1), the trimer (CD-*m*THPP (3:1) and the tetramer (CD-*m*THPP (4:1). In addition, the formation of many βCD^{-}-Na^{+} salts, complicated the purification of the product mixture. Although, the final strategy was successful and reproducible, it was preceded by numerous trials and methods. A short account of which is mentioned in the chapter below.

Initially, size exclusion chromatography (Sephadex G 25) was used directly after reaction, to purify small portions of crude solubilised in water. The sample was applied twice, on the same column (L x OD = 40 cm x 1.9 cm), varying the amount loaded by a factor of 20 and, but no band separation was observed (Figure 30 A/B). The inefficiency of separation was corroborated by TLC (silica gel 60, *i*PrOH : EtOAc : H_2O : NH_3 (5:3:3:1, *v/v*)): three spots were observed (black arrows), that glowed red under UV light (λ = 254 nm) and turned green after

being revealed with 4 % H_2SO_4 ethanolic solution (Figure 30 C). This observation indicated that the crude had more than one labelled product containing porphyrin, probably corresponding to the desired coupling products. To verify this assumption, a sample of the crude was analysed by mass spectrometry and the MALDI-TOF MS spectrum was recorded (Figure 30).

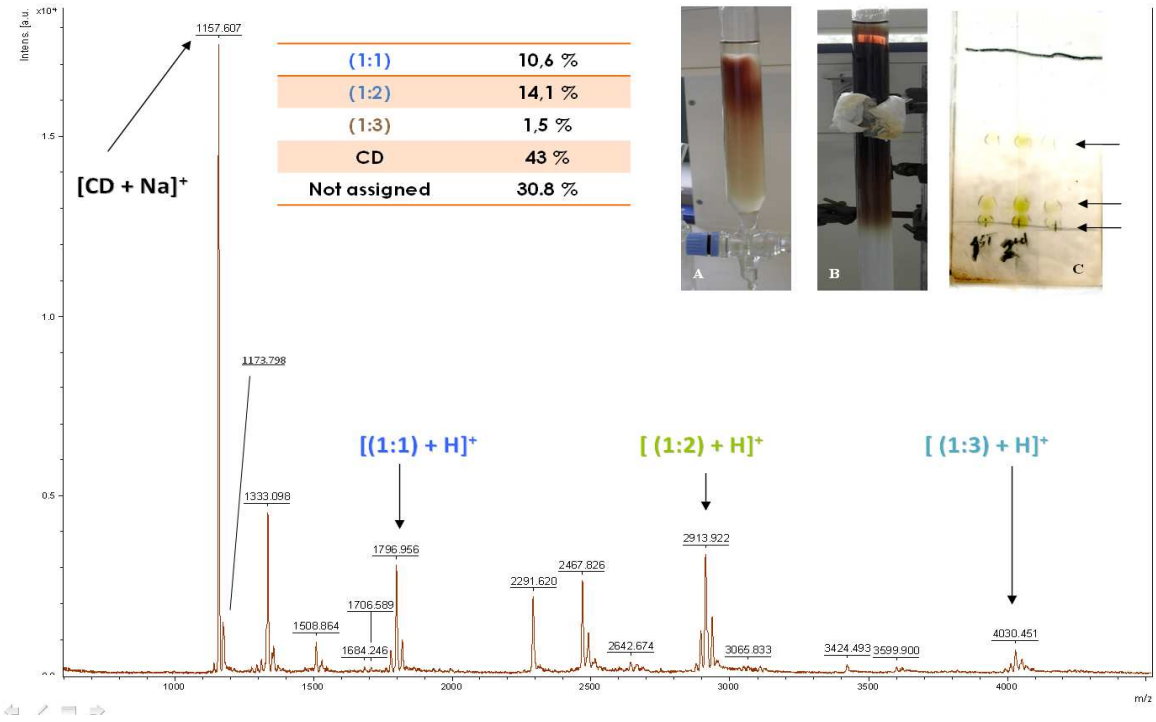

Figure 30. MS (MALDI-TOF) spectrum of crude, after size exclusion chromatography (Sephadex G 25). Insets: two column chromatography separations varying the amount applied: A) 1 mg crude in 2 mL of H_2O and B) 20 mg of crude in 5 mL H_2O; C) TLC monitoring of the fractions collected.

The MS spectrum revealed the presence of the expected coupling product (CD-*m*THPP), in a small amount (≈ 10 % *m/m*) and along with other coupling products, namely: CD-*m*THPP (2:1) ≈ 14 % (*m/m*) and CD-*m*THPP (3:1) ≈ 2 % (*m/m*). Additionally, a large excess of CD salts ≈ 43 % (*m/m*) and unassigned CD-related by-products were detected accounting for the remaining mass sample ≈ 30 % (*m/m*). The high amount of unrelated CD by-products can be explained by the excess βmTs used in the original procedure (4 molar eq. βmTs / 1 molar eq. *m*THPP), that under strong alkaline conditions can be lead to the undesired reactions, like discussed previously. Therefore, this experience proved that size exclusion chromatography was inadequately used as purification technique and the ratio of reactants used (βmTs / *m*THPP) could be reduced. Evidently, whatever their compositions are, the products in aqueous solution interacted with each other, forming supramolecular complexes of various compositions that are eluted indiscriminately by Sephadex. This outcome places doubts on the validity of the

previously published purification procedures [138] by size exclusion chromatography alone. Apparently, the prerequisite for a successful separation was the interactions of the solutes with the column packing material, indicating the use of silica gel was necessary.

Therefore, a second trial was carried out and the crude isolated was washed exhaustingly with MeOH, as alternative putification strategy that resulted in the isolation of a black insoluble solid. An aliquot of this solid sample was analysed by MALDI-TOF MS and the MS spectrum (Figure 31) revealed a relatively pure mixture, comprised of: two coupling products CD-*m*THPP (46 % *m/m*) and CD-*m*THPP (2:1) (46 % *m/m*) in an equal ratio and contaminated with traces of CD-*m*THPP (3:1) (5 % *m/m*) and *mono*-3,6-anhydro-βCD (3 % *m/m*). This trial revealed that other coupling products (CD-*m*THPP (2:1) and CD-*m*THPP (3:1)) could be selectively isolated, based on liquid-to-liquid extraction if the current purification method is further developed. Additionally, the continuous TLC monitoring during all of these trials was crucial, not only to assess the reaction progress but also to judge the efficiency of the purification trials.

Recalling the related work [135], where a similar conjugate (CD-*p*THPP) prepared from the reaction of βmTs with 5,10,15,20-tetrakis(*p*-hydroxyphenyl)-21,23*H*-porphyrin (*p*THPP). The conjugate CD-*p*THPP was painstakingly purified using RP-HPLC, with octadecylsilane (C_{18}) modified silica, as a stationary phase, and a linear gradient mobile phase starting from ammonium acetate ($AcNH_4$, pH = 5) and ending in acetonitrile (ACN). It was also reported the use of TLC (silica (RP-8), *i*PrOH : EtOAc : H_2O : NH_3 (5:1:3:2, *v/v*)). This data suggested that our coupling products should be eluted from a silica stationary phase, using a mixture of solvents with different affinities *i.e.* comprised of both aqueous and organic components.

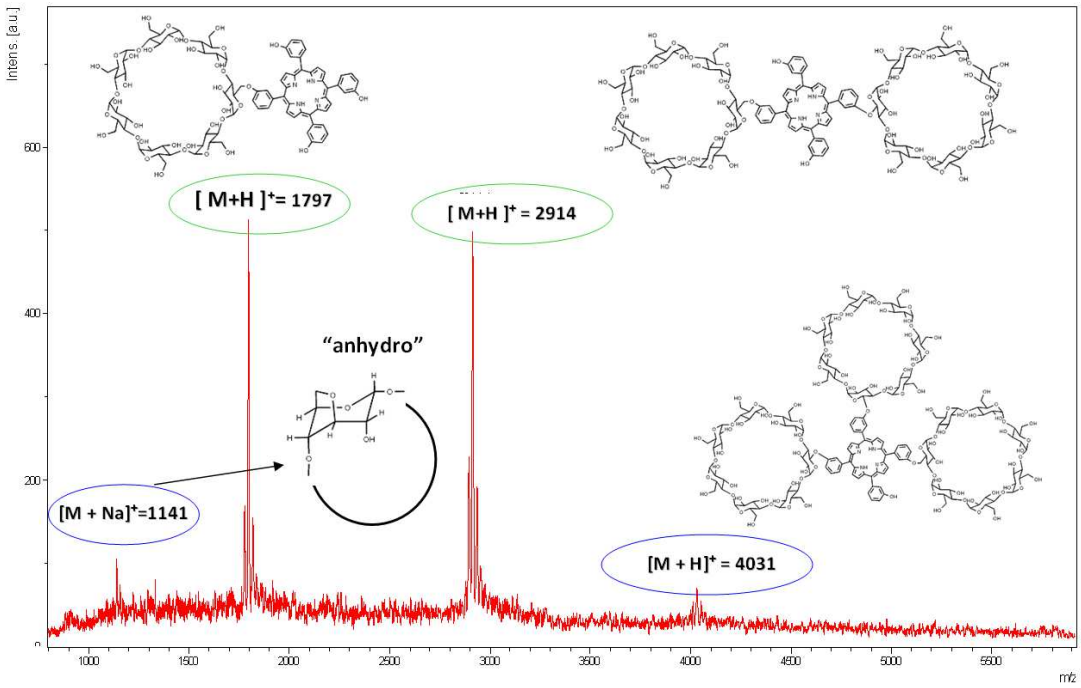

Figure 31. MS (MALDI-TOF) spectrum of a trial, where the crude was isolated after extensive MeOH washings.

Therefore, a series of TLC trials were conducted to improve the separation of several crude samples, using silica gel 60 as stationary phase and *i*PrOH :EtOAc : H_2O : NH_3 (5:3:3:1, *v/v*) as mobile phase. Figure 32 A shows the TLC of the crude diluted 1/10 in MeOH against βCD, *m*THPP and βmTs solutions used as controls. It shows that: i) *m*THPP is eluted as a red / brown spot that is not retained (R_F = 1.0), shows red fluorescence under UV light (λ_{exc} = 254 nm) and turns green when revealed with acidic solution (4 % H_2SO_4/EtOH); ii) the coupling products behave like mTHPP but, due to the attachment of CD units, it turns black after burning with 4 % H_2SO_4/EtOH; iii) finally, βCD, βmTs and any βCD related by-product are not UV active and will be revealed as black spots, upon burning with acidic solution. These observations agree with previous TLC data (Figure 30 C) and were corroborated by MALDI-TOF MS (Figure 30).

A sample of the same crude mixture previously treated by size exclusion chromatography, was applied and treated by preparative TLC chromatography (silica gel 60, *i*PrOH : EtOAc : H_2O : NH_3, (5:3:3:1, *v/v*)). Two TLC plates were loaded with 5 mg crude / 0.5 mL water (Figure 32 B) and with 20 mg crude / 0.5 mL (Figure 32 C) and after elution it was observed that only a limited amount of crude could be loaded onto a single plate, without compromising the degree of separation that corresponded to < 5 mg crude / 0.5 mL water.

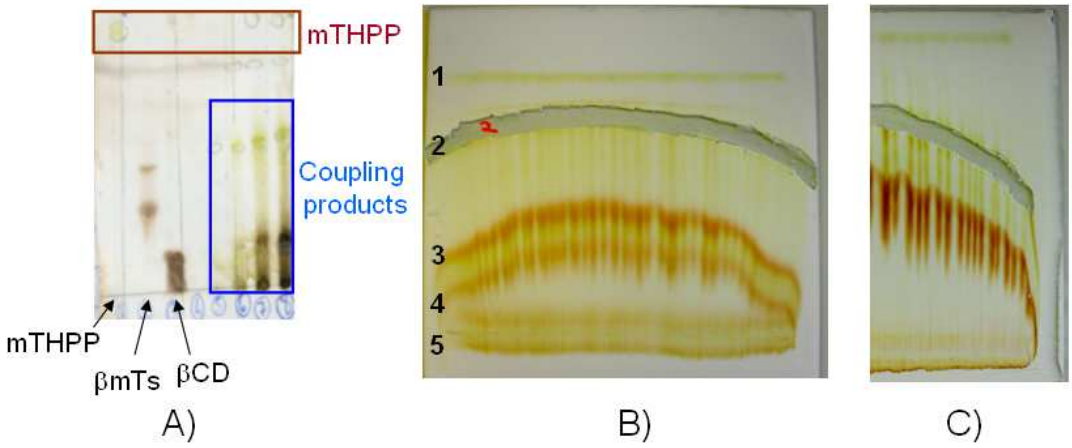

Figure 32. Degree of separation achieved in purification of crudes containing CD-*m*THPP: A) TLC of aggregated CD-*m*THPP in aqueous solution (D_2O, NMR tube) and preparative plates illustrating two separations where the amount of crude applied was varied: B) 5 mg crude / 0.5 mL H_2O and C) 20 mg crude / 0.5 mL H_2O. Silica gel 60, *i*PrOH : EtOAc : H_2O : NH_3, 5:3:3:1 (*v/v*).

Therefore, five plates were loaded each with 5 mg crude solubilised in water (0.5 mL). The TLC plate was developed, the five different bands isolated (1 to 5 – Figure 32 B) and subjected to MALDI-TOF MS analysis: i) band 1 spectrum revealed the presence of unreacted *m*THPP and *m*THPP salts; ii) band 2 corresponded to the desired conjugate product CD-*m*THPP and iii) bands 3, 4 and band 5 proved to be a mixture of CD-based by-products, other coupling products and unassigned impurities. The biggest drawback related with the usage of preparative TLC to purify CD-*m*THPP is that the conjugate was strongly bonded to the fine silica gel particles and could not be efficiently recovered.

This experiment revealed that a good degree of separation could be achieved once the proper ratio of silica/crude was found, which motivated further trials on the purification of these crudes using column chromatography. Different batch samples were applied to different column dimensions (L, cm) x (OD, cm) and the ratio between the amount of sample to be treated (crude, mg) and silica used to pack the column, was varied as described by Table 3. A proper purification was achieved through the use a relatively long column ((L, cm) x (OD, cm) = 62 cm x 2.2 cm), packed with 80 g of silica gel 60, loaded with 20 mg of crude solubilised in water / mobile phase (1:1) (# 4 Table 3).

Table 3. Dimensions of the columns used to treat the crude of the coupling reaction.

#	Dimensions (L, cm) x (OD, cm)	Silica (g)	Crude (mg)	ratio (silica, g / crude, mg)	Notes
1	32 x 2.2	40	53	0.8	Failure
2	62 x 2.2	67	31	2.1	Failure
3	53 x 4.4	167	113	1.5	Failure
4	62 x 2.4	80	20	4.0	Success

In some circumstances, different bands were noticed during CD-*m*THPP elution from the column, which can be understood in the light of: i) aggregation characteristic of porphyrin-related compounds in aqueous solvents; ii) the ability of porphyrin to coordinate with different positive ions (Na^+, NH_4^+) and iii) the promotion of acid-base equilibra between differently protonated species, motivated by the use of ammonia (NH_3) in the mobile phase.

Figure 33 A shows a TLC (silica gel 60, *i*PrOH : EtOAc : H_2O : NH_3 (5:3:3:1, *v/v*)) of a sample of CD-*m*THPP collected from an NMR (D_2O) into which it aggregated. The supernatant (Liquid, Figure 33 A), the solid that remained aggregated inside the NMR tube, solubilised in MeOH and iii) the conjugate CD-*m*THPP and iv) *m*THPP, both solubilised in MeOH were spotted: i) the aggregated form of CD-*m*THPP ("solid") revealed two strongly coloured spots with different R_F, as opposed to a single spot revealed by the supernatant (liquid) which proves how aggregation can affect the separation efficiency. Further, evidence supporting aggregation and the presence of multiple species in equilibrium was revealed by the application of a pure sample of CD-*m*THPP to the top of the column: Figure 33 B shows that during elution two different bands were collected from the column corresponding to the exact same compound as corroborated by MALDI-TOF MS spectra of each fraction.

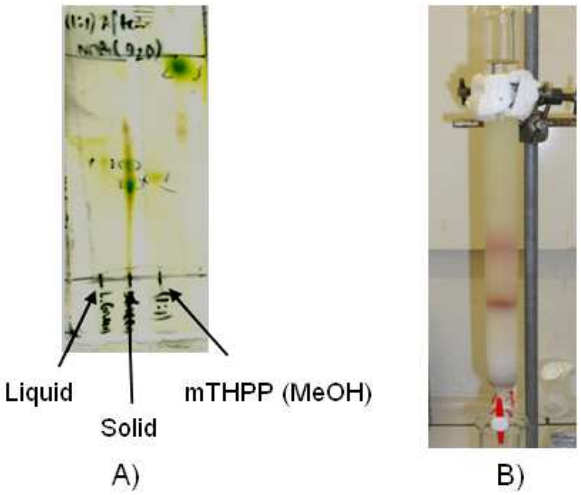

Figure 33. Evidence of aggregation during separation of CD-*m*THPP using A) TLC and B) column chromatography. Silica gel 60, *i*PrOH : EtOAc : H_2O : NH_3, 5:3:3:1 (*v/v*).

Aggregation and the presence of ammonia can modify the retention of CD-*m*THPP in the column. However, once collected these fractions were dialysed at slightly acidic pH (4 < pH < 5), which converts any excess of free ammonia into its water-soluble ammonium hydrochloride salt (NH_4Cl) that can then be cleared out from the isolated CD-*m*THPP.

Additional efforts were conducted to extract and purify other coupling products namely CD-*m*THPP (2:1) and CD-mTHPP (3:1) that have been identified by MS in prior experiments. Due to the high content of βCD units attached to the mTHPP core in CD-*m*THPP (2:1) and CD-*m*THPP (3:1), probably, these conjugates would present an improved water solubility and complexation ability when compared with CD-*m*THPP on its own. These separation experiments were supported by the following observations: after CD-*m*THPP was successfully isolated from the column, the presence of slightly coloured (green / brown) residue that remained at the top of the column was observed suggesting the presence of other porphyrin containing products, probably with high CD content.

Therefore, by applying the same purification strategy after the isolation of CD-*m*THPP by column chromatography (silica gel 60, *i*PrOH : EtOAc : H_2O : NH_3 (5:3:3:1, *v/v*), the mobile phase was changed and the column was flushed with to pure absolute ethanol (EtOH), followed by water (H_2O). Two fractions were selectively collected and revealed: i) red fluorescence under UV-Vis light (λ_{exc} = 254 nm) and ii) good water solubility. The MALDI-TOF MS (Figure 34) of the fraction collected with EtOH revealed the presence of a dimer, CD-*m*THPP (2:1) (m/z = 2916.6), with trace amounts of CD-*m*THPP (m/z = 1139.6). The small differences observed between the experimental values and those expected for CD-*m*THPP (m/z = 1135) and for CD-*m*THPP (2:1) (m/z = 2912) are explained by a small offset of the mass spectrometer, corresponding to m/z = 4.

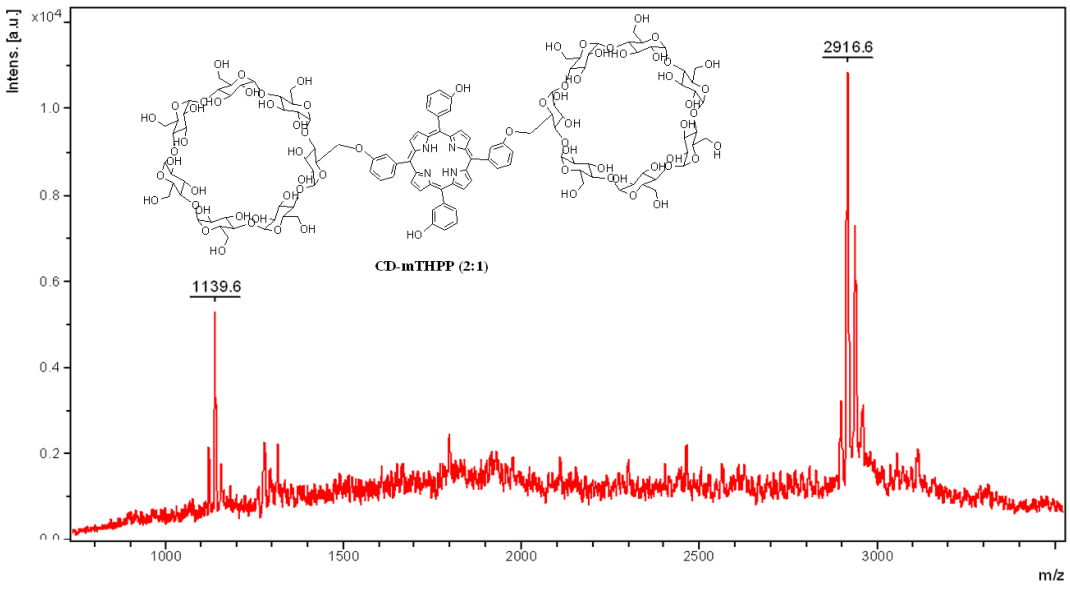

Figure 34. MS (MALDI-TOF) spectrum of a conjugate of higher stoichiometry (CD-*m*THPP (2:1)) isolated by column chromatography: silica gel 60, first washed with *i*PrOH : EtOAc : H_2O : NH_3, 5:3:3:1 (*v/v*) followed by absolute EtOH.

Therefore, the strategy employed lead to the isolation of very small amount of other coupling products (CD-*m*THPP (2:1)) present in most crudes. Due to the very small amounts of CD-*m*THPP (2:1) collected, the isolation of this extra product was not further explored. However, in a larger scale reaction, the isolation of this extra coupling product could result in an interesting future perspective.

4.2.2 Molecular characterization of CD-*m*THPP

Following the successful preparation and purification of CD-*m*THPP, several methods were used to characterize CD-*m*THPP namely: nuclear magnetic resonance (NMR) spectroscopy, elemental analysis, UV-Vis and emission fluorescence spectroscopy, TLC and by mass spectrometry (MALDI-TOF).

NMR spectroscopy was used to determine the structural features of the CD-*m*THPP in pure DMSO-d_6. This solvent was used because it enables the conjugate solubilisation in mostly monomeric form. and the observation of fast exchange protons (hydroxyl –OH and pyrrole -NH) of both starting materials namely: βCD (Figure 35 B) and *m*THPP (Figure 35 A).

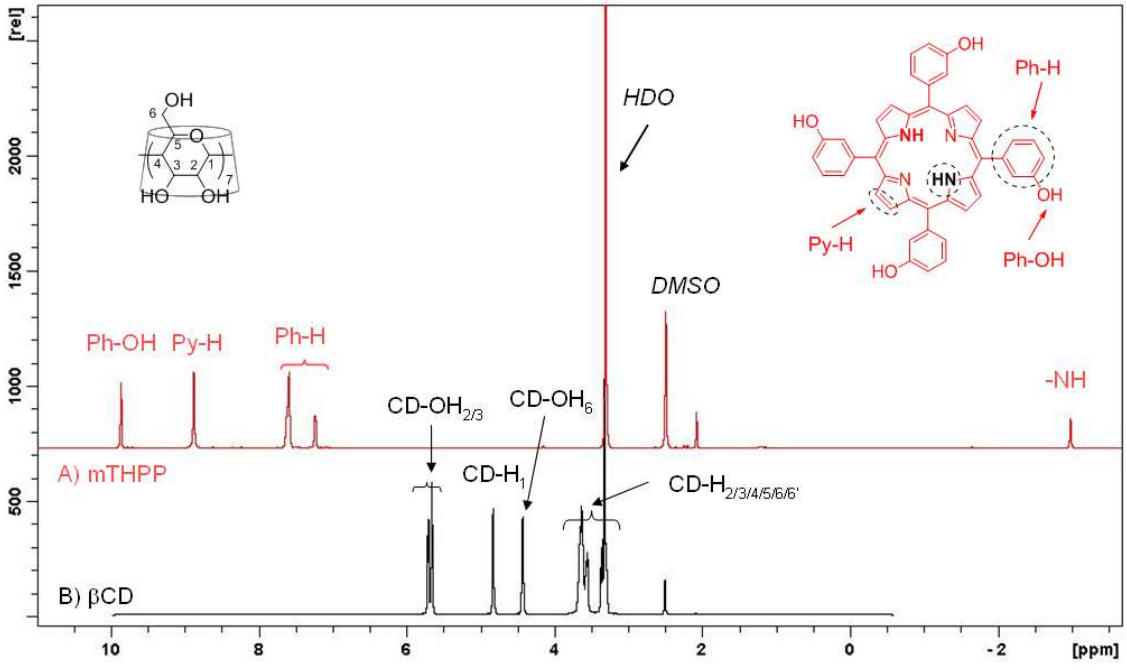

Figure 35. ^{1}H NMR spectra (DMSO-d_6, 500 MHz, 25 ° C) of A) *m*THPP and of B) βCD, illustrating the characteristic peaks of both macrocycles.

Figure 36 shows the ^{1}H NMR spectrum of CD-*m*THPP in DMSO-d_6 and it reveals that the isolated product presents structural features of both a βCD (Figure 36 A, black / blue colour) and *m*THPP (Figure 36 A, red colour) macrocycles, previously illustrated in Figure 35. The CD-*m*THPP exchangeable protons are observed: i) hydroxyl groups of βCD (CD-$OH_{2/3/6}$, 4.0 ppm – 6.0 ppm inset); ii) hydroxyls of *m*THPP (Ph-OH, ≈ 10.0 ppm) and also iii) the characteristic highly shielded pyrrole protons (-NH) of *m*THPP that resonates at ≈ - 3 ppm, due to the anisotropic effect of the aromatic macrocycle. All CD unit resonances are observed in the aliphatic region (3.0 ppm - 6.0 ppm): i) the characteristic anomeric proton connected to the carbon (C_1) (CD-H_1, ≈ 5 ppm) and all remaining proton signals (CD-H_2/H_3/H_4/H_5/H_6/$H_{6'}$, 3.0 ppm – 5.0 ppm). Finally, the signals from the *m*THPP macrocycle are observed in: i) the aromatic phenyl ring protons (Ph-H, 7.0 ppm - 8.0 ppm); ii) the pyrrole ring protons (Py-H_a/H_b, 8.0 ppm - 10.0 ppm).

The ^{1}H NMR of CD-*m*THPP (Figure 36 B) also supports the correct and desired connectivity, between one phenyl group of *m*THPP and one glucopyranose unit of βCD macrocycle like illustrated in Figure 36 A. Firstly, the signal of the anomeric proton (CD-$H_{1,}$ ≈ 5.0 ppm) is split into two unequal signals: a smaller blue coloured H_1 ≈ 4.9 ppm, Figure 36 C and a bigger black coloured $H_{1,}$ ≈ 4.8 ppm Figure 36 C). Secondly, the integration of the isolated signal at ≈ 4.05 ppm, corresponding to only one proton is assigned to a CD-H_5 signal (blue colour, Figure 36 C). These isolated signals corroborate the expected attachment of one phenyl ring of *m*THPP to one glucopyranose unit of the βCD macrocycle, like indicated by the blue coloured α-D-glucopyranose unit in Figure 36 A.

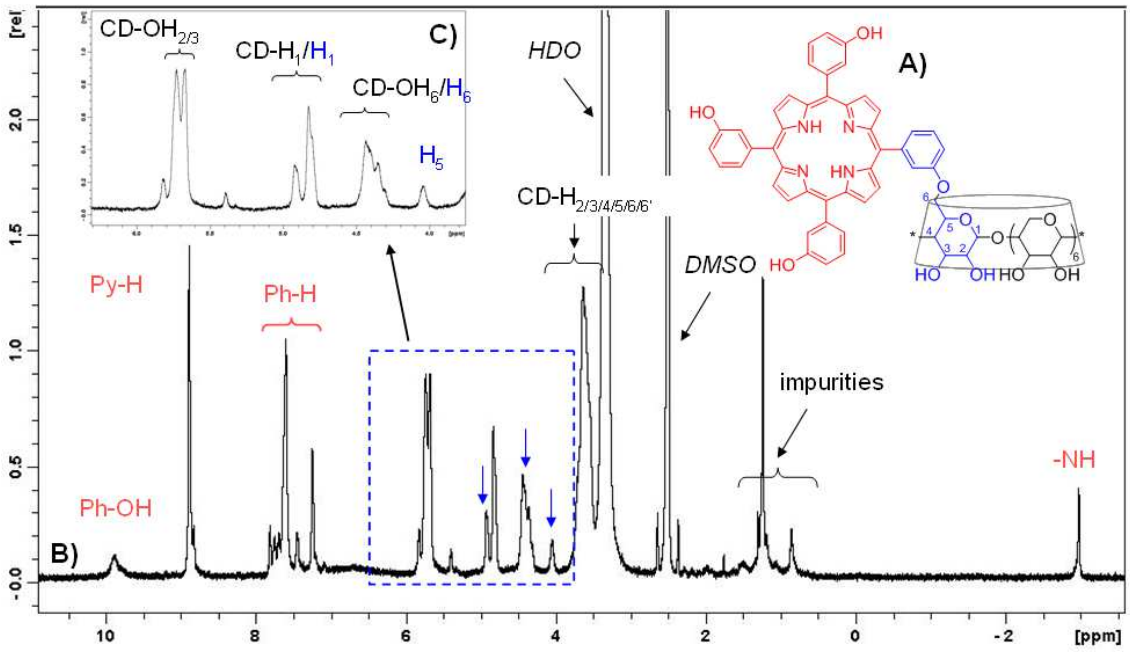

Figure 36. ^{1}H NMR spectrum (DMSO-d_6, 500 MHz, 25 ºC) of CD-*m*THPP: B) a full expansion, from -3.5 ppm to 11.0 ppm; C) an expansion in the aliphatic region, from 4.0 ppm to 6.0 ppm region.

2D HSQC NMR experiment (Figure 37 A) was used to assess the identity of CD-H_6, which is revealed as differently phased contours (red contour, ≈ 4.45 ppm, -CH_2) when compared to all other CD protons (black contours, -CHs). Therefore, having assigned CD-H_6,2D COSY NMR experiment (Figure 37 B) leads to CD-H_5 (≈ 4.05 ppm ,Figure 37 B). This corroborates the identity of CD-H_5 and of CD-H_6 of the glucopyranose unit, responsible for the ether bond between the *m*THPP and βCD forming the desired conjugate (CD-*m*THPP).

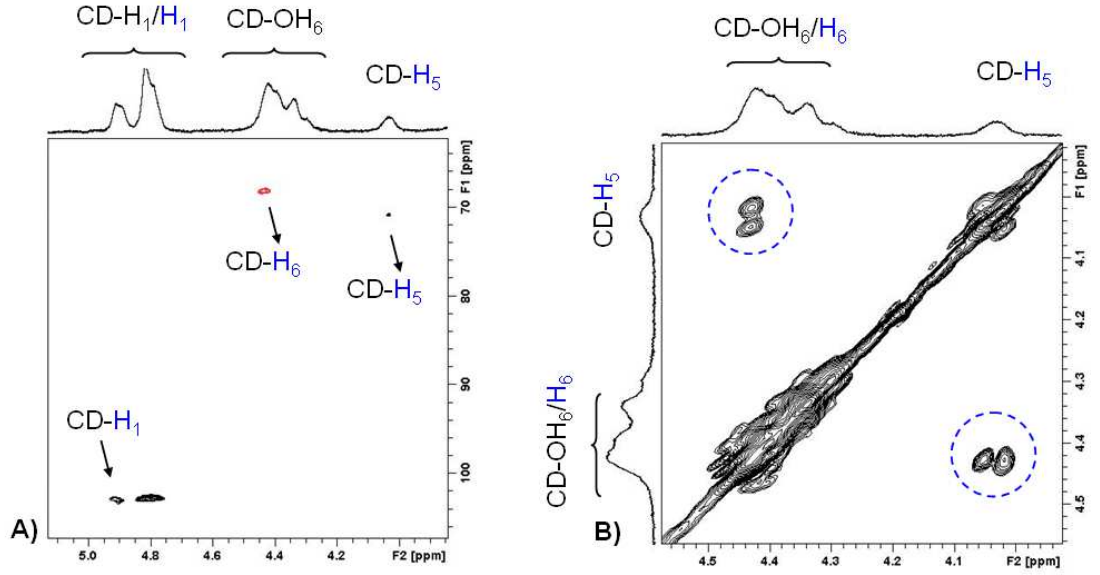

Figure 37. 2D NMR experiments (DMSO-d_6, 25ºC) of CD-*m*THPP: A) HSQC spectrum and B) COSY spectrum.

Although, the ^{1}H NMR of CD-*m*THPP is illustrative of the chemical modification achieved, more experimental evidence was required to fully characterize the identity and the purity of the CD-*m*THPP. MALDI-TOF mass spectrometry (positive mode, α-cyano-4-hydroxycinnamic acid matrix) was recorded (Figure 38) and shows a single major peak at m/z = 1796.8. This result is in excellent agreement with the expected value for the protonated molecular ion $[M+H]^+$ = 1795.7 of CD-*m*THPP, estimated for a molecular structure of $C_{86}H_{98}N_4O_{38}$. Additionally, no other high molecular weight coupling products were detected and CD-*m*THPP was isolated in excellent purity.

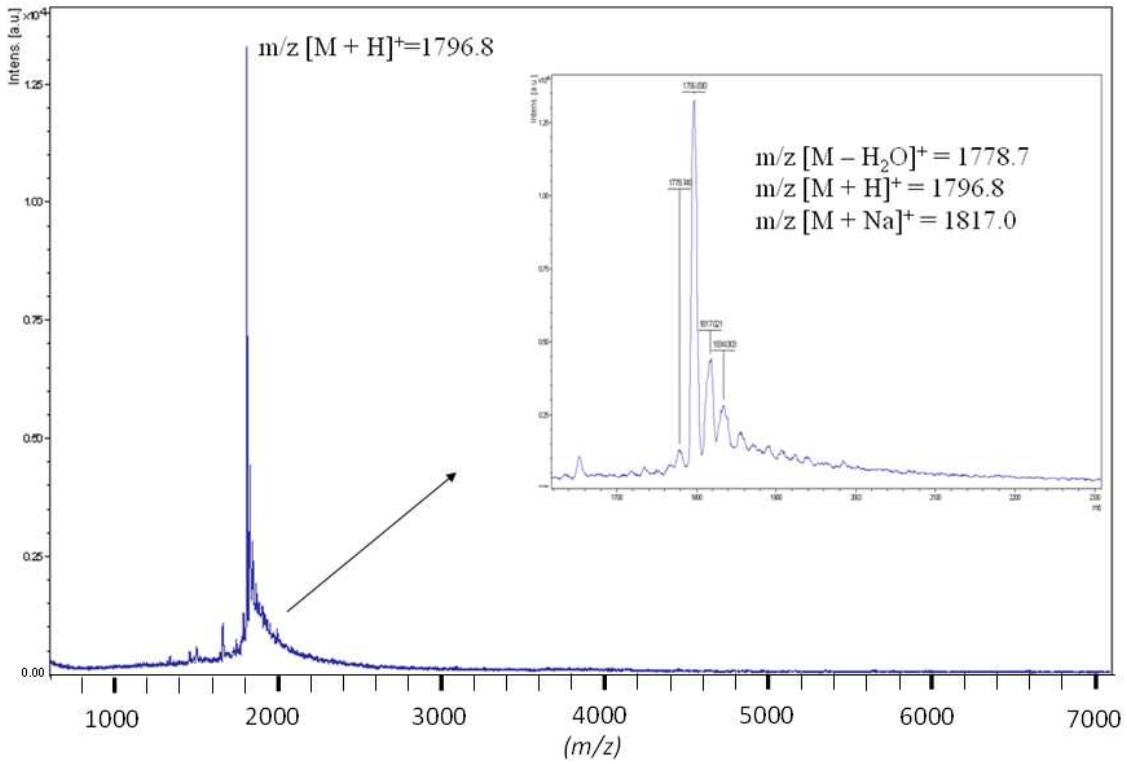

Figure 38. MS (MALDI-TOF) of CD-*m*THPP (positive mode, 2,5-dihydroxybenzoic acid (DHB) matrix): *m/z* calcd. for $C_{86}H_{98}N_4O_{38}$: 1795.70 [*M*]. Found: 1796.8 $[M+H]^+$ (100 %), 1817.0 $[M+Na]^+$ (33 %).

Further purity evidence was obtained from elemental analysis. The experimental result found (C: 51.18; H: 5.93; N: 3.11) revealed excellent agreement with estimated result for a chemical formula of $C_{86}H_{98}N_4O_{38}.9H_2O.NH_4Cl$ (C: 51.34; H: 6.02; N: 3.48). The addition of one molar eq. of ammonium chloride (NH_4Cl) agrees with the isolation / purification procedure of CD-*m*THPP, which involved: i) the use of ammonia (NH_3) in the mobile phase during column chromatography purification and is followed by ii) removal of NH_3 in acidic conditions (pH ≈ 5, H_2O / HCl) as a ammonium salt NH_4Cl though dialysis.

4.2.3 **Photophysical and other properties of CD-*m*THPP**

Solubility and aggregation

The porphyrin formation of aggregates in aqueous solutions has been studied in the literature and it is known to be dependent of factors like: i) the pH; ii) the ionic strength of the solution; iii) the concentration or iv) the solvent used to prepare the solutions [143, 68]. A CD-porphyrin conjugate based on 5,10,15,20-tetrakis(*p*-hydroxyphenyl)-porphyrin (*p*THPP) was prepared and studied in aqueous solutions, revealing poor aqueous solubility and a big tendency to aggregate. The corresponding loss in absorption/fluorescence properties was attributed to self-association, between CD cavity and the *p*THPP phenyl rings [148].

The pure conjugate CD-*m*THPP, isolated as a pure black solid, at room temperature is insoluble in water as it is. However, if CD-*m*THPP is first dissolved in a small amount of organic solvent (DMSO or MeOH), it can then be made water-soluble (μM range of concentration) and studied in aqueous media. Invariably, in aqueous solutions CD-*m*THPP always revealed a great tendency to aggregate and precipitate in the mM range of concentration. CD-*m*THPP showed good solubility in organic solvents (EtOH, MeOH or DMSO) but not in diethyl ether (EtOEt) where it was insoluble. This differential solubility towards EtOEt offered a tool for successful purification strategy for CD-*m*THPP (see section 10.1.4).

The solubility and aggregation tendency of CD-*m*THPP and *m*THPP were visually inspected in citrate and phosphate aqueous buffered solutions (pH = 3.8, 4.8, 6.0) and in phosphate buffer saline (PBS, pH = 7.4). CD-*m*THPP (and *m*THPP) was solubilised first in DMSO and further diluted to solutions (180 μM), with varying contents of DMSO (4 % and 9.1 %). Figure 39 shows the side pictures taken that illustrate the colour change and aggregation of buffered aqueous solutions, as the pH and amount of DMSO are changed keeping the temperature constant (10 – 15 ºC) over a period of 48 h.

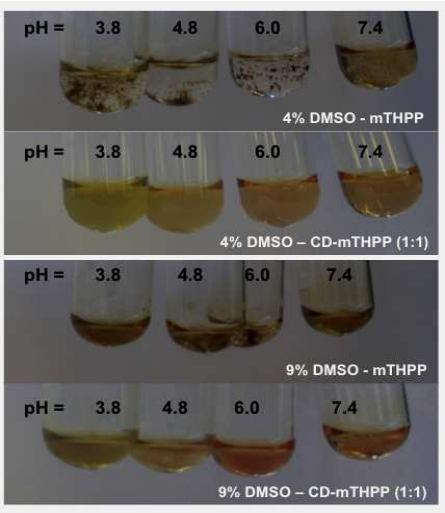

Figure 39. Solubility test of CD-*m*THPP (180 μM) and *m*THPP (180 μM), in buffered solutions (3.8 < pH < 7.4) modified with 4 % and 9.1 % of DMSO.

This experiment revealed that for solutions of 180 μM concentration: i) CD-*m*THPP shows better solubility than *m*THPP, independently of the amount of DMSO added to solution; ii) increasing the DMSO content in a solution of *m*THPP, from 4 % to 9.1 %, improved the solubility of *m*THPP but seemed to have no effect in aqueous solutions of CD-*m*THPP; finally, iii) the aggregation rate in solutions of *m*THPP was higher than the aggregation rate observed for aqueous solutions of CD-*m*THPP.

UV-Vis / fluorescence spectroscopy

The evaluation of the photophysical properties of CD-*m*THPP (3.6 μM) in aqueous solutions (4 % DMSO/PBS) and in pure DMSO were assessed by UV-Vis absorption and fluorescence. The results were compared to solutions of *m*THPP. The absorption spectra of CD-*m*THPP and *m*THPP were recorded in DMSO (Figure 40 A) and in 4 % DMSO/PBS (Figure 40 B).

The typical features of a porphyrin (*m*THPP) spectrum are preserved in the conjugate (CD-*m*THPP) spectrum in DMSO (Figure 40 A), with a strong Soret band (420 nm) and small Q bands (515 nm, 549 nm, 590 nm, 648 nm). In pure DMSO, molecules are less prone to aggregation and there is a nearly complete match of the UV-Vis absorption spectra of *m*THPP and CD-*m*THPP (Figure 40 A). However, in 4 % DMSO/PBS, the UV-Vis spectra of both porphyrin and conjugate (Figure 40 B) suffer some modifications: i) the maximum absorption achieved in 4 % DMSO/PBS is reduced when compared to pure DMSO and became broader; ii) the intensity of the Soret band in CD-*m*THPP (421 nm; 0.19 a.u.) is nearly double the intensity

of *m*THPP (428 nm; 0.11 a.u.); and iii) the Soret band of CD-*m*THPP is sharper than the Soret band of *m*THPP (Figure 40 B). These results that at 3.6 μM concentrations, aqueous solutions of CD-*m*THPP display a less aggregated profile when compared to *m*THPP solutions in 4 % DMSO/PBS.

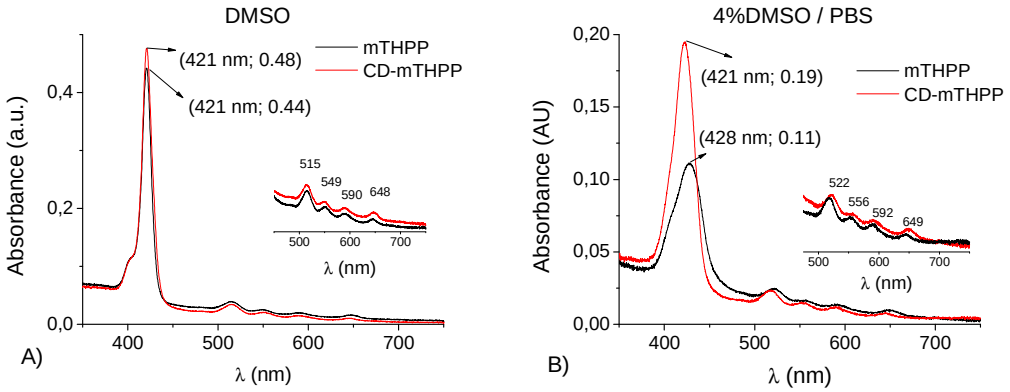

Figure 40. Absorption spectra for CD-*m*THPP (3.6 μM, red line) and for *m*THPP (3.6 μM, black line) in A) 100 % DMSO and B) 4 % DMSO/ PBS.

Additionally, Figure 41 shows the *m*THPP and CD-*m*THPP fluorescence spectra, following with excitation at the Soret band recorded for diluted 3.6 μM solutions, prepared in DMSO (Figure 41 A) and in 4 % DMSO/PBS (Figure 41 B). In DMSO (Figure 41 A), *m*THPP (654 nm; 17.5 a.u.) shows slightly higher fluorescence intensity than CD-*m*THPP (651 nm; 14.6 a.u.). However, in aqueous solutions 4 % DMSO/PBS, despite the overall fluorescence intensity is significantly lower than in DMSO, the conjugate in 4 % DMSO/PBS (650 nm; 5.6 a.u.) revealed much higher fluorescence intensity than *m*THPP (651 nm, 0.2 a.u). This corresponds to a 23-fold increase in emission fluorescence intensity (Figure 41 B), indicating that CD-*m*THPP recovers its emission properties at small (μM), but biologically relevant concentrations.

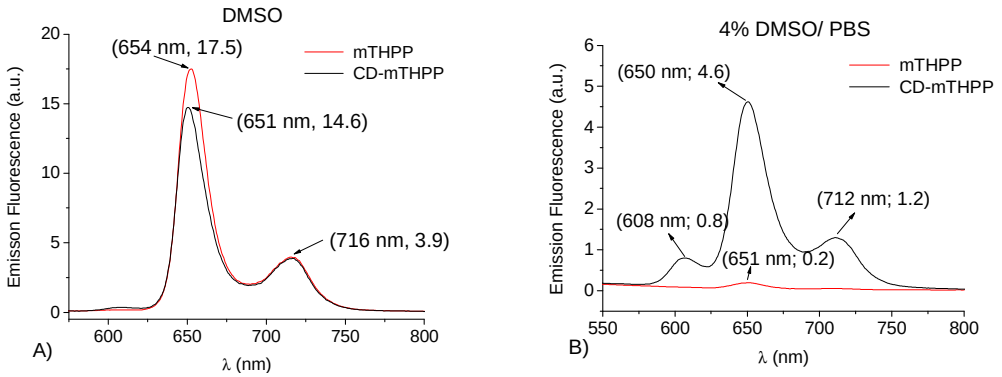

Figure 41. Fluorescence emission spectra of CD-*m*THPP (3.6 μM, black line) and for *m*THPP (3.6 μM, red line), following excitation at the Soret in: A) 100 % DMSO, with λ_{exc} = 421 nm for both CD-*m*THPP and *m*THPP; and B) in 4 % DMSO/ PBS, with λ_{exc} = 421 nm for CD-*m*THPP and λ_{exc} = 428 nm for *m*THPP.

These UV-Vis / fluorescence results revealed that in aqueous diluted solutions (3.6 μM), prepared in 4 % DMSO/PBS the aggregation phenomenon needs to be considered as it affects photophysical properties of both *m*THPP and CD-*m*THPP. Additionally, the conjugate is photoactive in aqueous 4 % DMSO/PBS solutions, preserving the typical UV-Vis and fluorescence spectral features of *m*THPP. CD-*m*THPP shows significantly less aggregation than *m*THPP solutions, resulting in improved absorbance and emission fluorescence intensities especially in 4 % DMSO/PBS.

pH dependence of UV-Vis properties

Given the well-documented influence of pH on the aggregation state of porphyrins and consequent effect on photophysical properties [143], it is reasonable to expect that CD-*m*THPP could display a similar pH dependence of its properties in aqueous solutions. Therefore, a comparative study between CD-*m*THPP and *m*THPP was performed to evaluate how the pH affects the photophysical properties and to determine at which the pH, both UV-Vis and fluorescence bands reach their maximum intensity. If successful, this experiment would result in the proper choice of a suitable pH to prepare aqueous solutions of CD-*m*THPP.

The absorption spectra were recorded for diluted solutions (2 μM) of *m*THPP (Figure 42 A) and of CD-*m*THPP (Figure 42 B), prepared in buffered solutions modified with 4 % of DMSO, as a function of the pH. The typical UV-Vis characteristics of the porphyrin and conjugate are preserved, with a strong Soret band ($\lambda \approx 420$ nm) and small absorption bands (Q bands), observed between 450 nm < λ < 700 nm. Variations on the wavelength and relative intensity of the bands were observed as the pH of both solutions was changed and, for simplicity, the changes on wavelength of the Soret (λ_{Soret}) and its intensity (absorbance) were recorded as a function of pH and were respectively plotted in Figure 42 C and D.

Figure 42 C reveals that in acidic pH (2 < pH < 3), the λ_{Soret} of CD-*m*THPP is 440 nm and when pH > 4, λ_{Soret} it drops abruptly to lower wavelength remaining approximately constant 420 nm < λ_{Soret} < 422 nm, thereafter, until pH = 11 resulting in a hypsochromic shifting by 18 nm. *m*THPP shows a high λ_{Soret} (440 nm) at acidic pH (< 3), but for 4 < pH < 6 λ_{Soret} gradually decreases down to 422 nm. λ_{Soret} remains constant until pH = 7 and rises gradually again, achieving a maximum at 432 nm at pH = 9, followed by a decrease in λ_{Soret} = 419 nm between 9 < pH < 11 which is in contrast with the constant value observed for the conjugate.

Figure 42 D shows that *m*THPP shows higher absorbance than CD-*m*THPP, for pH < 3 and for strong alkaline solution (pH > 10) and in the physiological range (6 < pH < 7). In all

other pH ranges namely in 3 < pH < 5 and between 8 < pH < 9, the absorption for CD-*m*THPP is higher than for *m*THPP.

To the best of our knowledge, the pH variation of UV-Vis spectral properties has not been assessed for any CD-porphyrin conjugate. However, the dependence of *m*THPP UV-Vis spectra has been assessed and compared with similar PS: i) the changes observed 4 < pH < 6 were related to different protonation of the imino nitrogens of the porphyrin core, and ii) the maximum absorbance was achieved at pH = 7 [55]. Interestingly, both *m*THPP and CD-*m*THPP reached their maximum absorbance at pH = 7, which is advantageous considering that most biological experiments are performed at physiological pH (= 7.4).

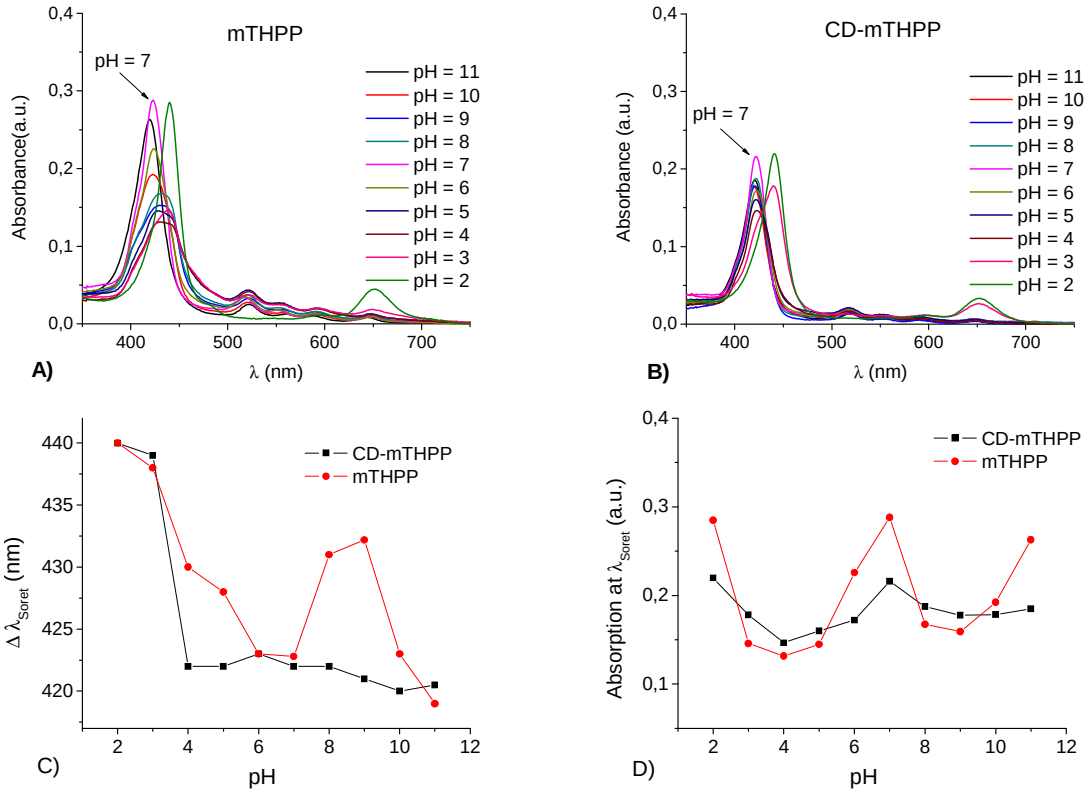

Figure 42. Absorption spectra as a function of pH change for A) *m*THPP and for B) CD-*m*THPP. Graphical representation of C) the Soret maximum (λ_{Soret}, nm) and of D) its intensity (Absorbance, a.u.) recorded for diluted solutions (2 μM) in 4 % DMSO/PBS*, (* - varying pH).

Less aggregated porphyrin solutions are expected to reveal improved UV-Vis spectral properties, than solutions where aggregation takes place. The aggregation of *m*THPP and CD-*m*THPP prepared in 4 % DMSO/PBS (pH = 7.0) was estimated, by the calculation of the full width at half maximum (FWHM) evaluated for the Soret band in the corresponding UV-Vis spectra. It was found that FWHM for *m*THPP (33 nm) > CD-*m*THPP (5 nm), indicating that

*m*THPP has a higher tendency to aggregate than CD-*m*THPP. This result is in line with our previous reported studies in 0.5 % DMSO/PBS solutions, where the aggregation tendency of *m*THPP and CD-*m*THPP was evaluated [144]. It has been shown that CD-*m*THPP revealed much smaller particles (≈ 13 nm, DLS) than *m*THPP (≈ 2000 nm, DLS) and *m*THPP, revealed a much bigger tendency to aggregate, than CD-*m*THPP.

Even though, diluted solutions were used (2.0 μM; 3.6 μM), aggregation of porphyrins proved to be a time-dependent and dynamic process in aqueous solutions, occurring even in the μM range of concentrations [68]. Probably, during the time it takes to: i) prepare of the initial stock solution; ii) diluting it to the desired concentration and iii) record the UV-Vis spectra of these solutions each solution both *m*THPP and CD-*m*THPP behave differently. Therefore, time between trials also affects the overall UV-Vis absorption spectra and needs to be assessed through carefully designed experiments.

pH dependence of fluorescence properties

Emission fluorescence spectra were recorded for dilute solutions (2 μM) of *m*THPP (Figure 43 A) and for CD-*m*THPP (Figure 43 B). *m*THPP shows a two band fluorescence spectra with peaks ($\lambda \approx 660$ nm and 725 nm) over the region $4 < pH < 11$ that turns into a single band spectra ($\lambda \approx 680$ nm) in acidic solutions ($pH < 4$). Likewise, CD-*m*THPP reveals a spectra three bands spectra ($\lambda \approx 623$ nm, 660 nm and 730 nm) for $4 < pH < 11$, which turns into a single band spectra ($\lambda \approx 677$ nm) when $pH < 4$. Figure 43 C shows that there are not significant changes on the wavelength of the strongest fluorescence band (λ_{MAX}) as the pH is changed, for solutions of *m*THPP and CD-*m*THPP. However, for ($3 < pH < 11$), the changes in intensity of the strongest fluorescence band recorded at λ_{MAX} (Figure 43 D) are more pronounced for CD-*m*THPP than for *m*THPP, except in very acidic ($pH = 2$) where *m*THPP fluorescence intensity is higher than CD-*m*THPP. The magnitude of the changes is roughly the same for *m*THPP and CD-*m*THPP and at $pH = 7$, it reached the maximum emission fluorescence intensity: CD-*m*THPP (70.6 a.u., $\lambda_{exc} = 422$ nm) ≈ 2.6 times higher than *m*THPP (26.4 a.u., $\lambda_{exc} = 422$ nm), when excited at the Soret maximum.

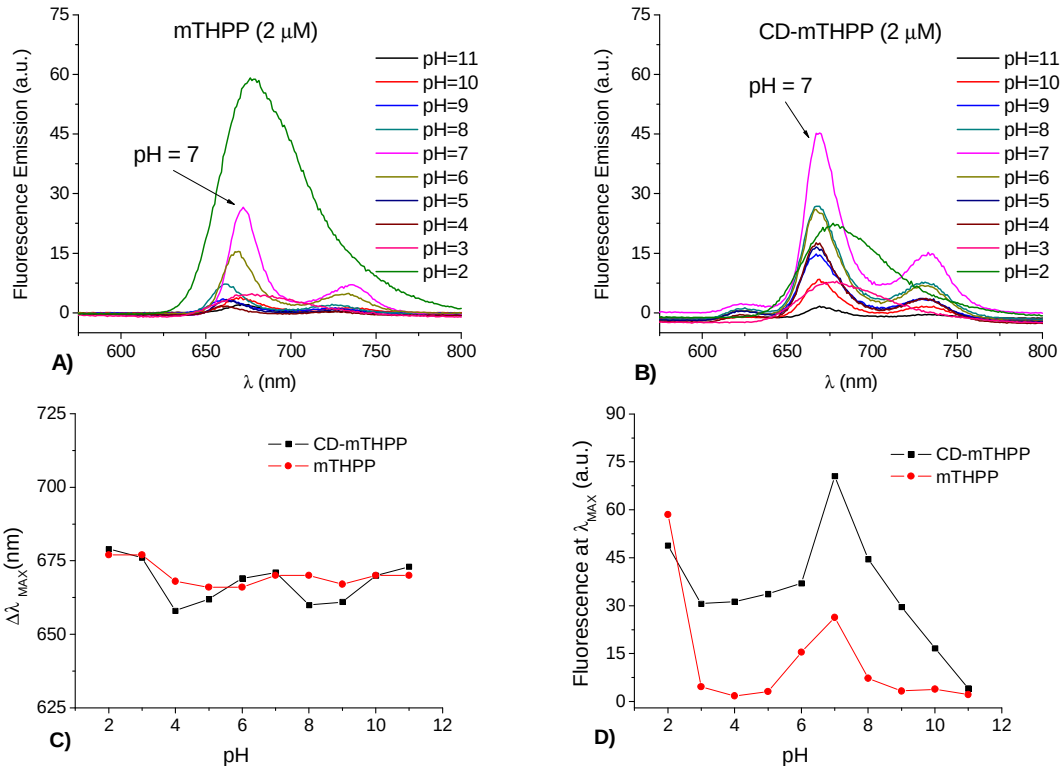

Figure 43. Fluorescence emission spectra as a function of pH for A) *m*THPP and B) CD-*m*THPP. Graphical representation of C) the intensest fluorescence band (λ_{MAX}, nm) and of D) its intensity (fluorescence, a.u.) recorded following excitation at Soret maximum for diluted solutions (2 μM) in 4 % DMSO/PBS*, (* - varying pH).

These results are in excellent agreement with measurements performed in collaboration with University of Catania [144], considering that: fluorescence emission intensity of CD-*m*THPP (5 μM, 0.5 % DMSO/PBS, ≈ 9 a.u.) *vs* *m*THPP (5 μM, 0.5 % DMSO/PBS, ≈ 2 a.u.), when excited at λ_{exc} = 512 nm.

The fluorescence spectral properties of *m*THPP and other photosensitizers have been studied as a function of the pH in phosphate buffered saline (PBS) modified with: i) 50 % (*v/v*) of methanol (MeOH) and by using non-ionic surfactant ii) Titron X-100 (20 %) modified with 0.6 % (*v/v*) of PBS [55]. *m*THPP revealed no fluorescence in PBS solution in a region 4 < pH < 10 and showed a fluorescence emission peak at 679 nm (λ_{exc} = 417 nm) in acidic pH < 4; its emission fluorescence intensity improved in solutions containing 50 % (*v/v*) MeOH/PBS, where two peaks were observed in 4 < pH < 10; however, when pH < 3, the spectrum changes and only one peak was observed at 683 nm. The improvement of the emission fluorescence spectra of *m*THPP (0.03 μM) in PBS, upon addition of 50 % MeOH was attributed to a decrease in aggregation. A reasonable explanation for the changes observed in the spectra for pH < 4 has been attributed to the protonation of the imino nitrogen of pyrrole group, which changes the porphyrin ring symmetry and results in a shift of the emission peaks [145].

In comparison with these published results, our results were obtained in aqueous solvents, in the presence of a limited amount of organic modifier (4 % *v/v* DMSO/PBS) as opposed to that reported (50 % v/ v MeOH) and, in addition, our concentration (2 μM) is nearly 70 times higher than the one reported (0.03 μM) *m*THPP. The improved emission fluorescence properties of CD-*m*THPP seems to be an intrinsic property of the molecule in aqueous solutions, where it reveals much less tendency to aggregate than *m*THPP in the same conditions (2 μM, 4 % DMSO/PBS pH = 7.0), evidently due to the attachment to the CD moiety.

4.3 Conclusions and future perspectives

The synthesis of CD-porphyrin conjugate (CD-*m*THPP) was accomplished by applying crucial modifications to a previous completely inappropriate purification methodology. The optimized improved procedure involved the use of column chromatography (silica gel 60, *i*PrOH : EtOAc : H_2O : NH_3 (5:3:3:1, *v/v*)) and dialysis to recover the pure CD-*m*THPP. The conjugate was obtained in 40 % yield, based on reacted *m*THPP. The moderate reaction yield is unavoidable, as many side products and processes are in operation and compete with the formation of CD-*m*THPP, but even this value it is much better than most literature reported yields. Most of unreacted *m*THPP can be successfully recovered and reused.

CD-mTHPP was obtained as a single molecular structure, constituted by one molecule of CD covalently connected to one molecule of porphyrin. Its physical-chemical properties were assessed by TLC, ^{1}H NMR spectroscopy, elemental analysis, MALDI-TOF mass spectrometry and UV-Vis / fluorescence spectroscopy. In its pure state, CD-*m*THPP preserves the porphyrin properties, namely it displays a typical UV-Vis absorption, red fluorescence and it is water-soluble in μM range of concentration, which are appropriate for *in vitro* biological studies.

In comparison to *m*THPP in the μM range of concentrations, CD-*m*THPP revealed improved emission fluorescence intensity (1.7-fold higher) in aqueous solutions modified with 4 % DMSO, which can be maximized using 4 % DMSO/PBS (pH = 7.0). CD-*m*THPP showed much smaller tendency for aggregation than for the *m*THPP in the same medium. However, the presence of aggregates at higher concentrations (mM range) indicates that efforts to improve its water solubility are required.

5. Large solubility enhancement of CD-*m*THPP complexed with of *per*(2,3,6-*O*-trimethyl)-βCD (pMβCD) and comparison with pMβCD complexes of mTHPP

5.1 Introduction

Methylated cyclodextrin (CD) derivatives are recognised for their distinctive properties: high solubility in commonly used organic solvents as well as in water and for their ability to accommodate guests molecules, through formation of cavity inclusion complexes [146]. In comparison to native CDs, the inclusion properties of methylated CDs are strongly related to the absence of sufficient hydroxyl groups (-OH), which gives extra flexibility in their cavity structure, due to lack of hydrogen bonding between adjacent OH groups in the secondary side [147]. The flexibility can be very advantageous because it allows the host to bend its macrocycle, in order to better accommodate more efficiently the incoming guest molecule [17]. Two examples of methylated CDs are heptakis(2,6-di-*O*-methyl)-βCD (DIMEB) and heptakis(2,3,6-tri-*O*-methyl)-βCD (pMβCD) (Figure 44).

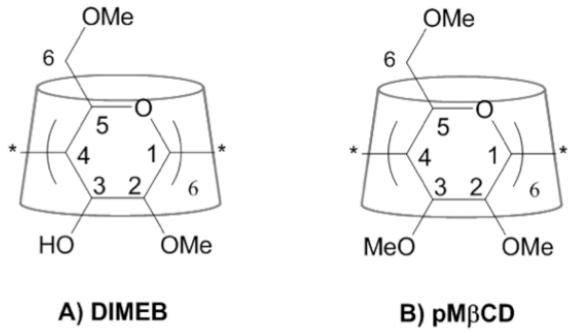

Figure 44. Two methylated βCD derivatives: A) DIMEB and B) pMβCD.

Methylated CDs became promising hosts for the complexation of chiral molecules, useful in separation of enantiomeric mixtures and very efficient solubilizers of porphyrins [148], namely 5,10,15,20-tetraphenylporphyrin (TPP) derivatives and water-soluble porphyrins often characterized by their high tendency to aggregate in aqueous solvents [67], as described in section 2.1.3. Methylated CDs are efficient solubilizers of water-soluble TPP derivatives, through formation of strong and water-soluble inclusion complexes characterized by 1:1 or 2:1 stoichiometries and high binding affinities [148]. The structure of these complexes has been determined through 1D and 2D NMR experiments. For example, the ^{1}H NMR spectrum of pMβCD changed after the gradual addition of water-soluble 5,10,15,20-tetra(*p*-sulfonatophenyl)-porphyrin ($TPPS_4$): i) new peaks were observed and attributed to the

formation of inclusion complexes (pMβCD / $TPPS_4$); ii) at the right stoichiometry ratio between (pMβCD / $TPPS_4$) = 2:1, a pure complex solution was obtained and a completely different spectrum was observed, solely assigned to the presence of the complex; iii) 2D NMR experiments, revealed interaction of the CD cavity internal protons (CD-H_3/H_5) and the phenyl rings of the $TPPS_4$ and iv) dipolar interactions of 3-OMe with CD-H_3/H_5 were detected, revealing that this methyl group is pointing towards the inside of the pMβCD cavity [149]. In a different example the water insoluble 5,10,15,20-tetra(*p*-pyridyl)-porphyrin (TPyP) interacted with two pMβCD molecules, with two of the four pyridyl moieties being deeply inserted into the pMβCD cavity [150]. These porphyrin-pMβCD inclusion complexes are so unusually strong, that dye inclusion single crystals (DISC) have been prepared and their X-ray structure determined (Figure 45) [151].

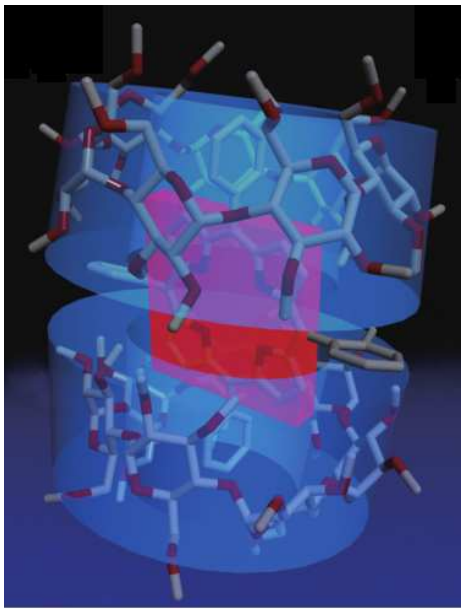

Figure 45. Structure of the inclusion complex between pMβCD and TPP, following a H:G = 2:1 stoichiometry [151].

Similar findings were also reported from the interaction of pMβCD with 5,10,15-(tris-(3,5-dicarboxylatophenyl)-20-phenylporphyrin), corresponding to the formation of an inclusion complex of different stoichiometry H:G = 1:1 [152].

UV-Vis and fluorescence spectroscopy have been used to determine both the stoichiometry and the binding constants of porphyrin and methylated CDs complexes: i) a solution of 5,10,15,20-tetrakis(*p*-carboxyphenyl)-porphyrin in the presence of pMβCD, prepared in 0.1 M aqueous buffer (pH = 7) revealed an increase in Soret intensity, when 3 molar

excess of pMβCD are added to the solution; the stoichiometry of the complex pMβCD: porphyrin was 2:1 [148]. In another example, 5,10,15,20-tetrakis[4-(3-pyridiniumpropoxy)phenyl]porphyrin tetrakisbromide (TPPOC3Py) was treated with increasing amounts of pMβCD solubilised in ethylene glycol : water (3:1) and an increase in the Soret intensity was observed and the curve fitting suggested a mixed equilibrium, between two stoichiometries comprising a 1:1 and a 2:1 equilibria [149].

In the previous section 4.2.1, the synthesis and characterization of CD-*m*THPP conjugate in its pure state was described and its aggregation and poor water solubility was observed. This impaired important studies namely inclusion studies in aqueous solution, in order to document the ability of CD-*m*THPP to carry guest molecules, specifically drugs with anticancer properties. Therefore, it was envisaged that by using pMβCD as solubilizer, the photophysical properties of CD-*m*THPP in aqueous solvents could be improved and the biological studies resumed. In this chapter, UV-Vis, fluorescence and NMR spectroscopies will be used to study complexation of pMβCD with *m*THPP and with CD-*m*THPP, namely:

i) Evaluate improvements in aqueous solubility of CD-*m*THPP and *m*THPP in the presence of pMβCD

ii) Determine a suitable range of concentrations (mM) to enable the NMR studies on the structural features of pMβCD complexes with CD-*m*THPP and *m*THPP

iii) Determine the equilibrium constant (K), the stoichiometry of complexation and mode of complexation *m*THPP and CD-*m*THPP

iv) Proceed with cell internalization experiments and

v) Study of complexation of poorly soluble molecules into CD-*m*THPP, solubilised by pMβCD

5.2 Results and discussion

5.2.1 Linear concentration range for *m*THPP and CD-*m*THPP in 4 % DMSO/PBS solutions

Prior to the evaluation of the improvements in aqueous solubility of CD-*m*THPP and *m*THPP promoted by addition of pMβCD, through a typical titration experiment based on UV-Vis / fluorescence, a preliminary UV-Vis study was required to determine a suitable concentration range (μM), under which titration experiments could be performed considering aggregation negligible.

UV-Vis spectroscopy was used to determine the linear range of concentration by application of Beer-Lambert law, which is followed when diluted solutions of chromophore are used. Deviation from linearity is observed when concentration of the chromophore is increased, signifying the onset of aggregation. The UV-Vis spectra of *m*THPP solutions recorded in DMSO (Figure 46 A) and in 4 % DMSO/PBS (Figure 46 B), reveal the typical UV-Vis spectra expected for CD-*m*THPP in DMSO (Figure 46 C) and in DMSO/PBS (Figure 46 D): i) an intense peak at ≈ 420 nm (Soret band) and ii) four weak bands between 450 – 700 nm (Q bands).

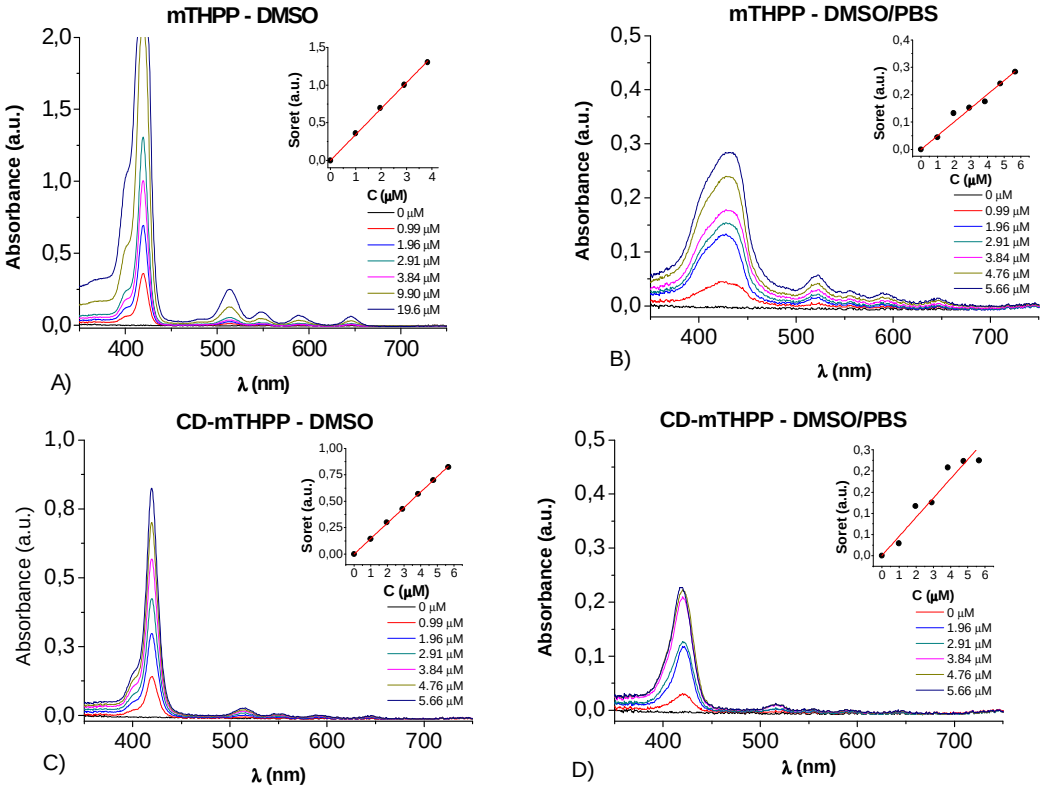

Figure 46. UV-Vis spectra of increasing amounts of: A) *m*THPP (0 – 20 μM) in DMSO; B) *m*THPP (0 – 5.6 μM) in 4 % DMSO/PBS; C) CD-*m*THPP (0 – 5.6 μM) in DMSO and D) CD-*m*THPP (0 – 5.6 μM) in in 4 % DMSO/PBS.

However, when the concentration of *m*THPP (or CD-*m*THPP) is increased both the aggregation and the intensity of the absorption bands (Soret and Q-bands) increase. For any given concentration (C = 3.84 μM) of active species (*m*THPP and CD-*m*THPP) in solution, the value of the full width at half-maximum (FWHM) can be calculated and used to judge aggregation tendency. Table 4 shows that in 4 % DMSO/PBS: $FWHM_{mTHPP}$ (58 nm) > $FWHM_{CD\text{-}mTHPP}$ (25 nm), whereas in DMSO: $FWHM_{CD\text{-}mTHPP}$ (14 nm) > $FWHM_{mTHPP}$ (8 nm) which suggest that in aqueous solutions (4 % DMSO/PBS), *m*THPP and CD-*m*THPP have a much higher degree aggregation than in pure DMSO. Moreover, in aqueous solutions and keeping the concentration constant (C = 3.84 μM), CD-*m*THPP is much less aggregated than *m*THPP, because $FWHM_{CD\text{-}mTHPP}$ = 25 nm < $FWHM_{mTHPP}$ = 58 nm which is in perfect agreement with previous reported data [144].

The summary of parameters (Table 4) obtained from the linear fittings, displayed as insets in Figure 46 reveal that: i) both CD-*m*THPP and *m*THPP possess a good linearity over a narrow range of concentrations (0 μM - 5 μM), both in DMSO (expected, since DMSO is a monomerizing solvent) and in 4 % DMSO/PBS, with most of the experimental data being explained by the linear fitting applied (calibration curve $R^2 \approx 1.0$; ii) the molar absorption coefficient (ε) of both compounds is higher in DMSO than in 4 % DMSO/PBS due to aggregation; and iii) although, CD-*m*THPP is less aggregated in 4 % DMSO/PBS than in *m*THPP, the ε value for the detection of *m*THPP is higher than the ε value for the detection of CD-*m*THPP independently of the solvent used – in DMSO (ε_{mTHPP} = 344501 $M^{-1}.cm^{-1}$ > $\varepsilon_{CD\text{-}mTHPP}$ = 146700 $M^{-1}.cm^{-1}$) whereas in 4 % DMSO/PBS (ε_{mTHPP} = 50400 $M^{-1}.cm^{-1}$ > $\varepsilon_{CD\text{-}mTHPP}$ = 45400 $M^{-1}.cm^{-1}$).

Table 4 – Experimental data on the calibration curves of *m*THPP and CD-*m*THPP, based on linear fitting adjustment (y = mx + b, with b = 0).

Example	Solvent	R^2	ε ($M^{-1}.cm^{-1}$)	Linear range	FWHM (C = 3.84 μM)
*m*THPP	DMSO	0.9996	344501	0 – 4 μM	8 nm
*m*THPP	DMSO/PBS	0.9915	50400	0 – 5 μM	58 nm
CD-*m*THPP	DMSO	0.9999	146700	0 – 5 μM	14 nm
CD-*m*THPP	DMSO/PBS	0.9778	45400	0 – 5 μM	25 nm

This suggests that the presence of aqueous buffered solutions (PBS) greatly affects the UV-Vis properties of *m*THPP and CD-*m*THPP, even when small amounts of organic modifier (4 % DMSO, *v/v*) are used in the preparation of solutions. However, if diluted solutions are used (0 μM – 4 μM) aggregation can be minimized to a reasonable level and titration experiments can be resumed.

Similar findings were observed for 5,10,15,20-tetrakis(*m*-hydroxyphenyl)-chlorin (*m*THPC) in MeOH, which showed good linearity over the concentration range 4.6 μM to 734 μM, but in opposition to our experiments, were determined following the intensity of the Q band I [153]. However, this can be compared with *m*THPP in DMSO (Figure 46 A) considering that at concentration of ≈ 10 μM it is no longer possible to record the intensity of Soret; therefore, it is possible to follow the Q-band I and go well above 20 μM in concentration. The good linearity in aqueous behaviour of *m*THPP in the range 0 μM – 5 μM agrees well, with linearity of 5,10,15,20-tetrakis(*N*-ethylpyridinium-2-yl)-porphyrin (TEPyP) in aqueous buffer, which showed deviations from Beer's law above 6 μM [150]. Pasternack and co-workers studied interactions of water-soluble porphyrins like tetra(*N*-methylpyridyl)-porphyrin (TMPyP), 5,10,15,20-tetrakis(*p*-carboxyphenyl)-porphyrin (H_2TPPC) and 5,10,15-tris(*p*-sulfonatophenyl)-20-phenylporphyrin (H_2TPPS_3) in aqueous buffered solutions at pH = 7.5 and found that these obeyed Beer-Lambert Law over a wide range of concentrations. However, in the presence of 0.1M KNO_3 added to their buffered solutions of TMPyP, H_2TPPS_3 and H_2TPPC substantial deviation from linearity was revealed, attributed to monomer-dimer equilibria of the free-base forms [154].

5.2.2 Titration experiments with pMβCD

Given the limited water solubility of CD-*m*THPP and considering the reported ability of *per*(2,3,6-trimethyl-6-deoxy)-βCD (pMβCD) to form inclusion complexes with tetraphenylporphyrin (TPP) [148], pMβCD was used as a solubilizer to improve the water solubility of CD-*m*THPP. *m*THPP was used as a model compound because its pMβCD complexes have been characterized and it was used as a starting material in the preparation of CD-*m*THPP, possessing similar structural features to the conjugate (Figure 47).

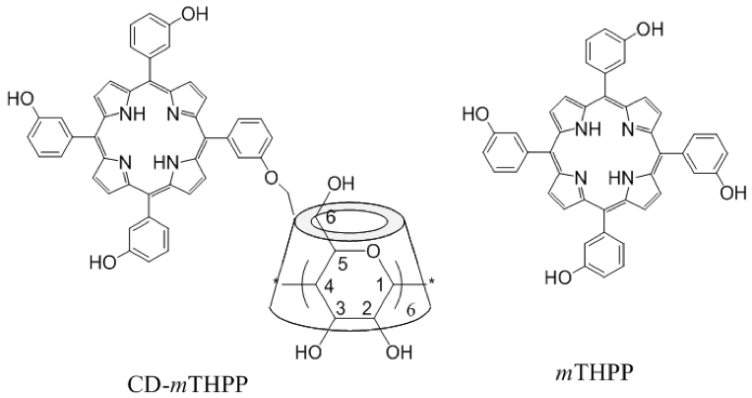

Figure 47. Structure of the conjugate (CD-*m*THPP) and of 5,10,15,20-tetrakis(*m*-hydroxyphenyl)-porphyrin (*m*THPP).

Titration experiments based on UV-Vis and fluorescence spectroscopy have been conducted, using 2 μM concentration to minimize aggregation phenomena and were prepared in 4 % DMSO/PBS (pH = 7.4). Solutions of porphyrin (*m*THPP) and conjugate (CD-*m*THPP) were titrated with pMβCD. Their UV-Vis (Figure 48 A) and fluorescence spectra (Figure 48 B) were recorded, following the addition of increasing amounts of pMβCD (molar eq.).

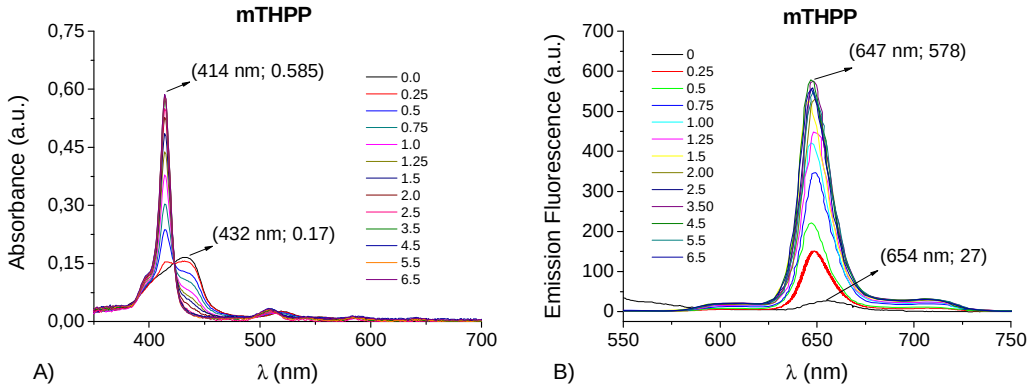

Figure 48. Spectral changes in A) UV-Vis absorbance and B) emission fluorescence intensity spectra for a solution *m*THPP (2 μM; 4 % DMSO/PBS), as pMβCD is added to the solution until it reaches 6.5 molar eq.

The initial UV-Vis spectrum of *m*THPP (2 μM; black line, Figure 48 A) upon addition of pMβCD solution gradually changes, from a broad Soret peak with negligible intensity (0.17 a.u.; 432 nm), to a well-defined spectrum with a sharp and intense Soret peak (0.59 a.u.; 414 nm), with increasing intensity as amount of pMβCD in solution is increased. This corresponds to a 3.4-fold increase in absorption maximum intensity, associated to a hypsochromic shift of the Soret (≈ 18 nm) after addition of 6.5 molar excess of pMβCD (Figure 48 A). The addition of more pMβCD resulted in no significant increase in the absorbance and a single isobestic point was observed at (λ = 423 nm, abs = 0.15 a.u.; Figure 48 A). Likewise, the initial fluorescence spectra (2 μM; black line, Figure 48 B) changes from a nearly negligible fluorescence intensity (27 a.u.; 654 nm), to a reasonable intense fluorescence emission (578 a.u.; 647 nm) after addition of 6.5 molar eq. of pMβCD. There is a total 21-fold increase associated with a hypsochromic shift of 7 nm (Figure 48 B). No increase in fluorescence emission was observed, upon further pMβCD addition.

The increase in UV-Vis and fluorescence intensity has been shown in the literature through titration experiments: i) 5,10,15-tri(3,5-dicarboxylatophenyl)-20-phenyl-porphyrin (20 μM; phosphate buffer, pH = 7) with 2,6-dimethyl-βCD [152]; charged 5,10,15,20-tetrasubstituted porphyrins TPPOC3Py (-C_6H_4-O-$(CH_2)_3$-Py^+Br^-, where Py^+ = alkylpyridinium, with pMβCD

[149] or even through the use of differently substituted CD derivatives like heptakis(2,6-di-*O*-n-octyl)-β-cyclodextrin (Oc-βCD) in the titration of TPP [155]. The appearance of a single isobestic point has been attributed to dimerization processes [69, 70]. This was observed for *m*THPP (2 μM) titrated with pMβCD in aqueous solutions, which corroborates well with previous observations regarding high propensity of *m*THPP to aggregate in aqueous media. However, as expected from the addition of pMβCD, this leads to the breakup of these dimeric species and to a reasonable recovery of the UV-Vis absorption intensity.

The same experiments were performed for diluted solutions of CD-*m*THPP (2 μM; 4 % DMSO/PBS) and as pMβCD was added to the host solution, both the UV-Vis absorption (Figure 49 A) and fluorescence spectra (Figure 49 B) were recorded: i) UV-Vis spectrum of CD-*m*THPP changed from a broad and weak Soret (0.13 a.u.; 422 nm), to a sharper peak and intense Soret band (0.21 a.u.; 414 nm) after the addition of 3 molar eq. of pMβCD above which no absorbance increase was noticed. This corresponded to a 1.6 fold increase in absorption maximum intensity associated to a hypsochromic shift of 8 nm (Figure 49 A). No isobestic points were observed. Fluorescence spectral changes starting from an initial solution of CD-*m*THPP (32 a.u.; 650 nm), following the addition of a total of 3 molar eq. of pMβCD, resulted in a 8-fold improvement of the fluorescence intensity associated to a hypsochromic shift of 3 nm and a much improved final fluorescence spectrum (256 a.u.; 647 nm) (Figure 49 B).

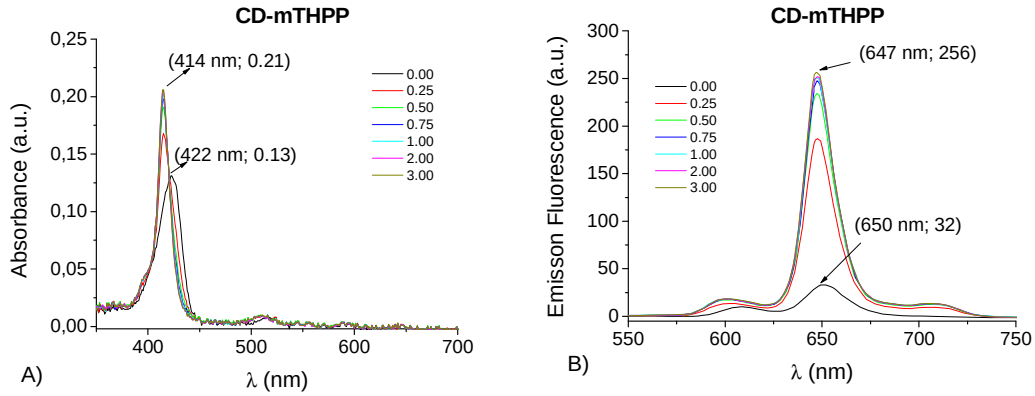

Figure 49. Spectral changes in A) UV-Vis absorbance and B) emission fluorescence intensity spectra for a solution CD-*m*THPP (2 μM; 4 % DMSO/PBS), as pMβCD is added to the solution until it reaches 3.0 molar eq.

These experiments revealed that the addition of pMβCD to aqueous buffered solutions of CD-*m*THPP and *m*THPP, promotes improvements in their UV-Vis absorbance and fluorescence emission. This suggests that the pMβCD complexes should display similarities given the structural similarities between the porphyrin and the conjugate. The amount of

pMβCD added to *m*THPP (6.5 molar eq.) is 2.2 higher than the one added to CD-*m*THPP (3.0 molar eq.), which probably indicates a different stoichiometry between the two complexes.

5.2.3 Stoichiometry estimation and stability of pMβCD complexes

Following the titration experiments by UV-Vis and fluorescence described previously, it is possible to estimate the stoichiometry of the complexation equilibrium, through a different graphical representation of the analytical data collected. Figure 50 A shows the changes in the absorption maximum (Soret intensity) for a 2 μM solution of *m*THPP, plotted against molar equivalents of pMβCD added to the solution during the titration. The changes on maximum intensity of fluorescence spectra upon excitation at the Soret maximum is shown in Figure 50 B. In both UV-Vis and fluorescence experiments, the intensities gradually increase and a plateau is reached when two molar eq. of pMβCD are added to *m*THPP (2 μM) (black arrow). Consequently, the complex is formed by adding two moles of pMβCD to one mole of *m*THPP, in an equilibrium following a two-to-one (2:1) stoichiometry.

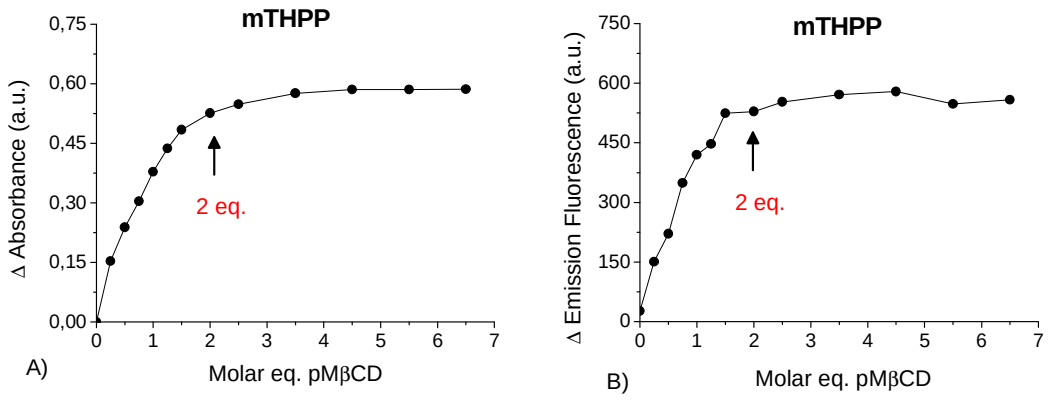

Figure 50. Titration experiment of *m*THPP (2 μM) with pMβCD (300 μM) in 4 % DMSO/PBS. For every pMβCD addition the A) absorption and B) fluorescence maximum were followed until an excess of 6.5 molar eq. are present in solution.

The 2:1 stoichiometry of the complex pMβCD/*m*THPP agrees with a reported example given by iron-tetrakis(4-sulfatophenyl)-porphyrin (Fe-TPPS) in the presence of pMβCD, where two molecules of pMβCD engulf a Fe-TPPS molecule, from opposite sides leading to a symmetrical substituted complex: Fe-TPPS/pMβCD (1:2) [156].

Likewise, the differences in the analytical response recorded for CD-*m*THPP, namely the increment in fluorescence (Figure 51 B) and absorbance (Figure 51 A) revealed complexation equilibrium involving a 1:1 stoichiometry.

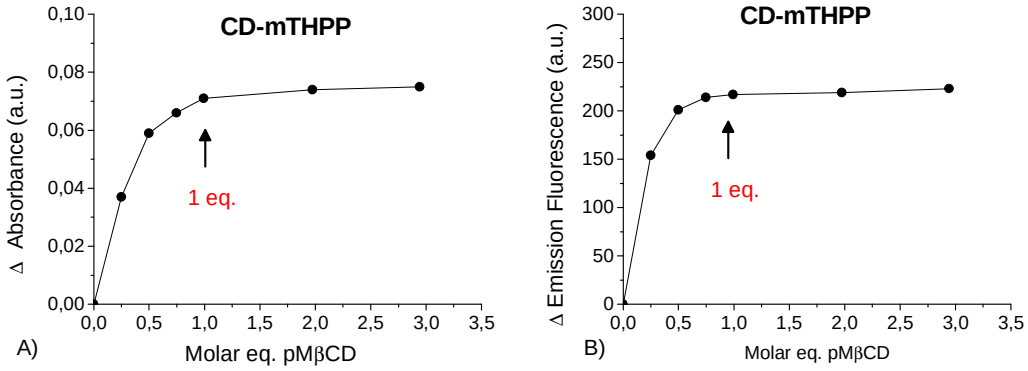

Figure 51. Titration experiment of CD-*m*THPP (2 μM) with pMβCD (300 μM) in 4 % DMSO/PBS. For every pMβCD addition the A) absorption and B) fluorescence maximum were followed until an excess of 3 molar eq. is present in solution.

In the literature, 1:1 complexes of pMβCD were reported with unsymmetrical substituted tetraphenylporphyrins like 5,10,15–tris(3,5-dicarboxylatophenyl)-20-phenyl-porphyrin. These were formed through inclusion of the only non-polar phenyl group, leaving excluded from the pMβCD cavity the bulky and polar substituent (3,5–dicarboxy-phenyl ring) [152]. The preferred 1:1 stoichiometry for these complexes is similar to the stoichiometry found for pMβCD/CD-*m*THPP and can be explained due to the steric hindrance offered by the βCD unit of CD-*m*THPP that blocks the access of more pMβCD units to adjacent phenyl groups in CD-*m*THPP structure.

These results show that pMβCD increased the solubility of both *m*THPP and CD-*m*THPP in aqueous solutions, leading to the decrease in aggregation attributed to the formation of water-soluble complexes of different stoichiometries.

Non-linear least square fitting method was used to determine the binding constants of complexation (K), based on UV-Vis titration data represented in Figure 50 A (pMβCD/*m*THPP) and Figure 51 A (pMβCD/CD-*m*THPP). Equations describing a 1:1 model of complexation were applied for pMβCD/CD-*m*THPP leading to $K_{(1:1)}$ = 3.8 ± 1.59 x 10^6 M^{-1} (goodness of fit, R^2 = 0.9954). The value of $K_{(1:1)}$ for the conjugate is in line with that reported for a similar conjugate, prepared from reaction of 5-(*p*-aminophenyl)-10,15,20-tris(*p*-sulfonatophenyl)-porphyrin with 6-deoxy-6-formyl-βCD, with pMβCD forming a 1:1 complex: $K_{(1:1)}$ = 3.0 × 10^6 M^{-1}, determined in 0.1 M ammonium carbonate, pH = 8.5) [157]. It also agrees with $K_{(1:1)}$ = 1.1 x 10^7 M^{-1}, found for complexation of pMβCD 5,10,15-tris(3,5-dicarboxylatophenyl)-20-

phenylporphyrin in phosphate buffer (0.1 M, pH = 7.4) [152]. In another example, βCD-dimers connected through flexible spacers were able to accommodate anionic porphyrins namely: 5,10,15,20-tetra(4-carboxyphenyl)-porphyrin (TCPP) and $TPPS_4$ and two different modes of complexation were identified for 1:1 complexes, with $K_{(1:1)} \approx 10^6\ M^{-1}$, determined in phosphate buffer (0.1 M, pH = 7) [158]. The strength of the binding of pMβCD with tetra(phenyl)-porphyrins depends on the charge of the included phenyl group, because anionic 5,10,15,20-tetra(4-sulfonatophenyl)-porphirin ($TPPS_4$), $K_{(1:1)} = 2.0 \pm 1.3 \times 10^4\ M^{-1}$ revealed stronger binding constant than cationic 5,10,15,20-tetrakis[4-(3-pyridiniumpropoxy)phenyl]-porphyrin (TPPOC3Py), $K_{(1:1)} = 2.3 \pm 0.9 \times 10^3\ M^{-1}$ determined in ethylene glycol (EG)-water (H_2O) (3:1) [149]. The binding of non-ionic tetraphenylporphyrins is even stronger.

The complex pMβCD/*m*THPP, through the application of a 2:1 model of complexation revealed an overall binding constant $K_T = K_{(1:1)} \times K_{(2:1)} = 4.9 \times 10^{12}\ M^{-2}$. The shape of the titration curve does not show two distinct binding steps (Figure 50 A) and thus a negligible concentration of intermediate 1:1 complex can be assumed in the determination of K_T for pMβCD/*m*THPP. This value is much larger than the values found for similar complexes of pMβCD: i) $K_T = 2.16 \times 10^7\ M^{-2}$ with cationic porphyrin TPPOC3Py, and ii) $K_T = 1.2 \times 10^9\ M^{-2}$ with anionic $TPPS_4$, determined in EG-H_2O (3:1) [149]. Explanations for this unusually high stability of pMβCD with tetraphenylporphyrins have been proposed and are related with the absence of strong hydrogen-bonding network in pMβCD, that in native βCDs keeps the cavity rigid, but in pMβCD facilitates porphyrin binding via the induced fit mechanism [17]. This model is usually applied to explain the binding between a substrate and a CD's cavity, whereby the substrate not matching the exact dimensions of a cavity, forces small changes in the CD structure enabling a better accommodation of the guest. A striking example of this phenomena is the double self-inclusion of two pMβCD moieties, covalently attached to the 4-positions of the phenyl groups of 10,20-bis(3,5-dicarboxylatophenyl)-5,15-diphenylporphyrin, which involves a 360° rotation of two glucopyranose units in the pMβCD moieties [146]. Therefore, pMβCD has an extremely strong tendency to include porphyrins in its cavity.

5.2.4 Structural features of pMβCD complexes

Nuclear Magnetic Resonance (NMR) spectroscopy was used to identify and determine the structure of the complexes of pMβCD, with CD-*m*THPP and with *m*THPP. The ^{1}H and ^{13}C NMR spectral assignment of pMβCD has been described in the literature [159]. ^{1}H NMR spectra were supported by 2D NMR experiments based on correlation spectroscopy through bonds (HSQC; HMBC; COSY; TOCSY) and through-space dipolar correlation spectroscopy, that relies on nuclear Overhauser effect (NOESY; ROESY).

mTHPP / pMβCD

The addition of *m*THPP solubilised in MeOD-d_4 to an aqueous solutions of pMβCD (10 mM), leads to a gradual change in the typical ^{1}H NMR spectrum of pMβCD (Figure 52 B) that involves: the reduction of pMβCD original signals (Figure 52 B) and the corresponding increase of new resonance peaks, gradually evolving to a new ^{1}H NMR spectrum attributed to the resonances of pure pMβCD/*m*THPP complex (8.9 mM / 5.6 mM, R = 1.6, Figure 52 A), in 11 % MeOD / D_2O. These features are typical of a slow exchange process between free and complexed components in the NMR time-scale, according to the equations described in section 1.2. The slow exchange regime is typically associated with very strong binding, confirming the very high titration constant, derived from the titration experiments.

The overall increase in solubility of the *m*THPP (≈ 5.6 mM) promoted by the addition of pMβCD, results in a well-resolved aromatic region of the spectra (7.0 – 10.0 ppm) (Figure 52 C). The formation of inclusion complexes between *m*THPP and pMβCD was corroborated by the strong shielding noticed by the cavity proton of pMβCD cavity (CD-H_3, ≈ 0.53 ppm).

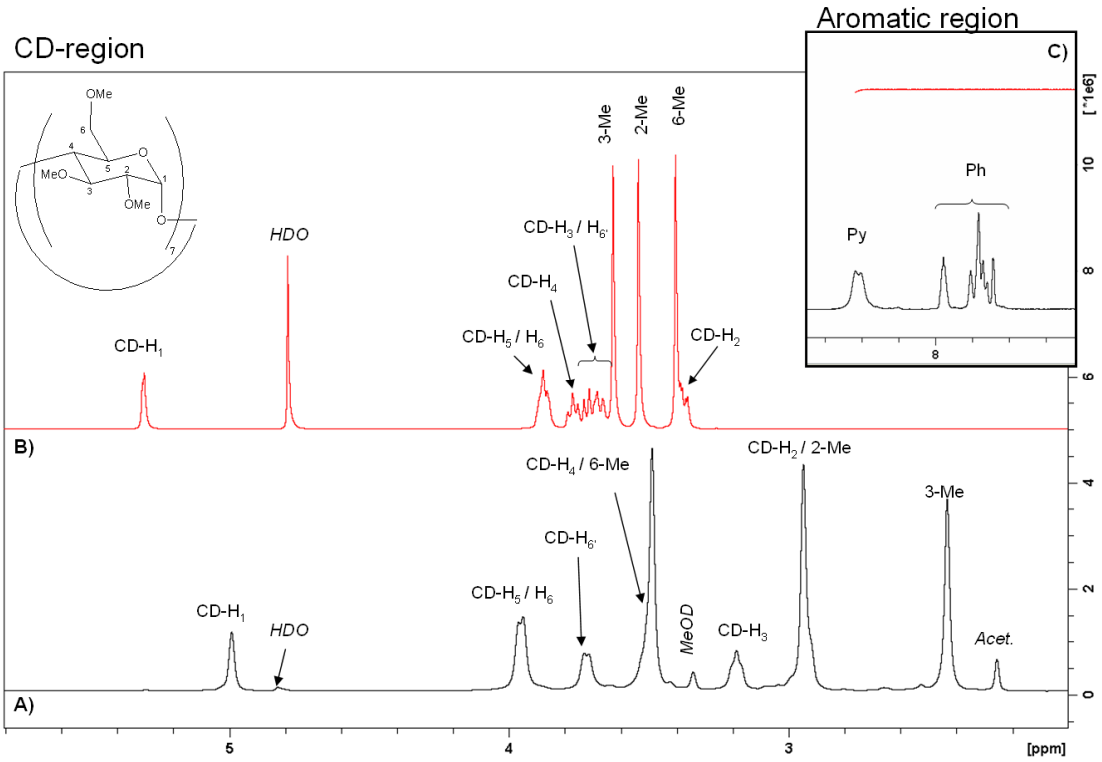

Figure 52. ^{1}H NMR spectra (500 MHz, 25 ºC) recorded in the aliphatic region (2.0 ppm – 6.0 ppm): A) pure complex pMβCD/*m*THPP (2:1) (8.67 mM / 5.6 mM, R = 1.54) in 11% MeOD-d_4/D_2O; B) pMβCD (8.67 mM) in D_2O and C) an expansion of the aromatic region (7.4 ppm – 8.6 ppm).

Further experimental evidence, supporting the existence of new species (complex: pMβCD/*m*THPP) was obtained from the 2D NMR HSQC experiments. These observations were possible due to a slow exchange equilibrium between *m*THPP, pMβCD (free / uncomplexed) and the complex pMβCD/*m*THPP. In the presence of a large excess of pMβCD (pMβCD/*m*THPP ≈ 4 (9.75 mM / 2.44 mM, R = 4), all *m*THPP added to the pMβCD solution is complexed and the remaining free pMβCD is in equilibrium with the complex, as observed by the multiple peaks corresponding to the uncomplexed (free) pMβCD and the complex (pMβCD/*m*THPP, green arrows, Figure 53 A). Following the addition of more mTHPP, the initial 2D HSQC spectrum evolves to a new 2D HSQC spectrum with only the complex is observed in solution (pMβCD/*m*THPP ≈ 2, 8.89 mM / 5.56 mM = 1.6, Figure 53 B).

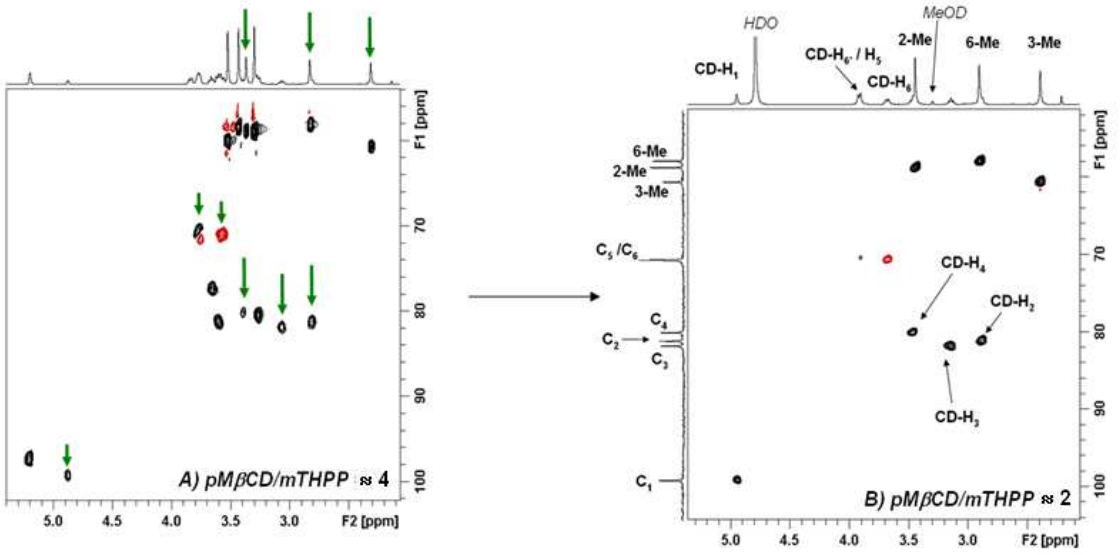

Figure 53. 2D NMR HSQC spectra (25 °C) expanded in the aliphatic region (2.0 – 5.5 ppm) in the presence of: A) excess of host pMβCD/*m*THPP ≈ 4 (9.75 mM / 2.44 mM, R = 4.0) and B) in equilibrium with pMβCD/*m*THPP ≈ 2 (8.67 mM / 5.56 mM = 1.6).

The 2D NMR ROESY experiments were conducted to determine the structure of the inclusion complex formed pMβCD/*m*THPP (Figure 54 A), with an estimated stoichiometry of two-to-one (2:1) illustrated by the proposed model of inclusion (Figure 54 B).

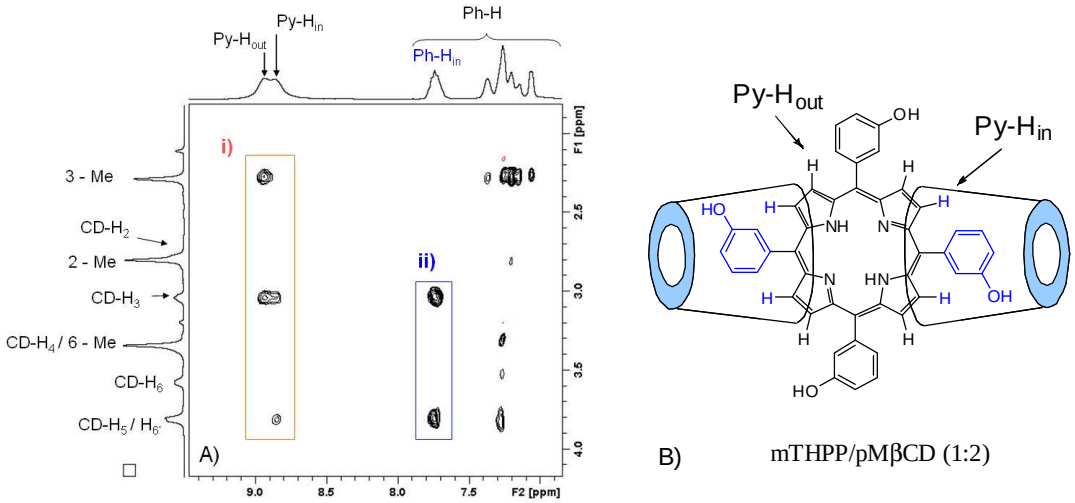

Figure 54. A) 2D NMR ROESY spectrum (25 °C) of the complex pMβCD/*m*THPP (2:1) (8.67 mM / 5.6 mM, R = 1.6) in 11 % MeOD-d_4 / D_2O revealing through-space correlations between βpen and *m*THPP, namely: i) two set of pyrroles (Py-$H_{out/in}$) and with ii) the included phenyl rings (Ph-H_{in}); B) proposed inclusion model following a 2:1 stoichiometry.

In complex pMβCD/*m*THPP, two pMβCD units approach one *m*THPP unit through opposite sides and capture two phenyl groups (blue Ph_{in}, Figure 54 B), which show strong dipolar interactions with CD-H_3/H_5 (Figure 54 A, ii). pMβCD captures the two opposed phenyl groups, through inclusion from the secondary side of the macrocycle which implies that pMβCD internal protons (CD-H_3/H_5) are closer to the pyrrolic protons included (Py-H_{in}) than to those not included (Py-H_{out}); these show interactions with 3-Me, CD-H_3 and CD-H_5 (Figure 54 A, i).

CD-mTHPP / pMβCD

Similarly, to evaluate the effect of adding pMβCD to a CD-*m*THPP solution, the ^{1}H NMR spectrum of a solution containing pMβCD was gradually recorded, following the addition of CD-*m*THPP diluted in DMSO. Figure 55 A shows the ^{1}H NMR spectrum of a solution containing pMβCD/CD-*m*THPP (4.79 mM / 2.49 mM; R = 1.92) and reveals peaks assigned to the complex pMβCD/CD-*m*THPP (*, Figure 55 A) and a reasonable amount of free pMβCD present in solution, when compared to the pMβCD spectrum (Figure 55 B).

The similarity between the chemical shifts observed for the complex pMβCD/CD-*m*THPP (*, Figure 55 A) and the pure pMβCD complex of the porphyrin (pMβCD/*m*THPP, Figure 52 A), indicates that both complexes possess similar structural features. Using approximately the same ratio (R) between host : guest to prepare both complexes (pMβCD/*m*THPP, R = 1.6 and pMβCD/CD-*m*THPP, R = 1.9), in pMβCD/CD-*m*THPP there is still an large excess of pMβCD in solution (Figure 55 A), which means that a different stoichiometry must be ruling the complexation of pMβCD/CD-*m*THPP. The stoichiometry of pMβCD/CD-*m*THPP complex was determined from the integration of the ^{1}H NMR signals (Figure 55 A), namely through integration of the signals in the aromatic region (24 H) attributed to Py-H and Ph-H and those in the aliphatic region (7 H), where CD-H_3 signal is expected (≈ 3.1 ppm). The value determined corresponds to a ratio of 24 H : 7.7 H, which is in agreement with the expected 24 H : 7 H suggesting a 1:1 stoichiometry, like determined from UV-Vis / fluorescence titration experiment.

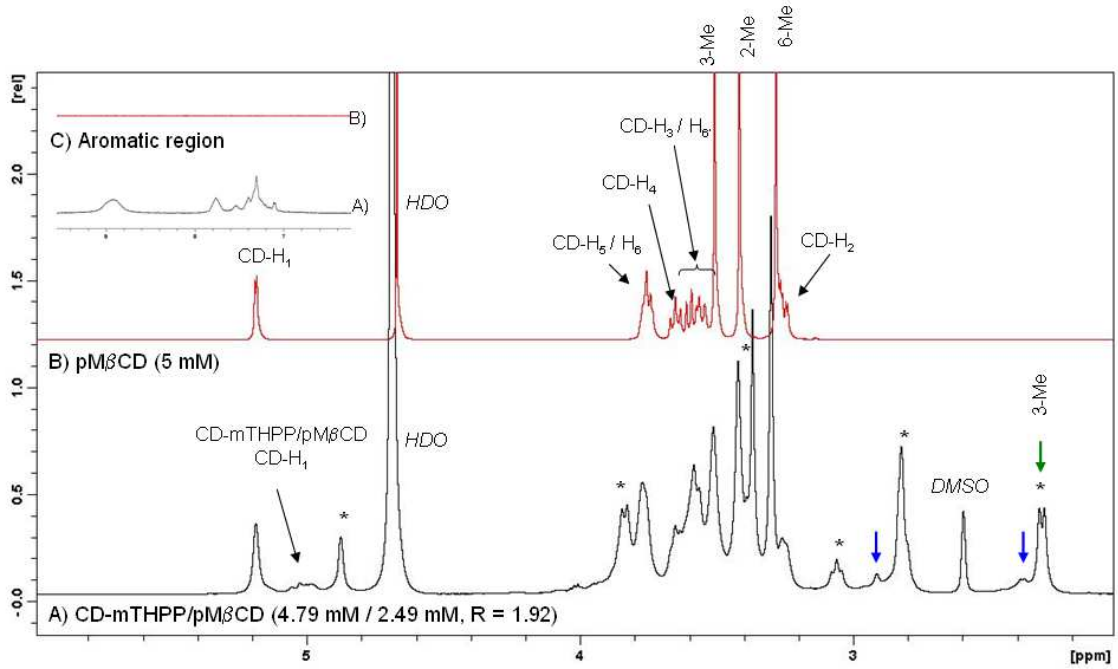

Figure 55. ^{1}H NMR spectra (500 MHz, 25 ºC) recorded in the aliphatic region (2.0 ppm – 6.0 ppm): A) pMβCD/CD-*m*THPP (4.79 mM / 2.49 mM; R = 1.92 in 4 % DMSO/D_2O; B) pMβCD (5 mM) in D_2O and C) an aromatic region expansion (6.5 – 9.5 ppm).

Additionally, the ^{1}H NMR spectrum of CD-*m*THPP in the presence of an excess of pMβCD (pMβCD/CD-*m*THPP, 4.79 mM / 2.49 mM; R = 1.92, Figure 55 A) reveals extra unexpected ^{1}H NMR peaks and features that are not observed for *m*THPP (pMβCD/*m*THPP, 8.67 mM / 5.6 mM, R = 1.6, Figure 52 A), even though the concentration of *m*THPP (5.6 mM) was higher than CD-*m*THPP (2.49 mM). The new ^{1}H NMR features comprise: i) small extra peaks (blue arrows) and ii) splitting of 3-Me peak (green arrow), both observed in Figure 55 A.

Likewise, the complex pMβCD/CD-*m*THPP revealed a 2D ROESY (Figure 56) with similar dipolar correlation peaks, to those observed for the complex pMβCD/*m*THPP with a 2:1 stoichiometry (Figure 54 A), namely: the engulfment of one phenyl ring by the pMβCD macrocycle (Figure 56, region ii) and the two set of pyrroles (Py-$H_{in/out}$) shifted into to signals, due to the approach of pMβCD cavity (Figure 56, region i). The proposed mode of inclusion for this 1:1 pMβCD/CD-*m*THPP complex is shown in Figure 57.

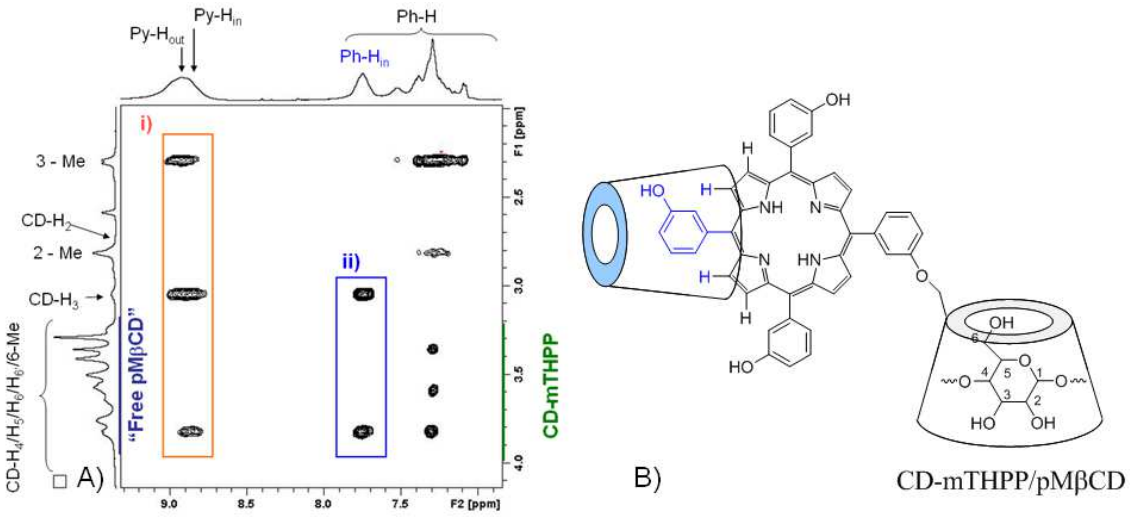

Figure 56. A) 2D NMR ROESY spectrum (25 ºC) of the complex pMβCD/CD-*m*THPP (4.79 mM / 2.54 mM, R = 1.88) in 4 % DMSO/D_2O revealing through-space correlations between βpen and CD-*m*THPP, namely: i) two set of pyrroles (Py-$H_{out/in}$) and with ii) the included phenyl rings (Ph-H_{in}); B) proposed inclusion model following a 1:1 stoichiometry.

In the presence of excessive pMβCD in solution two things can happen, which might explain the extra ^{1}H MNR features observed, namely: i) formation of diastereoisomeric forms of pMβCD/CD-*m*THPP (1:1) complexes (Figure 57), which explains the split in 3-Me peak (green arrow, Figure 55 A) or/and ii) formation of other inclusion complexes of higher stoichiometries (Figure 58), either through inclusion of one of the remaining phenyl groups in the 1:1, pMβCD/CD-*m*THPP complex (blue arrows, Figure 55 A) or through the formation of dimers.

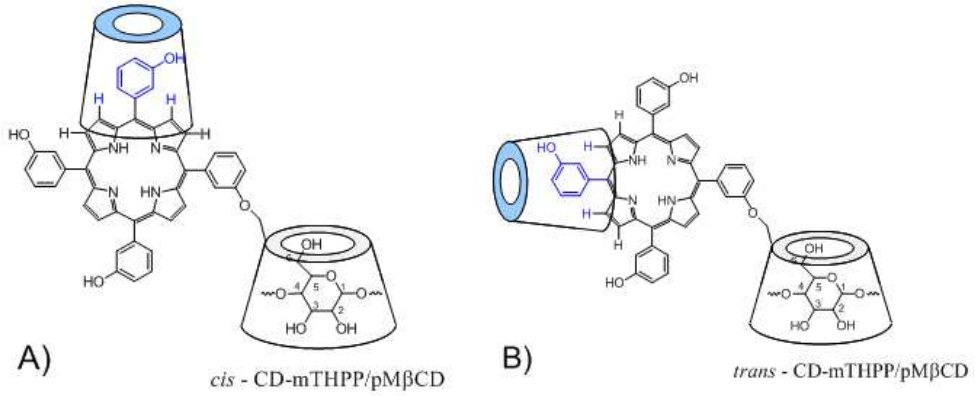

Figure 57. Diastereoisomeric forms of pMβCD/CD-*m*THPP (1:1) complexes: A) *cis*-pMβCD/CD-*m*THPP and B) *trans*- pMβCD/CD-*m*THPP.

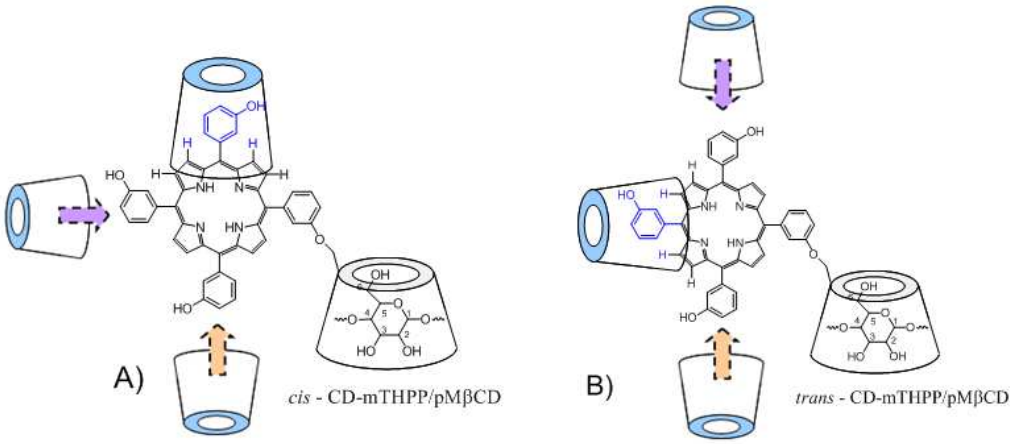

Figure 58. Formation of other inclusion complexes of higher stoichiometries, by attachment of free pMβCD units to the complex pMβCD/CD-*m*THPP (1:1). Multiple possibilities of approach A) *cis*-pMβCD/CD-*m*THPP and B) *trans*-pMβCD/CD-*m*THPP.

A product of the coupling reaction between 5-(*p*-aminophenyl)-10,15,20-tris(*p*-sulfonatophenyl)-porphyrin and 6-deoxy-6-formyl-βCD, formed a 1:1 complex with pMβCD with similar structural features [157]; however, the possibility of other pMβCD complexes has never been questioned.

In conclusion, both *m*THPP and CD-*m*THPP form stable water soluble, inclusion complexes with pMβCD. pMβCD/*m*THPP complex follows a well-defined 2:1 stoichiometry; whereas pMβCD/CD-*m*THPP, follows a major 1:1 stoichiometry but the existence of other complexes may not excluded, especially in the presence of excess of pMβCD. Aqueous solutions of pMβCD/*m*THPP reveal no signs of aggregation enabling NMR experiments using concentrations up to 5.6 mM, whereas pMβCD/CD-*m*THPP proved soluble in concentrations up to 2.5 mM. Additionally, pMβCD/*m*THPP (2:1) and pMβCD/CD-*m*THPP (1:1) showed very large binding constants in the order of 10^6 M^{-1} and 10^{12} M^{-2} for $K_{(1:1)}$ and $K_{(2:1)}$, respectively. These results suggest that in aqueous solution pMβCD is exclusively stationed on the *m*THPP moiety in CD-*m*THPP, leaving the βCD moiety available for further encapsulation of the guest. This possibility was studied next using selected guest molecules.

5.2.5 Complexation of selected guest molecules

After enhancing the solubility of CD-*m*THPP in 4 % DMSO/D_2O, through the use pMβCD acting as solubilizer, the complexation studies of selected guest molecules could be carried out.

Given the large binding constant of pMβCD/CD-*m*THPP (1:1) $K_{(1:1)} = 10^6\ M^{-1}$, it is expected that once formed, this pMβCD complex of CD-*m*THPP is stable enough not to be dissociated by any extra pMβCD. Thus, depending on the ratio of CD-*m*THPP to pMβCD used in the preparation the water-soluble complex pMβCD/CD-*m*THPP (1:1), there is always the question of knowing if the excess of pMβCD used as solubilizer will compete with the expected ability of the water-soluble complex (pMβCD/CD-*m*THPP, 1:1), to include and carry suitable-sized molecules. The presence of pMβCD as solubilizer poses more difficulties regarding the evaluation of analysis of inclusion phenomena by NMR spectroscopy, due to the large overlapping in the aliphatic region of the spectrum namely where the conjugate internal cavity protons (CD-H_3/H_5) signals are expected (3.2 ppm – 4.9 ppm). Therefore, to evaluate the formation of inclusion complexes between complexed CD-*m*THPP and any guest molecules, 2D NOE experiments will be performed in parallel, both for CD-*m*THPP alone and in the presence of the guest molecule.

To assess the availability of the cavity of CD-*m*THPP to accommodate suitable guest molecules, two model molecules have used: i) 1-adamantanamine (ADA-NH_3Cl), followed by *N*-desmethyltamoxifen (NDTAM.HCl) an anticancer drug (tamoxifen, TAM) major metabolite molecule.

1-Adamantanamine hydrochloride (ADA-NH_3Cl)

Starting from a clear solution of pMβCD/CD-*m*THPP (R = 0.91) prepared in 4 % DMSO/D_2O, the initial ^1H NMR spectrum was recorded (Figure 59 A). Then, ADA-NH_3Cl (0.36 μmol) dissolved in 4 % DMSO/D_2O was added to the solution and a second spectrum was recorded (Figure 59 B), followed by 2D NMR experiments. A complete solubilisation was achieved during the preparation of the complex pMβCD/CD-*m*THPP and after addition of ADA-NH_3Cl and their characteristic aliphatic: H_4/$H_{4'}$ (1 ppm), $H_{2'}$/H_3 (1.75 ppm) and H_2 (2.2 ppm) (Figure 59 B) could be detected. Given that the intensity of CD-H_1 of free pMβCD (5.1 ppm), does not change after the addition of ADA-NH_3Cl the integrity of the complex initially formed (pMβCD/CD-*m*THPP, R = 0.91) is not affected. Following the addition of ADA-NH_3Cl to the solution of pMβCD/CD-*m*THPP, the fine structure of spectra changed in the region between 3.4 ppm – 3.8 ppm, corresponding to the region where the internal protons of

pMβCD/CD-*m*THPP are expected (blue colour CD-H_3/H_5, Figure 59 A), which can attributed to the inclusion phenomenon. An expansion over the aromatic region (Figure 59 C) reveals a complete overlapping and good resolution, indicating that the structure of the inclusion complex formed (pMβCD/CD-*m*THPP, 1:1) does not changed by the addition of ADA-NH_3Cl.

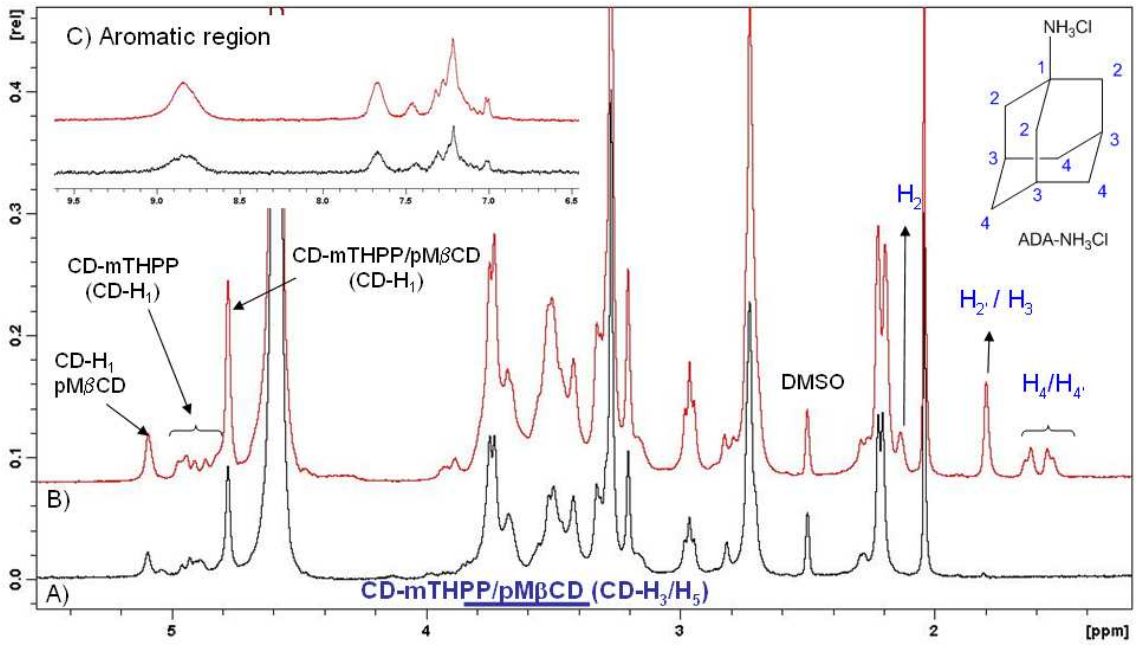

Figure 59. ^{1}H NMR spectra (4 % DMSO-d_6/D_2O, 500 MHz, 25 °C) of A) CD-*m*THPP : pMβCD = (2.21 mM / 2.00 mM; R = 1.10) and B) after the addition of ADA-NH_3Cl (0.36 µmol; 0.71 mM). C) expansion of ^{1}H NMR, comprising the aromatic region (6.5 ppm – 9.0 ppm).

To determine if the small changes in the aliphatic region of interest (3.4 ppm – 3.8 ppm) are due to complexation of ADA- NH_3Cl in the cavity of CD-*m*THPP, through-space interactions were determined by a 2D ROESY NMR experiment (Figure 60 A). The expansion over the region of interest, reveal strong interaction of protons of the base of adamantane moiety (H_4/$H_{4'}$) with the internal proton pMβCD/CD-*m*THPP (CD-H_5). This suggests a preferred orientation for the inclusion complex, with the charged amino group (-NH_3Cl) facing the secondary side of the cavity, with the adamanatane moiety being deeply inserted into the cavity, like illustrated by much stronger interaction of cavity proton H_3 with all other 1-adamantanamine protons (Figure 60 B).

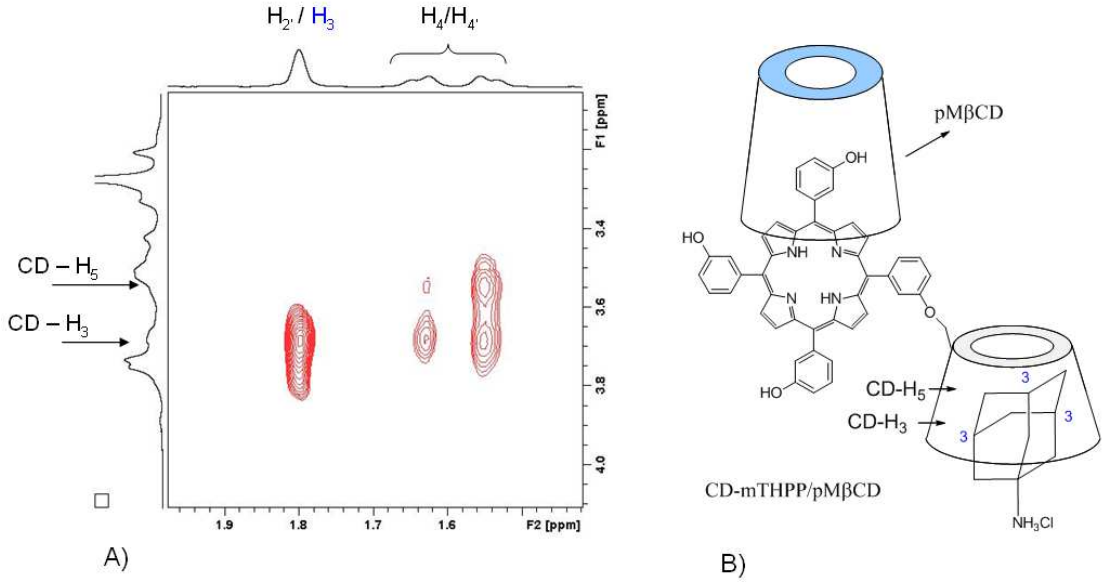

Figure 60. A) 2D NMR ROESY spectrum (25 ºC) revealing through space intermolecular interactions, between CD-*m*THPP cavity protons (CD-H_3/H_5) and ADA-NH_3Cl peaks; B) proposed model of inclusion.

Gemcitabine-adamantanamide (GEM-ADA amide)

GEM-ADA amide prepared in our group (see section 10.3.1) was tested as possible guest in a complexation study with CD-*m*THPP, in the presence of pMβCD used as a solubilizer. A host solution CD-*m*THPP : pMβCD (1.14 mM / 1.67 mM, R = 0.68) was prepared using an excess of pMβCD. Under these conditions, although the ^{1}H NMR spectrum (Figure 61 A) shows no peaks attributed to free pMβCD, the signals (green areas *, Figure 61 A) due to other inclusion species, possibly involved in solution were observed, once again, in the presence of an excess of pMβCD (≈ 1.46 molar excess). The identity of the signals was corroborated by 2D NMR ROESY experiment. After addition of GEM-ADA amide in excess (≈ 2 molar eq.) to this solution (4 % DMSO/ D_2O), it was observed that GEM-ADA is poorly water-soluble and to ease its solubilisation, the solution was sonicated and vortexed before the ^{1}H NMR and 2D NMR experiments were conducted to evaluate complexation equilibrium. The typical ^{1}H NMR spectrum of pMβCD/CD-*m*THPP, after addition of GEM-ADA amide revealed: i) the peaks corresponding to the adamantane moiety, between 2.0 ppm – 1.0 ppm (blue circle, Figure 61); ii) the aromatic protons of the pyrimidine ring (blue H_5/H_6) as well as iii) the hydroxyl groups (-OH) of the pentose unit, in position 3' and 5' of the in GEM-ADA amide shown in the expansion (Figure 61 C).

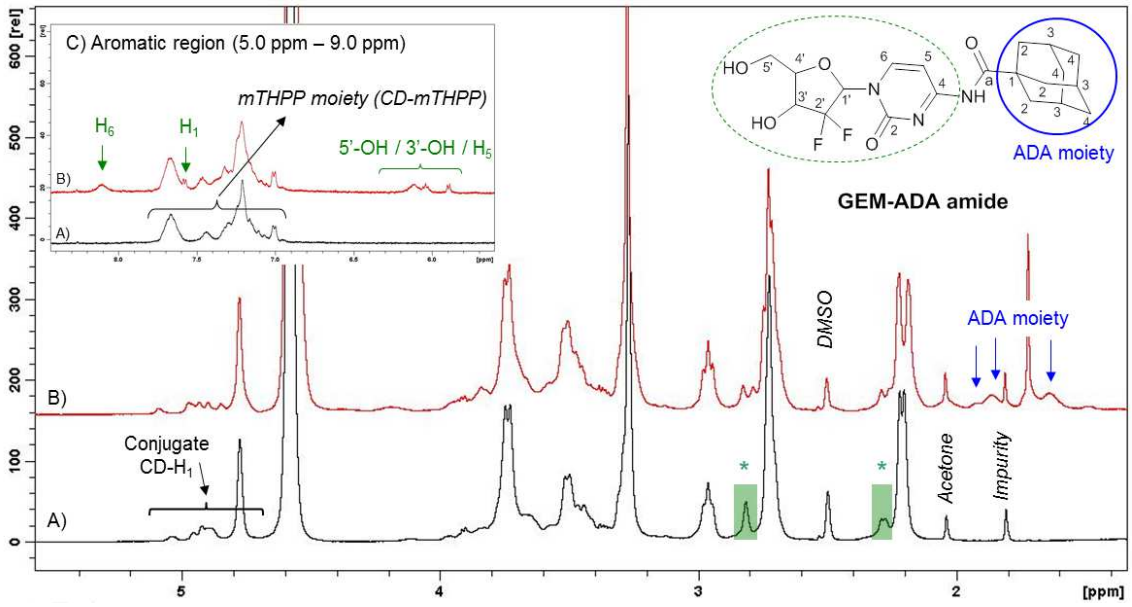

Figure 61. ^{1}H NMR spectra (4 % DMSO-d_6/D_2O, 500 MHz, 25 °C) of A) CD-*m*THPP / pMβCD (1.11 mM / 1.67 mM; R = 0.68) and B) after the addition of an excess of GEM-ADA amide (1.20 μmol; 2.45 mM) and C) an expansion comprising the aromatic region (5.0 ppm – 9.0 ppm).

The 2D ROESY NMR experiment performed (Figure 62 A) revealed through-space interactions, between pMβCD/CD-*m*THPP internal protons (CD-H_3/H_5, 3.6 ppm – 3.8 ppm) and GEM-ADA amide. The strong off-diagonal contours suggest the formation of inclusion complexes, with ADA moiety in GEM-ADA amide (blue circle, Figure 62 A) being deeply inserted into CD-*m*THPP cavity, interacting with CD-H_3/H_5 internal protons of the conjugate. The proposed model of inclusion suggests a similar mode of interaction to that shown by pMβCD/CD-*m*THPP and ADA-NH_3Cl. Additionally, 2D experiments applied to the structural characterization of GEM-ADA amide suggested that ADA moiety is spatially distant from the pentose and pyrimidine moieties, which corroborates the proposed geometry of inclusion involving the insertion of ADA moiety into CD-*m*THPP cavity of the complex pMβCD/CD-*m*THPP (1:1) (Figure 62 B).

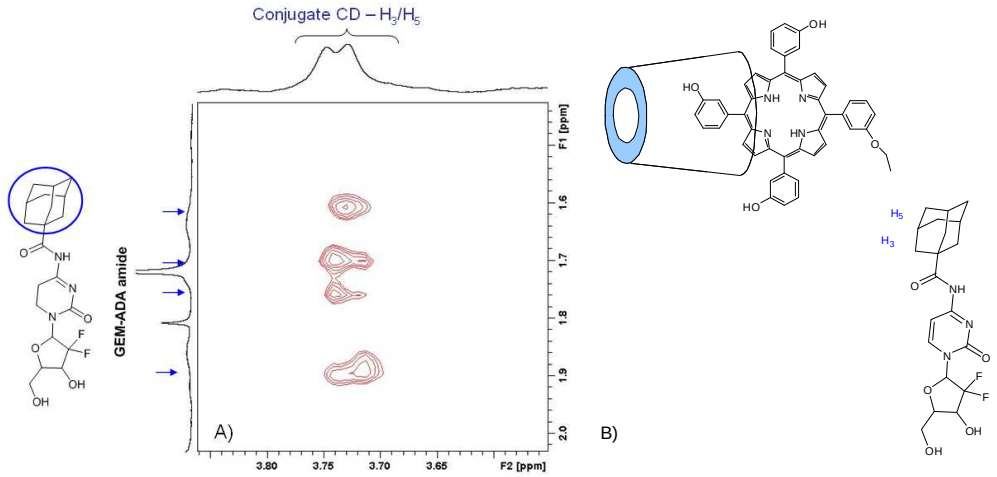

Figure 62. A) 2D ROESY NMR spectrum (500 MHz, 25 ºC) revealing through space intermolecular interactions, between CD-*m*THPP cavity protons (CD-H_3/H_5) and GEM-ADA amide peaks; B) proposed model of inclusion.

N-desmethyltamoxifen hydrochloride (NDTAM.HCl)

N-desmethyltamoxifen hydrochloride (NDTAM.HCl) is a major metabolite of the anticancer drug tamoxifen (TAM), whose properties are reviewed in section 6.1. CD-*m*THPP ability to include NDTAM.HCl was evaluated in 4 % DMSO/D_2O in the presence of pMβCD acting as solubilizer. Although, NDTAM.HCl has improved solubility comparatively to TAM, due to the strong red colour of pMβCD solutions of CD-*m*THPP it was difficult to evaluate visually the complete solubilisation of NDTAM.HCl of its addition to a pMβCD/CD-*m*THPP solution. The ideal compromise would be reached through the addition of only the right amount of free pMβCD, matching the exact stoichiometric ratio resulting in: i) the complete solubilisation of CD-*m*THPP; ii) ensure that all pMβCD in solution is complexed with the conjugate and there is no free pMβCD able to interact with the guest molecule (NDTAM.HCl) and finally, iii) this would maximize the inclusion of NDTAM.HCl by the soluble complex pMβCD/CD-*m*THPP

Therefore, a series of trials using different ratios of CD-*m*THPP, pMβCD and NDTAM.HCl have been performed to judge the complexation / inclusion of NDTAM.HCl in 4 % DMSO/D_2O (Table 5).

^{1}H NMR spectrum of pMβCD : CD-*m*THPP (1.96 mM : 1.06 mM : R = 1.83) in 4 % DMSO/D_2O (Figure 63 A) shows that: i) in the aliphatic region (3.0 ppm – 4.0 ppm), there is a big overlap between protons of free pMβCD (*, Figure 63 A) used in excess, and the signals of complex pMβCD/CD-*m*THPP. This solution was red coloured and visually showed no signs of

aggregation, corroborated by the very well-resolved spectrum in the aromatic region (6.0 ppm – 9.0 ppm, Figure 63 C) (Trial # 1, Table 5).

However, to avoid the excess of pMβCD in solution, more CD-*m*THPP (0.40 μmol) was gradually added as a solid, until no ^{1}H NMR signals corresponding to free pMβCD were observed. Unfortunately, the increase in concentration of conjugate from 1.06 mM to 1.86 mM, lead to cloudiness in the solution which is due to the poor solubility of CD-*m*THPP in 4 % DMSO/D_2O (Trial # 2, Table 5). This was corroborated by extra experiments, where the addition of CD-*m*THPP as a solid to an aqueous solutions of pMβCD resulted in precipitation, which was not observed if CD-*m*THPP was added prior to an initial solubilisation in DMSO. In the presence of a large excess of CD-*m*THPP with respect to pMβCD (2.32 mM : 0.66 mM : R = 3.51), the solution immediately precipitates and a 0.45 μm filter had to be used to remove most of insoluble material and clarify the solution (trial # 4, Table 5), The addition of NDTAM.HCl (0.51 μmol) to the clear solution resulted in cloudiness (trial # 5, Table 5), which indicated that NDTAM.HCl by itself shows limited solubility in solutions of pMβCD/CD-*m*THPP in 4 % DMSO/D_2O.

Table 5. Ratio of CD-*m*THPP, pMβCD and NDTAM.HCl used in the preparation of solutions for NMR experiments to test inclusion of NDTAM.HCl in CD-*m*THPP. Total volume of NMR tube 0.5 mL.

# Trial	CD-*m*THPP n (μmol), A	pMβCD n (μmol), B	NDTAM.HCl n (μmol)	R (B/A)	Notes / Observations
1	0.53	0.98	-	1.83	Clear solution
2	0.93	0.98	-	1.05	Addition of CD-*m*THPP / Cloudiness
3	0.93	0.98	0.43	1.05	Precip.
4	1.16	0.33	-	0.28	Heavy Precip. / Filtration
5	1.16	0.33	0.51	0.28	Cloudiness

Figure 63 B (trial # 3) shows the ^{1}H NMR spectrum of trial # 2 after addition of NDTAM.HCl (0.43 μmol), which resulted in cloudiness. NDTAM.HCl signals are observed in the aromatic region of the spectrum (6.8 ppm – 8.0 ppm), with peaks corresponding to the phenyl rings aromatic protons (Ph-$H_{a/b/c}$) indicated as black arrows in Figure 63 C. Therefore, even though different ratios of pMβCD/CD-*m*THPP are used to prepare clear solutions, the addition of NDTAM.HCl results in cloudiness.

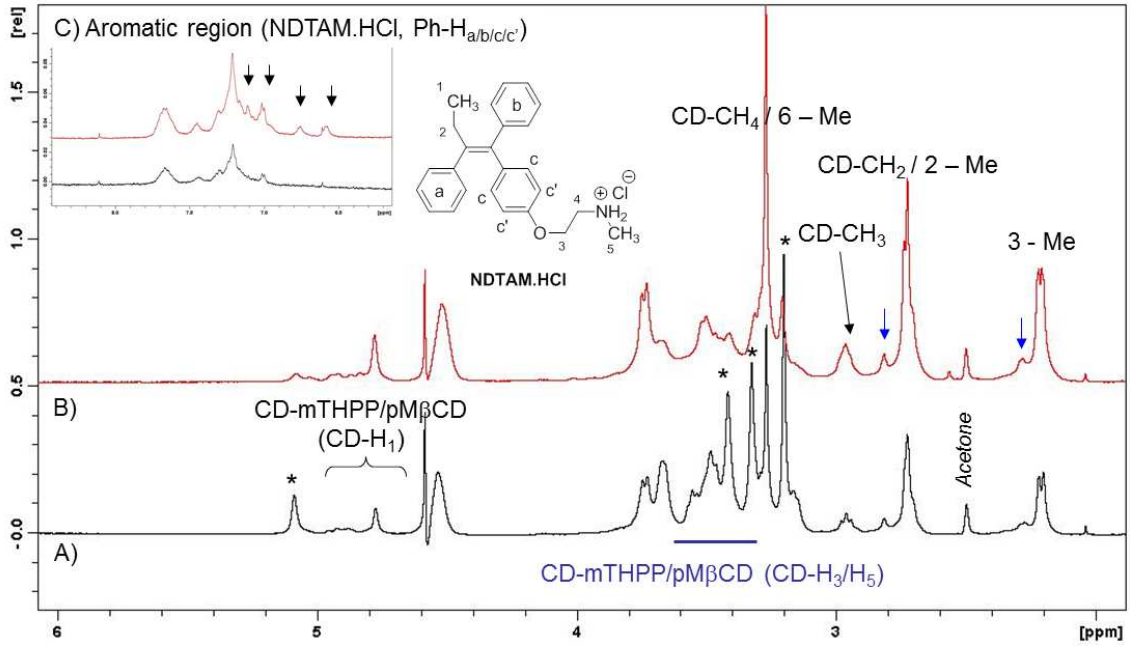

Figure 63. ^{1}H NMR spectra (4 % DMSO- d_6/D_2O, 500 MHz, 25 °C) of CD-*m*THPP / pMβCD A) before (# trial 1, Table 5); B) after the addition of NDTAM.HCl (# trial 3, Table 5) and C) an expansion comprising the aromatic region (5.0 ppm – 9.0 ppm).

The inclusion complex formation of pMβCD/CD-*m*THPP with NDTAM.HCl is expected to occur through interaction of the protons of βCD cavity of CD-*m*THPP and the phenyl rings (Ph-$H_{a/b/c}$) of NDTAM.HCl. Additionally, the inclusion is expected to occur through the secondary side of the CD unit and chemical shift differences (shielding of the inner protons CD-H_3/H_5) is expected. Besides, previous work in our laboratory has shown that NDTAM forms a strong enough complex with native βCD (K = 7 x 10^3 M^{-1}) via tritopic binding *i.e.* inclusion of each of the phenyl rings (Ph-$H_{a/b/c}$) in the cavity of βCD at any time [141].

Due to big overlap in the aliphatic region of spectrum (3.4 ppm – 3.8 ppm), where the internal protons of cavity of the conjugate in the complex are expected, this region is indicated in blue CD-H_3/H_5 in Figure 63 A.

Therefore, 2D HSQC NMR spectrum was used to determine and compare the chemical shifts differences of CD-H_3/H_5 of the conjugate in pMβCD/CD-*m*THPP, righ before (trial # 4, Table 5) and immediately after the addition of the NDTAM.HCl (trial # 5, Table 5). The comparison between 2D HSQC spectra before (Figure 64 A, i) and after the addition of NDTAM.HCl (Figure 64 A, ii) revealed that the signals corresponding to complexed pMβCD (CD-$H_{6'}$/CD-H_3/CD-H_4) and the only peaks changing are those attributed to the complexed conjugate conj (CD-$H_{6'}$/CD-H_3/CD-H_4). Furthermore, the two internal protons revealed significant shielding (blue boxes, Figure 64 A), which agrees with the formation of an inclusion

complex between NDTAM.HCl phenyl moieties and the conjugate pMβCD/CD-*m*THPP internal protons, namely: CD-H_3 (shielded, 0.06 ppm) and CD-H_5 (shielded, 0.106 ppm).

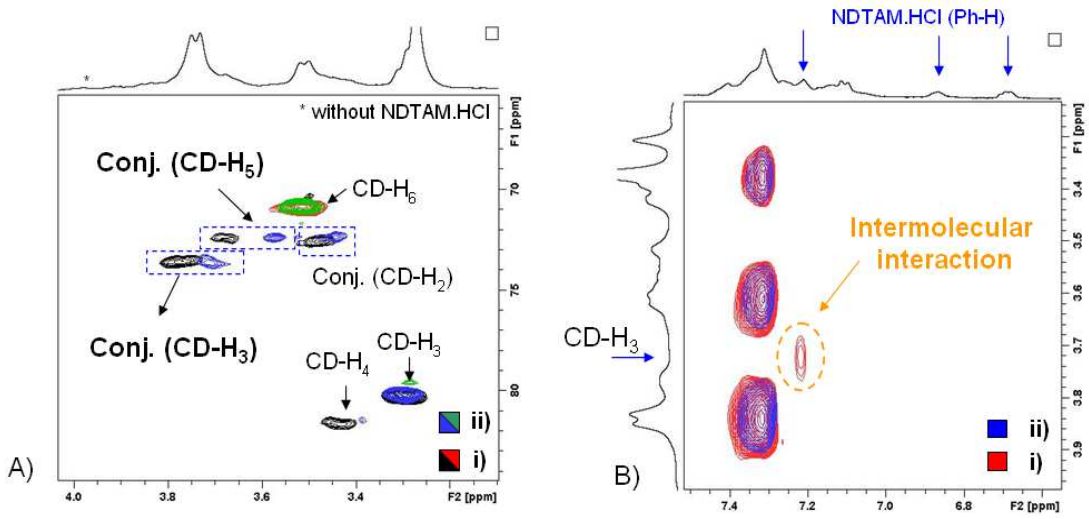

Figure 64. 2D experiments in 4 % DMSO- d_6/D_2O of pMβCD/CD-*m*THPP: A) 2D NMR HSQC spectra (25 ºC) in the presence of NDTAM.HCl (ii, trial # 5) and in the absence of it (i, trial # 4); and B) 2D NMR NOESY spectra (25 ºC) in the presence of NDTAM.HCl (i, trial # 2) and in the absence of it (ii, trial # 3).

Likewise, 2D NOESY experiments was performed to judge any dipolar interactions after addition of NDTAM.HCl, comparing solutions prior to (trials # 2, Figure 64 B ii) and after the addition of NDTAM.HCl (trials # 3, Figure 64 B i). The signals detected in the aromatic region are attributed to phenyl rings of NDTAM.HCl show one correlation with one of pMβCD/CD-*m*THPP internal cavity protons (CD-H_3 or CD-H_5). Assuming that CD-H_3 is closest to the secondary rim of βCD than CD-H_5, the strongest signal would be primarily due to interactions with CD-H_3, which from the 2D ROESY corresponds to a chemical shift of ≈ 3.72 ppm. Consequently, from the 2D HSQC the chemical shifts observed earlier, are attributed to CD-H_3 (≈ 3.8 ppm) than for CD-H_5 (≈ 3.5 ppm), the protons of the conjugate involved in complexation.

This experiment showed that NDTAM.HCl although is poorly soluble in 4 % DMSO/D_2O solution, can be solubilised using pMβCD/CD-*m*THPP. Inclusion complexes are formed between NDTAM.HCl and the cavity of the conjugate in the complex, which can potentially result in a suitable drug delivery system for the delivery of TAM derivatives to cancer cells.

5.2.6 Cell internalization of pMβCD/CD-*m*THPP

An important pre-requisite for an effective therapeutic effect of a specific drug is its ability to get in contact with the affected tissue or organ, either by systemic administration or more recently through active or passive targeting. Thus, the evaluation of cell inclusion is an important biological parameter to determine if: i) the molecules cross the biological membranes and reach the desired target tissue, ii) if it targets a specific cell compartment. Confocal microscopy can be used successfully to determine cell internalization or even the specific localization of molecules into different cell compartments and for this purpose, it relies on the fluorescence properties of suitable fluorescence dyes [160]. The use of porphyrins, or porphyrin related compounds like CD-*m*THPP, in cell experiments offers the potential advantage of good photophysical properties (fluorescence) that enables easy detection by confocal spectroscopy without the need to use additional fluorescence dyes. However, this is hardly the case because of limited aqueous solubility of porphyrins and their conjugates, which impairs most of these applications. Recalling CD-*m*THPP synthesis, the successful use of pMβCD as efficient solubilizer and its ability to complex relevant guest molecules it is important to assess if: CD-*m*THPP on its own and upon complexation with pMβCD is able to cross cellular membranes and be localized specifically in one or more cell compartments.

Confocal microscopy was used to record images of cells exposed to the solutions with the compounds (CD-*m*THPP and pMβCD/CD-*m*THPP) incubated at 37 ºC with an atmosphere saturated in 5 % CO_2. Two cell lines were tested: i) a breast cancer cell line MCF7 and ii) a prostate cancer cell line DU145 incubated for different time intervals (3h – 15 h). Two different media were used, namely phosphate buffered saline (PBS) and Roswell Park Memorial Institute medium (RPMI3).

In the first experiment cell internalization trial was performed in MCF7 cells, incubated for 3 h in PBS in the presence of CD-*m*THPP (10 μM) revealed poor internalization. The presence of 0.45 (Table 6 B) and 1.00 molar eq. of pMβCD, even when laser intensity was set at 100 % to record the pictures, the results were not satisfactory. However, when CD-*m*THPP (10 μM) used alone (Table 6 A), a small improvement was noticed and small red fluorescent dots were observed.

In a second trial DU145 cells were incubated for 15 h and pictures were recorded using a laser intensity set at 30 %. In PBS, with CD-*m*THPP (8 μM) showed some cells internalization. The observed dotted fluorescence implied lysosomal or endosomal localization and not diffuse cytoplasmic dispersion (Table 6 C). Additionally, the plates revealed good cell density after 15 h incubation period, indicating that the dark toxicity, if any, should be very small. There was an improvement in the cell internalization of CD-*m*THPP (8μM), when

DU145 cells are incubated in the presence of 0.5 molar eq. of pMβCD (Table 6 D). However, when DU145 are incubated for the same period in RPMI in the presence of CD-*m*THPP (8 μM), better internalization was revealed qualitatively corresponding to intense dotted red fluorescence. Cell density during observations revealed that DU145 cells were not affected by the conditions used and dark phototoxicity should remain within acceptable levels in RPMI (Table 6 E). Interestingly, in the presence 0.5 molar eq. of pMβCD added to CD-*m*THPP (8 μM), dotted and intense red fluorescence always restricted to dotted structures was observed and these pictures were preferred (Table 6 F).

Table 6. Confocal pictures of cell internalization experiments: A) MCF7, CD-*m*THPP (10 μM, PBS), 3 h (laser: 100 %); B) like A) in the presence of 0.45 molar eq. of pMβCD; C) DU145, CD-*m*THPP (8 μM, PBS), 15 h (laser: 30 %); D) like C) in the presence of 0.50 molar eq. of pMβCD; E) DU145, CD-*m*THPP (8 μM, RPMI), 15 h (laser: 30 %); F) like E) in the presence of 0.50 molar eq. of pMβCD (molar eq. = molar equivalent).

	CD-*m*THPP(10 μM)	CD-*m*THPP(10 μM) + 0.45 pMβCD
MCF7, 3 h Incubation	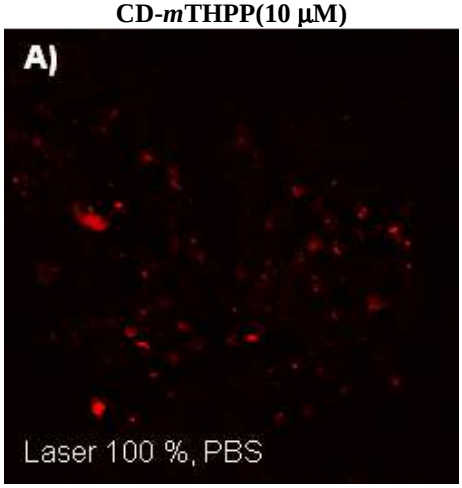	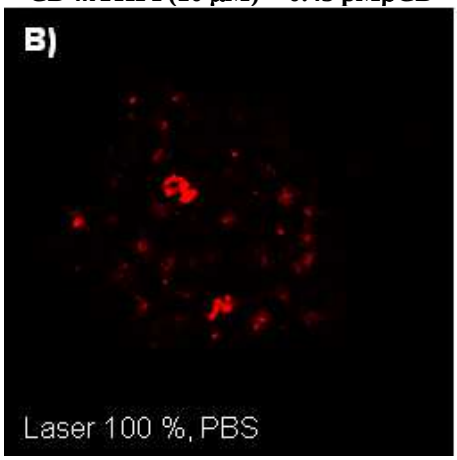
	CD-*m*THPP (8 μM)	**CD-*m*THPP (8 μM)+ 0.5 pMβCD**
DU145, 15 h Incubation	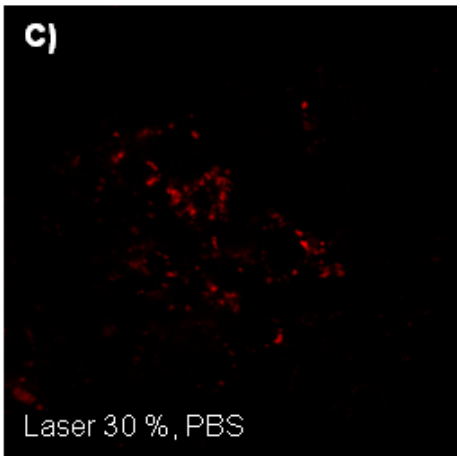	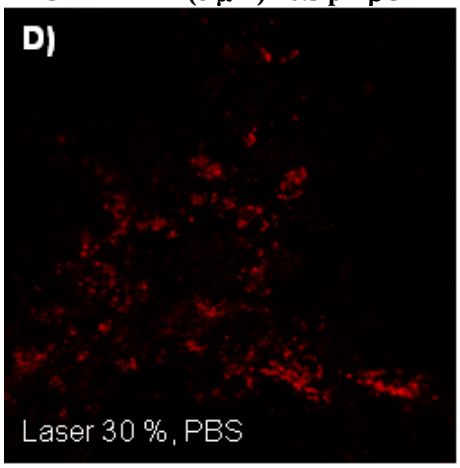
	CD-*m*THPP (8 μM)	**CD-*m*THPP (8 μM)+ 0.5 pMβCD**
DU145, 15 h Incubation	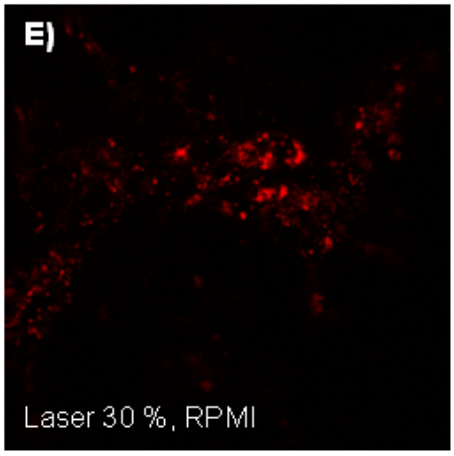	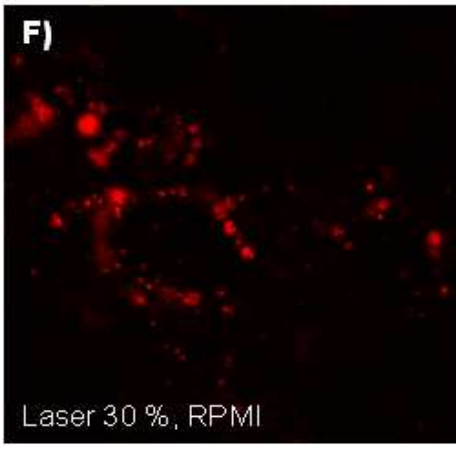

5.3 Conclusions and future perspectives

In this chapter, it was shown that the pure CD-*m*THPP conjugate revealed good properties acting as a bimodal molecular carrier. pMβCD used in stoichiometric amounts enhances the water solubility of CD-*m*THPP, through the formation of completely water-soluble complexes following a defined 1.1 stoichiometry.

The addition of an equimolar amount of pMβCD to solutions of CD-*m*THPP (2 μM, 4 % DMSO/PBS, pH = 7.4) resulted in 1.6-fold increase of UV-Vis absorbance and a 8-fold increase in fluorescence emission spectroscopy. The use of an excess of pMβCD enables the preparation of concentrated solutions of CD-*m*THPP (≈ 2.5 mM) suitable for structural analysis with no visual sign of aggregation. *m*THPP was used as a model compound and similar improvements were observed, but a 2:1 stoichiometry was ruling the slow equilibrium between pMβCD and *m*THPP. In both cases, pMβCD was anchored on *m*THPP moiety, leaving the βCD cavity of CD-*m*THPP free for inclusion.

Indeed, successful inclusion experiments of CD-*m*THPP in the presence of the model compound 1-adamantanamine (ADA-NH_3Cl) revealed that the cavity of CD-*m*THPP in the complex with pMβCD is available for inclusion with other molecules. Anticancer drug molecules, derivatives of tamoxifen (NDTAM.HCl) and of gemcitabine (GEM-ADA amide) proved successful guest molecules included into the cavity of pMβCD/CD-*m*THPP. The complexes, once formed, were not affected by the presence of excess of pMβCD in aqueous buffered solution (4 % DMSO/PBS, pH = 7.4), indicating the very high strength of binding. Indeed, the binding constants (K) for pMβCD/CD-*m*THPP 1:1 complex was $K_{(1:1)} \approx 3.8 \times 10^6$ M^{-1} and for the pMβCD/ *m*THPP 2:1 was $K_{(2:1)} \approx 4.9 \times 10^{12}$ M^{-2}.

Finally, CD-*m*THPP reveal good cell DU145 internalization properties, when incubated for a long period of time (15 h) using diluted solutions (8 μM – 10 μM) prepared in RPMI. CD-*m*THPP crossed the cell membrane, reached the cytoplasm and localized inside intracellular compartments. However, in the presence of ½ molar equivalent of pMβCD the intensity of the fluorescence emission was increased suggesting that the use of pMβCD may allow increase of administered concentration of CD-*m*THPP, alone or in a complex with suitable drug, thereby improving the delivery properties in aqueous media. The empty cavity of the βCD unit in the nanoaggregate (CD-*m*THPP) has been previously shown [144] to accommodate the nitrous oxide (NO) photodonor guest, thereby forming a supramolecular aggregate with diameter of about 16 nm, which preserved the fluorescence of the porphyrin core and was able to generate nitric oxide and singlet oxygen under illumination with visible light, conferring combined phototoxicity to cells, in agreement with the results presented here.

6. Modifications on selected anticancer drugs as guest molecules

6.1 Introduction

The discovery of new chemical entities (NCEs) is not as successful as it was in the beginning of the XIX century and currently, fewer NCE do actually reach the market. Currently drug discovery programs focus on identification of specific molecular targets, like enzymes, involved in critical biological activities and on the ability to design molecules (drugs) that interact with these specific targets by blocking its action. [161, 162].

Therefore, in an early stage of any formulation, the modulation of physicochemical properties of many NCEs can be achieved through proper chemical modification. An example of a critical property of any drug is its water-solubility that is related to bioavailability of the drug. It was estimated that 50 % of all the drugs approved for use as medicine display low aqueous solubility and most of the drugs administered orally, belong to class II (high permeability, low solubility) and class IV (low permeability, low solubility) of biopharmaceutical classification system (BCS) [163, 164].

Thus, a common challenge addressed by pharmaceutical technology is to find strategies to overcome the lack of water solubility of commonly administered drugs [165]. Reformulating any existing marketed drug should be cheaper, faster and safer than the effort considered for any NCE, as much of the information about the drug and biological effects are already known and can be used in advance [166]. Alternatively, direct chemical modifications of the structure of drugs may result in the modification of their physicochemical properties such as solubility.

In this chapter, one will explore the chemical modification of two drugs routinely used in cancer treatment (tamoxifen, TAM) and gemcitabine (GEM). The purpose of these chemical modification is: i) to increase the aqueous solubility of TAM, through preparation of of tamoxifen citrate salt (TAM-Cit) and one of its biological active metabolites, *N*-desmethyltamoxifen (NDTAM.HCl); ii) to prepare a starting material (NDTAM.HCl), suitable for chemical attachment to a fluorescence dye (fluorescein, FITC) resulting in NDTAM-FITC useful for cellular localization / distribution studies conducted by confocal microscopy; and, iii) preparation of and gemcitabine (GEM) attached to an adamantane (ADA) moiety tailored for complexation studies with CD-*m*THPP and CD-polymers.

6.2 Results and discussion

6.2.1 **Preparation of tamoxifen derivatives**

Tamoxifen

Cancer is associated with unusual growth of living cells in an organism. Many forms of breast cancer are a result of wrong signalling messages sent by sex hormones like estrogens. Estrogens are responsible for breast growth in women during puberty and they are delivered to the cells by serum proteins in blood. Once inside the cell, estrogens enter the cell nucleus and bind to a complex receptor protein (estrogens receptor), which then enables the synthesis of a protein involved in breast growth [167].

Tamoxifen (TAM) is an anticancer drug, very specific in its action. TAM exists in two different isomeric forms: *E*-isomer (*cis*-TAM) and *Z*-isomer (*trans*-TAM) [168]. *E*-isomer has agonist properties and only the *Z*-isomer of tamoxifen has pharmacological relevant properties acting as an antagonist of estrogens, *i.e.* it acts as a selective estrogen receptor modulator (SERM) compound.

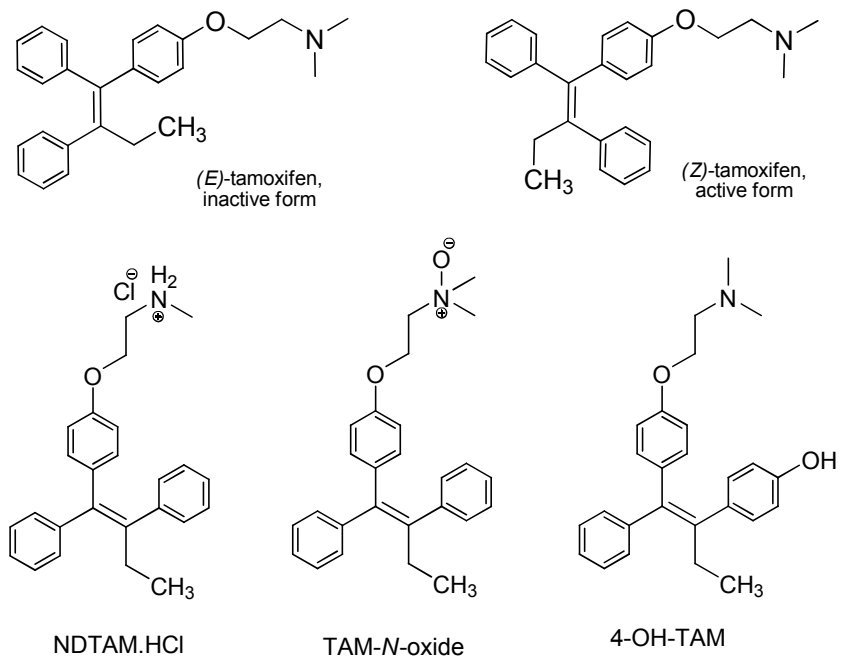

Figure 65. Structure of *(Z)*-tamoxifen and *(E)*-tamoxifen isomers and of *(Z)*-tamoxifen active liver metabolites: *N*-desmethyltamoxifen hydrochloride (NDTAM.HCl), tamoxifen-*N*-oxide (TAM-*N*-oxide) and 4-hydroxytamoxifen (4-OH-TAM).

Once inside the body TAM is converted into its active metabolites: 4-hydroxytamoxifen; *N*-desmethyltamoxifen (NDTAM) and tamoxifen-*N*-oxide (Figure 65) that

revealed enhanced affinity in the prevention of cancer, by blocking the specific site (estrogen receptors) competing with the natural hormone (estrogen) [168]. The water solubility of tamoxifen is very limited (0.1 mg/L, 20 ºC) [169] and its citrate salt is commercially used instead, due to its improved solubility (0.3 mg/L; 20°C) [170]. Commercial, tamoxifen citrate is sold as Novaldex® used in therapy for hormone receptor-positive breast cancer in pre-menopausal women.

Tamoxifen citrate (TAM-Cit)

The first approach to modify the TAM molecule by preparing its citrate salt was based on a reported procedure [171]. In their work it was described the formation of citrate salt (TAM-Cit) in a 2:1 or in a 1:1 stoichiometry. This suggested the possibility of isolating TAM-Cit, with varying stoichiometries because the commercially available TAM-Cit sold by Sigma-Aldrich shows a 1:1 stoichiometry [170].

In our hands, the reaction took place in acetonitrile (ACN) using approximately a two-fold molar excess of citric acid and the product was isolated directly from the solution, as it precipitates as a white solid - Figure 66.

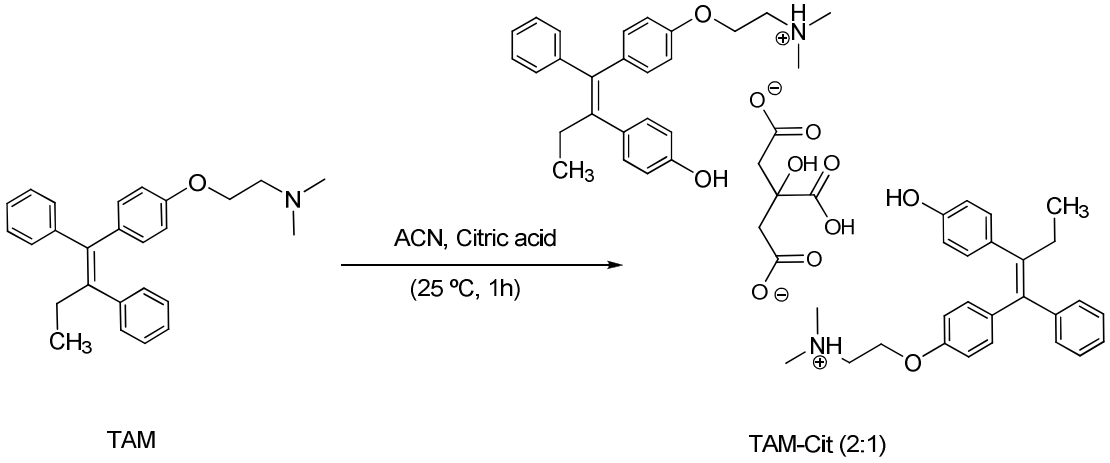

Figure 66. Synthesis of TAM-Cit (2:1) from the reaction of TAM with citric acid in acetonitrile (ACN).

The isolation and purification of the product involved extensive washings of the white solid with water, to take advantage of the difference in aqueous solubility between citric acid (CA) and TAM-Cit. Thus, it is expected that in the presence of a large excess of H_2O, mostly the unreacted citric acid (used in excess) will be washed away from the crude solid, leaving behind any insoluble material namely TAM-Cit.

The product TAM-Cit was prepared in a 63 % yield and was characterized by IR and ^1H NMR spectra in $CDCl_3$. In the aromatic region (7.0 ppm – 8.0 ppm) the compound displayed all

the signals from the TAM core. The assignment was straightforward and is shown in the appendix (Figure 120). The citrate moiety shows only one signal (≈ 2.8 ppm – 2.9 ppm) corresponding to the two methine groups in citric acid. Integrating the signal after careful data acquisition afforded a ratio TAM-Cit salt in a typical 2:1 stoichiometry. The comparison between IR spectrum of TAM-Cit and TAM, reveals that in TAM-Cit an extra peak at 1722 cm^{-1} characteristic of a carboxylic acid attributed to the citrate moiety, shown in appendix (Figure 121).

TAM-Cit (2:1) was successfully used in our group as guest molecule in several studies with CDs [172]. Additionally, the purification method developed, based solely on washings with water, illustrates a cheap and attractive way of obtaining a pure TAM derivative.

N-desmethyltamoxifen hydrochloride (NDTAM.HCl)

The second strategy to modify the chemical structure of TAM, dealt with a demethylation of the tertiary amine in TAM structure, to obtain *N*-desmethyltamoxifen hydrochloride (NDTAM.HCl). The synthetic procedure was based on the procedures described by Olofson [173] with some modifications implemented [174, 175]. The mechanism of demethylation of tertiary amines has been described elsewhere [176] and is shortly presented in Figure 67.

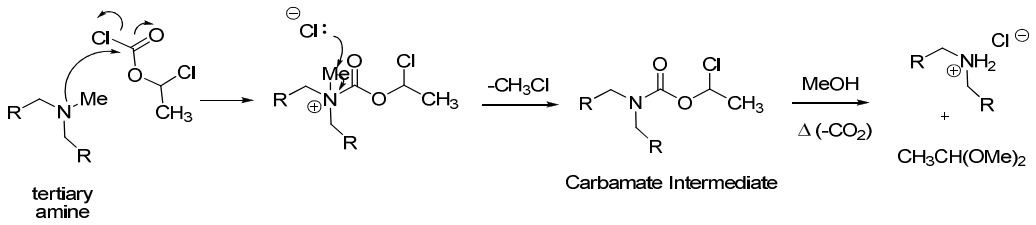

Figure 67. Mechanism of demethylation of amines using alkyl chloroformates.

It involves the use of a highly reactive species (α-chloroethylchloroformate) that is susceptible to nucleophilic attack by the tertiary amine resulting in the elimination of a methyl group as a chloroform molecule. The carbamate intermediate is subsequently decomposed by heating in methanol to the secondary amine hydrochloride. The structure of α-chloroethylchloroformate is very similar to that of 2,2,2-trichloroethylchloroformate, which as been used in the demethylation of tertiary methylamines [177]. The reaction proceeded by solubilising NDTAM.HCl in toluene at 0 ºC, followed by the addition of α-chloroethylchloroformate and refluxing the mixture, with periodic monitoring of reaction progress by TLC using CH_2Cl_2 : MeOH : NH_3 (95/5/0.3) as mobile phase, against an authentic

sample of NDTAM.HCl used as a standard. The reaction reached completion in ≈ 8 h and the product precipitated from the crude mixture, when poured directly into an excess of diethyl ether (EtOEt) (Figure 68).

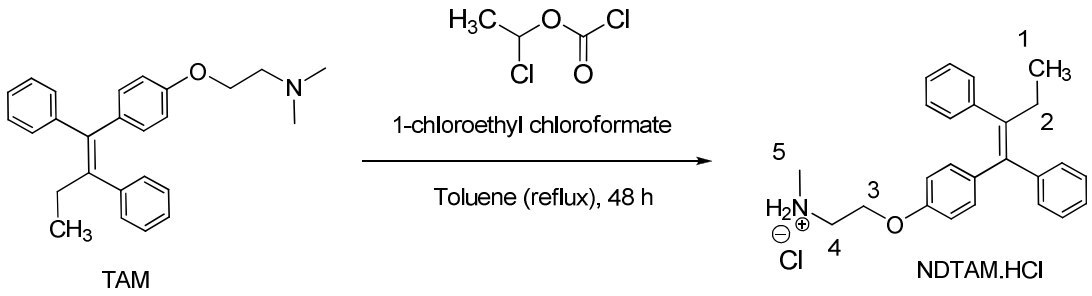

Figure 68. Synthesis of NDTAM.HCl from the reaction of TAM in refluxing toluene, using α-chloroethylchloroformate.

The overall yield of the reaction was 50 % and the product was characterized by NMR, IR spectroscopy and TLC. ^{1}H NMR spectrum in of NDTAM.HCl MeOH-d_4 (Figure 69), revealed a clean product free from impurities and the integration of methyl group (position 5, NDTAM.HCl in Figure 68 attached to the nitrogen atom) accounted for 3 H (≈ 2.67 ppm) corresponding to one methyl group, as expected. This is the only difference with respect to TAM spectra, where for the same resonance 6 H are expected, corresponding to two methyl groups. The identity of the sample was verified against a commercial sample of NDTAM.HCl (Sigma-Aldrich), both by IR spectroscopy and by TLC: the overlaid IR spectra of commercial sample and NDTAM.HCl obtained, revealed a complete matching in all regions of the spectra (appendix, Figure 117).

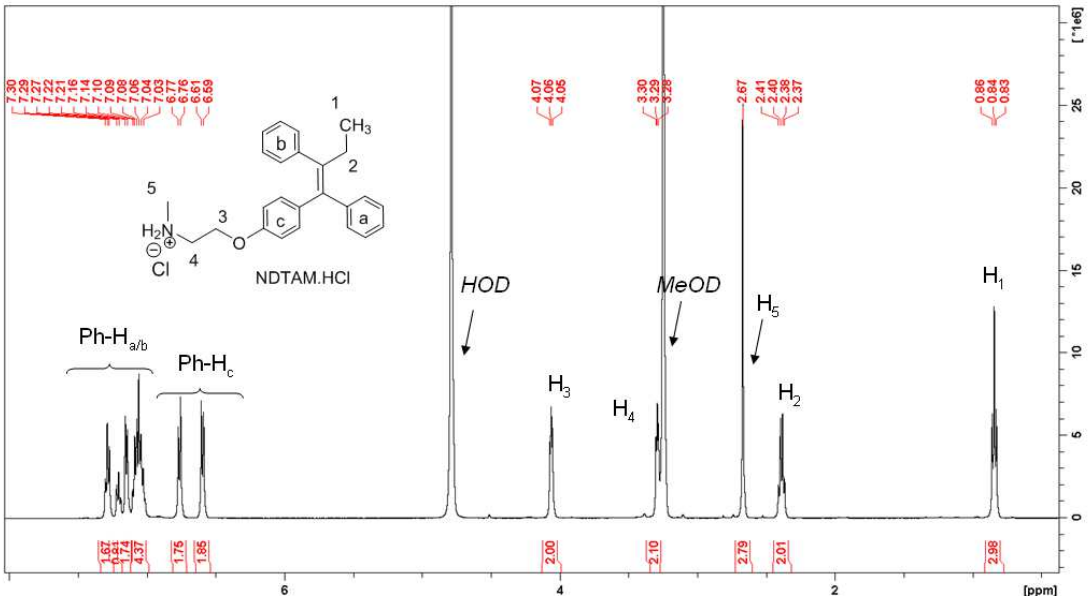

Figure 69. ^{1}H NMR spectrum (500 MHz, MeOD-d_4, 25 °C) of NDTAM.HCl.

In the literature, the preparation of NDTAM was described following at least three different procedures: In the first approach, TAM was solubilised in dichloroethane, in the presence of α-chloroethylchloroformate and was refluxed for 24 h. The crude mixture was then refluxed in MeOH for 3 h and the product was obtained from the residue, by recrystallization from EtOH and Et_2O to give NDTAM (86 % yield) [174]. The second procedure described used refluxing dichloromethane (boiling point, bp ≈ 40 ºC) for 24 h to obtain an oil, which was then, refluxed in MeOH for extra 3 h followed by column chromatography affording NDTAM (91 % yield) [178]. Alternatively, TAM was refluxed in toluene (bp ≈ 111 ºC) in the presence of 2,2,2-trichloroethylchloroformate and potassium carbonate. After 4h, the reaction was stopped to isolate the carbamate intermediate. This intermediate was stirred overnight in diglyme, acetic acid and zinc. Column chromatography was used followed by recrystallized from heptane to afford NDTAM (77 % yield) [174].

Although the yields reported are reasonably good these methodologies failed to distinguish if the actual product isolated is NDTAM.HCl or NDTAM. All of them involved refluxing MeOH to break the carbamate leading to the formation of the corresponding demethylated amine. Additionally, in the first approach, the only one avoiding column chromatography, is not clear in the description what solvent was used: 1,1-dichloroethane or 1,2-dichloroethane. Probably, the use of higher boiling point 1,2-dichloroethane (≈ 84 ºC) as opposed to 1,1-dichloroethane (bp ≈ 57 ºC), would ease the release of CO_2 during the reaction, thus avoiding the use of chromatographic methods and enabling the isolation of NDTAM by recrystallization.

In our hands, using the low boilng point $CHCl_3$ at reflux (bp ≈ 61 ºC) the reaction did not progress as the product was isolated in the presence of many impurities, after 72 h including MeOH reflux for 1 h. Column chromatography and even preparative plate chromatography were of no use, since it resulted in isolating NDTAM.HCl and many impurities. A critical point for the monitoring of the reaction progress towards the desired product was the use of TLC and a mobile phase composed of CH_2Cl_2 : MeOH : NH_3 (95:5:0.3, *v/v*), which enabled the distinction between: fast moving impurities (R_F = 0.94) or intermediate formed (carbamate), TAM (R_F = 0.32), the product identified using a commercial sample (R_F = 0.08) of NDTAM.HCl and non-moving impurities (R_F = 0) (Figure 70). Our successful strategy was to use a high boiling solvent (toluene) for an extended period of time (≈ 19 h / overnight) thus avoiding the need of methanol reflux step and proceed directly to the precipitation of NDTAM.HCl from EtOEt, isolated as a white solid of very good purity. In conclusion, demethylation of TAM using 1-chloroethylclhoroformate in refluxing toluene could be carried out in a simple procedure, compared to previously reported.

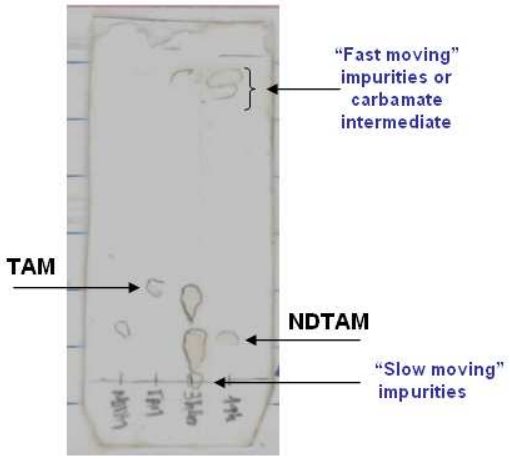

Figure 70. TLC monitoring of the demethylation reaction of TAM to obtain NDTAM.HCl. From left to right: i) commercial sample of NDTAM.HCl (NDTAM); ii) starting-material (TAM); iii) incomplete reaction after ≈ 4h and iv) complete reaction after (19 h, no TAM left to react).

NDTAM.HCl was used as guest molecule in complexation studies reported by our group [172] and additionally to react with fluorescein (isothiocyanate, FITC) in order to obtain NDTAM-FITC to study intracellular delivery and fate (see section 10.3.4). In addition, the method developed by our group presents a cheap and easy way of obtaining from affordable starting materials a very expensive TAM derivative.

Fluorescein labelling of NDTAM (NDTAM - FITC)

The preparation of NDTAM-FITC in our group previously relied on commercial samples of NDTAM.HCl as starting material. This posed a big problem in the developments of this specific synthetic procedure: the high price of starting material NDTAM.HCl limited all small-scale trials, which in turn limited complete optimization of the purification procedures. However, after the successful synthesis of NDTAM.HCl described earlier (see section 10.3.2), more material was available and therefore more trials could be performed and different purification strategies explored.

A general reaction explored in our group was the reaction between amines (R_1-NH_2) and isothiocyanate (R_2-N=C=S), to form thioureas (R_1-NH-C(=S)-NH-R_2). This kind of reactivity is greatly explored to link biologically relevant samples to several fluorescence probes and these have found wide applications in chemical biology specifically in:: immunochemistry; fluorescence *in situ* hybridization (FISH); cell tracing; receptor labelling; fluorescent analog cytochemistry and fluorescence resonance energy transfer (FRET) [179].

In our group, the procedure to attach a molecule of NDTAM.HCl to isothiocyanate moiety in fluorescein isomer 1 (FITC) was tried previously [180]. This procedure had a series of limitations associated with the low yield and the non-reproducibility in the preparation regarding the purity of the NDTAM-FITC. Therefore, the method for preparation and isolation of NDTAM-FITC should be revised. The general procedure involved the solubilisation of FITC in EtOH, followed by addition of NDTAM.HCl and *N*,*N*-diisopropylethylamine (DIPEA) to neutralize the salt. The reaction proceeded for 44 h at 40 ºC. The residue was dried and applied to a preparative TLC plate. NDTAM-FITC was isolated in 60 % yield, corresponding to the second band (R_F = 0.77) isolated from the preparative plate (Figure 71).

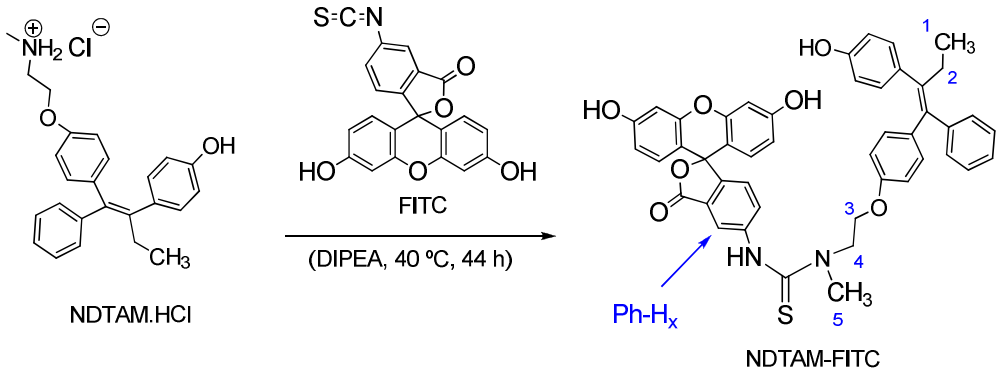

Figure 71. Synthesis of NDTAM-FITC from reaction of NDTAM.HCl with FITC in EtOH, to form a thiourea linkage.

FITC has been successfully attached to primary amines exploring the same kind of chemical connectivity – formation of thiourea linkage. FITC has been connected to octadecylamine, in anhydrous THF, at 60 ºC in 3 h but no details on the purification method used were given [181]. Moreover, in another example, FITC was connected to randomly deacetylated chitosan polymer (50 %), in water at neutral (pH = 6.9), at room temperature (not specified) for 24h, but no reference is made to difficulties faced with solubilisation of FITC in water. Additionally, the isolated fraction corresponded only to 6.6 % (*m/m*) probably due to inefficient mixture of the reactants [182].

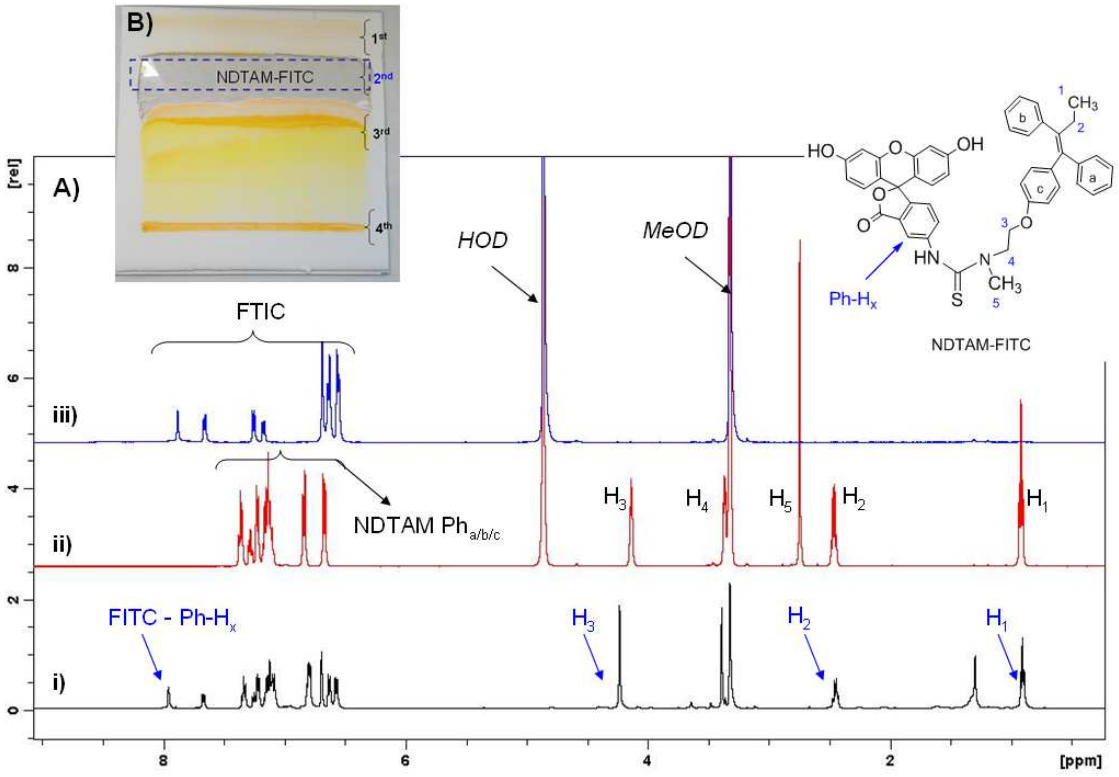

Figure 72. ^{1}H NMR spectra (MeOD-*d*$_4$, 500 MHz, 25 ºC) of i) NDTAM-FITC (2nd band scrapped from TLC plate B); ii) NDTAM.HCl and iii) FITC; B) inset picture, illustrates separation by preparative chromatography.

In our hands, using the fluorescent dye (FITC, yellow coloured) as a raw material means that at any stage the solution is always deeply coloured and poses a challenge to any separation/purification technique. TLC was used for monitoring the progress of reaction, but was of little use because there was no clear separation between spots, although various mobile phases have been used. Other trials involved the use of column chromatography, but with no success for similar reasons. However, an efficient method to purify this mixture of products was achieved through the application of small amounts of untreated crude (right after the

reaction), directly to a preparative plate (≈ 12 mg / 20 cm x 20 cm plate, silica gel, 500 μm thickness) solubilised in MeOH or in mobile phase $CHCl_3$/MeOH (3:1), which was the eluting solvent system. Five different bands were successfully isolated and through ^1H NMR analysis, the target compound was identified corresponding to the second (2^{nd}) fluorescence band isolated (NDTAM-FITC, R_F = 0.77, Figure 72 B). All of the other coloured bands (1^{st}, 3^{rd}, 4^{th}, 5^{th}), corresponded to undesired fluorescent impurities and were discarded afterwards. The overall yield of the separation is ≈ 60 % (*m/m*) and ≈ 80 % purity estimated from the average of NMR integration of NDTAM.HCl (H_1, H_2, H_3) with respect to FITC (Ph-H_x; 7.9 ppm: ≈ 1.6 H) considering the expected ratio Ph-H_x/$H_{1/2/3}$ (Figure 72 A).

Thus in our group perspective and considering that previously isolated NDTAM-FITC batches were not purified [180], the development of this purification method is important because this purified compound can now be applied in current / future works developed in our group.

6.2.2 **Preparation of a gemcitabine derivative**

Gemcitabine (GEM)

Gemcitabine (2,2'-difluorodeoxycytidine, dFdC or GEM) is a potent anticancer nucleoside drug analogue of deoxycytidine monophosphate (dCMP), a deoxyribonucleoside that is a component of deoxyribonucleic acid (DNA). dCMP is similar to ribonucleoside cytidine monophosphate (CMP), but with one hydroxyl group removed from the 2' position of the pentose unit. In GEM the hydrogens in position 2' of dCMP are substituted by fluorine, as displayed in Figure 73.

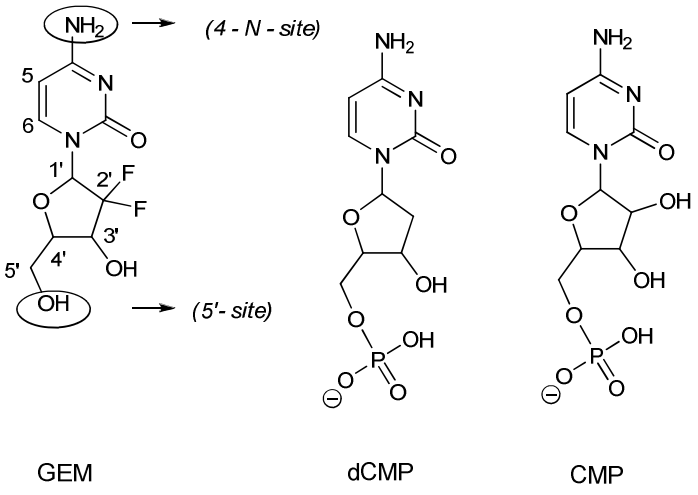

Figure 73. Chemical structure of gemcitabine (GEM), deoxycytidine monophosphate (dCMP) and ribonucleoside cytidine monophosphate (CMP)

GEM hydrochloride salt is marketed as Gemzar® (ELI Lilly) and is used in chemotherapy treatment of pancreatic and non-small lung cancer and other solid tumours. After intravenous administration, GEM is activated by deoxycytidine kinase (dCK) to its phosphorylated forms (GEM mono-, di-, and triphosphate nucleotides), following sequential phosphorylation steps. The active metabolites are then responsible for the anticancer activity of this drug, which comprises inhibition actions by competing with dCTP on DNA synthesis in rapidly divided cells. GEM is also deaminated to its inactive uridine metabolite (dFdU) by deoxycytidine deaminase and this presents a serious drawback [183], because it inactivates the drug. Thus, the drug displays poor bioavailability and efforts to increase GEM biological stability towards deamination have been focused on chemical modification at the drug, involving reactions on two different sites, namely on the pyrimidine (4-*N*-site) and on the pentose (5'-site) (Figure 73) [184].

The preferred modification involves the coupling of the amine (GEM) with a carboxylic acid (R_2-COOH) to obtain an amide bond (GEM-NH-CO-R_2), preferred to the ester derivatives because is of its improved stability regarding chemical and enzymatic hydrolysis [185]. This modification will produce a pro-drug with improved plasma lifetime after administration. Our aim has been to prepare an amide GEM prodrug that would be readily captured by βCD cavity for delivery.

Gemcitabine-adamantanamide (GEM-ADA amide)

The attachment of adamantyl (ADA) moiety into a gemcitabine (GEM) molecule is interesting from our perspective for two main reasons: firstly, the successful incorporation of an ADA moiety into GEM molecule, through an amide bond protects the unstable 4-*N*-site of GEM against undesired *in vivo* reactions (Figure 73). Secondly, ADA possess the exact geometry that fits βCD cavity forming a strong inclusion complex with estimated $K > 10^4$ M^{-1} [186] and has been extensively studied as model guest in complexation with βCD derivatives [187]. Additionally, one is also interested in the preparation / application of CD-based polymers with cell-penetrating properties and GEM-ADA would be a suitable guest molecule to test with polymer carriers, given the potential increase in solubility / stability that arise from the use of CD-polymers.

The modification of gemcitabine hydrochloride salt (GEM.HCl) with 1-adamantanecarboxylic acid (ADA-COOH) was explored using different coupling conditions, following various reported amide coupling reagents [188, 189] and procedures [190]. The coupling reaction between GEM.HCl and ADA-COOH, was optimally performed in a mixture of DMF:DMSO (3:1) at 25 ºC over a period of 48 h in the presence of 1.1 molar eq. of HATU and of 2.8 molar eq. of DIPEA resulting in GEM-ADA amide (Figure 74). Surprisingly, none of the strategies tried to isolate the desired product GEM-ADA amide were successful in our hands. These included, several liquid-to-liquid extractions strategies and column chromatography performed on crudes isolated after reaction. From all this experiment can be concluded that GEM-ADA amide is temperature sensitive and is affected by the presence of methanol.

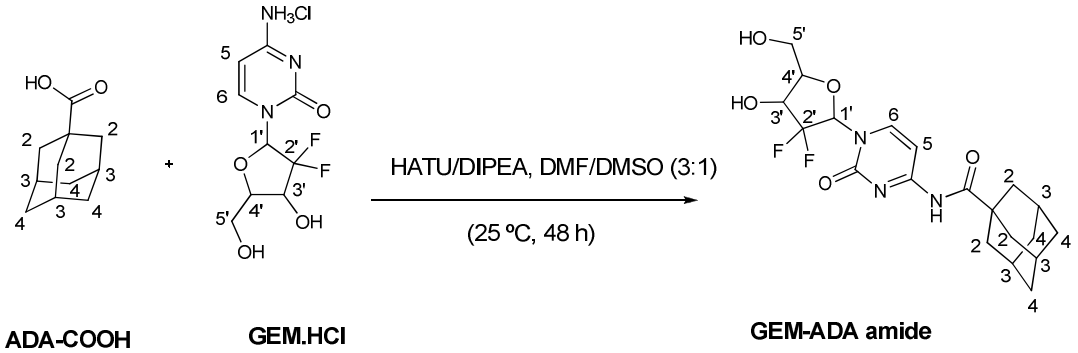

Figure 74. Synthesis of GEM-ADA amide, through the coupling reaction between gemcitabine (GEM.HCl) and 1-adamantanecarboxylic acid (ADA-COOH), activated by HATU/DIPEA.

Table 7 describes several conditions tested that resulted in the best experimental trial (Table 7, # 7). In this trial (# 7), TLC monitoring using a suitable mobile phase comprised of CH_2Cl_2 : acetone : EtOH (5:4:1) enable the identification of HATU-activated ADA-COOH (R_F = 0.99) that was subsequently converted into the UV-active desired product GEM-ADA amide (R_F = 0.78). The pure product (GEM-ADA amide) was obtained by liquid-to-liquid extraction [EtOAc / aqueous NaCl (10 % *m/v*)] to clean the organic phase (EtOAc), from any unreacted GEM.HCl and HATU-related by-products. Subsequently, by using small volumes of warm water (60 ºC), the pure GEM-ADA amide could be extracted and, on cooling was collected in 28.5 % yield, leaving behind an impurity as a light yellow residue. The pure GEM-ADA amide isolated was characterized by NMR spectroscopy in DMSO-d_6. The ^{1}H NMR (Figure 75) spectrum revealed: i) the characteristic ADA signals (three singlet between 2.2 ppm – 1.6 ppm); ii) the pyrimidine ring aromatic protons H_5/H_6 at 6.0 ppm and 8.2 ppm, respectively; iii) the pentose unit with signals $H_{5',a}/H_{5',b}/H_{4'}/H_{3'}/H_{1'}$ in the aliphatic region (3.6 ppm – 4.3 ppm). In DMSO-d_6 due to slow exchange on the NMR time scale with residual HDO in the solvent 5'-OH (6.34 ppm) /3'-OH (5.33 ppm) /amide –NH (10.5 ppm) protons were identified. A presaturation experiment involving irradiation at the HDO frequency resulted in the loss of their intensity, thereby revealing the frequency of these exchangeable protons.

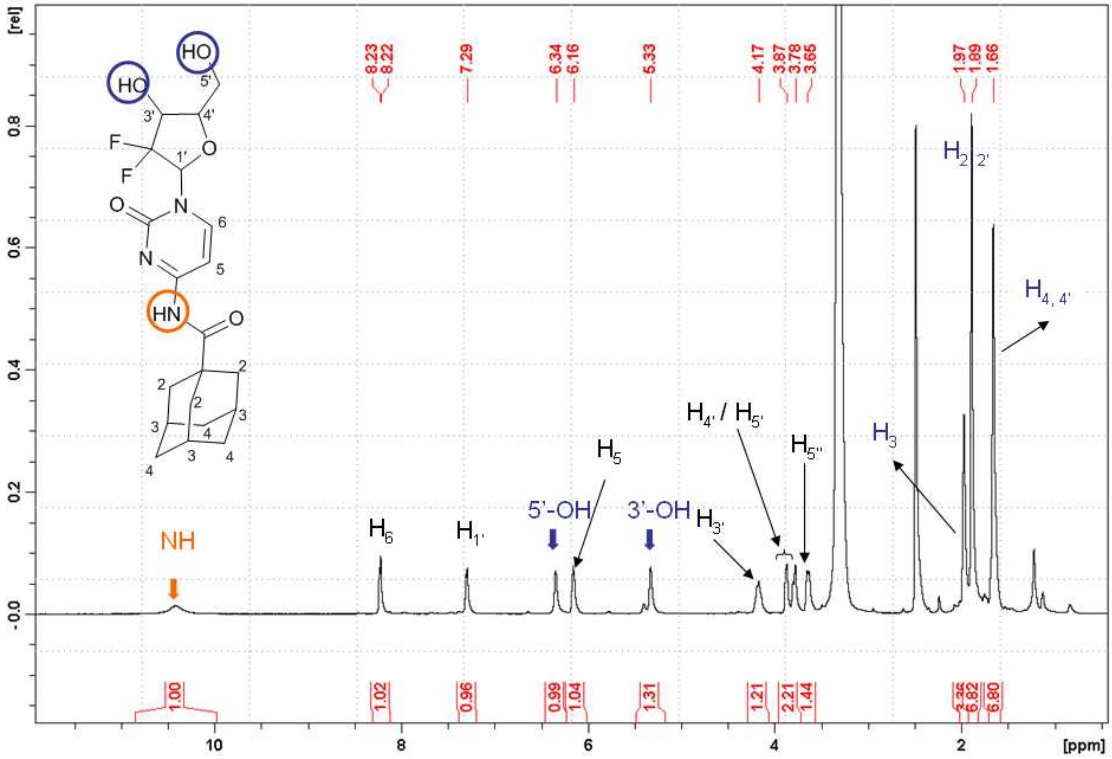

Figure 75. ^{1}H NMR spectrum (DMSO-d_6, 500 MHz, 25 °C) of GEM-ADA amide.

These structural features of GEM-ADA amide were corroborated by 2D HSQC NMR spectra, namely: the differently phased signals (CH_2) corresponding to H_5 /$H_{5'}$ on the pentose ring and H_2 /$H_{2'}$ and H_4 /$H_{4'}$ of the ADA moiety (Figure 76).

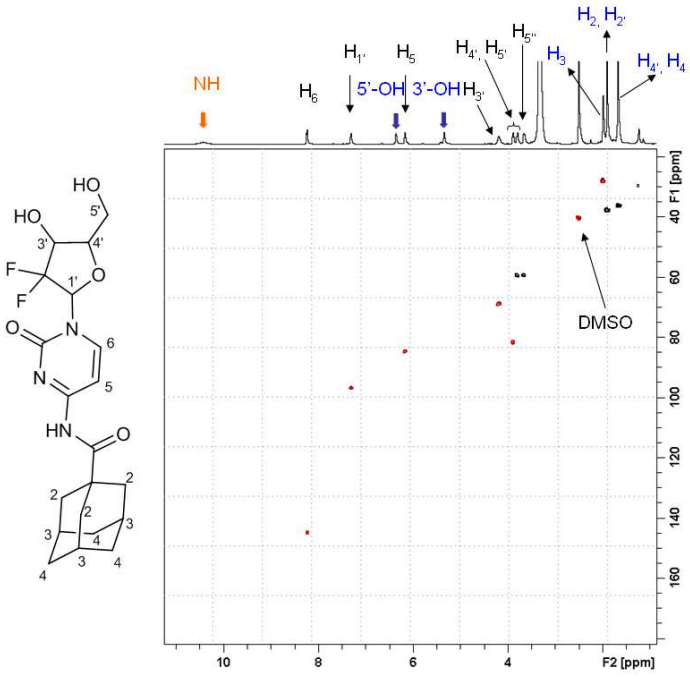

Figure 76. 2D NMR HSQC spectrum (DMSO-d_6, 25 °C) of GEM-ADA amide.

Additionally, the adamantyl moiety was located away from the pyrimidine and pentose moieties, because no nuclear Overhauser effect was observed during a typical 2D NOESY experiment, which detects through space interactions of spins up to a distance of ≈ 5 Å. Therefore, ADA moiety located in GEM-ADA amide is free to interact with a βCD derivative in a typical inclusion experiment. On the other hand, the above clearly excluded the possibility of attachment of ADA moiety to the 5'-OH site via an ester bond connection.

Table 7. Coupling conditions used in the preparation of GEM-ADA amide: reaction between GEM.HCl and ADA-CO_2H.

Trial	Coupling Conditions n (mmol) / n (mmol)	Solvent	ADA-CO_2H / GEM.HCl	Time / Temp.	Notes
1	EDC.HCl / DMAP 0.267 / 0.05	$CHCl_3$ (2 mL)	0.135 / 0.154	46 h / 25 ºC	Solvent not appropriate
2	EDC.HCl / DMAP 0.273 / 0.065	DMF (2 mL)	0.141 / 0.164	95 h / 25 ºC	Coupling conditions
3	DIC / HOBt 0.166 / 0.166	DMF (2 mL)	0.166 / 0.166	69 h / 35 ºC	Coupling conditions
4	EDC.HCl / NEM / HOBt 0.220 / 0.167 / 0.167	DMF/DMSO (3:1) (175 µL)	0.183 / 0.167	116 h / 55 ºC	Increase temperature and time of reaction
5	HATU / DIPEA 0.184 / 0.482	DMF/DMSO (3:1) (200 µL)	0.167 / 0.167l	26 h / 25 ºC	Coupling conditions Reduced volume
6	HATU / DIPEA 0.185 / 0.482	DMF/DMSO (3:1) (200 µL)	0.169 / 0.175	48 h / 25 ºC	Purification
7	**HATU / DIPEA 0.185 / 0.482**	**DMF/DMSO (3:1) (200 µL)**	**0.169 / 0.168**	**48 h / 25 ºC**	**Good trial**
8	HATU / DIPEA 0.194 / 0.482	DMF/DMSO (3:1) (200 µL)	0.186 / 0.178	50 h / 25 ºC	Product degradation
9	HATU / DIPEA 0.185 / 0.482	DMF/DMSO (3:1) (200 µL)	0.168 / 0.165	72 h / 25 ºC	Product degradation

During isolation of GEM-ADA amide, methanol was used to transfer small amounts of the product (mg) and a colour change in the solutions of GEM-ADA amide was observed: the initial solution (colourless) turned to yellow. The ^{1}H NMR spectrum of this yellow solution revealed extra peaks in the region, between 6.0 ppm – 9.0 ppm and an increase in the area of the peaks corresponding to the ADA moiety bellow 2.0 ppm (* in Figure 77 B).

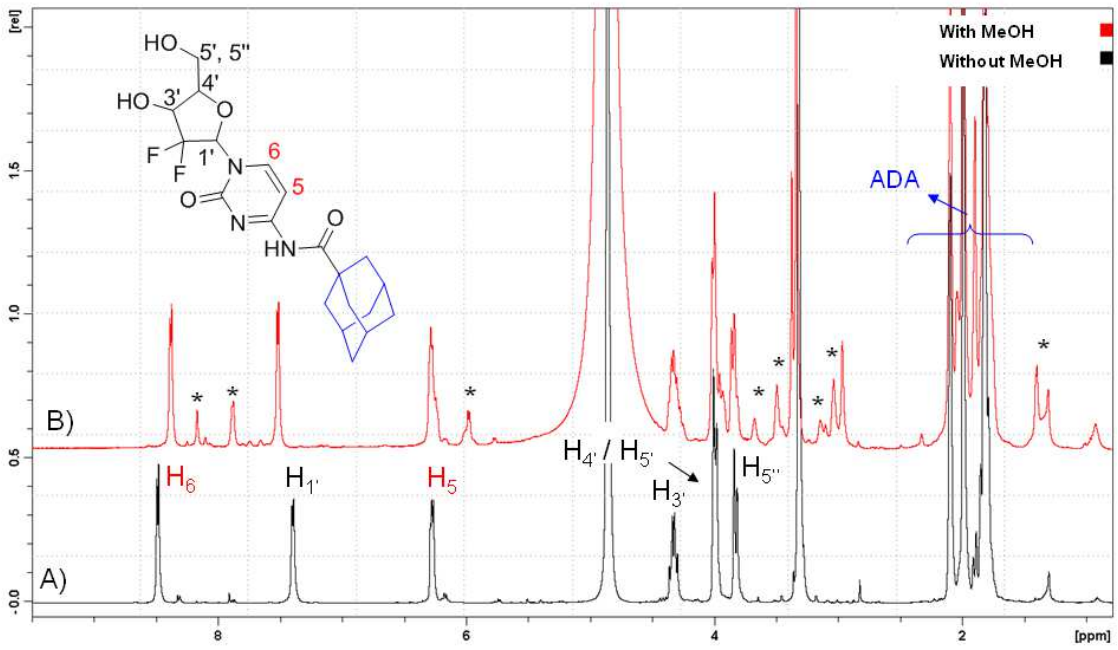

Figure 77. ^{1}H NMR spectra (MeOD-d_4, 500 MHz, 25 ºC) of A) GEM-ADA amide as it is after reaction isolation from warm water; and of B) GEM-ADA-amide after recovery using methanol, signals (*) due to extra species in solution.

A reasonable possibility is the formation of other coupling products or mixtures of them (3-OH and 5-OH, ester products) [191], all appearing together in the same spectral region but this would only be plausible in case of inefficient purification of the desired compound.

Probably, this unexpected behaviour regarding stability in MeOH could be explained by taking into account that methanol (MeOH), can effectively promote the formation of extra species in solution like hemiketals and ketals (Figure 78) [3].

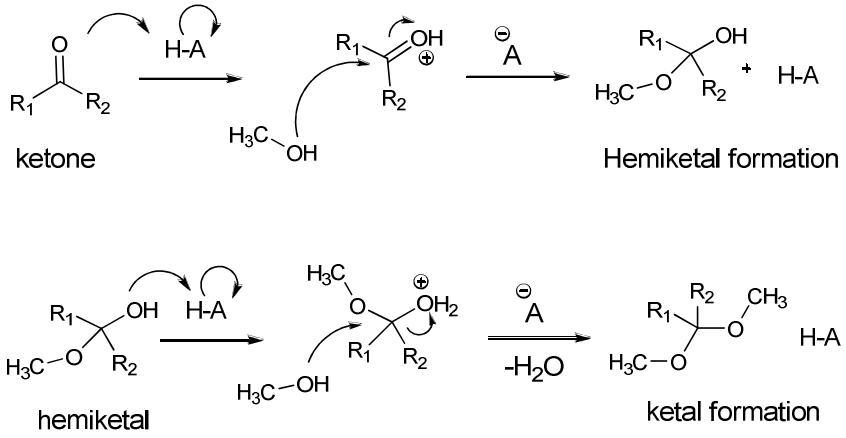

Figure 78. Formation of hemiketals and ketals through the reaction of methanol (CH_3-OH) with a kenote functionality.

This reversible reaction can account for the extra peaks in the aliphatic region of the spectra (*, below 2.0 ppm, Figure 77) and can explain the poor recovery of GEM-ADA amide (28.5 % yield).

6.3 Conclusions and future perspectives

The chemical modification of small molecules, tamoxifen and gemcitabine were implemented and found valuable for several reasons: i) they enable the synthesis in pure state of important TAM derivatives for inclusion study and confocal microscopy (NDTAM, TAM-Cit and NDTAM-FITC) and enabled anchoring of a βCD cavity suited moiety (GEM-ADA) for delivery via βCD carriers. This is of utmost importance in our group's perspective, because expensive anticancer drugs became available for experimentation, while our know-how was expanded, through the preparation and purification of these useful compounds. Most of these compounds have been used by our group members, in fruitful collaborations.

7. CD-polymers (CDPs) based on positively charged CDs

7.1 Introduction

Most of animal tissue cells possess an overall negative charge, attributed to the presence of sialic acid in their cell membrane, which facilitates interaction with positively charged substrates [192]. CD polymer research towards new DDS is still an area in expansion and their accurate characterization still faces many challenges. This has been attributed to the lack of controlled topology, defined structure, uniform molecular weight distributions, extended systemic biocompatibility and lack of toxicological studies [110]. Cationic βCD-based polymers (CPβCDs) have been prepared from βCD, epichlorohydrin and choline chloride and were characterized as drug carriers, revealing that high molecular weight and low cationic charge density, induced good drug inclusion and dissolution properties [193].

Amino-CD derivatives are examples of positively charged CDs that have been studied as biomimetic molecules [194]. *Per*(6-aminoalkylamino-6-deoxy)-CDs and *per*(6-guanidino-alkylamino-6-deoxy)-CDs are amino-CDs, that can display both amine ($-NH_2$) and ammonium salts ($-NH_4^+R^-$, $-NH_2^+R$) depending on the pH of the solution. These CD derivatives have been prepared and studied previously by our group and it was found that they possess good cell penetrating properties (CPCDs) and display moderate interaction with DNA [195]. Additionally, *per*(6-guanidino-6-deoxy)-CDs showed strong interactions through cavity inclusion with model nucleotides (5'-AMP, 5'-dCMP, 5'-dAMP) (Figure 79), but no interactions with nucleosides (2'-dC, 2'-dA). This was attributed to the dipole-dipole interactions that are guiding the inclusion phenomena, between the negatively charged phosphorylated groups in nucleotides and, the positively charged groups in CDs [196]. The electrostatic interactions offer additional stabilization to these inclusion complexes, resulting in the unexpected encapsulation of the pentose moiety of the nucleotides.

Therefore, nucleotide therapeutics can be achieved using CD-polymers containing CPCDs, opening a new and interesting field for the delivery of nucleotides and other anionic drugs.

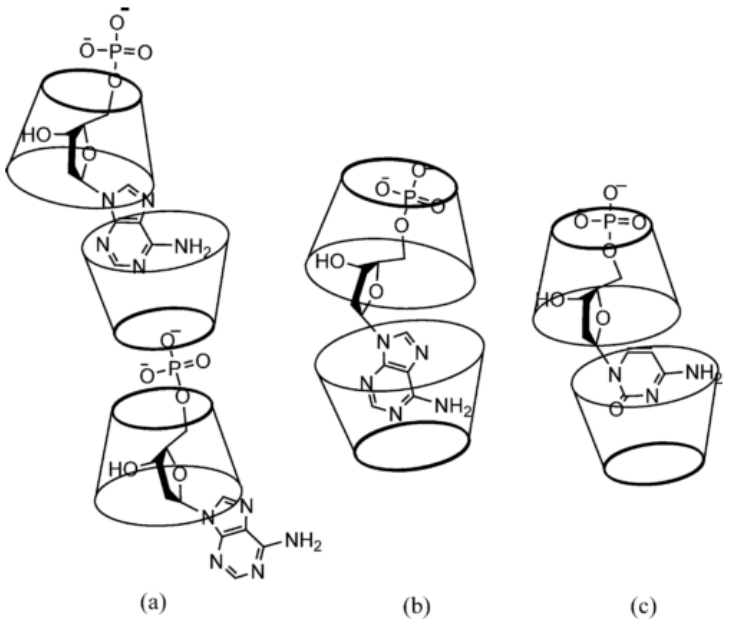

Figure 79. Suggested models of inclusion for the complex between: adenosine 5'-monophosphate (5'-AMP) with a) βguan and with b) γguan and between c) Deoxycytidine 5'-monophosphate (5'-dCMP) with βguan [196].

In this chapter it will be described the preparation of polymers based on a positively charged CDs, namely *per*(6-aminoethylamino-6-deoxy)-βCD, following different strategies. The CD-polymers prepared will be characterized and its ability to interact with model nucleotides such as adenosine 5'-monophosphate (5'-AMP) and gemcitabine monophosphate (GEM-MP) will be studied.

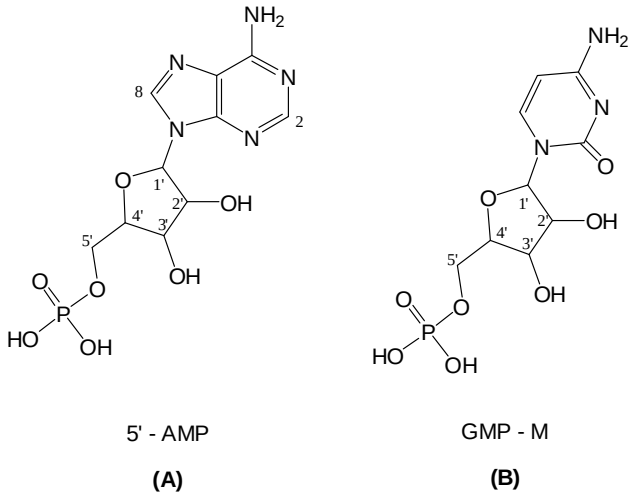

Figure 80. Structures of guest molecules: A) adenosine 5'-monophosphate (5'-AMP) and B) Gemcitabine Monophosphate (GEM-M).

Strategy for preparation of CD-Polymers (CDPs)

CDPs based on positively charged CDs were prepared following two different strategies outlined in Figure 81:

i) Reaction of a preformed polymer bearing suitable functional groups (*e.g.* poly-L-Lysine hydrobromide, pLys.HBr) of known average molecular weight, with a per-halogenated CD (*e.g.* heptakis(6-iodo-6-deoxy)-β-cyclodextrin, βpI) followed by reaction excess 1,2-diaminoethane (DAE) to generate pLys/βpen polymers (Figure 81 a)

ii) Direct reaction of heptakis(6-aminoethylamino-6-deoxy)-β-cyclodextrin (βpen), with epoxides [epichlorohydrin (EPI) and ethylene glycol diglycidyl ether (EGDE)] through ring-opening reactions in alkaline medium, to generate EPI/βpen and EGDE/βpen polymers (Figure 81 b)

The first approach is a costly reaction due to expensive pLys.HBr, starting material, that potentially offers some control over the molecular weights of the final polymers, because the starting material has a determined range of average molecular weight (AMW). The second approach is a cheap alternative that would use readily available epoxides as linkers (EPI and EGDE), but would offer no control over the AMW of the polymers. The details on the preparation of the linker (EGDE), that is not commercially available and on the modifications to the CD macrocycle (βpI and βpen) will be given, later in the chapter.

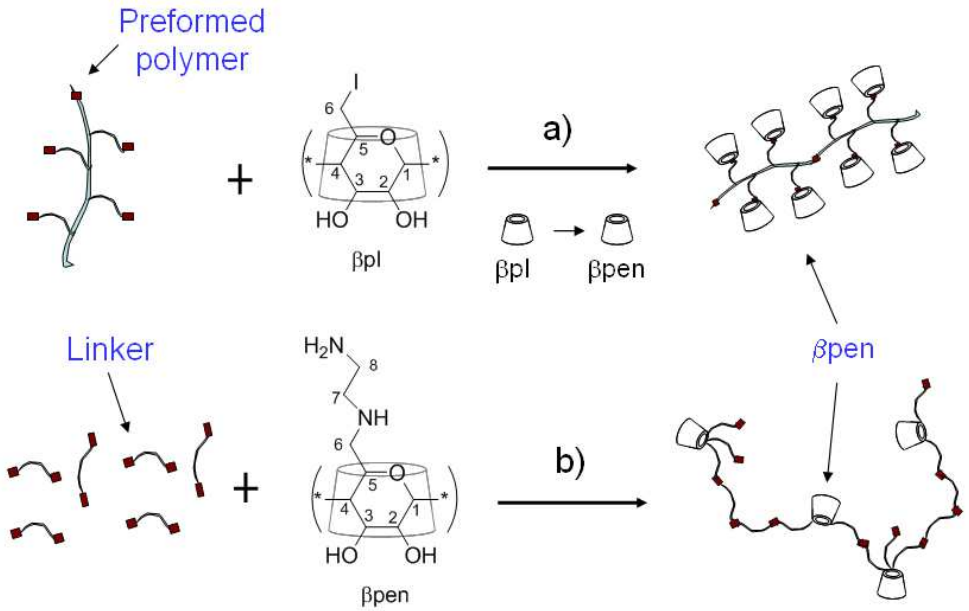

Figure 81. Polymerization strategies used in the preparation of CD-polymers based on: a) preformed polymer (pLys.HBr) and b) available linkers (EPI and EGDE).

7.2 Results and discussion

7.2.1 Preparation of *per*(6-aminoethylamino-6-deoxy)-βCD (βpen) polymers from poly-L-lysine (pLys)

Commercial poly–L-lysine hydrobromide (pLys.HBr) was used as a preformed polymer, following the first strategy outlined previously (Figure 81 a). This polymer is a polypeptide, composed by: i) a linear polymer connected by peptide backbone (amide bonds) and ii) a butylamine side chains displaying n repeating units, corresponding to lysine units (Figure 82). The ^{1}H NMR spectrum of pLys.HBr is shown in Figure 82.

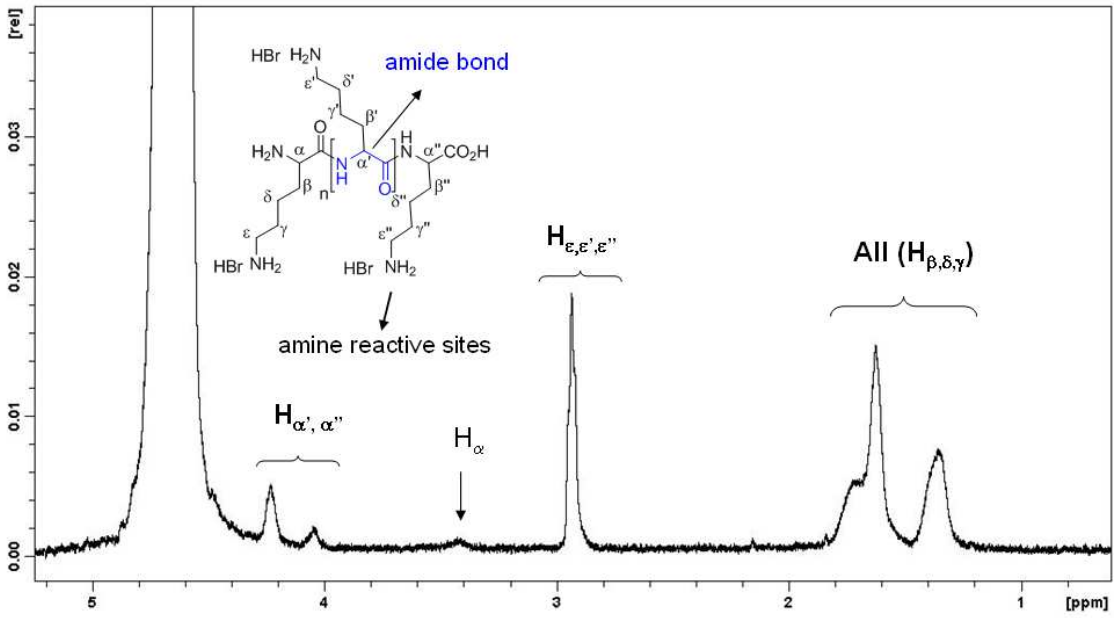

Figure 82. ^{1}H NMR spectrum (D_2O, 500 MHz, 25 °C) of poly-L-lysine hydrochloride, pLys.HBr (500 Da < AMW < 2000 Da).

Polymerization trials

To determine initial suitable polymerization conditions, a commercial batch of pLys.HBr (500 Da < AMW < 2000 Da) was used in three trials described in Table 8. The same amount of pLys.HBr (3.25 μmol) was first reacted with varying amounts of heptakis(6-iodo-6-deoxy)-β-cyclodextrin (βpI) at different temperatures (step 1, Table 8); followed by reaction wirh 1,2-diaminoethane (DAE), to generate βpen from the βpI (step 2, Table 8).

After the reaction is completed the work up procedure involved a dialysis step, through a snakeskin dialysis membrane (MW_{CO} = 3500 Da), used to clear out from the polymeric sample any traces of βpen (MW = 1430 Da). To evaluate the success of each reaction condition,

^{1}H NMR spectroscopy was used to determine the area anomeric proton signal (CD-$H_{1,}$, ≈ 5 ppm) and the area corresponding to the aliphatic peaks of pLys ($H_{\beta/\gamma/\delta}$ < 2 ppm). The experimental conditions that lead to polymers with the highest βpen content were those described for trial 3 (Table 8).

Table 8. Polymerization trials between pLys.HBr (500 Da < AMW < 2000 Da) and βpI.

Trial	βpI	DMF / KOH *	Step 1	Step 2
1	16 μmol	3 mL	70 ºC / 14 h	80 ºC / 8 h
2	21 μmol	1 mL	40 ºC / 14 h	80 ºC / 8 h
3	32 μmol	1 mL	60 ºC / 14 h	80 ºC / 8 h

** - pLys.HBr (500 Da < AMW < 2000 Da) (3.25 μmol)*

Consequently, following trial 3 conditions, three more trials were performed changing the AMW of the pLys.HBr used as starting material: a low (500 Da – 2000 Da), an intermediate (1000 Da – 5000 Da) and a high AMW pLys.HBr (4000 Da – 15000 Da) were used in the reaction. The intermediate pLys.HBr fraction (1000 Da – 5000 Da) revealed higher content of βpen and was used in the preparation of all pLys / βpen polymers.

In order to narrow further the AMW of the intermediate pLys.HBr (1000 Da < AMW < 5000 Da) fraction, this was sequentially dialysed using benzoylated (MW_{CO} = 2000 Da) and a snakeskin (MW_{CO} = 3500 Da) dialysis tubing. Three fractions were obtained: pLys A (1000 Da < AMW < 2000 Da, 35 % m/m_T); pLys B (2000 Da < AMW < 3500 Da, 52 % m/m_T) and pLys C (3500 Da < AMW < 5000 Da, 14 % m/m_T) and the number of lysine units (# Lys, Table 9) comprising in each pLys fraction was estimated taking into account: i) the molecular weight of one Lys chain (MW ($C_6H_{12}N_2O$) = 128 g/mol; ii) the MW_{CO} limits imposed by the dialysis membranes (MW_{CO} = 2000 Da and 3500 Da) used and iii) by the AMW of the starting pLys.HBr (1000 Da < AMW < 5000 Da).

Table 9. Fractioning of a batch of commercial pLys.HBr (1000 Da < AMW < 5000 Da; m_T = 100 mg) by dialysis to obtain pLys of different average molecular weights (AMW).

Fraction	AMW limits (Da)	# Lys groups (-NH_2)	% Mass recovered (m/m_T)
pLys A	(1000* < AMW < 2000)	8* < # < 16	35 %
pLys B	(2000 < AMW < 3500)	16 < # < 27	52 %
pLys C	(3500 < AMW < 5000)	27 < # < 39	14 %

* - lower limit: pLys A = lower AMW (1000) / MW of Lys (128) ≈ 8 # Lys.

The number of lysine units in the backbone (# Lys) of each fraction, should determine the maximum number of βpen units possible to be grafted onto each polymer backbone, assuming a highly efficient reaction. For every CD attached, the overall AMW of the polymer is

expected to increase by the mass of one βpen molecule (1430 g/mol). The ^{1}H NMR spectrum of starting material, pLys.HBr (1000 Da < AMW < 5000 Da) is comparable to those of fractions pLys A, B and C (Figure 83 A, B and C, respectively). All fractions isolated display signals in the same spectral regions as the starting material pLys.HBr and the mass recovered (m/m_T) is represented as a percentage of the total mass of pLys.HBr used (m_T = 100 mg).

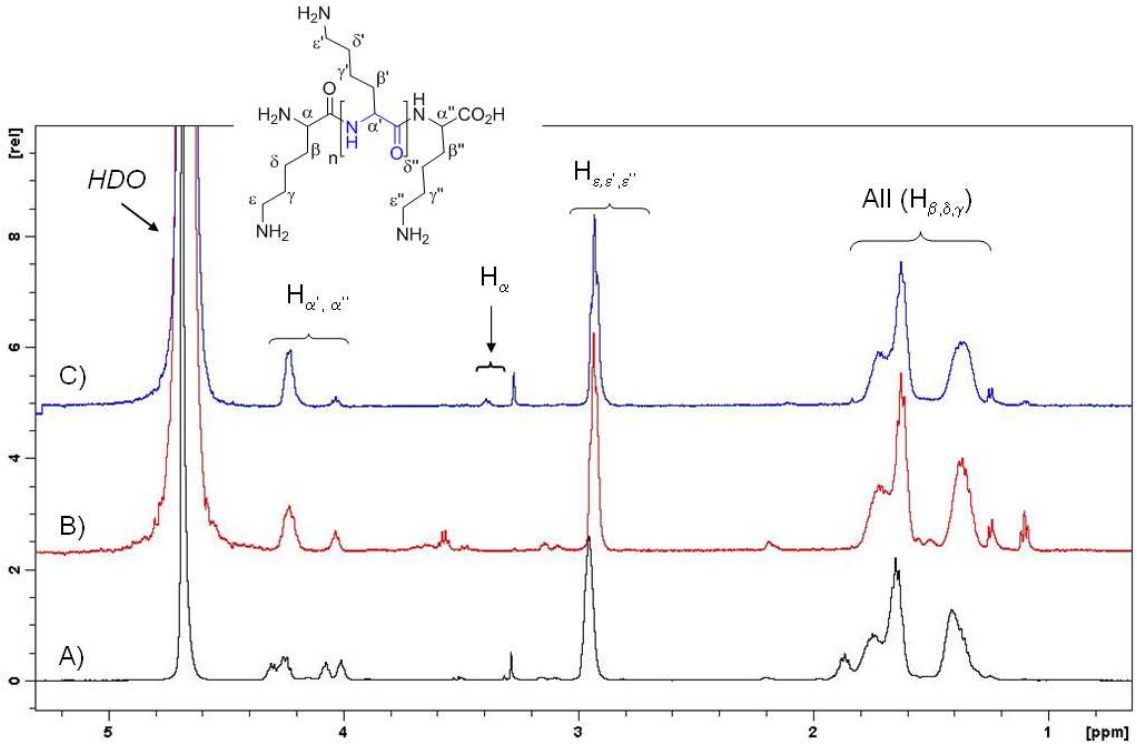

Figure 83. ^{1}H NMR spectra (D_2O, 500 MHz, 25 °C) of A) pLys A (1000 Da < AMW < 2000 Da); B) pLys B (2000 Da < AMW < 3500 Da); C) pLys C (3500 Da < AMW < 5000 Da).

Figure 83 A shows that the increased resolution of the peaks of fraction A, compared to the resolution of peaks in B and C, is probably due to the presence of small molecular weight oligomers in this fraction pLys A (1000 Da < AMW < 2000 Da). Inspection of the ^{1}NMR spectra reveals three major regions with assignable signals: 4.4 ppm – 4.0 ppm, 3.0 ppm – 2.9 ppm and 1.8 ppm – 1.3 ppm. The assignment was aided by Chemdraw ® software prediction of ^{1}H NMR resonances and by comparison with the spectrum of L-lysine itself. Therefore, the 4.4 ppm – 4.0 ppm region was assigned to $H_{\alpha'}$ and $H_{\alpha''}$ signals, the 3.0 ppm – 2.9 ppm region to H_{ε}, $H_{\varepsilon'}$ and $H_{\varepsilon''}$ signals and the 1.8 ppm – 1.3 ppm to all other protons (H_{β}, H_{γ}, H_{δ} of all kinds). The only group that remained separate is H_{α}, attributed to the *N*-terminal residue, with an expected signal between ≈ 3.5 ppm - 3.6 ppm. The integration of these signals (H_{α}), corresponding to the end-groups of the various oligomers present in each polymer (A, B and C), in comparison with the integrals of the rest of signals (H_{β}, H_{γ}, H_{δ}), would give the number of Lys units comprising

each polymer. Small peaks around 3.6 ppm – 3.5 ppm could be found and these were integrated in C (Figure 83 C) and with less accuracy in A (Figure 83 A), whereas in B (Figure 83 B) the region was masked with foreign peaks. In this manner, approximate numbers for monomers were determined and these fall within the expected range of AMW provided by the dialysis membrane molecular weight cut-off limits (MW_{CO}). Table 10 shows the results for the estimated value for # pLys (NMR) and the # pLys ("dialysis"), estimated after "dialysis" fractioning, following the procedure described in section 10.4.9.

Table 10. Estimated number of lysine units (# Lys) attached to polymer backbone: NMR based *vs* dialysis membrane based estimation.

Polymer AMW limits (Da)	# Lys (NMR)	# Lys (Dialysis)	Average (# Lys)
pLys.HBr (1000 < AMW < 5000)	-	-	24
pLys A (1000 < AMW < 2000)	12	8 < # Lys < 16	12
pLys B (2000 < AMW < 3500)	-	16 < # Lys< 27	22
pLys C (3500 < AMW < 5000)	35	27 < # Lys < 39	33

*Expected number of protons for pLys ($H_{\beta/\delta/\gamma}$) = 6 H.

7.2.2 Preparation of pLys/βpen polymers

The previously isolated polymer fractions pLys A, pLys B and pLys C were reacted with pβI following the reaction conditions outlined in Figure 84. The preparation of pLys / βpen polymers involved the reaction of pLys B (2000 Da < AMW < 3500 Da) with an excess of βpI, in alkaline water (KOH) and DMF for 48 h and at 60 ºC (Figure 84). In this first step, it is expected that the nucleophilic side chain amino groups, attached to pLys backbone will be able to substitute one or more iodo groups of βpI leading to the desired connectivity (pLys-βpI). The subsequent reaction in the presence of excess of 1,2-diaminoethane (DAE) performed for 12 h at 70 ºC, leads to the conversion of all remaining unreacted 6-iodo-βCD sites into *per*(6-aminoethylamino-6-deoxy)-βCD (βpen), leading to the desired pLys/βpen polymer.

After attachment of βpen on pLys B (see section 10.4.9) three fractions corresponding to increasing AMW ranges were obtained through dialysis treatment: BA' (1000 Da < AMW < 2000 Da); BB' (2000 Da < AMW < 3500 Da) and BC' (3500 Da < AMW < 5000 Da). A summary of overall results is presented in Table 11.

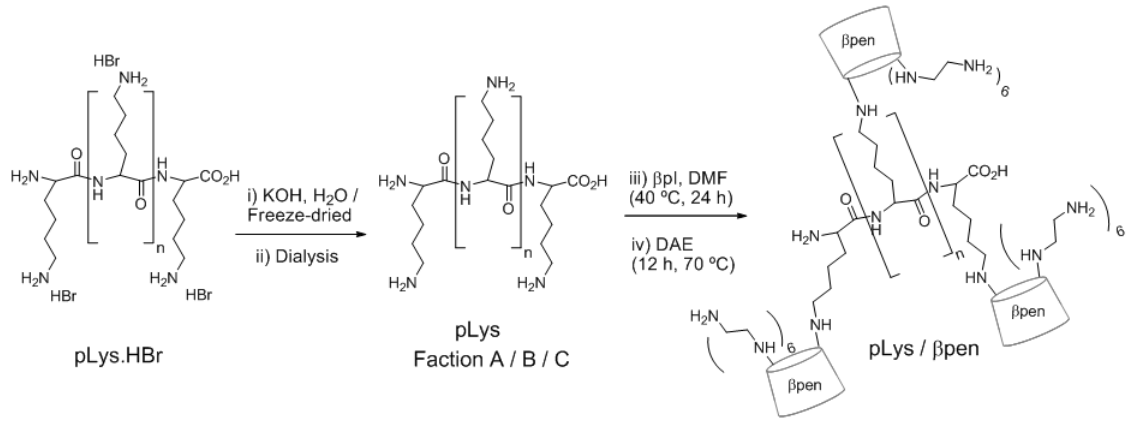

Figure 84. Preparation of pLys/βpen polymers: i) deprotection of pLys.HBr (1000 Da < AMW < 5000 Da) (KOH, H_2O) to obtain pLys; ii) fractioning of pLys.HBr (1000 Da < AMW < 5000 Da) into different fractions A / B / C of varying AMW; iii) attachment of βpI units, followed by iv) conversion to pLys/βpen polymer by reaction with DAE.

The smaller molecular weight fraction of all polymers of pLys/βpen A' (1000 Da * < AMW < 2000 Da) was discarded completely, as most of impurities resulting from the polymerization reaction were small molecular weight molecules (residual solvents DMF and DAE; traces of HI released from βpI attachment to pLys; βpI impurities (triphenylphosphine oxide, PPh_3) and small molecular weight oligomers). Likewise, the higher molecular weight fraction pLys/βpen C' (3500 Da < AMW < 5000 Da *) was also not used, because only small amounts were collected. Finally, the only usable fraction was pLys/βpen BB' (≈ 12 mg, Table 11), isolated from the reaction of the intermediate fraction B' (2000 Da < AMW < 3500 Da) after the fractioning dialysis procedure (see section 10.4.9).

Table 11. Results of polymerization reaction for each starting pLys polymer (A/B/C), after dialysis treatment to obtain different pLys/βpen fractions (A'/B'/C').

		Starting pLys fraction
pLys/βpen	**AMW Range (Da)***	**B**
A'	*1000* < AMW < 2000*	*BA' (-)*
B'	***2000 < AMW < 3500***	***BB' (12.1 mg)***
C'	*3500 < AMW < 5000**	*BC' (-)*

*- limits defined by the commercial AMW of pLys.HBr

A second polymer batch pLys/βpen T_2 was prepared following a similar reaction procedure, but using commercial pLys.HBr (1000 Da < AMW < 5000 Da) used as received without fractioning of pLys.HBr (see section 10.4.8). The work-up procedure involved only an extended dialysis (snakeskin dialysis, MW_{CO} = 3500 Da) step (12 h), followed by collection of

the inner contents of the membrane (3500 Da < AMW < 5000 Da) to afford pLys/βpen (T_2) (11.4 mg).

pLys/βpen BB´ and pLys/βpen T_2 were characterized in the following section and used in complexation / inclusion experiments (7.2.7).

7.2.3 Characterization of pLys/βpen polymers

pLys/βpen T_2 and pLys/βpen BB' were characterized by NMR and their spectra recorded in D_2O are respectively shown in Figure 85 C and in Figure 85 B. The first indication that the polymerization reaction was successful arrived from the comparison between ^{1}H NMR spectra of each polymer batch with that of βpen shown in Figure 85 A.

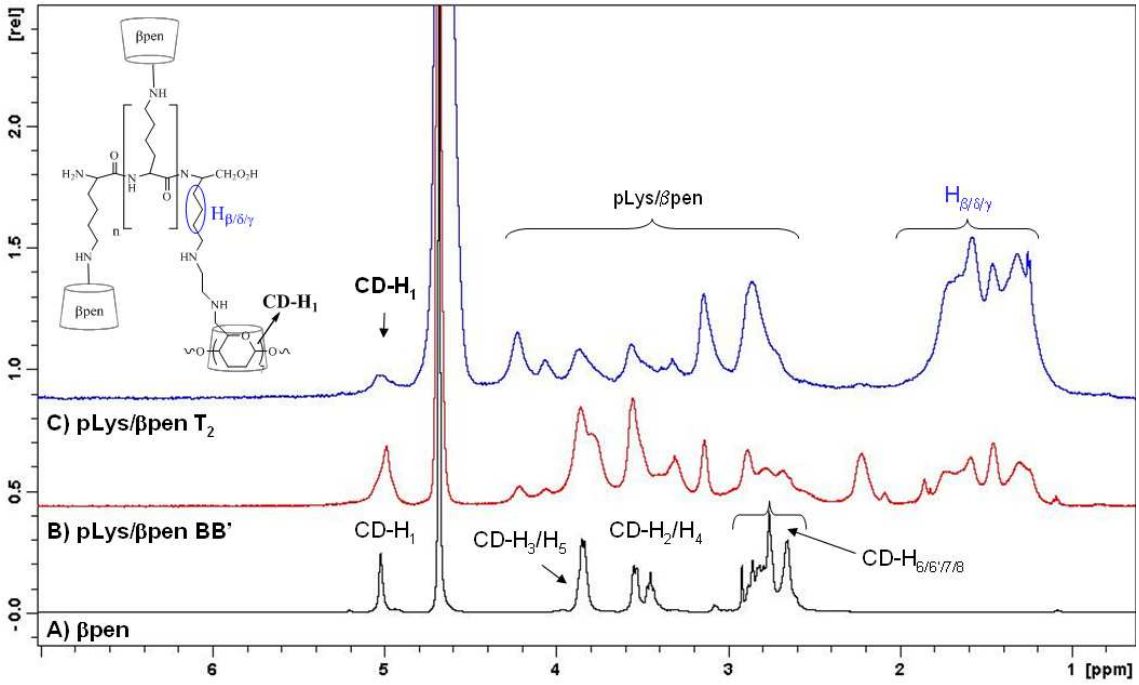

Figure 85. ^{1}H NMR spectra (D_2O, 500 MHz, 25 °C) of A) starting material βpen and two polymer batches: B) pLys/βpen BB' and of C) pLys/βpen T_2.

The ^{1}H NMR spectrum of pLys/βpen T_2 (Figure 85 C) revealed features of both βpen and of starting material pLys.HBr. βpen signals cover the area 3.9 ppm – 2.5 ppm, but the most characteristic is the anomeric peak (CD-H_1, ≈ 5.1 ppm), which is sharp in βpen (Figure 85 A) but broad in pLys/βpen T_2 (Figure 85 C). The presence of pLys is revealed by the characteristic

peaks $H_{\beta/\delta/\gamma}$ (≈ 1.0 ppm to 2.0 ppm) of the alkyl chain connected to the lysine pending groups on the polymer. In the region between 2.5 ppm to 4.5 ppm of pLys/βpen T_2, the signals of βpen and pLys overlap (Figure 85 C). Similar spectral features were observed for pLys/βpen BB' (Figure 85 B), namely: the presence of βpen, pLys signals, broad regions that overlap in the ^1H NMR spectrum of pLys/βpen BB', which difficult the analysis.

The estimation of the relative number of βpen units in pLys/βpen T_2 and in pLys/βpen BB' can be obtained considering the ratio R, between the area of the Lys group ($H_{\beta/\delta/\gamma}$ = 6H) and the areas of the anomeric proton CD-H_1 (≈ 5 ppm). Thus, for pLys/βpen T_2 (R_{T2} = 18.1 / 6 = 3.02) and for pLys/βpen BB' ($R_{BB'}$ = 4.1 / 6 = 0.68), which means that there are 4.4 times more Lys units with βpen attached in the pLys/βpen T_2 than in pLys/βpen BB'.

Moreover, assuming that for every 3.02 Lys units, there is one βpen attached in pLys/βpen T_2 and recalling the average number of Lys for the starting material used pLys.HBr (1000 Da < AMW < 5000 Da) (Table 10) that is ≈ 25 Lys residues, thus: βpen cups = 25 / 3.02 ≈ 8. Consequently, for pLys/βpen BB' polymer: βpen cups = 8 x ¼ ≈ 1.8, on average. Therefore, the above procedures resulted in a βpen rich pLys/βpen T_2 polymer, with a wide range of molecular weights as opposed to a Lys/βpen BB' polymer, with less βpen decoration but much narrower size distribution.

The higher βpen content in pLys/βpen T_2 can be attributed to a higher molecular weight distribution of pLys.HBr (1000 Da < AMW < 5000 Da), used in its preparation of pLys/βpen T_2. This is in opposition to the molecular weight of the fraction of pLys used in the preparation of pLys/βpen BB', which was narrowed down to pLys B (1000 Da < AMW < 3500 Da) through dialysis treatment.

Solubility, size and zeta potential

The initial reaction of βpI with pLys B and pLys C, after dialysis treatment resulted in six different polymer batches, namely: pLys/βpen AB', pLys/βpen BB', pLys/βpen CB', pLys/βpen AC', pLys/βpen BC' and pLys/βpen CC' (Table 12). Although, only pLys/βpen BB' was used in inclusion experiments, the residual amounts of all other pLys/βpen polymers were collected and were used in solubility tests performed in water, using concentration of 0.5 mg/mL at 25 ºC. Table 12 shows that some solutions, prepared from the freeze-dried solids (pLys/βpen), revealed cloudiness indicating poor solubility in water.

In the literature, the opalescence/cloudiness of solution observed during the preparation of nano- and micro-gels for drug delivery, was attributed to the hydrophilicity of the nanogels

[124]. γCD solutions revealed the same phenomenon, attributed to the ability of CDs to aggregate [197, 198]. Thus, it is expected that polymeric materials based on CD despite being water-soluble, may be prone to aggregation even in much diluted solutions. The two polymers of interest (pLys/βpen BB' and pLys/βpen T_2) are water-soluble. However, cloudiness was observed for solutions of pLys/βpen BB' as opposed to pLys/βpen T_2, which was a completely clear solution under the same conditions.

Table 12. Solubility of pLys/βpen polymers prepared from pLys A and pLys B fractions, tested in C = 0.5 mg/mL (25 ºC).

Polymer	pLys.HBr fraction	Aspect of solution
pLys/βpen AB'	B	Clear
pLys/βpen BB'	**B**	**Clear, with residue**
pLys/βpen CB'	B	Cloudy, with residue
pLys/βpen AC'	C	Clear
pLys/βpen BC'	C	Clear
pLys/βpen CC'	C	Cloudy

Dynamic light scattering (DLS) was used to determine the size and surface charge of the polymeric particles in aqueous solutions. All DLS experiments are based on the following assumptions: i) all particles are spherical; ii) particles have a homogenous / equivalent density and iii) the refractive index of the particles in the sample are known. Polymeric samples hardly meet all the DLS criteria for an ideal spherical particle and in addition to this, a typical DLS experimental result can be represented by at least three modes of size representation.

The size distribution (diameter, d, *nm*) of pLys/βpen BB' polymer, obtained from the DLS experiment was plotted as a function of: i) the number of particles; ii) the volume of the particles and iii) the intensity of the light scattered: i) the size/number distribution for pLys/βpen (BB') (Figure 86 A) shows two populations of sizes namely, a very small size ≈ 0.7 nm (9 %) and a moderate size ≈ 91 nm (14 %); ii) the size/volume representation (Figure 86 B) reveals a very small size population ≈ 0.8 nm (8 %) and a broader size population distribution with two maxima, at ≈ 105 nm (1.5 %) and ≈ 955 nm (5 %) and iii) the size/intensity (Figure 86 C) reveals a very small size population ≈ 1 nm (0.5 %) and a larger size population ranging from ≈ 164 nm (5 %) to a ≈ 615 nm (4 %). The result can be justified by the fact that larger particles scatter light more intensely than small ones. Thus, this representation was not chosen.

The results for the size of the particle differ, depending on the graphical representation of the results chosen. Additionally, filtration of the samples prior to DLS analysis was reported as a means to obtain reasonable DLS results from polymeric CD materials able to form

aggregates [199], but this procedure was not used and the size / number representation of the biggest population was determined and is shown in Table 13, for each polymeric material.

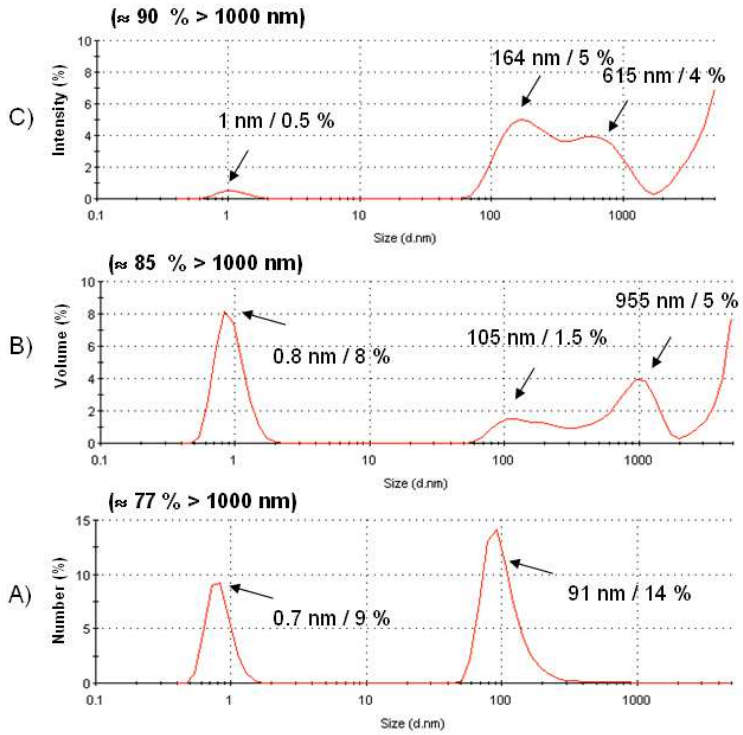

Figure 86. DLS results for pLys/βpen BB' polymer recorded in 0.5 mg/mL at 25 ºC: Size distribution by A) number; B) volume of particle and C) intensity of scattered light.

Recalling the AMW fractioning performed (Table 9), it is expected that the size of polymers prepared from the bigger fraction pLys C (3500 Da < AMW < 5000 Da) is larger than the size of polymers prepared from a smaller fraction pLys B (2000 Da < AMW < 3500 Da). The results show that for each polymer, there is no direct correspondence between the estimated AMW distribution of pLys fraction used as starting material and the size of the biggest particle detected in the final product. For example, the size of pLys/βpen BB' (≈ 91 nm, 14 %), prepared from pLys B (2000 Da < AMW < 3500 Da), is much bigger than the size of pLys/βpen BC' (≈ 3.1 nm, 17 %) prepared from a bigger size range pLys C (3500 Da < AMW < 5000 Da). The conformation of poly-L-Lysine has been determined [200] in aqueous solvents and it is dependent on factors like the solvent, pH value and temperature. Three different conformations were determined: i) a loosely PII-helix conformation 10 ºC (pH = 4); that becomes more tightly packed an ii) α-helix 10 ºC (pH = 11.6) conformation and is extended to iii) a β-sheet conformation by increase in the temperature 60 ºC (pH = 11.6). These data suggest that the 3D

structure of the polymeric products is difficult to predict and it affects the size distribution; therefore, DLS results should be interpreted with caution.

Table 13. Size and zeta potential for pLys/βpen B' and pLys/βpen C' determined by DLS (25 ºC).

Sample	AMW pLys fraction (Da)	Conc. (mg/mL)	Size / Number	pH	Zeta Potential (mV)
βpen	-	0.57	91 nm / 20 %	7	+ 10.6
pLys/βpen AB'	2000 < AMW < 3500	0.50	91 nm / 9.4 %	5	- 8.3
pLys/βpen BB'	2000 < AMW < 3500	0.50	91 nm / 14 %	9	-3.3
pLys/βpen CB'	2000 < AMW < 3500	0.50	141 nm / 18 %	8	-3.7
pLys/βpen AC'	3500 < AMW < 5000	0.50	190 nm / 17 %	7	+ 16.8
pLys/βpen BC'	3500 < AMW < 5000	0.50	3.1 nm / 17 %	7	+ 13.3
pLys/βpen CC'	3500 < AMW < 5000	0.50	7.5 nm / 13 %	7	+ 24.6

Table 13 also displays zeta-potential (ζ, *mV*) results recorded at a specific pH that enabled the determination of the surface charge displayed by a particle. pLys/βpen polymers containing βpen units grafted to their backbone, are expected to display both amine ($-NH_2$) and ammonium groups ($-NH_3^+$) depending on the pH of the solution, but the number of amine/ammonium is expected to increase for the same number carboxylic acid/carboxylate groups for the same polymeric backbone size. Polymers prepared from pLys B (2000 Da < AMW < 3500 Da) display a hard to rationalize negative charge as opposed to the positive charge particles of polymers prepared from pLys C (3500 Da < AMW < 5000 Da). pLys/βpen AC', BC' and CC' possess higher positive than βpen particles in solution: charge (from + 13.3 mV up to + 24.6 mV) than that of βpen particles (+ 10.6 mV). This agrees with a high content of βpen moieties that display ammonium ions at pH = 7. pLys/βpen AB', BB' and CB' possess negative charge, which can be explained by a poor NH_2/NH_3^+ these polymers.

7.2.4 Preparation of cross-linked polymers (EPI / βpen and EGDE /βpen)

The preparation of cross-linked polymers involved the use of suitable monomers based on the structure of epichlorohydrin (EPI), a crosslinking agent. It is cheap, readily available and has been widely used in the preparation of CD polymers based on βCD [193]. Furthermore, EPI is slightly soluble in water thus the reaction can be carried out in water.

The methodology used to polymerize βpen units to each other is described in Figure 87. It is based on the nucleophilicity of the primary amino groups of βpen that are expected to ring open EPI and initiate a polymerization process, under basic conditions (NaOH). βpen was dissolved in aqueous diluted NaOH and EPI was added slowly to the reaction mixture, at 60-70

ºC. However, under aqueous basic conditions (NaOH), there is the possibility of deprotonation of the secondary hydroxyl groups (2-OH / 3-OH) leading to undesired secondary reactions. In turn, this leads to the formation of alkoxide anions expected to compete with the polymer growth reaction, between βpen and EPI. In such an event, the cavities will be blocked from their wider side, a not desired outcome.

After 29 h the reaction was stopped, the products were recovered by precipitation from acetone, extensively dialysed through a benzoylated dialysis tubing (MW_{CO} = 2000 Da) to remove small MW side products and afford EPI/βpen polymers and finally, freeze-fried.

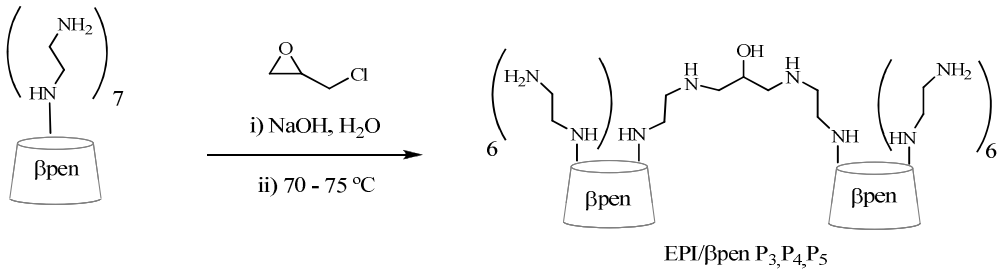

Figure 87. Preparation of EPI/βpen polymers, from reaction of EPI with βpen.

Three batches of EPI/βpen were thus prepared by varying the amounts of linker used according with the data displayed in Table 14. The characterization of EPI/βpen P_3/P_4/P_5 polymers and their use in several complexation / release experiments will be described in section 7.2.3. Unlike pLys / βpen polymers, due to the availability of raw materials (EPI and βpen), more material could be readily available and the characterization of these polymers was facilitated.

Table 14. Description of the polymer reaction conditions using EPI and βpen.

Polymer	Ratio (EPI/βpen)	n (EPI)	n (βpen)	Temp. (ºC)	Time	Amount
P_3	5	650 µmol	130 µmol	70 – 75 ºC	*29 h*	*240 mg*
P_4	10	1760 µmol	180 µmol	70 – 75 ºC	*2.5 h*	*229 mg*
P_5	20	3530 µmol	177 µmol	70 – 75 ºC	*2.5 h*	*225 mg*

In order to increase the hydrophilicity of the polymer, a symmetrical linker, ethylene glycol diglycidyl ether (EGDE) was prepared (see section 7.3.1) and used in the polymerization reaction with βpen, following a procedure similar to the one described for the preparation of EPI/βpen polymers. It is expected that the extra epoxide ring attached and EG linkage present in

EGDE unit, would offer equivalent reactivity of both ends and maybe higher AMW polymeric materials. The reaction is represented schematically in Figure 88.

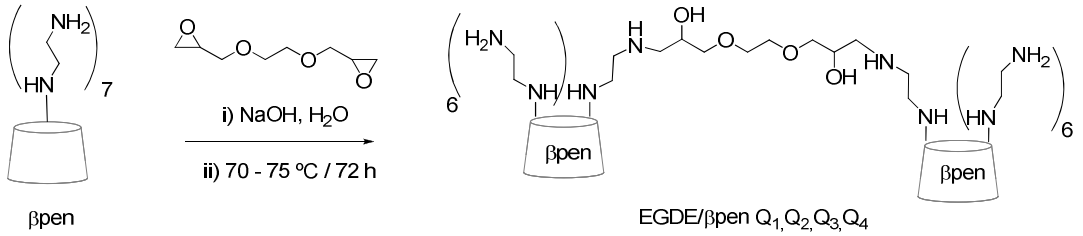

Figure 88. Preparation of EGDE/βpen polymers, from reaction of EGDE with βpen.

Four batches of EGDE/βpen polymers were prepared (Q_1, Q_2, Q_3, Q_4) varying the molar ratio between EGDE/βpen and the results are displayed in Table 15. EGDE/βpen polymers were characterized (see section 7.2.5), used in complexation studies and release experiments; the results were compared with those of EPI/βpen polymers.

Table 15. Description of the polymer reaction conditions using EGDE and βpen.

Polymer	Ratio (EGDE/βpen)	n (EGDE)	n (βpen)	Temp. (ºC)	Time (h)	Amount
Q_1	1	106 µmol	106 µmol	70 – 75 ºC	72 h	106 mg
Q_2	5	523 µmol	105 µmol	70 – 75 ºC	72 h	157 mg
Q_3	10	1050 µmol	109 µmol	70 – 75 ºC	72 h	241 mg
Q_4	20	1050 µmol	54 µmol	70 – 75 ºC	72 h	188 mg

7.2.5 Characterization of cross-linked polymers

Solubility, size and zeta-potential

The solubility and the appearance of aqueous solutions of EPI/βpen and EGDE/βpen, regarding the presence of aggregates, turbidity, gel formation was evaluated in diluted solutions (≈ 0.6 mg/mL) at 25 ºC. The results are summarized in Table 16 and these are in agreement with those found for pLys/βpen polymers, whereby all polymers enter the water phase but their aqueous solutions revealed cloudiness / turbidity.

Table 16. Aspect of the solutions of EPI/βpen and EGDE/βpen polymers tested for C = 0.6 mg/mL (25 ºC).

Polymer	Soluble
EPI/βpen P_3	Soluble; clear
EPI/βpen P_4	Soluble; cloudy
EPI/βpen P_5	Soluble; clear
EGDE/βpen Q_1	Soluble; clear
EGDE/βpen Q_2	Soluble; clear
EGDE/βpen Q_3	Soluble
EGDE/βpen Q_4	Soluble

The size distribution (diameter, d, *nm*) and zeta-potential (ζ, *mV*) for EPI/βpen and EGDE/βpen polymers were determined by DLS and are shown in Table 17. For DLS analysis polymeric solutions were not centrifuged. Additionally, only the most intense peak was represented as a percentage of the total size distribution (Table 17). The results are compared to those of βpen (Entry 1, Table 17). The results show that EGDE/βpen polymer particles are much bigger than EPI/βpen polymer particles. The size of EPI/βpen polymers particles seems to increase only above a ratio of EPI/βpen = 20, for P_5 (≈ 51 nm) and remain constant (≈ 33 nm) for ratios of EPI/βpen = 5 and 10 respectively for P_3 and P_4.. All EGDE/βpen and EPI/βpen polymers are positively charged and the charge is roughly the same for P_3 (+ 34 mV) and P_4 (+ 32 mV) but slightly higher for P_5 (+ 43 mV). Moreover, the polymers maintain a higher (3-4 fold) positive charge, compared to βpen, as planned.

Table 17. Size and zeta potential for EPI/βpen and EGDE/βpen polymers determined by DLS (25 ºC).

#	Sample	Concentration (mg/mL)	Size / Number (d, nm / %)	pH -	Zeta Potential (ζ, mV)
1	βpen	0.57	91 nm / 20 %	7.2	+ 10.6
2	EPI/βpen P_3	0.64	32 nm / 28 %	7.1	+ 34.0
3	EPI/βpen P_4	0.66	33 nm / 29 %	6.9	+ 32.0
4	EPI/βpen P_5	0.63	51 nm / 28 %	7.1	+ 43.0
5	EGDE/βpen Q_2	0.65	79 nm / 25 %	7.1	+ 34.0
6	EGDE/βpen Q_3	0.65	122 nm / 21 %	7.1	+ 45.5

Structure of the polymers

NMR spectroscopy was used to evaluate the polymerization products. Figure 89 compares the ^{1}H NMR spectra of EPI/βpen (P_3/P_4 and P_5, Figure 89 A, B and C) with that of βpen (Figure 89 D) used as starting material. The ^{1}H NMR spectrum of βpen (Figure 89 D) shows well-resolved signals with the characteristic anomeric peak (CD-H_1, ≈ 5 ppm), the

internal protons (CD-$H_{3/5}$, ≈ 4 ppm); CD-H_2 and CD-H_4 (3.8 ppm – 3.9 ppm) and CD-$H_{6/6'}$ is overlaid with alkyl chain ($H_{7/8}$). The broadness of the EPI/βpen (CD-H_1) in Figure 89 A is a characteristic signal such pLys/βpen polymers. This broad signals are in contrast, when compared with the signals of βpen (a sharp and defined spectrum).

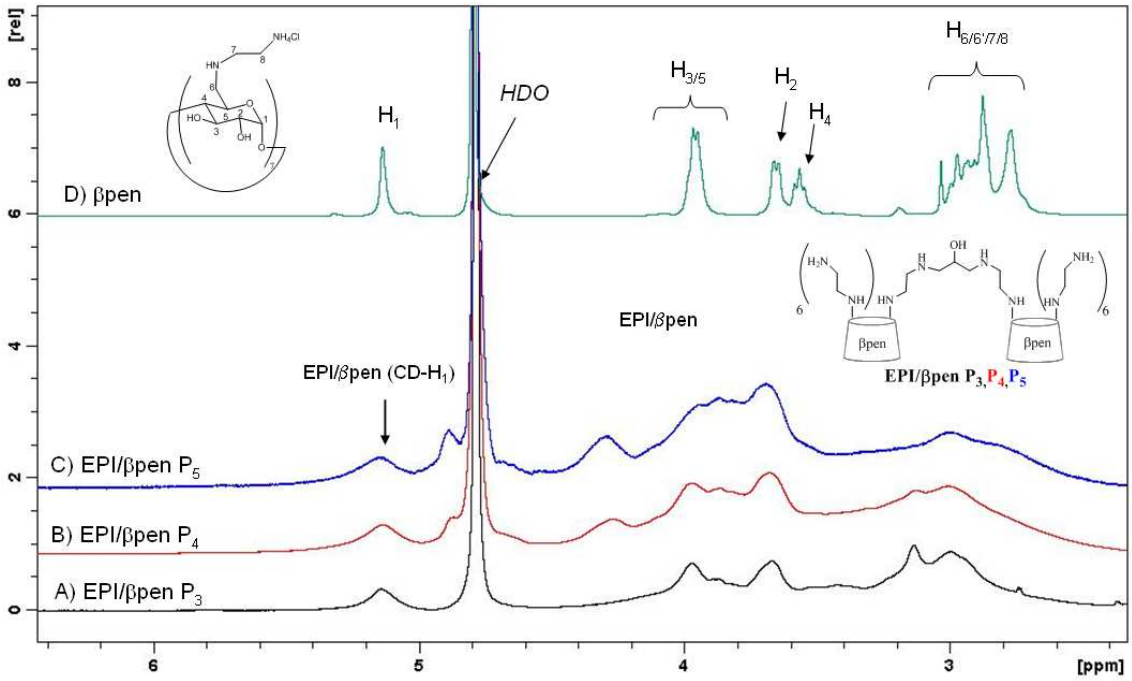

Figure 89. ^{1}H NMR spectra (D_2O, 500 MHz, 25 °C) of EPI/βpen polymers A) P_3; B) P_4; C) P_5 and D) starting material, βpen.

EPI/βpen is different from pLys/βpen, because the broad signals of EPI/βpen spread over the region, where signals of βpen are also expected (2.4 ppm to 4.6 ppm). The potentially useful signals of the hydroxyl groups (-OH), generated upon ring-opening reaction of epoxides, cannot be observed in D_2O, because they are in fast exchange with HDO in the NMR time scale. Furthermore, the ^{1}H NMR signals of the linkers overlap with the signals of polymeric βpen. Therefore, it will not be possible to estimate the relative ratio of CD units in each polymer, using the well-defined peak of CD-H_1 in βpen, like previously done for pLys/βpen polymers.

The polymeric character of EPI/βpen P_3, P_4 and P_5 was also assessed from the ^{13}C NMR spectra, comparatively to ^{13}C NMR spectrum of βpen (Figure 90). Broad signals in the ^{13}C NMR spectra of polymers (Figure 90 A, B, C) were observed, which agree with the multiple

connections typical of many polymeric matrix and are in opposition to the sharp peaks observed for βpen.

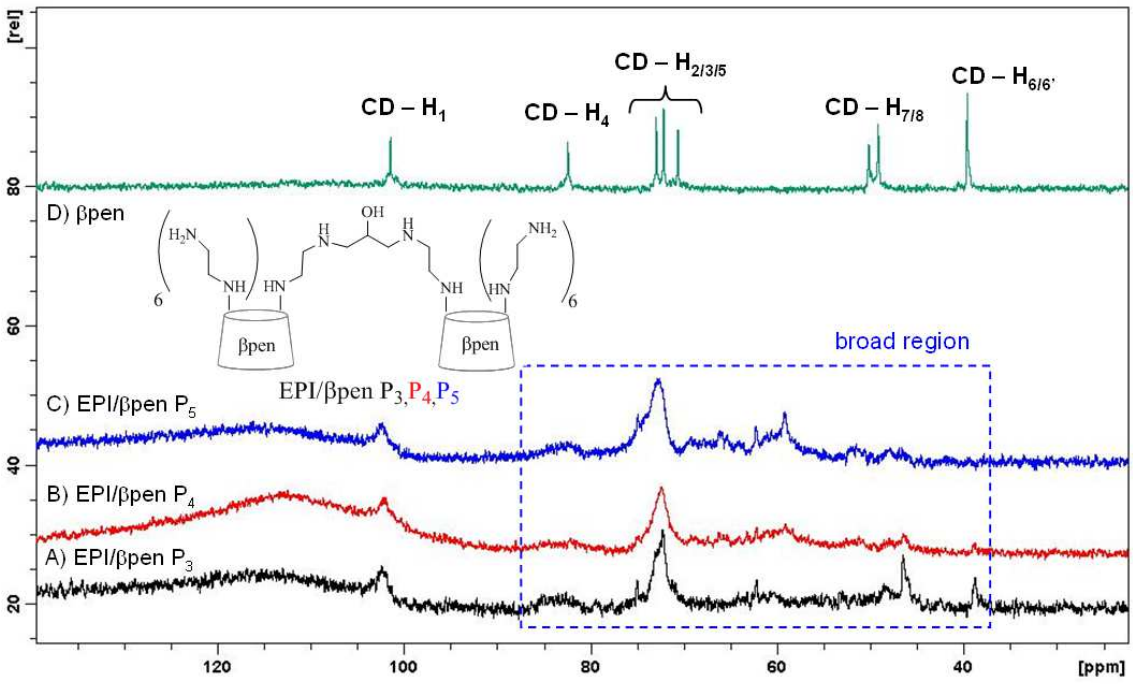

Figure 90. ^{13}C NMR NMR spectra (D_2O, 125 MHz, 25 °C) of EPI/βpen polymers A) P_3; B) P_4; C) P_5 and D) starting material, βpen.

In addition, 2D HSQC NMR experiment was performed on a sample of EPI/βpen P_3 and it revealed that in the aliphatic broad region of the ^{1}H NMR spectrum (Figure 90 A, 2.4 ppm – 4.6 ppm), there are many differently phased contours (–CH and –CH_2) corresponding to the cross-linked matrix of EPI / βpen P_3 polymer (Figure 91). A Chemdraw prediction based on a tentative polymer structure revealed good agreement between the ^{13}C NMR chemical shifts expected for EPI/βpen P_3 (35 ppm – 85 ppm) and those actually observed in the 2D HSQC (Figure 91).

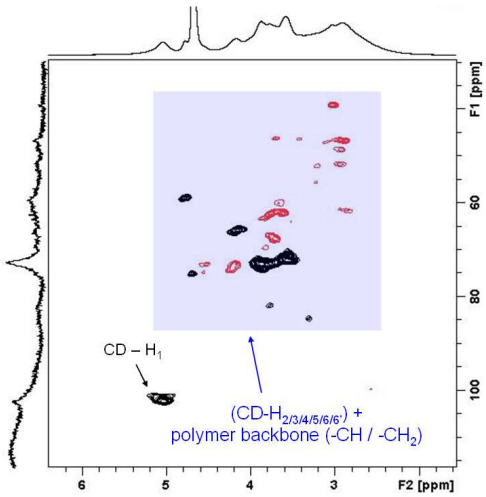

Figure 91. 2D HSQC NMR spectrum (D_2O, 25 °C) of EPI/βpen P_3.

Similarly, the ^1H NMR spectra of EGDE/βpen polymers Q_1, Q_2 and Q_3 shown respectively in Figure 92 A, B, C were compared to the ^1H NMR spectrum of βpen (Figure 92 D). Once again, broad signals and overlaid regions were observed in the aliphatic region of EGDE/βpen polymers (2.4 ppm – 4.2 ppm), indicating the success of the polymerization reactions. Although it is possible to identify the presence of βpen unit connected to the EGDE/βpen polymers, by the presence of resolved and isolated signal of the anomeric proton (CD-H_1, ≈ 5 ppm), the relative ratio of CD units in EGDE / βpen cannot be estimated for EGDE / βpen polymers from the NMR spectra. Therefore, other experimental methods will be used to estimate the amount of βpen content in each polymer.

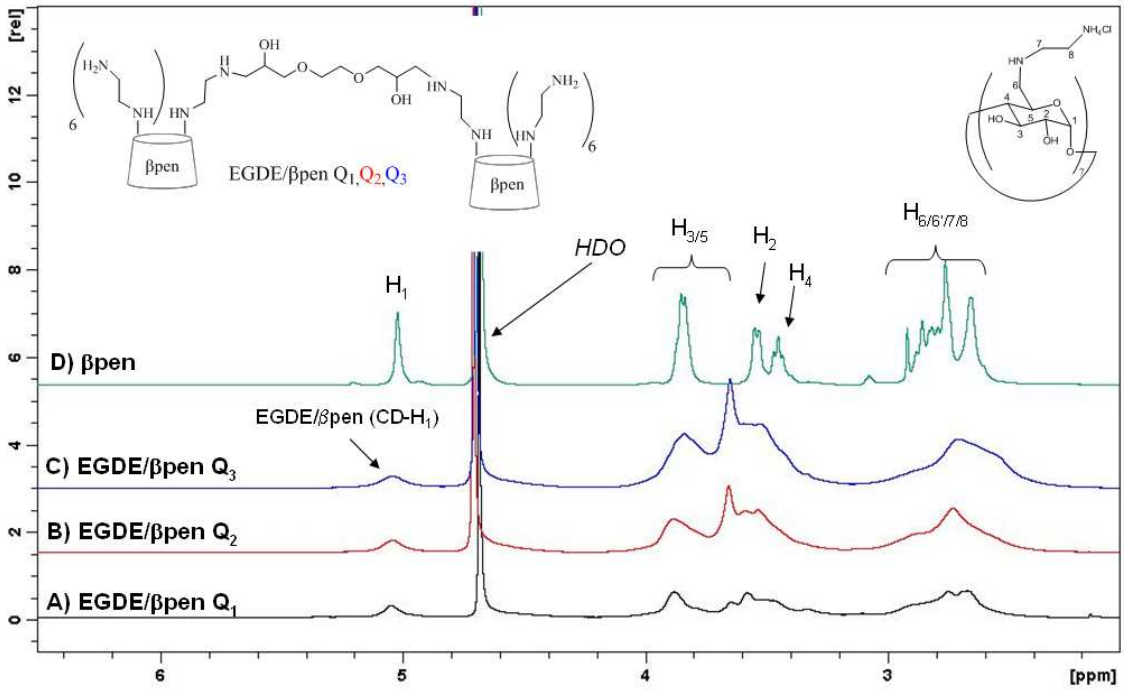

Figure 92. ^{1}H NMR spectra (D_2O, 500 MHz, 25 ºC) of EGDE/βpen polymers A) Q_1; B) Q_2; C) Q_3 and starting material βpen.

X-ray powder diffraction (XRD)

XRD is a useful technique to judge the degree of crystallinity of any solid sample, characterized by an X-ray diffraction pattern, which gives a graphical representation, of X-ray intensity as a function of the angle of diffraction (2θ). Any crystalline sample is characterized by well-defined diffraction pattern (sharp lines at specific 2θ values) and a corresponding graph with very sharp peaks, which contrasts with a poor diffraction pattern (broad shaded regions) and a 2θ graph with broad peaks/regions typical of an amorphous sample.

The diffraction patterns and 2θ graphs of EPI/βpen P_5 was determined and compared to that of βpen (Figure 93). Although βpen is not a crystalline material, it revealed a semi-crystalline phase with very sharp peaks (Figure 93 A). After reaction, βpen loses its crystallinity and gives rise only to broad peaks in EPI/βpen P_5 (Figure 93 B). The similarities between the maximum values observed for (2θ ≈ 20) in βpen and in EPI/βpen P_5, agrees with the expected structural similarity between βpen and EPI/βpen P_5. The remaining polymeric batches (EPI/βpen and EGDE/βpen polymers) revealed similar features in comparison to βpen, thus verifying the amorphous nature of the polymeric materials prepared.

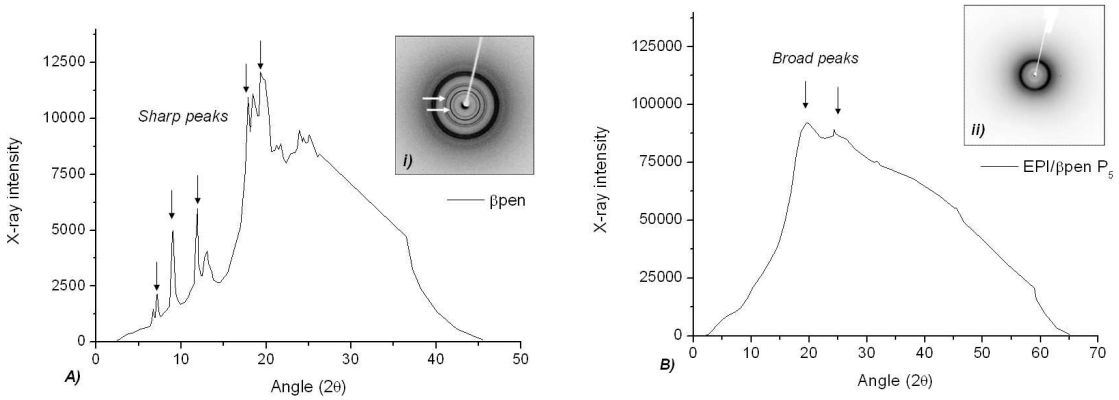

Figure 93. Graphical representation of 2θ curves for A) βpen and B) EPI/βpen P_5 and of both diffraction patterns shown as insets.

The X-ray results indicate that the polymerization reaction was successful in linking βpen units to a polymeric backbone. After, polymerization βpen loses its semi-crystalline features (sharp peaks, Figure 93 A) and an amorphous material is formed, EPI/βpen P_5 (broad peaks, Figure 93 B), in agreement with NMR results.

Elemental Analysis

Elemental analysis was used to determine the relative percentage of nitrogen (% N), present in each cross-linked polymers (EPI/βpen and EGDE/βpen). Since the only source of nitrogen (N) in the polymer comes from βpen, the higher the nitrogen content (% N) in a polymer the more βpen units it will contain. The nitrogen content of βpen (% $N_{\beta pen}$ = 10.83), estimated for a molecular formula of βpen.7HCl.7H_2O ($C_{56}H_{133}N_{14}Cl_7O_{35}$), was used as a reference in the estimation of the CD content of each polymer. The quotient (R, Table 18) between the nitrogen content of the polymer (% N) and that of βpen (% $N_{\beta pen}$), gives a relative amount of βpen attached to the polymer backbone and an estimation of the amount of CD in each polymer. Table 18 displays elemental analysis results for EPI/βpen and EGDE/βpen.

Table 18. Elemental analysis data for EPI/βpen and EGDE/βpen polymers.

Polymeric Samples	βpen / Linker	C (%)	H (%)	N (%)	R = N / $N_{\beta pen}$
βpen	-	39.9	7.1	10.8	1.00
EPI/βpen P_4	(1:10)	41.7	7.7	7.9	0.68
EPI/βpen P_5	(1:20)	42.0	7.5	7.0	0.60
EGDE/βpen Q_1	(1:1)	43.6	7.9	9.9	0.85
EGDE/βpen Q_2	(1:5)	45.3	8.4	7.6	0.66
EGDE/βpen Q_3	(1:10)	47.5	8.6	6.5	0.56
EGDE/βpen Q_4	(1:20)	45.0	8.0	5.0	0.43

The results show that for EPI/βpen P_4 (1:10); R = 0.68 > EPI/βpen P_5(1:20); R = 0.60 indicating that: the higher the linker content, the smaller is the number of CDs attached to the polymer backbone. Additionally, comparing EPI/βpen P_4 (1:10); R = 0.68 to EGDE/βpen Q_3 (1:10); R = 0.56 it seems that: the extra epoxide ring in EGDE structure promotes a high crosslinking of the polymers, instead of promoting further points of attachment for new βpen units.

Average Molecular Weight

The determination of polymer average molecular weight (AMW) is important because the magnitude of AMW often determines most of polymer macroscopic properties like the glass transition temperature (T_g), the modulus (or stiffness) and tensile strength [201]. The AMW value of a polymer depends on the experimental technique used. Suitable techniques are dynamic light scattering (DLS), size exclusion chromatography (SEC), vapour pressure osmometry (VPO) and viscometry [202]. Often these techniques rely on standards to calibrate the instrumental apparatus like polymers of "known" molecular weight, resulting in AMW average values with reasonable uncertainties. An alternative method that offers more reliable results is mass spectrometry MS, using matrix-assisted laser desorption ionization with time of flight detection (MALDI-TOF). MS (MALDI-TOF) provides direct access to molecular weight data rather than average values and could allow the direct observation of different end groups. However, accurate and reproducible results are often dependent on the matrix selection and methods for the preparation of sample [203].

From our perspective, the determination of AMW value is important because it would enable: i) the calculation of the exact amount of polymeric material to be used for the release experiments and ii) it would be possible to relate the ratio between host – guest molecules, with the expected stoichiometry of the interaction if available. Table 19 shows AMW values for EPI/βpen and EGDE/βpen polymers determined by: vapour pressure osmometry (VPO), static light scattering (SLS) and mass MS (MALDI-TOF).

AMW determined by VPO revealed an AMW = 2130 Da for EPI/βpen P_3, which agrees with MALDI-TOF MS results for EPI/βpen P_4, P_5 and for EGDE/βpen Q_1, Q_2 and Q_3 indicating small average molecular weight, heavily cross-linked polymers containing few CD units. The AMW of EGDE/βpen Q_1, Q_2 and Q_3 determined by static light scattering (SLS) revealed very high molecular weight polymers, which is contradictory with the result obtained from MALDI-TOF MS analysis for the same polymer batch. However, the inconsistency in these results can be understood in the light of the limited water solubility revealed by polymeric solutions, given

that the method used to record SLS results relies on the preparation of a series of aqueous solutions with varying concentrations.

Therefore, the most reliable results were based on MALDI-TOF MS revealing that all EPI/βpen and EGDE/βpen polymers, on average, are represented as a distribution of masses of small average molecular weight ranging from ≈ 2500 to ≈ 3400 Da (Table 19). The small increase in the molecular weight of the polymers, noticed as the amount of linker (EPI or EGDE) added increases, corresponds to an increase in the crosslinking of the polymeric materials (EPI or EGDE), which corroborates the elemental analysis results.

Table 19. Average molecular weight of EPI/βpen and EGDE/βpen polymers determined by different analytical methods;

Polymer	MALDI-TOF MS (AMW)	Vapour Pressure Osmometry(VPO)	Static Light Scattering (SLS)
EPI/βpen P_3	**-**	**2130**	**-**
EPI/βpen P_4	2557	-	-
EPI/βpen P_5	2596	-	-
EGDE/βpen Q_1	2640	-	19800
EGDE/βpen Q_2	2935	-	60600
EGDE/βpen Q_3	3012	-	81000
EGDE/βpen Q_4	3381	-	-

The attachment of βpen units to both polymers would promote the increase in AMW, by at least 1430 g/mol corresponding to the molecular weight of one βpen unit. The MALDI-TOF MS of EPI/βpen P_4 (Figure 94 A) revealed the loss of βpen and at least one more peak at ≈ 5000 m/z, indicating the presence of a small percentage of higher molecular weight polymer. Likewise, the MALDI-TOF MS of EGDE/βpen Q_4 (Figure 94 B) revealed the loss of βpen and the presence of small percentage of high molecular weight polymer fractions, with peaks corresponding to ≈ 7000 m/z and ≈ 11000 m/z. However is the regular heptet observed, with the corresponding to 7 fragments, attributed to the loss of EGDE (≈ 174). This indicates that instead of acting as a polymer linker in connecting different βpen units, EGDE is probably blocking all seven amino groups, limiting the success of the polymerization strategy and increasing the crosslinking degree in EGDE/βpen polymers.

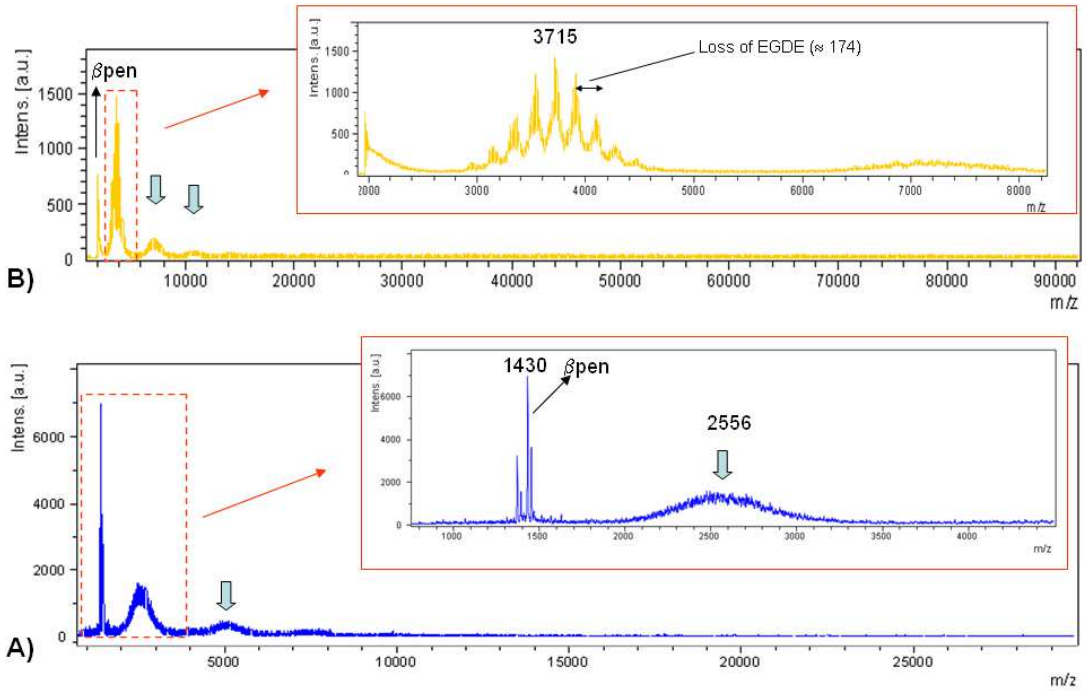

Figure 94 – MS (MALDI-TOF) of A) EPI/βpen (10:1) P_4 and of B) EGDE/βpen (20:1) Q_4.

The preparation of positively charged polymers through the incorporation of βpen into polymer matrices, based on preformed polymers and on the usage of linkers proved to be of limited success. Although the connectivity of the βpen to each polymer was achieved, the small amount of material collected poses restrictions on both the characterization and application studies of these promising CD-polymers, which were nevertheless studied in selected cases, regarding their ability to act as host and as release rate modulators of model guest molecules and nucleotides.

7.2.6 **Inclusion complexes of βpen with selected guest molecules**

βpen as a model host

In order to evaluate the ability of EPI/βpen and EGDE/βpen polymers to interact with potential useful molecules, βpen (Figure 95 A) was used as model host because: i) βpen is part of EPI/βpen and EGDE/βpen polymeric structures and ii) βpen as been prepared and characterized in our group by NMR spectroscopy. The model guests used for evaluate the complexation with bpen and with CD-polymers prepared were adenosine 5'-monophosphate (5'-AMP, Figure 95 B) and 4-aminobenzoic acid (PABA, Figure 95, C).

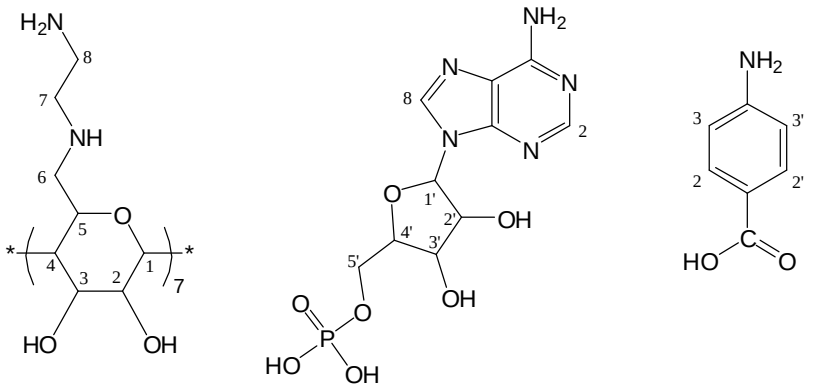

Figure 95. Structures of host (βpen) and guest molecules (5'-AMP and PABA).

PABA has been used because: i) at physiological pH, it is mostly present as a carboxylate anion which maximizes the interaction with positively charged CD like βpen; iii) PABA has the perfect size/shape to fit the cavity of βpen and it shows a very simple ^{1}H NMR spectrum; finally, iv) PABA find most of its applications as UV filter in sunscreens. On the other hand, 5'-AMP was used because it is a readily available, cheap nucleotide and revealed interactions through formation of inclusion complexes with *per*(6-guanidino)-CDs (α-, β-, γ-guan), following several stoichiometries and modes of interaction [196]. If successful, a similar strategy can be applied and used to study the interaction of gemcitabine monophosphate with CD-polymers.

NMR spectroscopy was used to study the intermolecular interactions between the model guest molecules (5'-AMP and PABA) and the host βpen macrocycle. ^{1}H NMR and 2D ROESY NMR experiments were performed in phosphate buffered saline (PBS, pH = 7.4) at 25 ºC.

4-Aminobenzoic acid (PABA) with βpen

The ^{1}H NMR spectrum of βpen was recorded before and following the addition of the guest (PABA). A chemical shift difference was observed in the aliphatic region (3.7 ppm – 3.9 ppm), corresponding to the region of βpen internal protons (CD-H_3/H_5). 2D ROESY NMR experiment revealed strong dipolar interactions, between PABA-$H_{3/3'}$ and βpen CD-H_3 and between PABA-$H_{2/2'}$ and CD-H_5 (Figure 96 A). These intermolecular interactions support by a preferred mode of interaction, with the carboxylate moiety of PABA molecule oriented towards the primary side of βpen, leaving the amino group facing the secondary side of the host molecule (Figure 96 B).

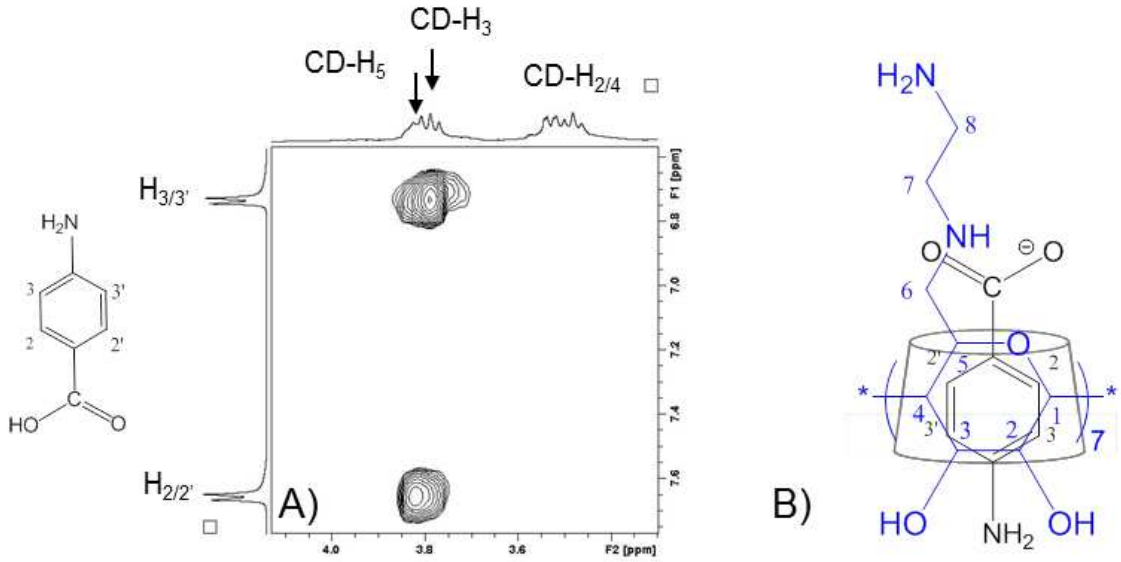

Figure 96. A) 2D NMR ROESY (25 ºC) spectrum expansion revealing intermolecular dipolar interactions between βpen and PABA. B) Mode of inclusion proposed for the complexation between these two molecules, based on NMR data.

Adenosine 5'-monophosphate (5'-AMP) with βpen

5'-AMP interaction with βpen was evaluated by NMR spectroscopy. The ^{1}H NMR of βpen was recorded before the addition of 5'-AMP, which promotes a change in the chemical shift of βpen internal protons resonances (CD-$H_{3/5}$). After addition of 5'-AMP in 4-fold excess to maximize interactions, the ^{1}H NMR spectrum revealed shielding of CD-$H_{3/5}$ and deshielding of CD-$H_{2/4}$ and CD-$H_{6/6'/7/8}$. The 2D ROESY NMR experiment (Figure 97 A) revealed that the internal protons of βpen (CD-$H_{3/5}$), showed many interactions with different protons of 5'-AMP, namely with: i) the ribose protons ($H_{1'/2'/3'/4'/5'}$, Figure 97 C, D) and with ii) the protons

from the nucleobase (H_2, H_8) (Figure 97 B). All of these interactions both with the primary/secondary side of βpen cavity and with multiple sites of the 5'-AMP molecule suggest a complexation equilibrium involving multiple species and perhaps a complex stoichiometry.

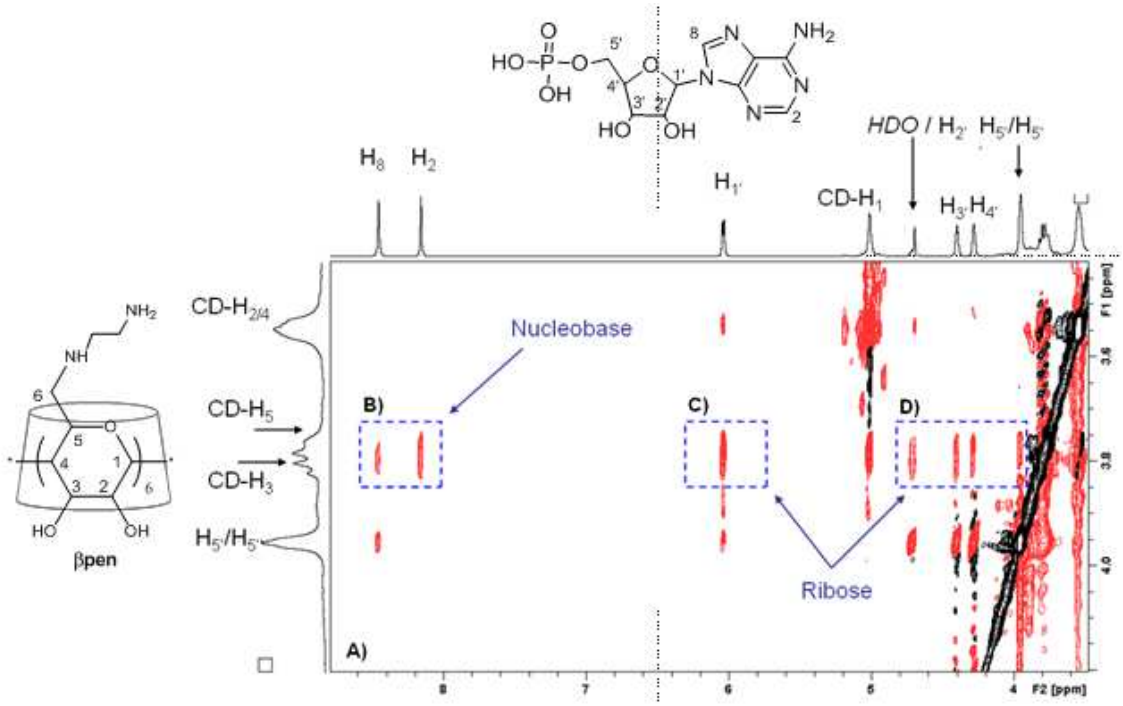

Figure 97. A) 2D ROESY NMR spectrum (25 ºC) with an expansion revealing multiple intermolecular dipolar interactions between βpen and 5'-AMP. B) Region of the spectra corresponding to CD-$H_{3/5}$ interactions.

The table of multiple intermolecular dipolar interactions (Table 20 A), between every proton of βpen and of 5'-AMP was obtained from the intensity of the contour peaks in a 2D ROESY experiment (Figure 97 A).

Table 20. 5'-AMP / βpen complex: i) table of intermolecular dipolar interactions between 5'-AMP and βpen; ii) proposed model of inclusion for this complex, following a 2:1 stoichiometry (G:H).

A)

5' – AMP \ βpen	H_3	H_5	$H_{6,6'}$	$H_{7,8}$
H_2	✔	✔		
H_8	✔			
$H_{1'}$	✔	✔		
$H_{2'}$	✔			
$H_{3'}$	✔	✔		
$H_{4'}$	✔	✔	✔	✔
$H_{5'}$	✔	✔	✔	✔

B)

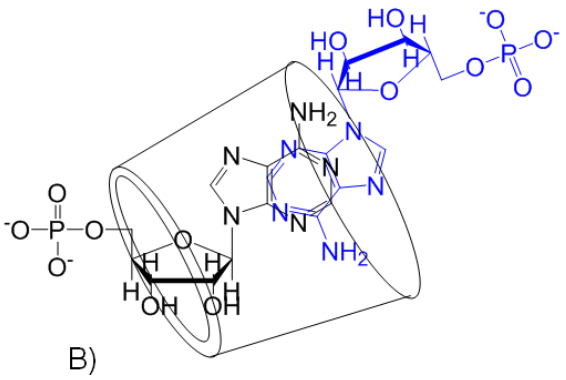

The continuous variation method (Job' plots) was applied to determine the stoichiometry of complexation, between βpen (host, H) and 5'-AMP (guest, G). ^{1}H NMR spectroscopy was used to evaluate proton chemical shift changes (Δδ), resulting from the addition of a G solution to an initial solution of H, both kept constant and equal to 10 mM, prepared in deuterated phosphate buffer saline (PBS). The resulting Job' plots (Figure 98) revealed that there is inclusion of 5'-AMP into βpen resulting in:

i) shielding of βpen internal proton (CD-H_5) observed by a positive chemical shift change (+ Δδ), attributed to inclusion

ii) deshielding of the aminoethylamino group (CD-H_7 /CD-H_8) justified by a negative chemical shift change (- Δδ), due to the presence of phosphate anion group facing the primary side of the macrocycle

The Job' plots maximum (CD-H_5) and minimum (CD-H_7 /CD-H_8) were observed to ([H] / ([H] + [G]) = 0.3, corresponding to a stoichiometry of complexation 5'-AMP / βpen = 2:1 and confirming the multiple interactions observed from the 2D ROESY experiment (Figure 97 A).

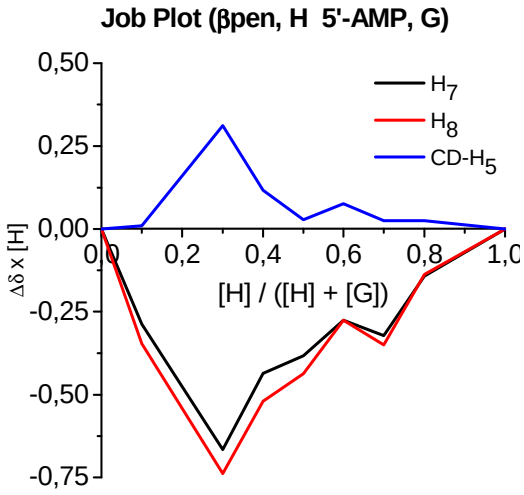

Figure 98. Job plot for titration of βpen in the presence of 5'-AMP.

Considering the above data, a suggestion of an inclusion model is depicted in Table 20 B. The model is consistent with the inclusion of one 5'-AMP with the phosphate group toward the positively charged amino side as previously observed [196], but illustrates the known

tendency of the nucleotides to dimerise *via* head-to-head stacking of the flat aromatic base moieties.

7.2.7 Inclusion complexes of polymers with selected guest molecules

EPI/βpen P_3 with PABA

Following the successful complexation experiment of βpen with PABA, the same guest molecule (PABA) was used to determine if βpen cavities in EPI/βpen P_3 polymer (see chapter 7.2.6) were available and free for inclusion. The initial ^{1}H NMR spectrum of EPI/βpen P_3 was broad and unresolved and after the addition of an excess of PABA (≈ 4.8 molar eq.) to the polymer solution, a slight change in the peaks of aliphatic broad region of the spectra was observed. 2D ROESY NMR experiment (Figure 99 A) revealed strong dipolar intermolecular interactions, between βpen internal protons (CD-H_3/H_5) and PABA aromatic signals ($H_{2/2'}$/$H_{3/3'}$) suggesting that βpen cavity grafted to EPI/βpen P_3 backbone interacts with PABA and is therefore free to load other molecules, like nucleotides (5'-AMP). A proposed model of inclusion for the complexes with PABA is depicted in Figure 99 B.

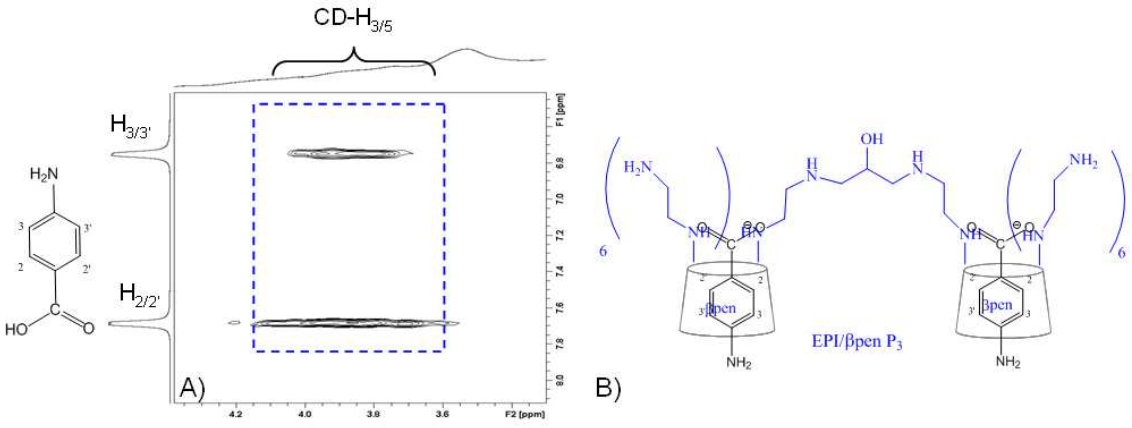

Figure 99. A) 2D NMR ROESY spectrum (25 ºC) expansion revealing intermolecular dipolar interactions, between EPI/βpen P_3 and PABA; B) Mode of inclusion proposed for the complexation between these two molecules.

This successful result shows that EPI/βpen polymers can be used as carriers for other molecules such as 5'-AMP and will be explored as host systems and tested as modifiers of release of 5'-AMP through a dialysis membrane (see section 7.2.9).

pLys.βpen BB' with PABA

PABA was likewise used as model guest to evaluate the availability of βpen cavities in pLys/βpen BB' polymers for inclusion. ^{1}H NMR spectrum of pLys / βpen BB' was recorded, followed by addition of an excess of PABA. The presence of PABA in solution is observed by its characteristic aromatic peaks, but the detection of CD-H_3/H_5 chemical shifts was not possible from the ^{1}H NMR spectra of pLys.βpen BB', due to the big overlap in the aliphatic region (3.7 ppm - 3.9 ppm). The assignment of the region between 3.7 ppm – 3.9 ppm to the resonances of CD-H_3/H_5 was obtained from 2D HSQC spectrum (Figure 100 A) and 2D ROESY NMR spectrum (Figure 100 B) revealed dipolar interactions, between PABA-$H_{2,2',3,3'}$ and the internal protons of the βpen (CD-H_3/H_5), grafted to pLys.βpen BB' (3.7 ppm - 3.9 ppm, blue region Figure 100 A and Figure 100 B). Likewise, the successful inclusion of PABA into βpen cavities of pLys/βpen BB' polymer, indicates that these cavities are also accessible for inclusion of other suitable guest molecules.

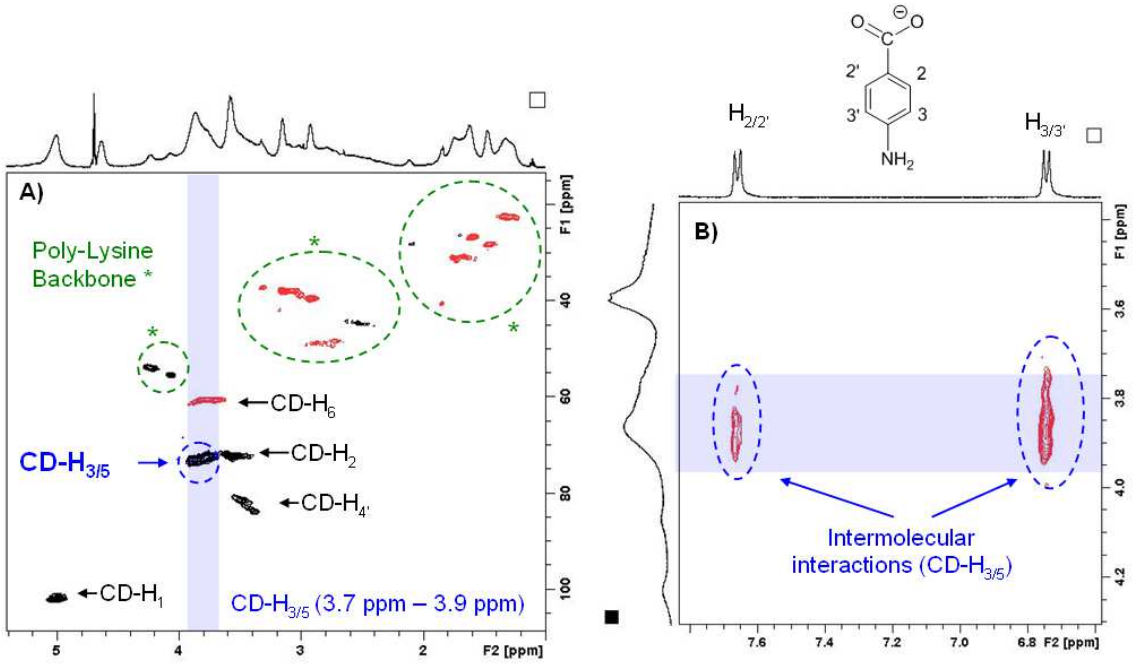

Figure 100. 2D NMR experiments (25 ºC) of pLys/βpen BB' (1.2 mg / 0.5 mL D_2O) in the presence of an excess of PABA: A) 2D NMR HSQC and B) 2D NMR ROESY.

pLys/βpen T_2 with 1-adamantanamine hydrochloride (ADA-NH_3Cl)

The evaluate the usefulness of pLys/βpen polymers as versatility host systems, the inclusion studies were extended to 1-adamantananime hydrochloride (ADA-NH_2.HCl). In addition, it is structurally very similar to 1-adamantanecarboxylic acid (ADA-COOH), a starting material used in the preparation of gemcitabine-adamantanamide (GEM-ADA amide), a molecule that revealed limited solubility in water and posed stability problems in methanol solutions.

The ^{1}H NMR characteristic signals of ADA-NH_2.HCl in D_2O are expected in the aliphatic region of the spectrum (< 2.3 ppm) [187]. The ^{1}H NMR spectrum of pLys/βpen T_2 solubilised in D_2O was recorded before and after the addition of ADA-NH_2.HCl: all regions of the spectrum revealed broad peaks and overlapping regions. As previously, 2D ROESY NMR experiment revealed strong intermolecular interactions between, the internal protons of βpen (CD-H_3/H_5, 3.8 ppm – 4.0 ppm) and those of ADA-NH_2.HCl (1.6 ppm – 2.4 ppm), which are attributed to the formation of an inclusion complex (Figure 101 B): positively charged amino-end of ADA-NH_2.HCl, will be facing the secondary side of βpen cavities in the polymer. This agrees with the expected electrostatic repulsion between the positively charged amino group of ADA-NH_2.HCl and the positively charged primary side of the βpen in the polymer with the several aminoethylamino chains.

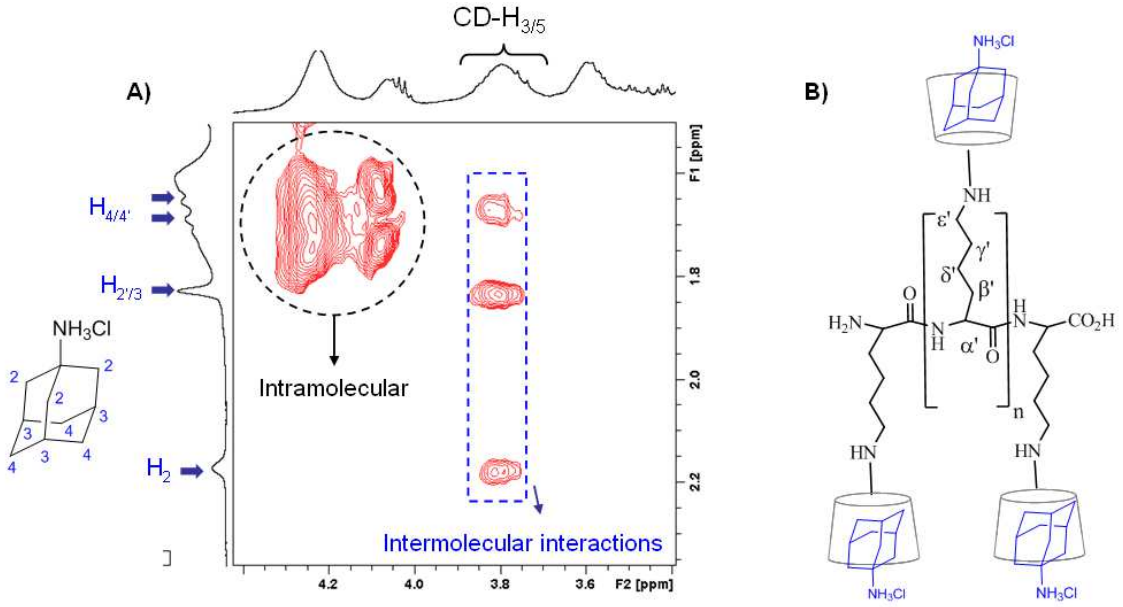

Figure 101. A) 2D NMR ROESY spectrum (25 °C) of pLys/βpen T_2 in the presence of ADA-NH_2.HCl; B) the proposed model of inclusion for this complex.

7.2.8 **Inclusion studies of polymers with gemcitabine-adamantanaminde (GEM-ADA amide)**

pLys/βpen BB' with GEM-ADA amide

The initial ^{1}H NMR spectrum of a pLys/βpen BB' polymer solution was recorded, followed by the addition of GEM-ADA amide. 2D ROESY NMR experiment (Figure 102 A) revealed strong intermolecular interactions, between ADA-moiety of GEM-ADA amide (1.6 ppm – 2.2 ppm) and the internal protons of βpen in the polymer (CD-H_3/H_5, 3.7 ppm – 3.9 ppm). The proposed model of inclusion (Figure 102 B) suggests that GEM-ADA amide in included in βpen cavities of pLys/βpen BB', through insertion of ADA moiety into the secondary side of the CD macrocycle.

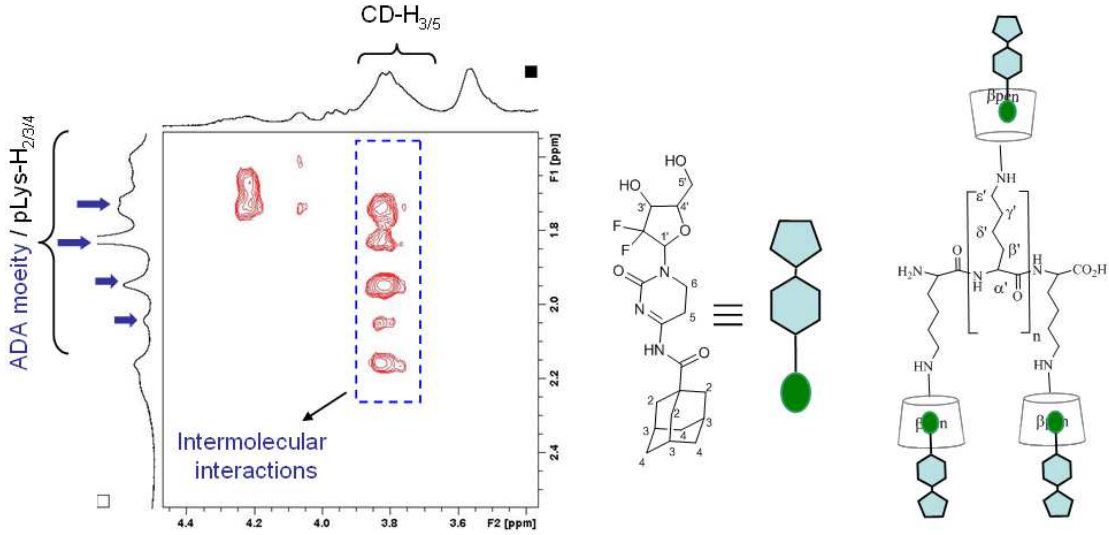

Figure 102. A) 2D NMR ROESY spectrum (25 ºC) of pLys/βpen BB' (1.0 mg / 0.5 mL D_2O) in the presence of an excess of GEM-ADA amide and B) proposed model of inclusion for the complex between GEM-ADA amide and pLys / βpen BB'.

These preliminary trials reveal that pLys/βpen polymers are suitable for inclusion of charged molecules, which offers advantages regarding the potential stability of sensible formulations based on gemcitabine. Additionally, the attachment of an ADA moiety to the GEM.HCl structure offered additional chemical protection to GEM structure and added a ADA moiety suitable for inclusion into CD polymers, such pLys.βpen BB'.

7.2.9 Polymers as release rate modifiers of selected nucleotides

One of the fundamental characteristics of a polymeric material in a formulation is its ability to modulate the release rate of a drug. CD-polymers are known to modify the release rates of several drugs and the manner by which this is achieved has been described [109].

To evaluate the ability of CD-polymers to complex and delay the release of nucleotides into solution, a modified Franz cell was used to study the release of a model nucleotide (5'-AMP) through a permeable membrane (benzoylated dialysis tubing, MW_{CO} = 2000 Da) in phosphate buffer saline (PBS, pH = 7) at 37 ºC (see section 9). A Franz cell apparatus is shown in Figure 103 and comprises: a donor and a receptor compartment, separated by a hollow junction to which a dialysis membrane (MW_{CO} = 2000 Da) is attached, it is filled with media and is kept at constant temperature (37 ºC) under constant magnetic stirring. The analyte to be tested (5'-AMP, 1 mM in PBS) is added to the donor side and at a given time intervals, the content of the receptor is sampled, replacing each time the volume taken with fresh solvent (PBS). It was assumed that: i) the benzoylated dialysis tubing (MW_{CO} = 2000 Da) is permeable to 5'-AMP; ii) 5'-AMP diffuses from the donor to the receptor at a constant rate for a given temperature and concentration of 5'-AMP.

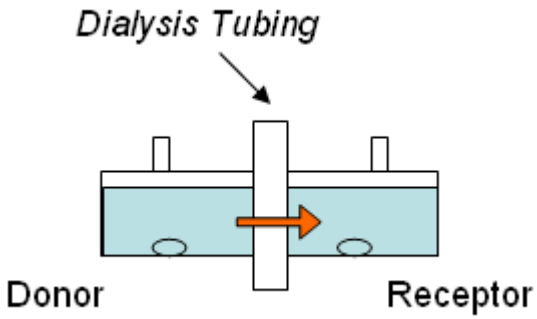

Figure 103. Modified Franz-cell set up used for the determination of the release rates, with two compartments separated by a hollow junction to which is attached a benzoylated dialysis tubing MW_{CO} = 2000 Da.

The rate of release can be calculated by determining the amount of 5'-AMP released into the receptor, if equal volumes are collected, at fixed time intervals (0, 60, 120, 180, 240, 300 and 360 min), followed by replacement with fresh PBS in the compartment each time. The drawn liquid were subsequently analysed with HPLC.

UV-Vis spectroscopy was used for identifying a suitable wavelength (λ) for the detection 5'-AMP. Figure 104 A shows the UV-Vis spectrum of an aqueous solution of 5'-AMP

(62 μM) prepared in PBS and λ was chosen close to the maximum of absorption (λ = 258 nm). Consequently, a calibration curve for 5'-AMP (Figure 104 B) revealed a linear response for 5'-AMP prepared in concentrations ranging from 5 μM to 250 μM, with detection wavelength (λ = 254 nm).

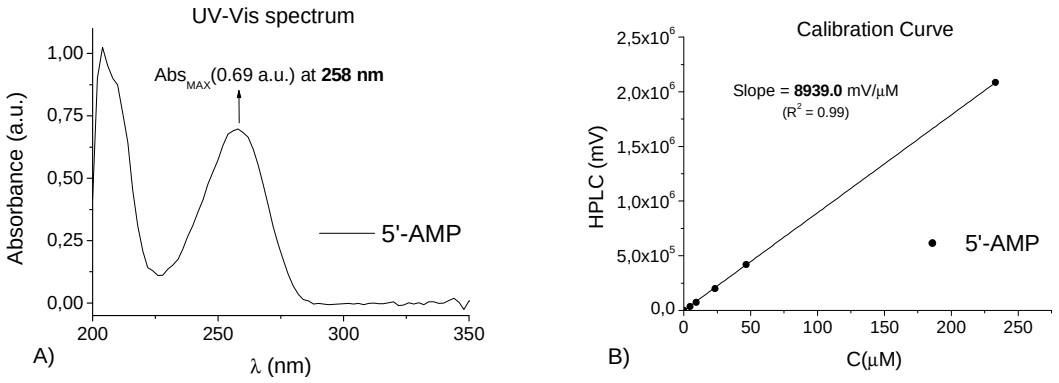

Figure 104. A) UV-Vis absorption spectrum of 5'-AMP (62.5 μM; PBS) and B) calibration curve for 5'-AMP determined by HPLC analysis with UV-detection at λ = 254 nm.

Several trials were executed to evaluate the capacity at polymers prepared to release 5'-AMP in aqueous buffered solutions (1 mM, PBS, pH = 7.4), through a dialysis membrane using the modified Franz-cell (Figure 103).

Figure 105 A shows the release rates of: i) 5'-AMP (1 mM, PBS) used as a blank experiment; ii) 5'-AMP (1 mM, PBS) in the presence of EPI/βpen P_5 (3.2 mg/mL, PBS) and iii) 5'-AMP (1 mM, PBS) in the presence of βpen.HCl (1 mM, PBS) used as model complexation agent. Comparison shows that the release rates of: 5'-AMP (18.0 μM/h) > 5'-AMP + βpen.HCl (13.8 μM/h) > 5'-AMP + P_5 (9.0 μM/h). Therefore, 5'-AMP will diffuse through the benzoylated dialysis tubing (MW_{CO} = 2000 Da) 1.3 times faster than 5'-AMP in the presence of an equimolar solution of βpen.HCl, which can be explained by the formation of an inclusion complex between 5'-AMP and βpen.HCl. However, 5'-AMP in the presence of EPI/βpen P_5 (9.0 μM/h) is released twice as slow in the donor side, than 5'-AMP alone (1 mM; 18.0 μM/h) . That can be explained by: i) inclusion / complexation with βpen present in EPI/βpen P_5 and ii) the possible entanglement, between different polymer chains, can physically delay the diffusion of 5'-AMP through the membrane. Given the cloudiness that is noticed during the preparation of polymeric aqueous solutions, namely those of EPI/βpen (Table 16), it is reasonable to expect that aggregation can affect the release rate of 5'-AMP in solution, even starting from diluted solutions like 1 mM in donor compartment.

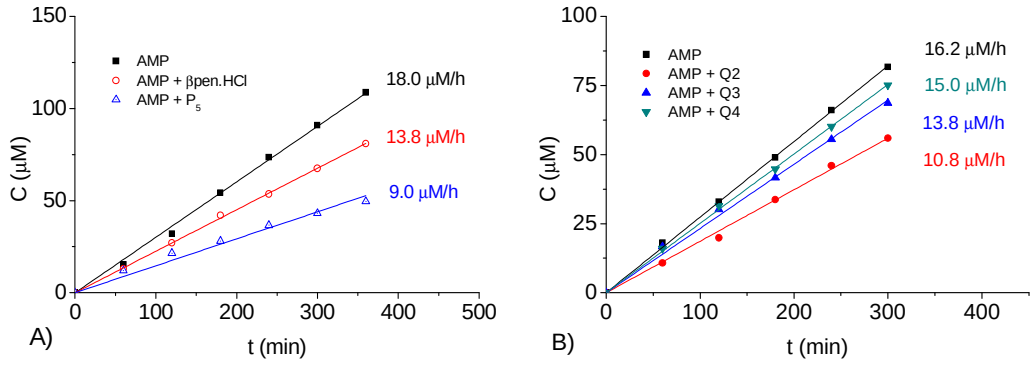

Figure 105. Release rates experiments: trial 1: 5'-AMP as a blank; AMP + βpen.HCl and 5'-AMP + P_5. Effect of changing the polymer content of linker (EGDE/βpen Q_2, Q_3 and Q_4) on the release rate of 5'-AMP, through a dialysis membrane.

Similar results were found when the release rate of 5'-AMP (1 mM, PBS) used as a reference, was determined in the presence of EGDE/βpen Q_2, Q_3 and Q_4 (1.6 mg/mL, PBS) polymers Figure 105 B: i) the release of 5'-AMP (16.2 μM/h) agrees with the value found previously (average = 17.1 μM/h); ii) 5'-AMP is retained longer in EGDE/βpen polymers, with similar release rates: Q_2 (10.8 μM/h), Q_3 (13.8 μM/h) and Q_4 (15.0 μM/h); iii) EGDE/βpen Q_2, Q_3 and Q_4 polymers show higher release rates than EPI/βpen P_5, meaning that EGDE/βpen polymers are less effective in retaining 5'-AMP than EPI/βpen polymers. A reason for these changes in the release rate of different CD-polymers might be related to the different βpen content in each polymer.

Therefore, the release rate of 5'-AMP (1 mM, PBS) was determined in the presence of different amounts of βpen.HCl, keeping 5'-AMP a constant concentration (1 mM, PBS) (Figure 106 A). The results showed that: i) the release rate of 5'-AMP (19.8 μM/h) is comparable to the previous trials (average = 18.0 ± 1.8 μM/h) and ii) the release rates of 5'-AMP is affected by the presence of increasing amounts of βpen.HCl: 19.2 μM/h; 5'AMP + βpen.HCl (R = 0.65) > 10.2 μM/h; 5'-AMP + βpen.HCl (R = 1.03), considering $R = n_{\beta pen} / n_{5'\text{-}AMP}$. This indicates that the presence of more βpen enhances the retention of 5'-AMP on the donor compartment, due to inclusion into the βpen units of the polymer.

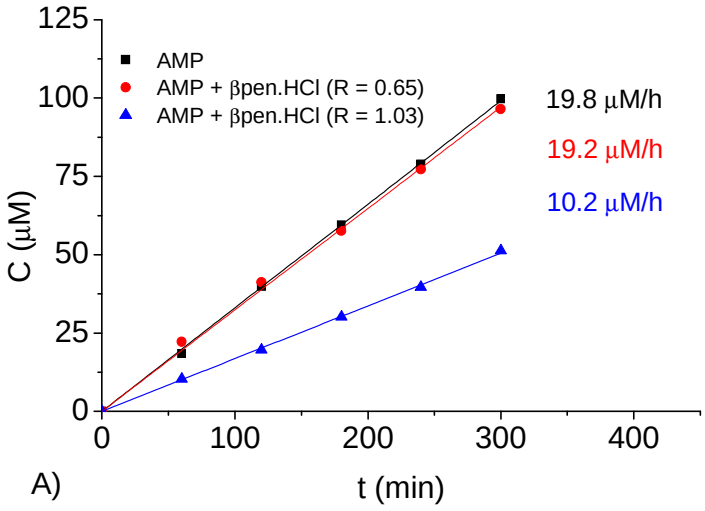

Figure 106. Release profile experiments of 5'-AMP: effect of addition of increasing amount of βpen / 5'-AMP, with R = $n_{βpen}$ / $n_{5'\text{-}AMP}$.

Additional trials using increasing amount of polymer EGDE/βpen Q_3 (1, 2.5 and 7.5 mg/mL in the donor compartment revealed that: i) solutions became cloudy during preparation and ii) release rates results under these conditions were not reproducible. In addition, the limitations found in the determination of the accurate number of βpen content in each polymer limits the proper analysis of release rate results, because a direct correspondence to the number of CD cavities responsible for inclusion cannot be made. However, it is expected that a high content of βpen.HCl in the polymers promote a stronger binding of 5'-AMP and decreased rate of release through the membrane.

Finally, following the strategy outlined for the determination of the release rate of 5'-AMP, the release rate of gemcitabine monophosphate (GEM-MP, 1 mM, PBS) was determined in the presence of pLys/βpen polymer BB' using the same experimental set up (Figure 103). A calibration curve for GEM-MP (Figure 107 A) previously determined in our group was used as a reference, against which the concentrations of GEM-MP from the release experiment were calculated. Therefore, 5'-AMP (1 mM, PBS) and GEM-MP (1 mM, PBS) release rates through the benzoylated dialysis tubing (MW_{CO} = 2000 Da) were determined (Figure 107). The release rate for 5'-AMP (27.6 μM/h) is higher than the one found for GEM-MP (22.2 μM/h, 1 mM, PBS), which is due to stronger interactions of GEM-MP with the pLys/βpen BB' polymer.

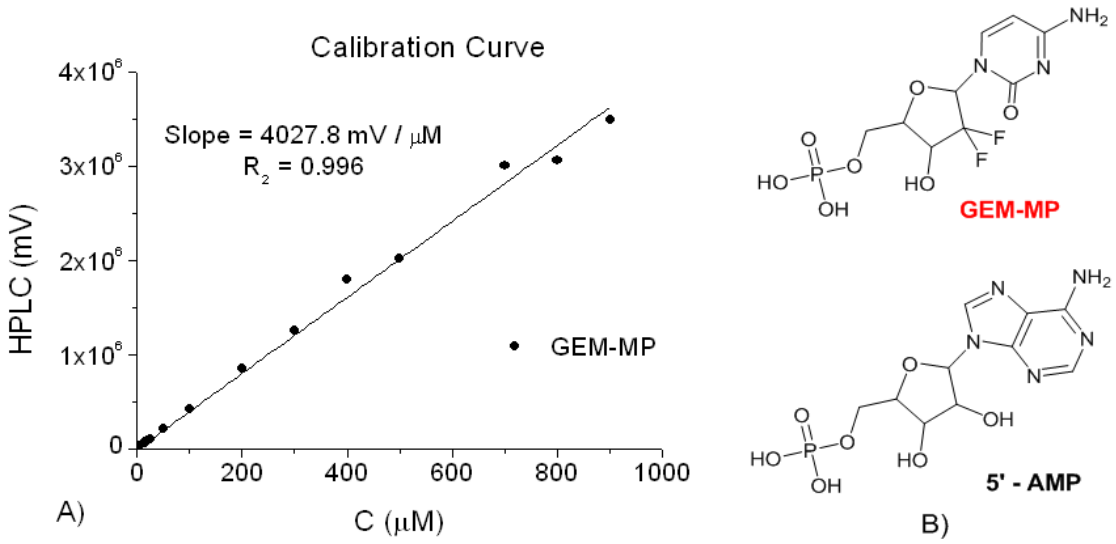

Figure 107. A) Calibration curve for GEM-MP determined by HPLC analysis with UV-detection at λ = 254 nm. B) Host-molecules: adenosine 5'-monophosphate (5'-AMP) and gemcitabine monophosphate (GEM-MP).

In summary, the release rate of 5'-AMP through a benzoylated dialysis membrane (MW_{CO} = 2000 Da) can be modified modified simple by adding βpen.HCl to the donor compartment. However, with positively charged polymers like EPI/βpen P_5, EGDE/βpen Q_2, Q_3 or Q_4 the release rate of 5'-AMP through the membrane can be decreased leading to a modified release of the host molecule. Interestingly, preliminary trials using pLys/βpen BB' to modify the release of 5'-AMP and GEM-MP suggest that the polymer can interact with the membrane, resulting in increase of rate. Our studies were limited by the aggregation phenomena, limited amount of polymers obtained and the relative uncertainty in the determination of the βpen content / molecular weight of the polymers. However, we have explored methods and approaches towards polymers with multiple bpen cavities and charges, potentially useful for delivery of negatively charged drugs.

7.3 Preparation of monomers

7.3.1 Ethylene glycol diglycidyl ether (EGDE)

Epoxides are cyclic ethers rings, with three atoms that due to high bond strain in its ring, are much more reactive than other ethers, namely towards nucleophilic substitution via ring opening [3]. The ring opening reaction of an epoxide generates an alkoxy (or hydroxyl) and when combined with other good leaving group, or a second epoxide ring, offers a difunctional and versatile monomer for polymerization reactions.

Ethylene glycol diglycidil ether (EGDE, Figure 108) is not commercially available, but can be found from Sigma-Aldrich as a polymer with average molecular weight, ranging from 500 g/mol to 6000 g/mol [204]. However, Peng *et. al.* [205] reported the preparation of EGDE, from the controlled reaction between ethylene glycol (EG) and epichlorohydrin (EPI) in mild conditions. EGDE was isolated in ≈ 27 % yield, from a crude oil obtained by liquid-to-liquid extraction, subsequent distillation followed by column chromatography. However, no TLC data regarding the separation of the EGDE and any related impurities was described.

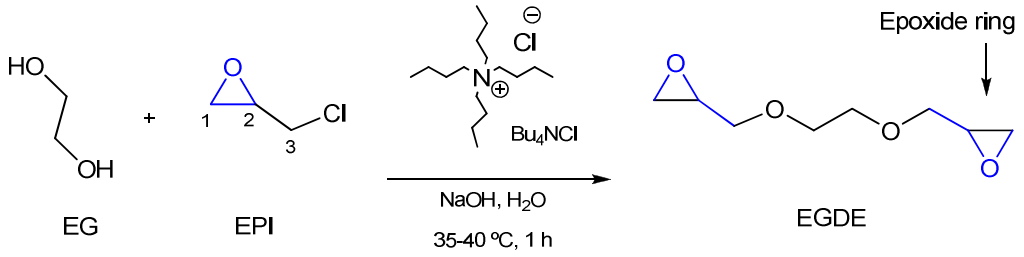

Figure 108. Synthesis of EGDE starting from EPI and EG.

In our hands based on the Peng's reported procedure [205], EGDE was obtained as a pure compound isolated from a mixture of three products, after reaction in mild (35 ºC – 40 ºC, 1 h) alkaline conditions (H_2O / NaOH) in the presence of tetra-butyl-ammonium chloride (Bu_4NCl), a phase-transfer catalyst used to enhance the solubility between two immiscible reactants, EG and EPI (Figure 108).

After 1 h, the reaction was stopped; liquid-to-liquid extraction was used followed by column chromatography to isolate the desired crude mixture. TLC monitoring during column elution (silica gel; EtOAc : EtOEt (5:1)) revealed three different products: fraction 1, 2 and 3 (Figure 109 A). ^{1}H NMR analysis of each fraction revealed that EGDE corresponded to fraction 3 (Figure 109 B). EGDE, isolated as a yellow oil, was further characterized by ^{13}C NMR with assignments corroborated by both 2D COSY and HSQC experiments, which agree with literature data [205]. Fractions 1 and 2 (impurities) were discarded based their ^{1}H NMR spectra, not related to the ^{1}H NMR features expected for EGDE.

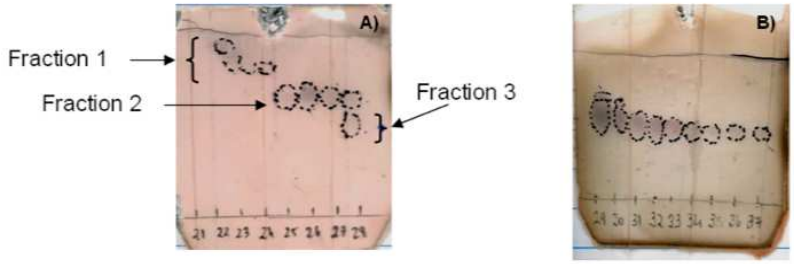

Figure 109. TLC monitoring of column fractions (1, 2, 3) collected during EGDE purification: (A) initial purification stage with collection of three different fractions and (B) a later stage in the separation, where the desired EGDE isolated as a clean product (fraction 3).

The poor yield obtained (12 %) deserved some attention and a series of modifications were performed to the original procedure, trying to improve the reaction yield:

i) the molar ratio (EPI/EG) was changed from the reported EPI/EG = 6 down to EPI/EG = 2, which lead to an economy of the reactants

ii) the reaction was performed in the absence of water, to avoid undesired and competing reactions such as the nucleophilic attack of $^{-}$OH to an epoxide ring, resulting in faster reactions rates in the presence of water (precipitation / cloudiness would start much faster)

Therefore, as a general strategy to stop the reaction and avoid heavy precipitation, whenever the cloudiness of the solution and viscosity started to increase (visual detection), the trials were stopped and the reaction crude separated. Interestingly, a failed trial revealed that if the temperature of the reaction mixture rises above ≈ 40 ºC, even if for a short while, massive precipitation leads to untreatable reaction crudes. The overall yield of EGDE remained low (12 %) in spite of these efforts.

One of the reasons for the poor yields described and achieved is the lack of selectivity on the ring opening reaction and the possibility of competitive reactions that lead to the formation of mono-glycidyl ethers and several oligomers [205]. This can be schematically illustrated in Figure 110.

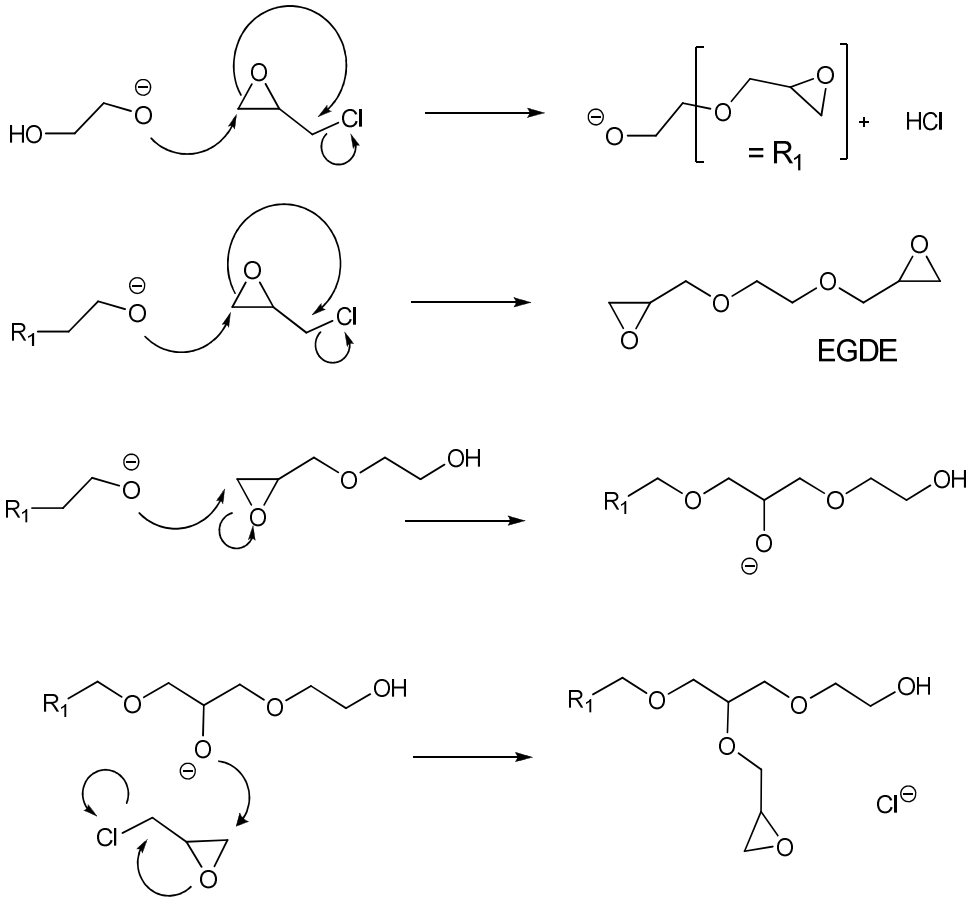

Figure 110. Schematic representation of the multiple possibilities of nucleophilic substitution reactions (S_N2) between an alkoxide species ($R - O^-$) and an epoxide ring (EPI).

Thus, EGDE was successfully obtained as mixture of three products, which is typical of any polymerization reaction. Comparatively to the reported literature, although EGDE was obtained in smaller yield our approach is preferred because: i) a TLC method for the reaction monitoring was developed and ii) the time-consuming distillation method was avoided.

7.3.2 *Per*(6-iodo-6-deoxy)-βCD (βpI)

In order to generate and incorporate CDs in any polymer backbone, versatile building blocks are required. Heptakis(6-iodo-6-deoxy)-βCD (βpI) and/or heptakis(6-bromo-6-deoxy)-βCD (βpBr) are two per-halogenated CDs prepared from βCD following a typical per-halogenation reaction (Figure 111), suitable for preparation of CD containing polymers as they are multifunctional CDs.

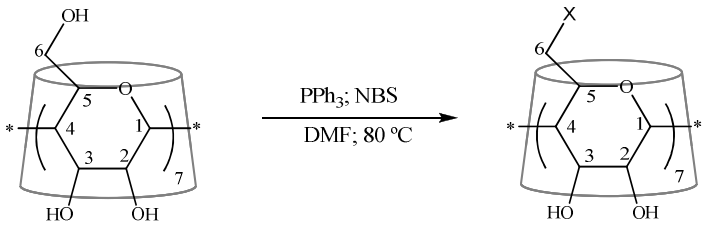

Figure 111. Synthesis of a per-substituted derivative βpX (X = I or Br) starting from βCD.

The reaction followed a modified procedure based on the work reported by Defaye [33]. It involves, the reaction between *N*-bromosuccinimide (NBS) [206] and triphenylphosphine (PPh_3) in dry dimethylformamide (DMF), followed by addition of βCD. Depending on the halogen (-X) donor used, different derivatives can be achieved namely: i) *per*-iodo derivatives using iodine (I_2), and ii) *per*-bromo derivatives using bromide (Br_2) or NBS.

βCD was therefore converted into βpBr (94.3 % yield) and into βpI (88.3 % yield). The exact same synthetic procedure (see section 7.3.2) was applied to prepare α-, β- and γ-CD leading to a multigram preparation of all *per*-halogenated CDs. The advantage in the strategy applied involved the TLC (silica, dioxane / NH_3 / *i*PrOH (10:7:3, *v/v*)) monitoring of the reaction progress until completion (Figure 112). It revealed: i) the presence of any unreacted βCD; ii) the formation of the desired product βpBr; iii) the presence of the typical intermediate products: under-brominated derivatives, triphenylphosphine oxide (PPh_3=O) and over-brominated derivatives.

The purification steps involved water (H_2O) and methanol (MeOH) washings, resulting in a light brown solid (βpBr). It was found that with H_2O, most of the UV-active impurities (PPh_3=O) could be removed. However, methanol (MeOH) is not selective and washes away most of UV-active impurities, over-brominated CD products and the desired product βpBr. Therefore, given that βpBr is soluble in MeOH, a compromise should be reached between the number of washings, the amount of MeOH used to wash the product.

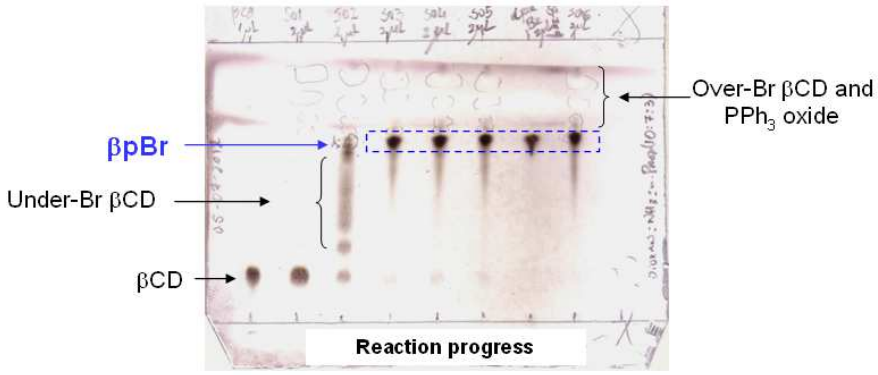

Figure 112. TLC monitoring of the bromination of βCD (NBS method).

βpBr was obtained as a light yellow solid, it was characterized by ^{1}H NMR and ^{13}C NMR spectra. Typical NMR features of βpBr in DMSO-d_6 are: i) the absence of ^{1}H NMR signals due to OH_6 resulting from substitution by Br and ii) ^{13}C NMR reveals a large chemical shielding of C_6 signal that, after per-substitution, shift from 60.3 ppm in βCD to 34.5 ppm in βpBr. Additionally, if the purification procedure is not successful, traces of undesired impurity (PPh_3=O) can be revealed by their ^{1}H NMR characteristic signals in the aromatic region (7 – 8 ppm) and the purification refined.

Previously reported methods [207, 33] fail to describe any TLC data, which was critical to evaluate reaction progress and assess purification achieved. In our group perspective, these findings were even more relevant as all *per*-halogenated (I, Br) CDs have been prepared in multigram scale, which in our laboratory experience was never achieved before. This was possible due to a short collaboration, between our group and Cyclolab in Hungary.

The major advantage of the bromination and iodination procedures is the insertion of good leaving groups in the narrow periphery of CDs, making βpBr and βpI useful derivatives towards nucleophilic substitution reactions. βpBr and βpI were used in the preparation of *per*(6-aminoethylamino-6-deoxy)-βCD (βpen) (see next section) and in the preparation of polymers based on pLys structure, described in section 7.2.1.

7.3.3 *Per*(6-aminoethylamino-6-deoxy)-βCD (βpen)

The synthesis of *per*(6-aminoethylamino-6-deoxy)-βCD (βpen) and its hydrochloride salt (βpen.HCl) from per-halogenated CDs (βpI or βpBr), followed a patented strategy developed in our group [208] with minor modifications. The reported preparation involves the reaction of βpBr with an excess of 1,2-diaminoethane (DAE), acting both as solvent and

reactant, in an autoclave, under pressure (7 atm) at 80 °C for 3 - 4 days. βpen was isolated as a βpen.HCl salt in 18 % yield, after precipitation in cold acetone, acidification and dialysis at pH = 7.0 (Sigma dialysis cellulose tubing, benzoylated) for extra 3 days. A modified general procedure was adopted herein (Figure 113). It involved the reaction of βpI (or βpBr), with an excess of DAE at 80 ºC.

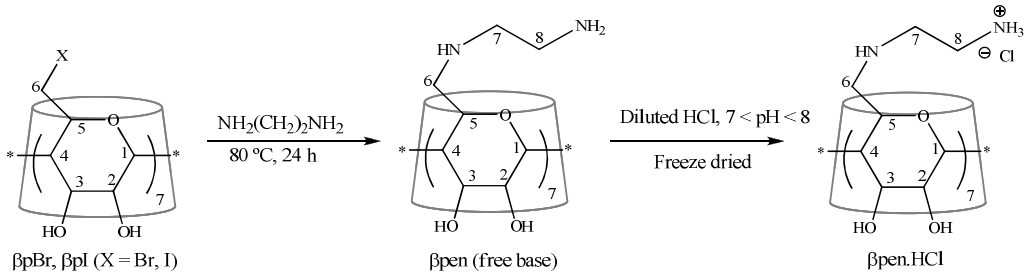

Figure 113. Synthesis of βpen (freebase) and βpen .HCl from βpBr or βpI.

The reaction was monitored by TLC (silica, *i*PrOH : EtOAc : H_2O : NH_3 (5:3:3:1, *v/v*)) and after nearly 24 h it reached completion, with the simultaneous consumption of βpBr . βpen (freebase) can be precipitated from the reaction mixture, when poured directly into an excess of DMF, followed by washings with ethanol (EtOH). Alternatively, βpen (freebase) can then be easily converted into its hydrochloride salt (βpen.HCl), by solubilisation in dilute HCl (0.1 M) until pH ≈ 7 – 8 followed by freeze-drying. βpen.HCl is yellowish compound and has better water solubility than βpen (freebase), that is white powder and is sparingly water-soluble.

βpen (freebase) was analysed by MALDI-TOF MS and characterized by NMR. The MS of βpen (freebase) revealed excellent agreement with the expected value and the mass fragments detected correspond to the aminoethylamino tails lost (Appendix, Figure 116). The ^{1}H NMR and ^{13}C NMR spectra in D_2O agree with reported data [208], but the appearance of the ^{13}C is greatly affected by the pH of the βpen solution (freebase) and the best results were obtained at pH ≈ 4 corresponding to the formation of the βpen.HCl in solution, with all amino groups charged thus the molecule is symmetrical and the spectrum is simple.

In summary, the modifications implemented to the original procedure enable:

i) the monitoring of the reaction progress by TLC, that reaches completion with the complete consumption of the starting material βpBr (or βpI)

ii) a faster reaction lasting only 1 day as opposed to at least 3 - 4 days, performed in a small glass flask avoiding the use of the autoclave

iii) the isolation of the pure βpen (freebase) by precipitation in DMF, directly from the reaction mixture

In addition, βpen possesses simultaneously i) good nucleophilic properties due to the presence of primary and free amino groups and ii) positively charge, due to both primary and secondary amino groups. The methodology developed offers a selective purification method for the removal of water-insoluble βpBr (or βpI) from reaction mixtures, through the generation of water-soluble (βpen). This strategy will be used in the preparation of positively charged CD polymers.

Finally is worth noting that it has earlier been shown that, βpen and similar derivatives are charged in neutral pH and display two pKa values (pK_{a1} = 6.5 and pK_{a2} = 9.5), while protonation occurs at the secondary amino groups [195].

7.4 Conclusions and future perspectives

CD-polymers based on a positively charged CD (βpen) were prepared using two different strategies: i) based on a commercial preformed polymer (pLys.HBr) and ii) based on readily available monomers such as EPI and EGDE. Although it was possible to prepare, characterize and use these CD-polymers their extensive application was impaired because of lack of low reproducibility in the preparation and difficulties in the scale-up due to limited availability of the expensive raw-materials pLys.HBr.

Despite these limitations, all polymers revealed good water solubility properties and the successful attachment of βpen to polymeric backbone, demonstrated by NMR spectroscopy, enabled: i) the evaluation of release rates of nucleotides through a dialysis membrane in a Franz cell set up and ii) the study of inclusion / complexation with model molecules.

Regarding the complexation ability polymers EPI/βpen P_3 and pLys/βpen BB' can complex p-aminobenzoic acid (PABA). In addition, polymer pLys/βpen T_2 can successfully complex 1-adamantanamine (ADA-NH_3Cl) and polymer pLys/βpen T_2 proved a suitable host for anticancer gemcitabine modified with adamantyl group (GEM-ADA amide). Additionally, polymers EPI/βpen P_5 and EGDE/βpen Q_1, Q_2, Q_3, Q_4 could modify the rate of release of adenosine 5'-monophosphate (5'-AMP) by decreasing its rate of release through a dialysis membrane. However, polymer pLys/βpen BB' showed the opposite effect towards a nucleotide drug gemcitabine monophosphate (GEM-MP); these results merit optimization, as each type of nucleotide constitutes a unique case. In this sense, these preliminary results are promising towards new CD-polymers for drug delivery systems.

EXPERIMENTAL

8. Materials

All solvents were reagent grade and were used as received. Deuterated NMR solvents D_2O, DMSO-d_6, $CDCl_3$ and MeOD-d_4 were purchased from Deutero GmbH (Kastellaun, Germany). Dry dimethylformamide (DMF), gemcitabine hydrochloride (GEM), 1-adamantanamine hydrochloride (ADA-NH_3Cl), 1-adamantanecarboxylic acid (ADA-COOH), tamoxifen (TAM), sodium hydroxide (NaOH), 4-toluenesulfonyl chloride (TsCl), hydrochloric acid (HCl), triphenylphosphine (PPh_3), potassium hydroxide (KOH), *N*-bromosuccinimide (NBS), sodium methoxide (CH_3ONa), 1,2-diaminoethane (DAE), epichlorohydrin (EPI), ethylene glycol (EG), ammonium chloride (NH_4Cl), magnesium sulphate ($MgSO_4$), *N*,*N'*-diisopropylethylamine (DIPEA), 1-[bis(dimethylamino) methylene]-1*H*-1,2,3-triazolo[4,5-b]pyridinium 3-oxid hexafluorophosphate (HATU), gemcitabine hydrochloride (HCl), sodium chloride (NaCl), 1-chloroethylchloroformate (CECF), citric acid (CA), fluorescein isothiocyanate isomer 1 (FITC), preformed polymers poly-L-lysine hydrobromide (pLys.HBr, 500 Da < AMW < 1000 Da; 1000 Da < AMW < 5000 Da and 4000 Da < AMW < 15000 Da), benzoylated cellulose dialysis membrane (MW_{CO} = 2000 Da) was purchased from Sigma Aldrich (Germany). Snake skin pleated dialysis tubing (MW_{CO} = 3500 Da) was purchased from Thermo Scientific. 5,10,15,20-tetrakis(*m*–hydroxyphenyl)-21,23*H*-porphyrin (*m*THPP) was purchased from Innochem Ltd (Carnforth, Lancashire, UK). β-cyclodextrin (βCD) and *per*(2,3,6-trimethyl)-β-cyclodextrin (pMβCD) was purchased from Cyclolab (Budapest, Hungary).

9. Methods

Chromatography

Sample was applied to TLC plates using glass capillaries or calibrated micropipettes (1 – 5 μL). TLC plates were examined under ultra-violet light of λ = 365 nm or λ = 254 nm) and were visualized using one to the following revealing solutions (RS):

- RS A – 4 % H_2SO_4 / EtOH (*v/v*), prepared by solubilising concentrated sulphuric acid (H_2SO_4, 2 mL) into ice-cold ethanol (EtOH, 50 mL).
- RS B – anisaldehyde solution: prepared by mixing *p*-anisaldehyde (9.2 mL), with acetic acid (AcOH, 3.75 mL), ethanol (EtOH, 338 mL) and sulphuric acid (H_2SO_4, 12.5 mL).

Preparative chromatography was performed using glass plates (20 cm x 20 cm) coated with silica gel GF (thickness = 500 μm). Flash column chromatography was performed using a glass column (length (L), cm x outer diameter (OD), cm) and silica gel (pore size 60 Å, 70-230 mesh, 63-200 μm).

pH measurements

The pH was measured using an MP200 Mettler Toledo pH meter. Before each measurement, the electrode system was calibrated in hydrogen ion concentration units ($pH = -\log[H^+]$) using buffer reference standard solutions (Scharlau) at 25 ºC. Alternatively, universal-indicator paper (range pH 1.0-11.0, Sigma-Aldrich) was used for pH checking on reaction progress.

UV-Vis / fluorescence spectroscopy (UV-Vis / Fluor)

UV-Vis spectra were collected on: i) an Agilent Cary 60 UV-Vis spectrometer, using a quartz cuvette (1 cm path length) or ii) on a JASCO double beam spectrophotometer (V-560). The baseline was corrected using the solvent spectrum as a reference. Fluorescence spectra were recorded using a: i) Varian Cary Eclipse fluorescence spectrometer or ii) a JASCO spectrofluorimeter (FP-777) using a quartz cell with 1 cm path length.

Infrared spectroscopy (IR)

Infrared (IR) spectra were collected on a Thermo Scientific Nicolet 6700 FTIR, with N_2 purging system and a common deuterated triglycine sulphate (DTGS) detector. Spectra were acquired using a single reflection ATR (Attenuated Total Reflection) SmartOrbit accessory equipped with a single-bounce diamond crystal, with a spectral range (10000 – 55 cm^{-1}) and a 45º angle of incidence. 32 scans were collected in the range 4000–400 cm^{-1} and taken a resolution of 4 cm^{-1}.

Nuclear magnetic resonance (NMR)

All NMR experiments were recorded at 298 K. 1D and 2D NMR spectra were acquired either on a Bruker Avance III spectrometer at 250.13 MHz for ^1H and 62.90 MHz for ^{13}C or on a Bruker Avance DRX 500 spectrometer at 500.13 MHz for ^1H and 125.77 MHz for ^{13}C. ^1H NMR spectra recorded in D_2O were referenced on the HOD signal at $\delta = 4.79$ ppm. 2D ROESY spectra were acquired with presaturation of the residual water resonance and a mixing (spin-

lock) time of 350 ms at a field of ~2 kHz with the TPPI (time proportional phase increments) method, using a 1024 K time domain in F2 (FID resolution 5.87 Hz) and 460 experiments in F1. 2D NOESY spectra were acquired using mixing times of 1-1.5 s, TPPI detection and HDO presaturation. Processing was carried out with zero-filling to 2K in F1 using sine or qsine (F2) and qsine (F1) window functions, respectively. All chemical shifts (δ) are reported in parts *per* million (ppm) and coupling constants (*J*) are reported in Hz. Structural assignments of compounds and inclusion complexes were corroborated by 2D NMR experiments namely through: correlation spectroscopy (COSY), Heteronuclear Single-Quantum Coherence (HSQC), heteronuclear multiple-bond correlation (HMBC), total correlation spectroscopy (TOCSY), nuclear Overhauser effect spectroscopy (NOESY) and rotating frame nuclear Overhauser effect spectroscopy (ROESY).

Mass Spectrometry (MS)

Matrix assisted laser desorption ionization with time of flight detection (MALDI-TOF) mass spectra (MS) were recorded on an AutoflexBruker mass spectrometer, operating in a linear mode and in positive polarity using either 4-hydroxy 2,5-dihydroxybenzoic acid (DHB) or α-cyano-4-hydroxycinamic acid (HCCA) to prepare the matrix solutions (Ronzoni Institute, Milan, Italy) under service contract.

Elemental analysis

The elemental analysis assays were performed using a Perkin Elmer 2400 CHN elemental analyser.

X-Ray powder diffraction (XRD)

The analysis was determined using a Rigaku R-AXIS IV imaging plate detector mounted on a Rigaku RU-H3R rotating anode X-Ray generator. The dry solid sample was ground to a fine powder and was placed inside a glass capillary (Hampton Research, USA) with the following dimensions: length (L) x outer diameter (OD) x wall thickness (WT) = (80 x 1 x 0.01) mm. Samples were collected at a distance (d; mm) from the detector and were irradiated during (t, min).

Vapour pressure osmometry (VPO)

Experiments were performed using a vapour pressure osmometer K–7000 from Knauer. The solvent used in all measurements was water and the temperature was 40 °C. Polyvinyl pyrrolidone (AMW = 10 kDa) was used as a standard and concentrations were reported in molality (*mol* solute / *kg* solvent). The experiments were performed on a stage at the University of Iceland, Faculty of Pharmacy.

Static light scattering (SLS)

Molecular weight determinations were performed using a Malvern Zetasizer Nano ZS instrument running a Static Light Scattering (SLS) method. The samples were studied at different concentrations at 25 °C applying the Rayleigh equation. The measurements were a kind contribution from Cyclolab S.A. Budapest, Hungary.

Dynamic light scattering (DLS)

DLS measurements of size (d, nm) and zeta potential (ζ, mV) were performed using a Zetasizer Nano Series (Malvern Instruments Ltd), equipped with a MPT-2 autotitrator and disposable folded capillary cells (DTS 1060 / DTS 106). The wavelength of detection was 633 nm and temperature of all experiment was 25 ºC. Titration experiments were conducted in water, with the pH ranging from 3.0 < pH < 8.0. Experimental data was processed using Zetasizer software version 6.34 (Malvern Instruments Ltd).

High performance liquid chromatography (HPLC)

HPLC measurements were performed using a Shimadzu system composed of: i) an UV-Vis detector (SPD-10A); ii) a pump (LC-10AT VP) with a degasser (DGU-14A) and iii) a C18 Supelco HPLC column (L x OD) = 25 cm x 4.6 mm, with 5 μm particle size. No temperature control was used and all injections were 20 μL. The detection wavelength of adenosine 5'-monophosphate (5'-AMP) and gemcitabine monophosphate (GMP) was λ = 254 nm using a mobile phase of acetonitrile : water (75:25, *v/v*).

Modified Franz cell set-up

The modified Franz cell device was constituted by two compartments, a donor (D) and a receptor (R), each of a fixed volume (3.5 mL) and separated by a hollow junction (diffusion

area = 3.14 cm^2) to which a semi-permeable membrane (benzoylated dialysis tubing MW_{CO} = 2000 Da) was attached. The system was thermostated with warm water (37 ºC ± 0.5 ºC) through both cells for 30 min, before each experiment. All the R volume (3.5 mL) was collected at a fixed time intervals (60 min; 120 min; 180 min; 240 min; 300 min; 360 min), followed by replacement with fresh R phase maintained at (37 ºC ± 0.5 ºC).

Confocal microscopy

A Biorad MRC 1024 ES laser scanning confocal microscope was used. The coverslips were washed twice with PBS or RPMI and placed over the 639 oil immersion quartz objective (NA 1.3). Intracellular CD-*m*THPP fluorescence was excited using the 568 nm line of an argon–krypton laser (30 % of total laser power). CD-*m*THPP fluorescence was collected with the use of a long-pass filter at ≥ 585 nm, whereas FITC-type fluorescence was collected through a bandpass filter centred at 522 (± 35) nm. During image acquisition a Kalman level 3 (three iterations per image) smoothing routine was applied each time to eliminate spurious signal. The contribution of cell autofluorescence was checked each time in untreated cells and was, in all cases, found to be negligible.

Cells were washed with PBS and mounted on microscope slides for confocal fluorescence live cell imaging. The slides were placed under the 60· oil immersion quartz objective (NA 1.3) of a Biorad MRC 1024 ES laser scanning confocal microscope. Intracellular NDMTAM-FITC was excited using the 488 nm line of an argon–krypton ion laser, whereas the internalized probes were excited by the 568 nm line of the same laser. NDTAM-FITC fluorescence was collected through a band-pass filter centred at 522 (± 35) nm, while organelle probe fluorescence was collected after a long-pass filter at ± 585 nm. During image acquisition a level 3 (three iterations per image) Kalman smoothing routine was applied in all occasions to eliminate spurious signals.

10. Synthesis

10.1 CD derivatives

10.1.1 **6-*O*-Monotosyl-β-cyclodextrin (βmTs)**

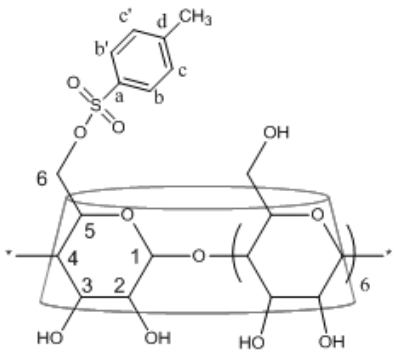

βmTs

β-cyclodextrin (βCD, 2.0 g, 1.76 mmol) was added in small portions, to a sodium hydroxide solution (NaOH, 0.4 M, 60 mL) and was vigorously stirred in an ice bath (0 ºC – 5 ºC). After βCD was completely dissolved, 4-toluenesulfonyl chloride (TsCl, 0.8 g, 4.2 mmol, 2.43 molar eq.) was added to the mixture and the whole was stirred for 2 h in the ice bath (0 ºC – 5 ºC). Afterwards, a second portion of TsCl (1.2 g, 6.3 mmol, 3.58 molar eq.) was added to this mixture and it was stirred for 3 h more. The reaction was stopped, the crude was filtered through a plug of celite 545 coarse (20 g – 25 g) to separate unreacted TsCl. The alkaline filtrate (12 < pH < 13) was kept at 0 ºC – 5 ºC and under constant magnetic stirring was adjusted to pH = 1.5, by the addition of hydrochloric acid (HCl, 0.1M). The product precipitated as a white solid, it was filtered, washed with cold water (100 mL) and dried in the vacuum oven at 60 ºC for 24 h. The filtrate was left to rest in the fridge overnight (12 h – 18 h) and the filtration step was repeated to collect any remaining product (second crop). The purity of the product 6-*O*-monotosyl-β-cyclodextrin (βmTs) was assessed by TLC (silica gel 60; dioxane : NH_3 : *i*PrOH (10:7:3, *v/v*); RS A; R_F = 0.47) and it was obtained as a white solid (40 %, 0.89 g). ^{1}H NMR (DMSO-d_6, 250 MHz, 25 ºC): δ (ppm) 7.72 (d, *J* = 8 Hz, H_a, 2H), 7.40 (d, *J* = 8 Hz, H_b, 2H), 6.00 - 5.75 (m, 2-OH, 3-OH, 14H), 4.76 (d, H_1, 7H), 4.60 – 4.00 (m, 6-OH, 7H), 3.80 – 3.40 (m, H_3, H_5, H_6, $H_{6'}$, 28H, overlapping with residual HDO), 3.40 – 3.00 (m, H_4, H_2, 7H, overlapping with residual HDO), 2.39 (s, CH_3, 3H). ^{13}C NMR (DMSO-d_6, 62.5 MHz, 25 ºC): δ (ppm) 144.9 (C_a), 133.0 (C_d), 130.1 (C_b/$C_{b'}$), 128.0 (C_c/$C_{c'}$), 102.0 (C_1), 81.5 (C_4), 74.3 – 71.3 (C_2, C_3, C_5), 60.0 (C_6), 21.1 (CH_3). Characterization data presented agrees with literature [209].

10.1.2 **Heptakis(6-bromo-6-deoxy)-β-cyclodextrin (βpBr)**

[N-Bromosuccinimide (NBS) method]

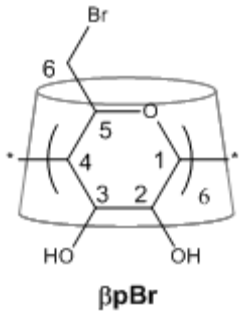

βpBr

In a water bath at room temperature (20 ºC – 25 ºC), dry dimethylformamide (DMF, 100 mL) was added to a flask, equipped with a drying tube filled with potassium hydroxide (KOH) and was vigorously stirred. Triphenylphosphine (PPh_3, 39.4 g, 0.15 mol) was added to the DMF, in small portions and a temperature drop (25 ºC *to* 17 ºC) was noticed. *N*-bromosuccinimide (NBS, 28.6 g, 0.16 mol) was added in portions, while the temperature was kept bellow 40 ºC, by addition of ice to the water bath. During the addition of NBS, the colour of the solution changed (white *to* dark red) and its viscosity increased which was controlled by addition of DMF to ensure a constant and vigorous stirring. β-cyclodextrin (βCD, 11.4 g, 0.01 mol, white powder) was added to the mixture at once leading to an increase in the temperature and to a colour change (dark red *to* dark green). Afterwards, this solution was transferred to an oil bath (70 ºC – 80 ºC) and the reaction progress was monitored by TLC (silica gel 60; dioxane : NH_3 : *i*PrOH (10:7:3, *v/v*), RV A). The reaction was stopped after consumption of the starting material (βCD). The mixture was cooled in a water bath (20 ºC – 25 ºC) for 10 min, until the temperature droped down to 40 ºC – 50 ºC. Methanol (MeOH, 50 mL) was added and the solution was poured into a large excess of MeOH (500 mL). The pH of the methanolic solution was checked ($2 < pH < 3$, universal paper) and adjusted to ($7 < pH < 8$, universal paper), by addition of sodium methoxide (CH_3ONa, 3.21 g). The mixture was stirred for 5 min and left to stand for 10 – 15 min leading to the precipitation of the product as a light brown solid. The product was extensively washed with MeOH/water to remove impurities: over-brominated, under-brominated products and traces of PPh_3. The purity of the product heptakis(6-bromo-6-deoxy)-β-cyclodextrin (βpBr) was assessed by TLC (silica gel 60; dioxane : NH_3 : *i*PrOH (10:7:3, *v/v*); RS A; $R_F = 0.68$) and it was obtained as a light yellow powder (94.3 %, 14.9 g). ^{1}H NMR (DMSO-d_6, 500 MHz, 25 ºC): δ (ppm) 6.04 (d, $J = 7.0$ Hz, 2-OH, 7H), 5.91 (br s, 3-OH, 7H), 4.98 (d, $J = 3.0$ Hz, H_1, 7H), 4.01 (d, $J = 10.0$ Hz, H_6, 7H), 3.83 (t, $J = 8.5$ Hz, H_5, 7H), 3.66 (q, H_3, $H_{6'}$, 14H), 3.48 – 3.35 (m, H_2, H_4, 14H). ^{13}C NMR (DMSO-d_6, 125 MHz, 25 ºC): δ (ppm) 102.1 (C_1), 84.6 (C_4), 72.3 (C_3), 72.1 (C_2), 71.0 (C_5), 34.5 (C_6). Characterization data presented agrees with literature [33].

10.1.3 **Heptakis(6-aminoethylamino-6-deoxy)-β-cyclodextrin (βpen)**

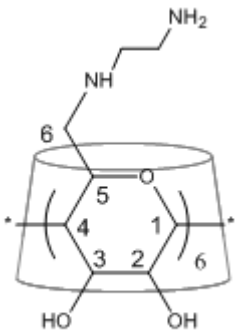

βpen

Heptakis(6-bromo-6-deoxy)-β-cyclodextrin (βpBr, 3.04 g, 1.93 mmol) was dissolved in 1,2-diaminoethane (DAE, 15.0 mL) and a light brown solution was obtained. The mixture was warmed to 80 ºC, kept under vigorous magnetic stirring and under an argon atmosphere. The reaction was monitored by TLC (silica gel 60; dioxane : NH_3 : *i*PrOH (10:7:3, *v/v*), RS A). After 24 h the reaction crude was left to cool to room temperature (20 – 25 C) and poured into an excess of dimethylformamide (DMF, 75 mL). A white solid was obtained that was filtered through a filter paper (Whatman, nº 5), washed with ethanol (EtOH, 50 mL) and was dried in an oven (vacuum, 80 ºC) for 24 h. The product heptakis(6-aminoethylamino-6-deoxy)-β-cyclodextrin (βpen) was obtained as a white solid (1.78 g; 64.7 %).

^{1}H NMR (acidic D_2O (pH ≈ 4), 500 MHz, 25 ºC): δ (ppm) 5.04 (br s, 7H, H_1), 3.88-3.86 (m, 14H, H_5/H_3), 3.56-3.54 (m, 14H, H_4/H_2), 2.99 (br s, 14H, $H_6/H_{6'}$), 2.89-2.79 (m, 28H, H_7/H_8). ^{13}C NMR (D_2O, 125 MHz, 25 ºC): δ (ppm) 101.5 (C_1), 82.5 (C_4), 73.0 (C_5), 71.7 (C_2), 70.7 (C_3), 50.2 / 49.2 (C_7/C_8), 40.0 (C_6). Characterization data presented agrees with the literature [210, 211]. MS (MALDI-TOF): *m/z* calcd for $C_{56}H_{112}N_{14}O_{28}$ 1428.78 [M]. Found: 1430.3 $[M+H]^+$ (100 %), 1452.3 $[M+Na]^+$ (77 %).

10.1.4 β-cyclodextrin-*meso*-tetrakis(*m*-hydroxyphenyl)-porphyrin conjugate (CD-*m*THPP)

5,10,15,20-tetrakis(*m*-hydroxyphenyl)-21,23*H*-porphyrin (*m*THPP, 61 mg, 0.089 mmol) was dissolved in dry dimethylsulfoxide (DMSO, 2 mL) and the mixture was stirred at 40 °C, in an argon atmosphere and protected from light. Sodium hydroxide (NaOH, 23.5 mg, 0.59 mmol) was added and the reaction mixture was stirred for 15 min. 6-*O*-monotosyl-β-cyclodextrin (βmTs, 125.5 mg, 0.097 mmol) solubilised in dry DMSO (4 Å molecular sieves, 24 h) (1.0 mL) and added to the reaction mixture in portions over 1 h (0.25 mL / 15 min). The reaction was monitored by TLC (silica gel 60; *i*PrOH : EtOAc : H_2O : NH_3 (5:3:3:1, *v/v*); RS A) until all βmTs was consumed. The reaction was stopped after 72 h. The desired product appeared as a brown spot (R_F = 0.61), showed red fluorescence under ultraviolet light irradiation (λ_{ex} = 254 nm) and turned green upon spraying with RS A. A mixture of EtOH : H_2O (1:1, *v/v* ~2 mL) and hydrochloric acid (HCl (1 M), 1.1 mL) was added to the crude mixture (until the pH ~ 6.0) and it was dialysed (benzoylated dialysis membrane, MW_{CO} = 2000 Da), against distilled water for ~ 24 h. The solvent (H_2O) was removed in ratovapor, using EtOH to avoid bumping and the dried material was collected and washed with ethyl acetate (EtOAc, 100 mL), to remove most of unreacted *m*THPP and *m*THPP salts. The solid obtained was subjected to column chromatography using a long column (L x OD = 60 cm x 2.4 cm) packed with silica gel 60 (80 g) and using *i*PrOH : EtOAc : H_2O : NH_3 (5:3:3:1, *v/v*) as the mobile phase. Loading had to be restricted to a small portion of crude (~20 mg) per column. The first fraction collected was unreacted *m*THPP (20 mg in total), followed by CD-*m*THPP. Subsequently, the solvent (mobile phase - *i*PrOH : EtOAc : H_2O : NH_3) was evaporated under vacuum and the residue (1 – 2 mL) was adjusted to pH ≈ 5 and dialyzed for 18 h (benzoylated dialysis membrane, MW_{CO} = 2000 Da). The purity of the product β-cyclodextrin-5,10,15,20-tetrakis(*m*-hydroxyphenyl)-porphyrin conjugate (CD-*m*THPP) was assessed by TLC (silica gel 60; *i*PrOH : EtOAc : H_2O : NH_3 (5:3:3:1, *v/v*); RV A; R_F = 0.61) and was obtained as a black powder (43 mg, 40 %, calculated based on reacted porphyrin). ^{1}H NMR (DMSO-d_6, 500 MHz, 25 ºC): δ(ppm) 9.80 (s, Ph-OH, 3H), 8.88 (s, Py-H, 8H), 8.00 – 7.00 (s, Ph-H, 16H), 6.00 – 5.50 (br d, CD-OH_2/CD-OH_3, 14H), 4.90 (s, CD-H_1 connected *m*THPP, 1H), 4.80 (s, CD-H_1, 6H), 4.50 – 4.20 (br m, CD-OH_6, 6H), 4.10 (s, CD-H_5 connected to *m*THPP, 1H), 3.90 - 3.00 (m, CD-H_2 / H_3 / H_4 / H_5 / H_6/ $H_{6'}$, 42H, overlapping with residual HDO), -3.00 (s, -NH, 2H). MS

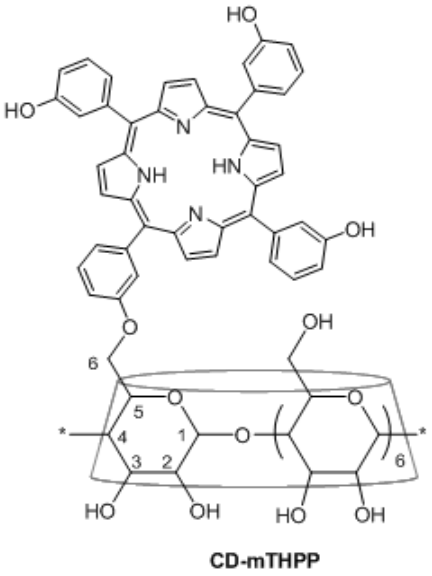

CD-mTHPP

(MALDI-TOF): *m/z* calcd for $C_{86}H_{98}N_4O_{38}$ 1795.70 [M]. Found: 1796.8 $[M+H]^+$ (100 %), 1817.0 $[M+Na]^+$. Anal. Calcd. (%) for $C_{86}H_{98}N_4O_{38}.9H_2O$. NH_4Cl: C: 51.34, H: 6.02, N: 3.48. Found: C: 51.18; H: 5.93; N: 3.11. UV-Vis (DMSO, C = 3.6 μM) = 420 (0.48); 514 (0.03); 551 (0.02); 590 (0.02), 645 (0.01). UV-Vis (4 % DMSO/PBS, C = 3.6 μM) = 422 (0.19); 517 (0.02); 553 (0.01); 589 (0.01), 644 (0.01).

Recovery of pure CD-mTHPP from pMβCD complexes

The complexed CD-*m*THPP in the form of pMβCD/CD-*m*THPP collected from any complexation experiment study, was solubilised in water and was dialysed (benzoylated dialysis tubing, MW_{CO} = 2000 Da) for 8 h. The resulting clear, dark red solution was dried until a small residue (1 – 2 mL) was obtained. It was transferred to a glass tube, it was vortexed and a large volume of diethyl ether (EtOEt, 10 – 12 mL) was added gradually. The desired product (CD-*m*THPP) precipitates as a dark red / black solid free from any pMβCD, which is washed away by the supernatant EtOEt (discarded). The product purity was assessed by TLC (silica gel 60; *i*PrOH : EtOAc : H_2O : NH_3 (5:3:3:1, *v/v*); RV A; R_F = 0.61) and can be reused.

10.2 Monomers - linker

10.2.1 **Ethylene glycol diglycidyl ether (EGDE)**

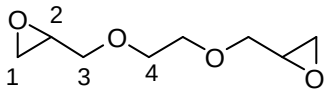

EDGE

Epichlorohydrin (EPI, 20 mL, 0.255 mol), sodium hydroxide (NaOH, 9.55 g, 0.239 mol) and tetrabutylammonium chloride (TACl, 0.55 g, 2 mmol) were solubilised in water (1 mL) at room temperature (20 – 25 ºC) to obtain a light yellow solution. Ethylene glycol (EG, 1.115 mL, 20 mmol) was added slowly in two portions (2 x 560 µL) and the reaction mixture was kept in a water bath (T = 10 ºC) and after 10 min turned cloudy. The crude mixture was finally transferred to an oil bath (35 – 40 ºC) and was stirred for 30 min. The reaction was stopped and the white precipitate was filtered and washed with water (20 mL) and with chloroform (150 mL). The organic phase was collected, washed with saturated ammonium chloride (NH_4Cl, sat. sol., 3 x 120 mL) until the pH ≈ 5. It was dried over magnesium sulphate anhydrous (30 min) and evaporated under vacuum in the rotary evaporator (50 ºC) until a light yellow residue was obtained. The desired product was purified from the light yellow crude obtained (666 mg) by column chromatography using a column (OD x L = 2.6 cm x 53 cm), packed with silica gel (73 g) and using EtOAc : EtOEt (5:1, *v/v*) as mobile phase. The purity of the desired product ethylene glycol diglycidyl ether (EGDE) was assessed by TLC (silica gel 60; EtOAc : EtOEt (5:1, *v/v*); RV B; R_F = 0.57) and was obtained as an oil (12 % yield; 79.9 mg) stored in the freezer. ^{1}H NMR ($CHCl_3$-d_1, 500 MHz, 25 ºC): δ (ppm) 3.83 – 3.76 (m, $H_{3'}$, 2H), 3.75 – 3.59 (m, H_4, 4H), 3.48 – 3.36 (m, H_3, 2H), 3.16 (m, H_2, 2H), 2.78 (t, H_1, 2H), 2.60 (br s, $H_{1'}$, 2H). ^{13}C NMR ($CHCl_3$-d_1, 125 MHz, 25 ºC): δ (ppm) 72.0 (C_3), 70.7 (C_4), 50.8 (C_2), 44.2 (C_1). Characterization data presented agrees with literature [205].

10.3 Selected anticancer molecules

10.3.1 **Gemcitabine-adamantanamide (GEM-ADA amide)**

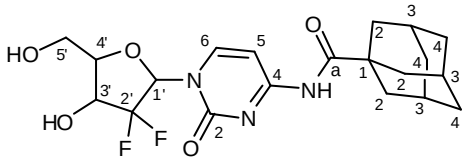

GEM-ADA amide

In a small flask (10 mL) 1-adamantanecarboxylic acid (ADA-COOH, 30.4 mg; 0.17 mmol) was solubilised in dry mixture of DMF:DMSO (3:1, *v/v*) (200 µL), followed by addition of *N*,*N'*-diisopropylethylamine (DIPEA, 84 µL; 0.48 mmol) and 1-[bis(dimethylamino) methylene]-1*H*-1,2,3-triazolo[4,5-b]pyridinium 3-oxid hexafluorophosphate (HATU.PF_6, 70.3 mg; 0.19 mmol). This light yellow solution was stirred for 60 min at 10-15 C and it turned dark brown in colour. Gemcitabine hydrochloride (GEM.HCl, 50.3 mg; 0.17 mmol) was added to the mixture and the temperature was raised to 25 ºC. The flask was then flushed with argon (Ar), reaction was periodically checked by TLC (silica gel 60; CH_2Cl_2 : acetone : EtOH (5:4:1, *v/v*); RV B) revealing the activated ADA-COOH (R_F = 0.99) being converted into the UV-active desired product GEM-ADA amide (R_F = 0.78). The reaction was stopped after 48 h and a dark orange colour developed. Liquid-to-liquid extraction was used: ethyl acetate (EtOAc, 2 mL) was first added to the mixture and it was transferred to a separation funnel, followed by addition of aqueous sodium chloride (NaCl, 10 % *m/v*, 6 x 2 mL). The aqueous layer (NaCl 10 %, 12 mL) was washed with EtOAc (6 x 10 mL) and all organic layers were combined and dried. The product gemcitabine-adamantanamide (GEM-ADA amide) was recovered from the organic layer with warm purified water (60 ºC) and a white solid was obtained (GEM-ADA amide, 20.4 mg, 28.5 %). ^{1}H NMR (DMSO-d_6, 500 MHz, 25 ºC): δ(ppm) 10.2 (br s, amide -NH, 1H), 8.22 (d, H_6, 1H), 7.29 (s, $H_{1'}$, 1H), 6.34 (s, 5'-OH, 1H), 6.16 (s, H_5, 1H), 5.33 (s, 3'-OH, 1H), 4.17 (m, $H_{3'}$, 1H), 3.87 (s, $H_{5'}$, 1H), 3.78 (s, $H_{4'}$, 1H), 3.66 (s, $H_{5''}$, 1H), 1.97 (s, ADA-H_3, 3H), 1.89 (s, ADA-$H_{2,\,2'}$, 6H), 1.66 (s, ADA-$H_{4,\,4'}$, 6H). ^{13}C NMR (DMSO-d_6, 125 MHz, 25 ºC): δ(ppm) 178.9 (C_a), 164.1 (C_4), 154.8 (C_2), 145.2 (C_6), 123.6 (t, J_{CF} = 23 Hz, $C_{2'}$), 97.0 (C_5), 85.1 – 84.8 ($C_{1'}$), 81.7 ($C_{4'}$), 69.1 – 68.8 ($C_{3'}$), 59.4 ($C_{5'}$), 42.5 (ADA-C_1), 37.8 (ADA-C_2), 36.3 (ADA-C_4), 28.1 (ADA-C_3).

10.3.2 *N*-desmethyltamoxifen hydrochloride (NDTAM.HCl)

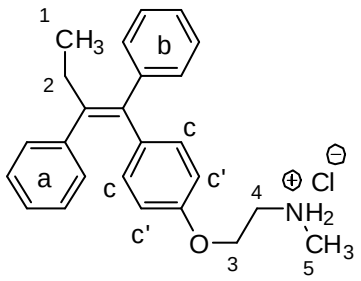

NDTAM.HCl

Tamoxifen (TAM, 151 mg, 0.410 mmol) was dissolved in toluene (6 mL) at 0 °C followed by addition of 1-chloroethylchloroformate (CECF, 100 μL, 0.93 mmol). After 15 min stirring at 0 °C, the reaction was heated to reflux with periodic monitoring of its progress by TLC (silica gel 60; CH_2Cl_2 : MeOH : NH_3 (95:5:0.3, *v/v*) and UV-Vis irradiation at 365 nm. The reflux was continued until all TAM is consumed (19h). Toluene was evaporated in the rotary evaporator (60 ºC) until an oily yellow residue (2 – 3 mL) was obtained. The desired product was then precipitated, by addition of an excess of diethyl ether (EtOEt, 25 mL), followed by extensive washings with EtOEt to recover NDTAM.HCl as a white solid (81 mg; 50 % yield). The purity of *N*-desmethyltamoxifen hydrochloride (NDATM.HCl) was assessed by TLC (silica gel 60; CH_2Cl_2 / MeOH / NH_3 (95:5:0.3, *v/v*); R_F = 0.08). The identity of the product was confirmed by comparison of its spectra with those of an authentic sample of NDTAM.HCl (Sigma). ^{1}H NMR (MeOD-d_4, 500 MHz, 25 ºC) δ (ppm) 7.31 – 7.03 (m, Ph-H_a/Ph-H_b, 10 H), 6.78 – 6.58 (dd, $J_{cc'}$ = 8 Hz, Ph-H_c/$H_{c'}$, 4 H), 4.06 (t, H_3, 2 H, J = 4.3 Hz), 3.29 (t, H_4, 2 H, J = 5.0 Hz), 2.67 (s, H_5, 3 H), 2.39 (q, H_2, 2 H), 0.84 (t, H_1, 3 H). ^{13}C NMR ($CDCl_3$, 125 MHz, 25 ºC): δ (ppm) 132.1 – 113.3 (Ph-C_a/C_b/C_C), 63.1 (C_3), 48.4 (C_4), 33.6 (C_5), 29.3 (C_2), 13.7 (C_1). Characterization data presented agrees with literature [178].

10.3.3 **Tamoxifen citrate (TAM-Cit, 2:1)**

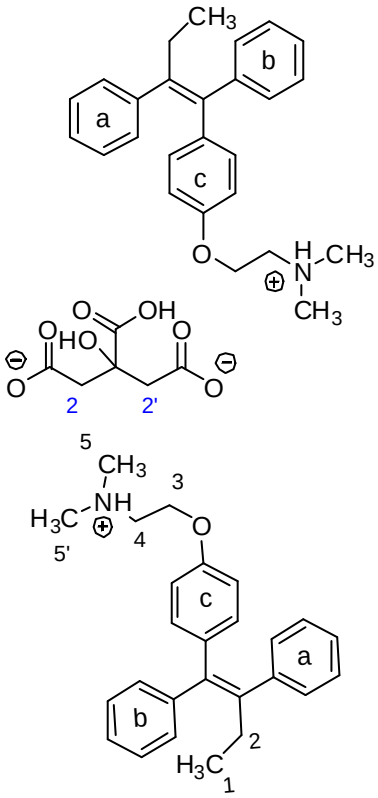

Tamoxifen (TAM, 51.5 mg, 0.09 mmol) was solubilised in acetonitrile (ACN, 2 mL) and the solution was stirred at room temperature (20 ºC – 25 ºC) in an oil bath. Citric acid (CA, 55.0 mg, 0.26 mmol) was added to the solution and cloudiness was developed as the solid (CA) deposits in the bottom of the flask. The reaction was stirred vigorously for 40 min and it changes its aspect, turning from clear with solid in the bottom, to cloudy with white solid dispersed as very fine white particles. Reaction was stopped and the solid was filtered through a paper filter (Whatman number 4) and was extensively washed with water (H_2O, 3 x 20 mL) to wash from the final product any excess of unreacted CA. A white solid was obtained (24.7 mg, 63.3 %) in a form of TAM-Cit with a stoichiometry of tamoxifen / citrate (2:1). ^{1}H NMR ($CDCl_3$, 500 MHz, 25 ºC): δ (ppm) 7.35 – 7.11 (m, Ph-H_a/Ph-H_b, 10 H), 6.80 – 6.5 (dd, J = 8.0 Hz, Ph-H_c, 4H), 4.22(s, H_3, 3H), 3.29 (s, H_4, 3H), 2.78 (s, H_5, $H_{5'}$, 6H), 2.67 (br d, CH_2-citric acid, 4H), 2.46 (q, H_2, 2H), 2.67 (t, H_1, 3H). ^{13}C NMR ($CDCl_3$, 125 MHz, 25 ºC): δ (ppm) 136 – 109 (Ph-C_a/C_b/C_c), 62.5 (C_3), 56.9 (C_4), 46.2 (citric acid - C_2/$C_{2'}$), 44.0 (C_5/$C_{5'}$), 29.3 (C_2), 13.8 (C_1). Characterization data presented agrees with literature [212].

10.3.4 *N*-desmethyltamoxifen-fluorescein (NDTAM-FITC)

Fluorescein isothiocyanate isomer 1 (FITC, 10 mg, 25.7 μmol) was solubilised in ethanol (EtOH, 2 mL) to get a clear yellow solution, followed by the addition of *N*,*N*-diisopropylethylamine (DIPEA, 10 μL, 57.4 μmol). The colour changed from yellow to orange. *N*-desmethyltamoxifen (NDTAM.HCl, 9.4 mg, 23.9 μmol) was added to the mixture and the reaction was stirred at 40 ºC, protected from the light and under inert atmosphere (argon). After 44 h, the reaction was stopped and it was dried in the ratory evaporator (40 ºC) to an orange residue. The residue (≈ 12.0 mg) was solubilised methanol (MeOH, 1 mL) and the solution was applied to a preparative TLC plate (silica gel 60; 20 cm x 20 cm plate, 500 μm thickness), using $CHCl_3$ / MeOH (3:1) as a mobile phase. Five different bands were collected and NDTAM-FITC was isolated in a 70 % (*m*/*m*) as an orange powder. The purity of the product *N*-desmethyltamoxifen-fluorescein (NDTAM-FITC) was assessed by TLC (silica gel 60; $CHCl_3$: MeOH (3:1, *v*/*v*); R_F = 0.77), corresponding to the second band and was obtained as an orange solid (10.5 mg, 62 % m/m_T purity, with m_T = total mass applied to the TLC plate). ^{1}H NMR (MeOD-d_4, 500 MHz, 25 ºC): δ (ppm) 7.66 (s, Ph-H_x, 1H), 7.35 – 6.50 (Ph-$H_{a/b/c}$, Ph-$H_{d,e,f}$, 22H), 4.23 (s, H_3, 2H), 3.42 – 3.26 (H_4, H_5, MeOD, 5H), 2.45 (q, H_2, 3H), 0.84 (t, -CH_3, 3H).

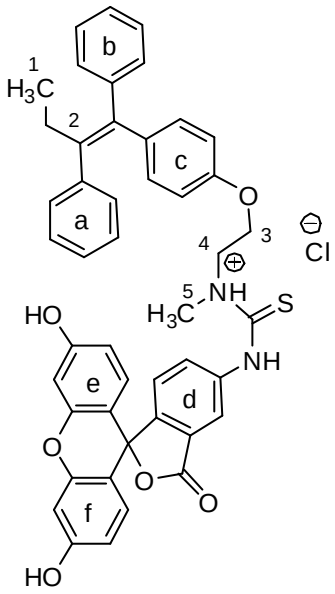

NDTAM - FITC

10.4 CD-Polymers

10.4.1 **Epichlorohydrin/βpen (EPI/βpen, 5:1, P_3)**

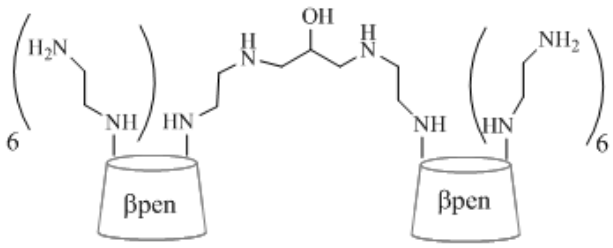

EPI/βpen P_3,P_4,P_5

Heptakis(6-aminoethylamino-6-deoxy)-β-cyclodextrin (βpen , 185 mg, 129.5 μmol) was solubilised in water (2 mL) and a light yellow solution was obtained. Its pH was to ≈ 11 - 12 by addition of a diluted solution of sodium hydroxide (NaOH, 0.1 M). The solution was stirred in an oil bath (70 ºC – 75 ºC) under argon atmosphere for 0.5 min. Epichlorohydrin (EPI, 50 μL, 648 μmol) was added dropwise to the mixture and after 29 h the reaction was stopped. The pH of the mixture was adjusted to ≈ 7.0, acetone (10 mL) was added and a pale yellow solid precipitated followed by extensive washings with acetone (4 x 10 mL). The solid was decanted, solubilised in water (1 mL) and was dialysed at pH = 7 in a benzoylated dialysis tubing (MW_{CO} = 2000 Da), for 24 h with continuous water exchange. After freeze-dried a yellow solid corresponding to polymer EPI/βpen (P_3, 240 mg) was obtained. ^{1}H NMR (D_2O, 500 MHz, 25 ºC) δ (ppm) 5.5 – 4.9 (br m, CD-H_1), 4.5 – 2.3 (CD-H_2,H_3,H_4,H_5,$H_{6,6'}$,$H_{7,7'}$,$H_{8,8'}$) and (EPI-CH,CH_2 aliphatic chains).

10.4.2 **Epichlorohydrin/βpen (EPI/βpen, 10:1, P_4)**

Prepared like P_3 with the following modifications: βpen (251.5 mg; 175.9 μmol); sodium hydroxide NaOH (0.05 M, 6 mL); EPI (138 μL, 1.76 μmol); 2.5 h reaction. EPI/βpen (P_4, 229 mg) was obtained. ^{1}H NMR (D_2O, 500 MHz, 25 ºC) δ (ppm) 5.5 – 4.9 (br m, CD-H_1), 4.5 – 2.3 (CD-H_2,H_3,H_4,H_5,$H_{6,6'}$,$H_{7,7'}$,$H_{8,8'}$) and (EPI-CH,CH_2 aliphatic chains).

10.4.3 **Epichlorohydrin/βpen (EPI/βpen, 20:1, P_5)**

Prepared like P_4 with the following modifications: βpen (252.5 mg; 177 μmol); EPI (277 μL, 3.53 μmol). EPI/βpen (P_4, 225 mg) was obtained. ^{1}H NMR (D_2O, 500 MHz, 25 ºC) δ

(ppm) 5.5 – 4.9 (br m, CD-H_1), 4.5 – 2.3 (CD-H_2,H_3,H_4,H_5,$H_{6,6'}$,$H_{7,7'}$,$H_{8,8'}$) and (EPI-CH,CH_2 aliphatic chains).

10.4.4 Ethylene glycol diglycidyl ether/βpen (EDGE/βpen, 1:1, Q_1)

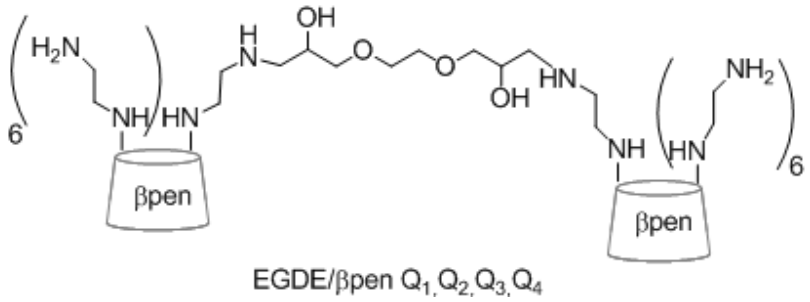

EGDE/βpen Q_1, Q_2, Q_3, Q_4

Heptakis(6-aminoethylamino-6-deoxy)-β-cyclodextrin (βpen, 151.1 mg, 106 μmol) was solubilised in diluted sodium hydroxide solution (NaOH, 0.05 M, 5 mL) and a light yellow solution was obtained. The solution was stirred in an oil bath (70 ºC – 75 ºC) under argon atmosphere for 0.5 min. Ethylene glycol diglycidyl ether (EGDE, 16.5μL, 106 μmol) was added to the mixture and after 72 h the reaction was stopped. The pH of the mixture was adjusted to ≈ 7.0, acetone (10 mL) was added and a pale yellow solid precipitated followed by extensive washings with acetone (4 x 10 mL). The solid was decanted, solubilised in water (1 mL) and was dialysed at pH = 7 in a benzoylated dialysis tubing (MW_{CO} = 2000 Da), for 24 h with continuous water exchange. After freeze-dried a yellow solid corresponding to polymer EGDE/βpen (Q_1, 106 mg) was obtained. ^{1}H NMR (D_2O, 500 MHz, 25 ºC) δ(ppm) 5.4 – 4.8 (br m, CD-H_1), 4.3 – 2.3 (CD-H_2,H_3,H_4,H_5,$H_{6,6'}$,$H_{7,7'}$,$H_{8,8'}$) and (EGDE-CH,CH_2 aliphatic chains).

10.4.5 Ethylene glycol diglycidyl ether/βpen (EDGE/βpen, 5:1, Q_2)

Prepared like Q_1 with the following modifications: βpen (150 mg; 105 μmol); sodium hydroxide NaOH (0.05 M, 5 mL); EGDE (83 μL, 523 μmol). EGDE/βpen (Q_2, 157 mg) was obtained. ^{1}H NMR (D_2O, 500 MHz, 25 ºC) δ(ppm) 5.4 – 4.8 (br m, CD-H_1), 4.3 – 2.3 (CD-H_2,H_3,H_4,H_5,$H_{6,6'}$,$H_{7,7'}$,$H_{8,8'}$) and (EGDE-CH,CH_2 aliphatic chains).

10.4.6 Ethylene glycol diglycidyl ether/βpen (EDGE/βpen, 10:1, Q_3)

Prepared like Q_2 with the following modifications: βpen (155 mg; 109 μmol); sodium hydroxide NaOH (0.05 M, 5 mL); EGDE (166 μL, 1.05 mmol). EGDE/βpen (Q_3, 241 mg) was

obtained. ^{1}H NMR (D_2O, 500 MHz, 25 ºC): δ (ppm) 5.4 – 4.8 (br m, CD-H_1), 4.3 – 2.3 (CD-$H_{2,}H_{3,}H_{4,}H_{5,}H_{6,6'},H_{7,7'},H_{8,8'}$) and (EGDE-CH,$CH_2$ aliphatic chains).

10.4.7 **Ethylene glycol diglycidyl ether/βpen (EDGE/βpen, 20:1, Q_4)**

Prepared like Q_3 with the following modifications: βpen (76.6 mg; 54 μmol); sodium hydroxide NaOH (0.05 M, 2.5 mL); EGDE (166 μL, 1.05 mmol). EGDE/βpen (Q_4, 188 mg) was obtained. ^{1}H NMR (D_2O, 500 MHz, 25 ºC): δ (ppm) 5.4 – 4.8 (br m, CD-H_1), 4.3 – 2.3 (CD-$H_{2,}H_{3,}H_{4,}H_{5,}H_{6,6'},H_{7,7'},H_{8,8'}$) and (EGDE-CH,$CH_2$ aliphatic chains).

10.4.8 **Poly-L-lysine/βpen (pLys/βpen, T_2)**

A stock of poly-L-lysine hydrobromide (pLys.HBr, 1000 < MW_{CO} < 5000) was prepared by solubilising pLys.HBr (25 mg) in water (2 mL). Its pH was adjusted to pH ≈ 11, by addition of aqueous potassium hydroxide (KOH, 0.24 mM, 200 μL) to neutralize the hydrobromide salt (HBr) and obtain pLys (1000 - 5000). pLys (1000 - 5000) (1.1 mL, 12.5 mg, ≈ 4.17 μmol*) was freeze dried, dimethylformamide (DMF, 3 mL) was added, followed by heptakis(6-iodo-6-deoxy)-β-cyclodextrin (βpI, 53 mg, 27.8 μmol). The solution was stirred in an oil bath (70 ºC – 75 ºC) and after 29 h the reaction was stopped, followed by addition of 1,2-diaminoethane (DAE, 2 mL) to insure in 12 h at 70 ºC – 75 ºC the *in situ* generation of βpen. This reaction was monitored by TLC (silica gel 60; *i*PrOH : EtOAc : H_2O : NH_3 (5:3:3:1, *v/v*); RV A) revealing that pLys / βpen (1000 - 5000) is not eluted (R_F = 0) as opposed to βpI (R_F = 0.66). The reaction was stopped after 12 h at 70 ºC – 75 ºC, its contents dried and the residue was dialysed at pH ≈ (8 – 9) in a snakeskin dialysis (MW_{CO} = 3500 Da) for 12 h with continuous water exchange. The contents of the dialysis membrane were dried and a yellow solid corresponding to polymer pLys/βpen (2000 Da < AMW < 3500 Da) (T_2, 11.4 mg) was obtained, dried by freeze-drying. ^{1}H NMR (D_2O, 500 MHz): δ (ppm) 5.3 – 4.8 (br m, CD-H_1), 4.4 – 2.5 (CD-$H_{2,}H_{3,}H_{4,}H_{5,}H_{6,6'},H_{7,7'},H_{8,8'}$ and pLys-$H_{\alpha,\varepsilon}$), 2.0 – 1.0 (pLys-$H_{\beta,\delta,\gamma}$). (* Considering AMW[pLys (1000 - 5000)] = 3000 g/mol).

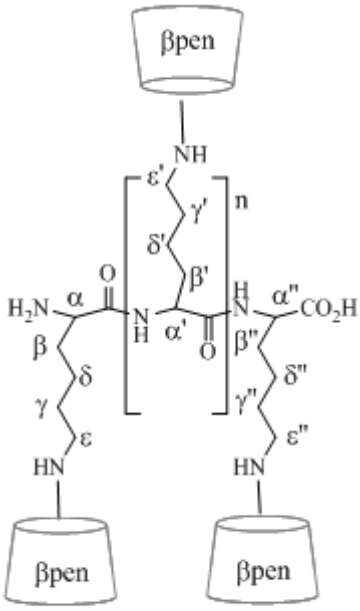

pLys / βpen T_2, BB'

10.4.9 **Poly-L-lysine/ βpen (pLys/βpen, BB')**

Fraction pLys/βpen B' (2000 Da < AMW < 3500 Da) (52 mg, ≈ 18.9 μmol*) resulting from the fractioning of pLys.HBr was dissolved into dimethylformamide (DMF, 2 mL). Aqueous potassium hydroxide (KOH, 2.85 mM, 30 μL) was added and the solution was stirred at 30 ºC for 4 h (solution turned cloudy). More DMF (2 mL), KOH (2.85 mM, 30 μL) were added and the pH was checked and adjusted to (≈ 7 – 8). Heptakis(6-iodo-6-deoxy)-β-cyclodextrin (βpI, 60 mg, 31.5 μmol) was added and reaction proceeded for 48 h at 60 ºC. The reaction was monitored by TLC (silica gel 60; *i*PrOH : EtOAc : H_2O : NH_3 (5:3:3:1, *v/v*); RV A) and revealed that the desired product pLys/βpen (BB') was not eluted (R_F = 0) as opposed to the remaining βpI (R_F = 0.66). The reaction was stopped and 1,2-diaminoethane (DAE, 3 mL) was added to the reaction mixture and it proceeded for 12 h more, until all remaining βpI was consumed (TLC data). The reaction was stopped and was fractioned by using fractioning procedure described for pLys.HBr. Fractioning of polymers was followed by freeze-drying to obtain pLys/βpen BB' (2000 Da < AMW < 3500 Da) (12.1 mg, 23 % *m/m*). ^{1}H NMR (D_2O, 500 MHz) δ (ppm) 5.3 – 4.8 (br m, CD-H_1), 4.4 – 2.5 (CD-$H_{2,}H_{3,}H_{4,}H_{5,}H_{6,6'},H_{7,7'},H_{8,8'}$ and pLys-$H_{\alpha,\varepsilon}$), 2.0 – 1.0 (pLys-$H_{\beta,\delta,\gamma}$). (* Considering AMW of pLys/βpen B' = 2750 g/mol.).

Dialysis fractioning of pLys.HBr (1000 Da < AMW < 5000 Da)

Commercial poly-L-lysine hydrobromide (pLys.HBr, 1000 Da < AMW < 5000 Da), pLys.HBr (100 mg = m_T) was solubilised in water (1 mL), its pH was adjusted to pH ≈ 7, by addition of KOH (0.1 M), and was dialysed against destiled H_2O (2 x 300 mL) using two dialysis membranes in the following order: i) benzoylated dialysis tubing (MW_{CO} = 2000 Da) and ii) skinsnake dialysis tubing (MW_{CO} = 3500 Da). Three fractions of pLys were isolated: fraction A (pLys A) isolated from the liquid lost through membrane (MW_{CO} = 2000 Da); fraction B (pLys B) collected from liquid lost through the second membrane (MW_{CO} = 3500 Da) and fraction C (pLys C) recovered from the contents of the second membrane (MW_{CO} = 3500 Da). The contents of each fraction were freeze-dried to obtain fractions A/B/C with different molecular weight ranges, taking into consideration the lower MW limit (1000 Da) and upper MW limit (5000 Da) of commercial pLys.HBr (1000 Da < AMW < 5000 Da). Fractioning of pLys.HBr (1000 Da* < AMW < 5000 Da *) (100 mg = m_T): pLys fraction A (1000 Da * < AMW < 2500 Da) (35 mg, 35 % m/m_T); pLys fraction B (2000 Da < AMW < 3500 Da) (52 mg, 52 % m/m_T) and pLys fraction C (3500 Da < AMW < 5000 Da *) (14 mg, 14 % m/m_T).

11. Evaluation of Properties

11.1 Linear range of concentrations

11.1.1 ***m*THPP in DMSO (*4 % DMSO/PBS*)**

A stock solution of 5,10,15,20-tetrakis(*m*-hydroxyphenyl)-porphyrin (*m*THPP, 100 μM) was prepared solubilising *m*THPP (3.39 mg, 4.99 μmol) in dimethylsulfoxide (DMSO, 50 μL). Six diluted solutions of varying concentrations (C_1 = 0.99 μM; C_2 = 1.96 μM; C_3 = 2.91 μM; C_4 = 3.84 μM; C_5 = 4.76 μM; C_6 = 5.66 μM) were prepared by taking volumes of stock *m*THPP (100 μM, DMSO: V_1 = 10.0 μL; V_2 = 20.0 μL; V_3 = 30.0 μL; V_4 = 40.0 μL; V_5 = 50.0 μL; V_6 = 60.0 μL) into DMSO (1 mL). The UV-Vis spectra of each solutions (1 - 6) was recorded and the maximum intensity (Soret band) was plotted as a function of the concentration, followed by linear regression used to fit experimental data to the best line (y = mx + b). (*The experiment was repeated in 4 % DMSO/PBS were prepared by diluting the same volumes of mTHPP stock (100 μM, DMSO) in a mixture of 4 % DMSO/PBS (1 mL)*).

11.1.2 **CD-*m*THPP in DMSO (*4 % DMSO/PBS*)**

Like described for *mTHPP in DMSO (4 % DMSO/PBS*), but starting from a stock solution of CD-*m*THPP (100 μM, DMSO) prepared by: i) first, solubilising CD-*m*THPP (2.8 mg, 1.56 μmol) in DMSO (0.5 mL) and then ii) by diluting it further, by adding 32 μL of this stock to a total volume of DMSO (968 μL).

11.2 UV-Vis / fluorescence pH dependence

11.2.1 **Preparation of PBS solutions of varying pH**

A stock solution of phosphate buffered saline (PBS; pH = 7.4) was prepared by solubilising: sodium chloride (NaCl, 0.40 g, 6.85 mmol), potassium chloride (KCl, 0.01 g, 0.14 mmol), potassium dihydrogen phosphate (KH_2PO_4, 12.0 mg, 0.09 mmol) and disodium hydrogen phosphate (Na_2HPO_4, 72.0 mg, 0.51 mmol) in 50 mL of distilled water (H_2O) and the pH was checked (pH = 7.4). Through the addition of HCl (0.1 M) to the initial PBS solution, the pH was adjusted to pH = 2 and a small volume (2 mL) was widrawn, stored in a vial and kept in the fridge. Then, following the gradual addition of sodium hydroxide solution NaOH (0.1 M) to this starting solution (pH = 2), other aqueous buffered solutions (pH = 3, 4, 5, 6, 7, 8, 9, 10, 11) were prepared and stored.

11.2.2 ***m*THPP in 4 % DMSO/PBS of varying pH**

The *m*THPP stock (50 μM, DMSO) was prepared by: i) first, solubilising *m*THPP (2.2 mg, 3.24 μmol) in DMSO (0.5 mL) and then ii) by diluting it further, by adding 7.7 μL of this stock in a total volume of DMSO (993 μL). Diluted solutions of *m*THPP (2 μM; 4 % DMSO/PBS*) were prepared, by adding 80 μL of *m*THPP stock (50 μM, DMSO) to vials containing phosphate buffered solution (PBS*, 1920 μL) of varying pH = 2, 3, 4, 5, 6, 7, 8, 9, 10, 11. For every solution at different pH, the UV-Vis and fluorescence spectra were recorded and spectral changes plotted as a function of the pH.

11.2.3 **CD-*m*THPP in 4 % DMSO/PBS of varying pH**

Like described for *mTHPP in 4 % DMSO/PBS of varying pH,* but starting from a stock solution of CD-*m*THPP (50 μM, DMSO) prepared by: i) first, solubilising CD-*m*THPP (2.8 mg, 1.56 μmol) in DMSO (0.5 mL) and then ii) by diluting it further, by adding 16 μL of this stock to a total volume of DMSO (984 μL).

11.3 Stoichiometry of pMβCD complexes

11.3.1 **Titration pMβCD/CD-*m*THPP (UV-Vis / Fluorescence)**

A diluted solution of CD-*m*THPP (2 μM, 4 % DMSO/PBS), prepared by adding 80 μL of a stock of CD-*m*THPP (50 μM) into 1920 μL of PBS. Small aliquots (5 μL) of a concentrated solution of pMβCD (300 μM, 4 % DMSO/PBS) was added stepwise to the initial guest solution. The UV-Vis and fluorescence spectral changes were recorded before and after each addition, until no more changes are observed. The stoichiometry and binding constants of the complexation were determined, by plotting Soret maximum and fluorescence as a function of the molar equivalents of pMβCD added.

11.3.2 **Titration pMβCD/*m*THPP (UV-Vis / fluorescence)**

Like described for *Titration pMβCD/CD-mTHPP (UV-Vis / Fluorescence),* but starting from a stock solution of *m*THPP (50 μM, DMSO).

11.3.3 **Estimation of the binding constant**

pMβCD/CD-mTHPP (1:1) equilibrium

Non-linear least square fitting of the UV-Vis titration data using the GraphPad Prism 2.01 software using a suitable equation for 1:1 binding, as follows: If G is the guest, H is the host, and HG is the formed complex, the association constant, *K*, can be defined as:

K = [HG]/[H][G], (Eq. 1)

[G] = [G_0]−[HG] (Eq. 2)

[H] = [H_0]−[HG] (Eq. 3)

where, [H_0] and [G_0] being the total host and guest concentrations, respectively. Combining all (Eq.2) and (Eq. 3) in (Eq. 1), [HG] can be written as:

$$[HG] = \frac{([G0]+[H0]+1/K) - \sqrt{[-([G0]+[H0]+1/K)]^2 - 4[G0][H0]}}{2} \quad \text{(Eq.4)}$$

The experimental data were fitted to the equation $\Delta A = \varepsilon_{\Delta HG}[HG]$ (Eq. 5), with ΔA = the observed difference in absorbance, yielding $K_{(1:1)}$ = 3.8 (± 1.59) X 10^6 M^{-1} (goodness of fit, R^2 = 0.9954).

pMβCD/mTHPP (2:1) equilibrium

For the 2:1 case, we assume negligible [HG] concentration, thus

K = [H_2G]/[H]^2[G] (6)

[G0] = [G]+[H_2G] (7)

[H0] = [H]+2[H_2G] (8)

Set mole fractions, αo = [H]/[H0], α2 = 2[H_2G]/[H0] and (α0 + α2) = 1. Assuming that the free guest, *m*THPP, does not contribute to the observed absorbance due to its nearly zero solubility,

$$\Delta A = \alpha 2 \Delta A_{max} \Rightarrow [H_2G] = \frac{\Delta A[H0]}{2\Delta A_{max}} \quad , \quad \text{with} \quad [H] = [H0](1 - \frac{\Delta A[H0]}{\Delta A_{max}}) \quad \text{and}$$

$$[G] = [G0] - \frac{\Delta A[H0]}{2\Delta A_{max}}.$$

Therefore,

$$K = \frac{(\frac{\Delta A[H0]}{2\Delta A_{max}})}{(\frac{[H0]-(1-\Delta A[H0])}{\Delta A_{max}})^2([G0]-(\frac{\Delta A[H0]}{2\Delta A_{max}}))}$$

By plugging in values for concentrations and absorbance differences observed near the break point of the 2:1 binding curve, [H0] = 2 X 10^{-6} M, ΔAM_{max} = 0.526, ΔA = 0.585, the binding constant is obtained was $K_{(2:1)}$ = 4.9 X 10^{-12} M^{-2}.

11.4 Structural features by pMβCD complexes by NMR

11.4.1 **pMβCD/*m*THPP (2:1)**

The initial ^{1}H NMR spectrum of pMβCD (8.67 mM, 0.5 mL, D_2O) was recorded. A diluted solution of *m*THPP (50 μM, MeOD-d_4) was added stepwise in small volumes (12.5 μL) to the initial pMβCD solution and ^{1}H NMR was recorded, until no more peaks corresponding to pMβCD were observed in the spectra. Finally, 2D NMR experiments were recorded to determine the structural features of the complex pMβCD/*m*THPP. *[Final concentration:* pMβCD/*m*THPP *(8.67 mM / 5.6 mM, R = 1.54) in 11 % MeOD / D_2O]*.

11.4.2 **pMβCD/CD-*m*THPP (1:1)**

The ^{1}H NMR spectra of pMβCD (5.0 mM, D_2O) was recorded. A small amount of CD-*m*THPP (2.1 mg; 1.67 μmol) was solubilised in DMSO (20 μL), followed by the addition of 0.45 mL of pMβCD (5.0 mM, D_2O). All NMR spectra including 2D NMR experiments were recorded at 25 ºC. *[Final concentration:* pMβCD/CD-*m*THPP *(4.79 mM / 2.49 mM, R = 0.52) in 4 % DMSO / D_2O]*.

11.5 Inclusion / complexation studies of selected molecules

11.5.1 **Job plots (NMR) for 5'-AMP : βpen**

Continuous variation Job plots of the βpen cavity protons (CD-H_3, H_5) chemical shifts were evaluated from ^{1}H NMR (deuterated PBS, 25 ºC) in the presence of varying amounts of adenosine 5'-monophosphate (5'-AMP). Initial concentrations of βpen.HCl and 5'-AMP were 10 mM prepared in PBS. For a total volume corresponding to one NMR tube (1 mL), different

volumes of βpen (10 mM) were mixed with 5'-AMP (10 mM), in the following ration (R = $V_{\beta pen}$ / $V_{5'\text{-}AMP}$): 0.2/0.8, 0.4/0.6, 0.6/0.4, 0.8/0.2 mL) were mixed. Chemical shift changes of cavity protons (H_3, H_5) were plotted as a function of the mole fraction of βpen.HCl in the NMR tube and the stoichiometry was determined.

11.5.2 **5'-AMP : βpen**

βpen.HCl (11.7 mg; 6.94 μmol) was solubilised in deuterated PBS (pH = 7.4; 0.45 mL) to obtain a clear slight yellow solution. The ^{1}H NMR spectrum was recorded. Adenosine 5'-monophosphate, 5'-AMP (2.40 mg; 6.91 μmol) was added to the previous NMR tube and the solid added completely solubilises. The ^{1}H NMR spectrum was recorded again followed by 2D ROESY NMR experiment (spinlock time = 350 ms). *[Final concentration:* βpen.HCl/5'-AMP *(15.4 mM / 15.4 mM, R = 1.00) in PBS]*.

11.5.3 **PABA : βpen**

βpen.HCl (6.33 mg; 3.76 μmol) was solubilised in deuterated PBS (pH = 7.4; 0.6 mL) to get a clear slight yellow solution. The ^{1}H NMR spectrum was recorded. Excess of *p*-aminobenzoic acid, PABA (2.13 mg; 15.5 μmol) was added to the previous NMR tube and the solid added completely solubilises. The ^{1}H NMR spectrum was recorded again followed by 2D ROESY NMR experiment (spinlock time = 350 ms). *[Final concentration: βpen.HCl/PABA (6.3 mM / 25.8 mM, R = 1.00) in PBS]*.

11.5.4 **ADA-NH_3Cl : CD-*m*THPP**

In a dry vial CD-*m*THPP (2.01 mg; 1.12 μmol) and pMβCD (1.45 mg; 1.01 μmol) were solubilised in DMSO-d_6 (20 μL), vortexed for 1 - 2 min followed by the addition of D_2O (480 μL) to obtain a clear dark red 4 % DMSO/D_2O solution. The ^{1}H NMR spectrum was recorded followed by addition of ADA-NH_3Cl (6.7 μL; 54.3 mM, 4 % DMSO/D_2O). ^{1}H NMR spectrum and 2D NMR spectra (HSQC / NOESY) were subsequently recorded. *[Final concentration*: pMβCD/CD-*m*THPP *(2.00 mM / 2.21 mM, R = 0.91) + ADA-NH_3Cl (0.71 mM) in 4 % DMSO / D_2O]*.

11.5.5 **GEM-ADA amide : CD-*m*THPP**

In a dry vial CD-*m*THPP (1.0 mg; 0.557 μmol) and pMβCD (1.2 mg; 0.839 μmol) were solubilised in DMSO-d_6 (20 μL), vortexed for 1-2 min followed by the addition of D_2O (480 μL) to obtain a clear dark red solution (4 % DMSO/D_2O). ^{1}H NMR (relaxation delay, d_1 = 5 s) was recorded, followed by addition of GEM-ADA amide (T_9) (0.5 mg; 1.175 μmol) stirring (5 min; not soluble), followed by sonication for 60 min. ^{1}H NMR spectrum and 2D NMR spectra (2D ROESY / NOESY) were subsequently recorded. *[Final concentration: pMβCD/CD-mTHPP (1.67 mM / 1.14 mM, R = 1.46) + GEM- ADA amide (2.45 mM) in 4 % DMSO / D_2O]*.

11.5.6 **NDTAM.HCl : CD-*m*THPP**

In a dry vial CD-*m*THPP (0.96 mg; 0.53 μmol) and pMβCD (1.4 mg; 0.98 μmol) were solubilised in DMSO-d_6 (20 μL), vortexed for 1-2 min followed by the addition of D_2O (480 μL) to obtain a clear dark red solution (4 % DMSO/D_2O). The ^{1}H NMR (relaxation delay, d_1 = 5 s) and 2D HSQC experiments were recorded, followed by addition of NDTAM.HCl (0.17 mg; 0.43 μmol) and repetition of the same NMR experiments. 2D NOESY experiment was recorded using a different molar ratio namely: CD-*m*THPP (1.7 mg; 0.93 μmol); pMβCD (1.4 mg; 0.98 μmol); NDTAM.HCl (0.17 mg; 0.43 μmol). *[Final concentration: pMβCD/CD-mTHPP (1.96 mM / 1.06 mM; R = 1.85) + NDTAM.HCl (0.86 mM) in 4 % DMSO / D_2O]*.

11.5.7 **PABA : EPI/βpen P_3**

P_3 (6.13 mg) was solubilised in deuterated PBS (pH = 7.4; 0.5 mL) to get a clear slight yellow solution with a residue in the bottom of the tube. The ^{1}H NMR was recorded. *Para*-aminobenzoic acid, PABA (2.0 mg; 14.6 μmol) was added to the previous NMR tube and the solid added completely solubilises. The ^{1}H NMR was recorded again followed by 2D ROESY NMR experiment (spinlock time = 350 ms).

11.5.8 **PABA : pLys/βpen BB'**

pLys/βpen BB' (1.2 mg; 0.6 μmol) was solubilised D_2O (0.5 mL) to get a clear colourless solution. The ^{1}H NMR spectrum was recorded. *Para*-aminobenzoic acid, PABA (20 μL; D_2O) of a 30.6 mM solution prepared by solubilising PABA (4.2 mg; 30.6 μmol) in D2O (1

mL). The ^{1}H NMR spectrum was recorded again followed by 2D ROESY NMR experiment (spinlock time = 350 ms) and 2D HSQC.

11.5.9 **GEM-ADA amide : pLys/βpen BB'**

pLys/βpen BB' (1.0 mg; 0.5 μmol) was solubilised D_2O (0.5 mL) to get a clear colourless solution. The ^{1}H NMR spectrum was recorded. GEM-ADA amide (0.6 mg; 1.4 μmol) was added to the previous solution and the ^{1}H NMR spectrum was recorded again followed by 2D ROESY(spinlock time = 350 ms) and a 2D HSQC NMR experiments.

11.5.10 **ADA-NH_3Cl : pLys/βpen T_2**

pLys/βpen T_2 (5.0 mg) was solubilised D_2O (0.6 mL) to get a clear light yellow solution. The ^{1}H NMR spectrum was recorded. 1-Adamantanamine, ADA-NH_3Cl (12 μL, 55.9 mM, D_2O) was added to the previous NMR tube and the solid added completely solubilises. The ^{1}H NMR spectrum was recorded again followed by 2D ROESY (spinlock time = 350 ms) NMR experiment.

11.5.11 **5'-AMP : pLys/βpen T_2**

pLys/βpen T_2 (5.0 mg) was solubilised D_2O (0.6 mL) to get a clear light yellow solution. The ^{1}H NMR spectrum was recorded. Adenosine 5'- monophosphate, 5'-AMP (96 μL, 20.2 mM, D_2O) was added to the previous NMR tube. The ^{1}H NMR spectrum was recorded, followed by 2D ROESY (spinlock time = 350 ms) NMR experiment.

11.6 HPLC calibration curve of 5'-AMP

HPLC with UV-Vis detection at λ = 254 nm was used to determine the calibration curve of 5'-AMP. A stock solution A, containing 5'-AMP (8.1 mg; 23.3 μmol) was solubilised in phosphate buffer saline (PBS, pH = 7.4). Five solutions were prepared by diluting small volumes of solution A (1 mL; 5 mL; 2.5 mL; 1 mL; 0.5 mL) respectively into (100 mL; 25 mL; 25 mL; 25 mL; 25 mL) to get five solutions of concentrations of (C_x = 233.0 μM; 46.7 μM; 23.3 μM; 9.3 μM; 4.6 μM) respectively. All solutions were injected in duplicate (2 x) in the HPLC system and the analytical response (area under the peaks) was measured and plotted as a function of C_x (μM).

12. Cell experiments

Cell experiments were conducted on human prostate cancer cell line (DU145) and on breast cancer cell line (MCF7). Cell medium used Roswell Park Memorial Institute (RPMI) medium and phosphate buffered saline (PBS). Incubation times used were 3 h or 15 h. Imaging was performed by confocal spectroscopy at λ_{exc} = 647 nm and λ_{em}~680 nm.

12.1 CD-mTHPP

A stock solution of CD-*m*THPP (10 mM; DMSO) was prepared solubilising CD-*m*THPP (0.82 mg; 0.45 μmol) into DMSO (46 μL). The stock solution was diluted twice: CD-*m*THPP (400 μM; 4 % DMSO/PBS) and CD-*m*THPP (8 μM; cultured media). DU145 cells were incubated for 15 h in the presence of CD-*m*THPP (8 μM; cultured media). A second set of experiments was performed in RPMI instead of PBS.

12.2 pMβCD/CD-mTHPP

A stock solution of pMβCD/CD-*m*THPP (10 mM in CD-*m*THPP; DMSO) and was prepared by solubilising CD-*m*THPP (0.72 mg; 0.40 μmol) and pMβCD (0.30 mg; 0.21 μmol) into DMSO (400 μL). This stock solution was diluted twice: CD-*m*THPP (400 μM; 4 % DMSO/PBS) and CD-*m*THPP (8 μM; media). DU145 cells were incubated for 15 h in the presence of CD-*m*THPP (8 μM; cultured media). A second set of experiments was performed in RPMI instead of PBS.

APPENDIX

13. Additional characterization data

13.1 Conjugate CD-mTHPP

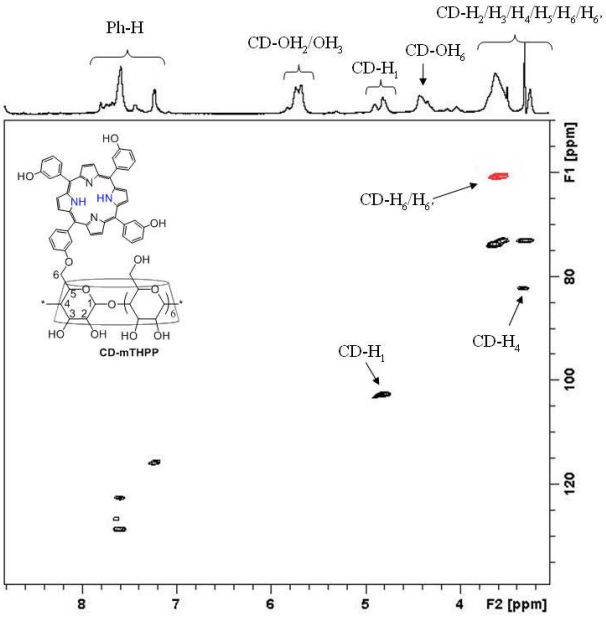

Figure 114. 2D HSQC NMR experiment (DMSO-d_6, 500 MHz, 25 ºC) of CD-*m*THPP.

13.2 Per(6-aminoethylamino-6-deoxy)-βCD (βpen)

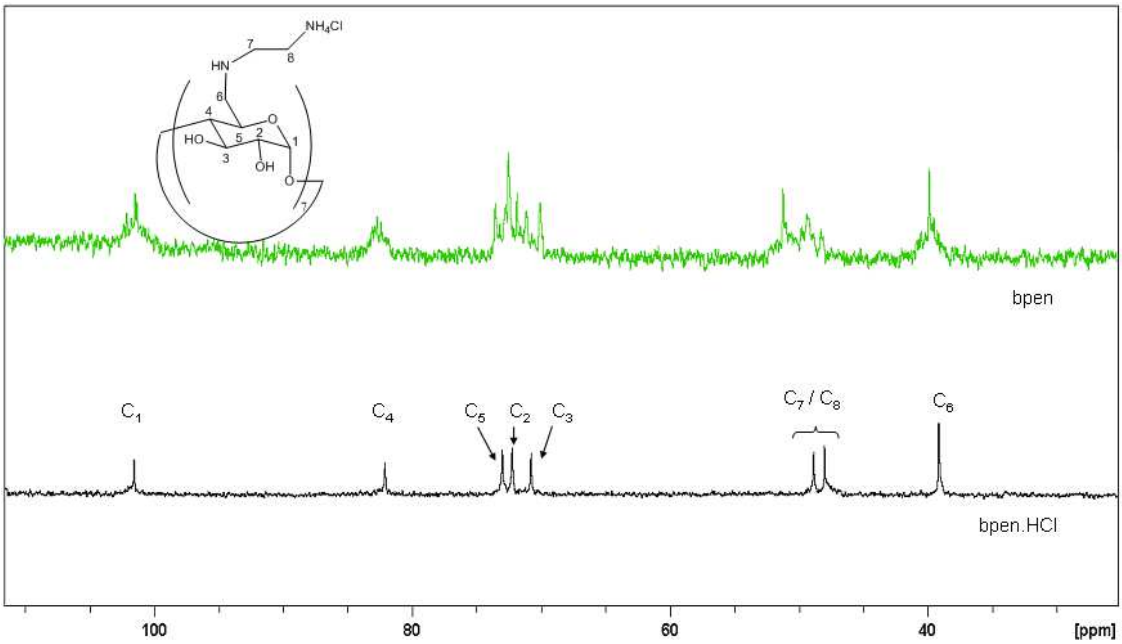

Figure 115. ^{13}C NMR spectrum (D_2O, 500 MHz, 25 ºC) spectra of βpen (white powder) in D_2O (10 < pH < 11) and of βpen.HCl (pH ≈ 4).

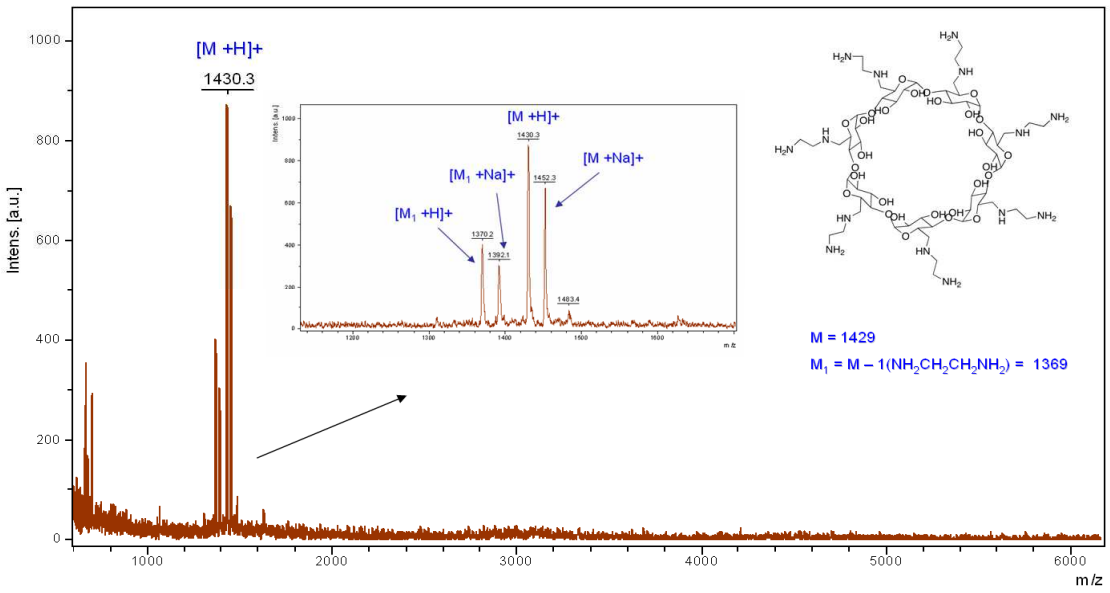

Figure 116. MS (MALDI-TOF) βpen **freebase (5 mg/mL), using 2,5-dihydroxybenzoic acid (DHB) as a matrix.**

13.3 N-Desmethyltamoxifen hydrochloride (NDTAM.HCl)

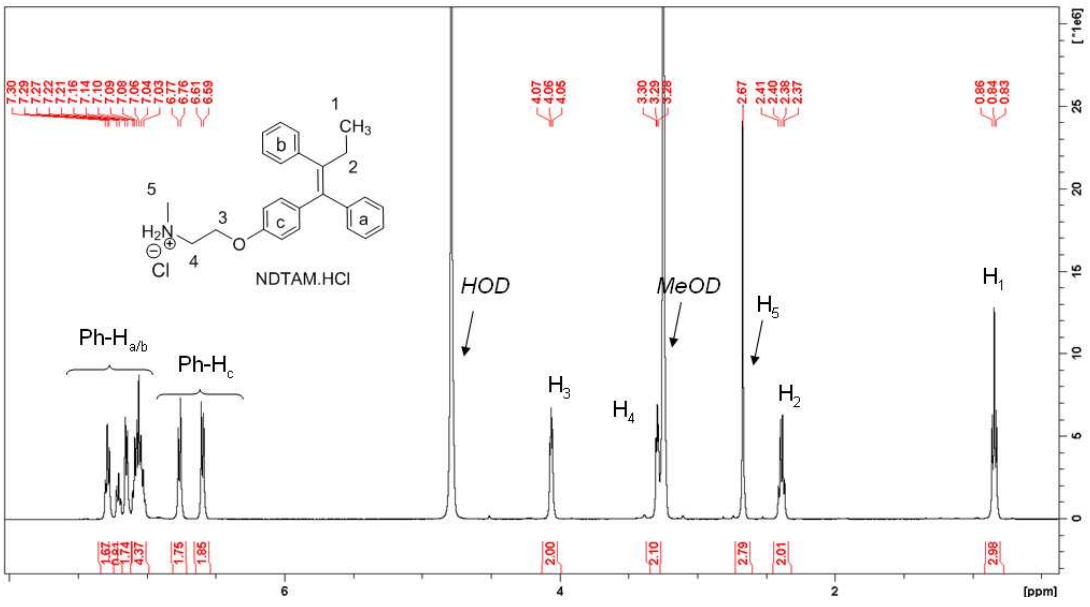

Figure 117. ^{1}H NMR spectrum (MeOD-d_4, 500 MHz, 25 °C) of NDTAM.HCl.

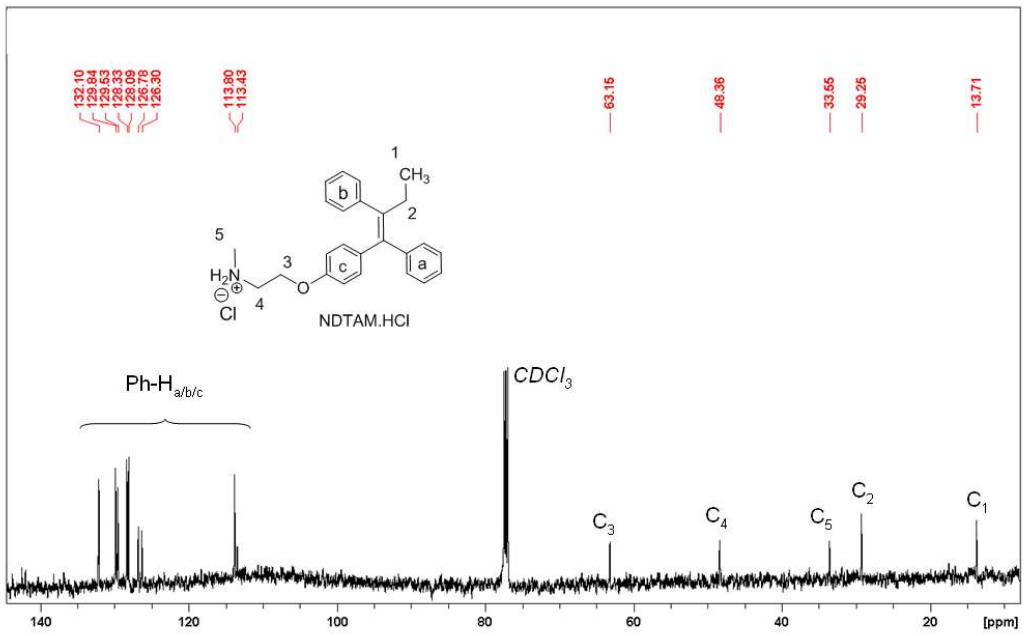

Figure 118. ^{13}C NMR spectrum ($CDCl_3$, 500 MHz, 25 °C) of NDTAM.HCl.

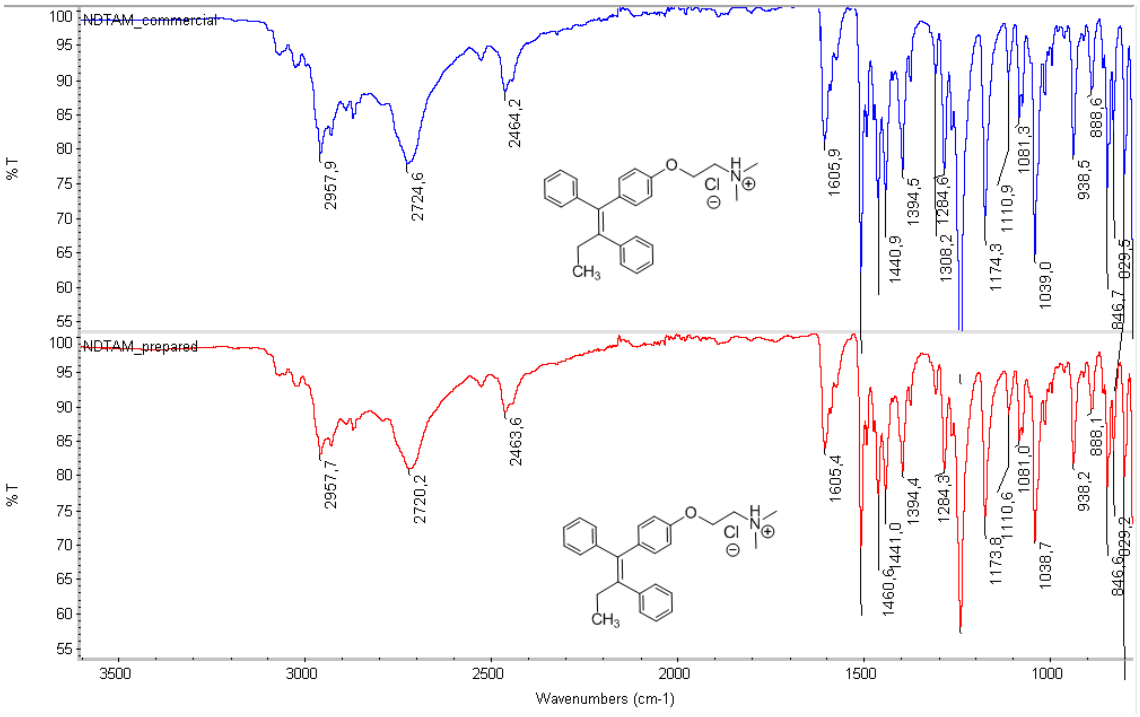

Figure 119. IR spectra of commercial NDTAM.HCl (blue line) and of NDTAM.HCl experimentally obtained (red line).

13.4 Tamoxifen citrate (TAM-Cit, 2:1)

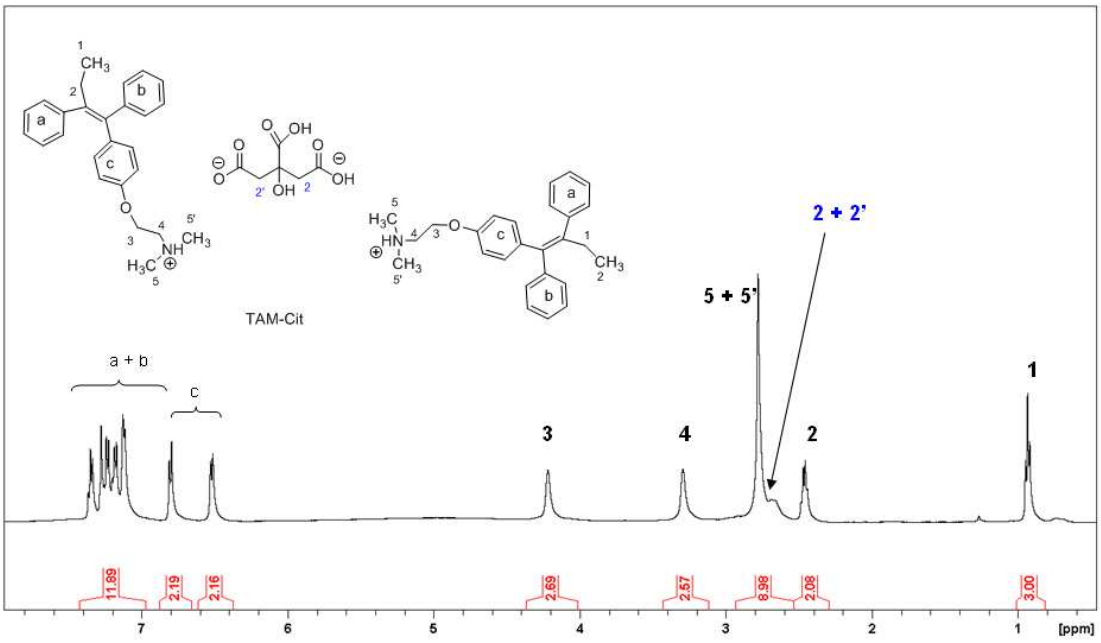

Figure 120. ^{1}H NMR spectrum ($CDCl_3$, 500 MHz, 25 °C) of TAM-Cit (2:1).

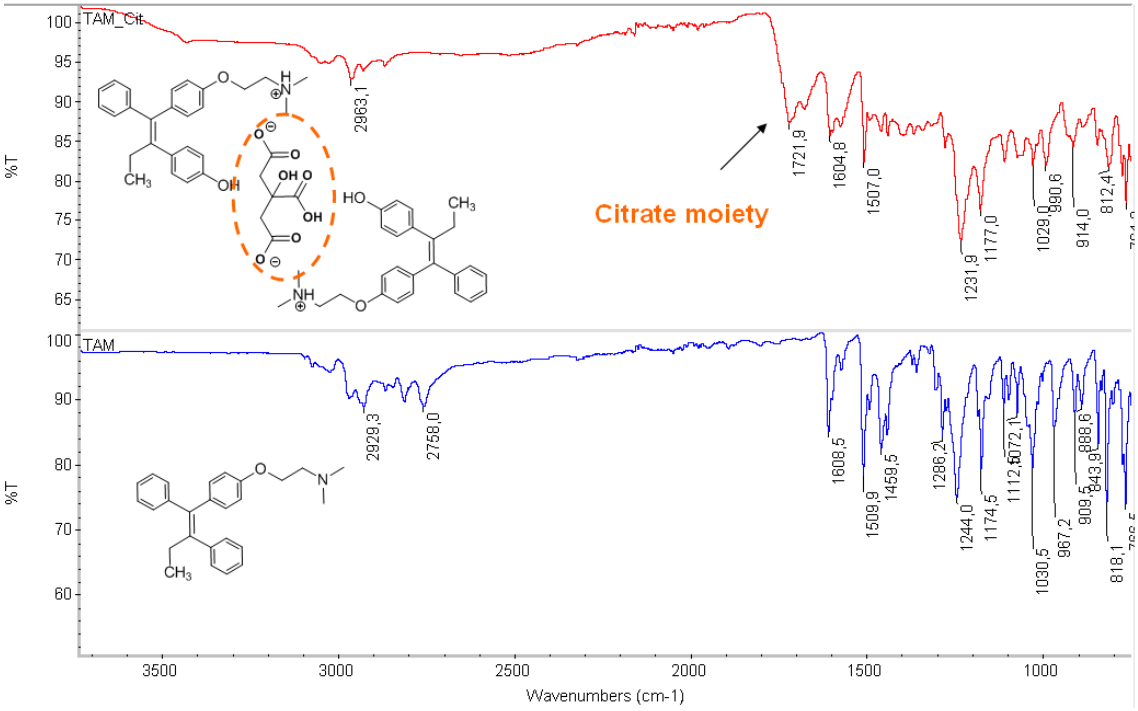

Figure 121. IR spectra of commercial TAM (blue line) and of TAM.Cit (2:1) (red line).

13.5 Gemcitabine-adamantanamide (GEM-ADA amide)

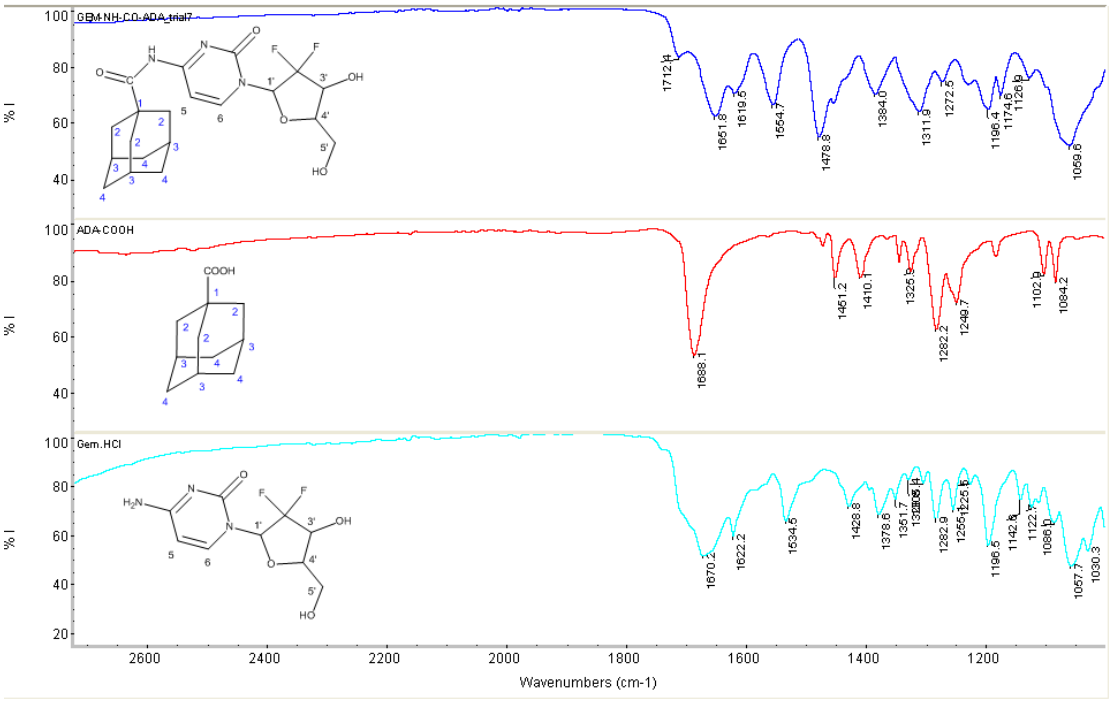

Figure 122. IR spectra of commercial GEM.HCl (light blue), ADA-COOH (red line) and of GEM-ADA amide (blue line).

REFERENCES

1 - Ghazarian, H.; Idoni, B.; Oppenheimer, S. B. A glycobiology review: carbohydrates, lectins and implications in cancer therapeutics. *Acta Histochem.* **2011**, *113*, 236-247.

2 - Hakomori, S.-I. Carbohydrate - carbohydrate interaction as an initial step in cell recognition. *Pure Appl. Chem.* **1991,** *63*, 473-482.

3 - Solomons, T. W. G.; Fryhle, C. B. Organic Chemistry, 7th ed. *John Wiley & Sons*, **2002.**

4 - McNaught, A. D. Nomenclature of carbohydrates - recommendations 1996. *Pure Appl. Chem.* **1996** *68*, 1919 - 2008.

5 - Saenger W.; Jacob, J.; Gessler, K.; Steiner, T.; Hoffmann, D.; Sanbe, H.; Koizumi, K.; Smith, S.M.; Takaha, T. Structures of the common cyclodextrins and their larger analogues beyond the doughnut. *Chem. Rev.* **1998**, *98*, 1787-1802.

6 - Integrated relational Enzyme database (IntEnz): EC 2.4.1.19 - Cyclomaltodextrin glucanotransferase. http://www.ebi.ac.uk/intenz/query?cmd=SearchEC&ec=2.4.1.19 (accessed Oct 31, 2011).

7 - Nam, S.-W.; Park, H.-Y.; Kim, J.-H.; Seo, J.-H.; Han, N.-S.; Kim, B.-W. Expression of Bacillus Macerans cyclodextrin glucanotransferase gene in Sacharomyces Cerevisiae. *Biotechnol. Lett.* **2001**, *23*, 727-730.

8 - Loftsson, T.; Duchene, D. Cyclodextrins and their pharmaceutical applications. *Int. J. Pharm.* **2007**, *329*, 1-11.

9 - Szejtli, J. Past, present, and future of cyclodextrin research. *Pure Appl. Chem.* **2004**, *76*, 1825-1845.

10 - Szejtli, J. Introduction and general overview of cyclodextrin chemistry. *Chem. Rev.* **1998**, *98*, 1743-1754.

11 - Loftsson, T., Brewster, M. E. Pharmaceutical applications of cyclodextrins. 1. Drug solubilization and stabilization. *J. Pharm. Sci.* **1996**, *86*, 1017-1025.

12 - Srivastava, A.; Hunter, J. M. Reversal of neuromuscular block. *Br. J. Anaesth*. **2009**, *103*, 115-129.

13 - Easton, C. J.; Lincoln, S. F. Modified cyclodextrins. *Imperial College Press* (London) **1999**, 4-5.

14 - Uekama, K.; Hiayama, F.; Irie, T. Cyclodextrin drug carrier systems. *Chem. Rev.* **1998**, *98*, 2045–2076.

15 - Li, S.; Purdy, W. C. Cyclodextrins and their applications in analytical chemistry. *Chem. Rev.* **1992**, *92*, 1457–1470.

16 - Dodziuk, H. ed. Cyclodextrins and their complexes: chemistry, analytical methods, applications. *John Wiley & Sons*, **2006**.

17 - Liu, L.; Guo, Q.-X. The driving forces in the inclusion complexation of cyclodextrins. *J. Incl. Phenom. Macrocycl. Chem.* **2002**, *42*, 1–14.

18 - Rekharsky, M. V; Inoue, Y. Complexation thermodynamics of cyclodextrins. *Chem. Rev.* **1998**, *98*, 1875–1917.

19 - Thordarson, P. Determining association constants from titration experiments in supramolecular chemistry. *Chem. Soc. Rev.* **2011**, *40*, 1305–1323.

20 - Schneider, H.-J.; Hacket, F.; Rüdiger, V.; Ikeda, H. NMR studies of cyclodextrins and cyclodextrin complexes. *Chem. Rev.* **1998**, *98*, 1755–1786.

21 - Connors, K. A. Binding constants: the measurement of molecular complex stability. *John Wiley & Sons*, **1987**.

22 - Kleckner, I. R.; Foster, M. P. An introduction to NMR-based approaches for measuring protein dynamics. *Biochem. Bioph. Acta.* **2011**, *1814*, 942–968.

23 - Zouvelekis, D.; Yannakopoulou, K.; Mavridis, I. M.; Antoniadou-Vyza, E. The self-association of the drug acemetacin and its interactions and stabilization with β-cyclodextrin in aqueous solution as inferred from NMR spectroscopy and HPLC studies. *Carbohydr. Res.* **2002**, *337*, 1387–1395.

24 - Kokkinou, A.; Yannakopoulou, K.; Mavridis, I. M.; Mentzafos, D. Structure of the complex of β-cyclodextrin with β-naphthyloxyacetic acid in the solid state and in aqueous solution. *Carbohydr. Res.* **2001**, *332*, 85–94.

25 - Sollogoub, M. Site-Selective Heterofunctionalization of Cyclodextrins: Discovery, Development, and Use in Catalysis. *Synlett.* **2013**, *24*, 2629-2640.

26 - Boger, J.; Corcoran, R. J.; Lehn, J. M. Cyclodextrin chemistry. Selective modification of all primary hydroxyl groups of α- and β-cyclodextrins. *Helv. Chim. Acta.* **1978**, *61*, 2190–2218.

27 - Khan, A. R.; Forgo, P.; Stine, K. J.; D'Souza, V. T. Methods for selective modifications of cyclodextrins. *Chem. Rev.* **1998**, *98*, 1977–1996.

28 - Melton, L. D.; Slessor, K. N. Synthesis of monosubstituted cyclohexaamyloses. *Carbohydr. Res.* **1971**, *18*, 29–37.

29 - Peter, R. A.; Ellwood, P.; Staton, I.; Stoddart, J. F. Synthesis and characterisation of per-3,6-anhydro cyclodextrins. *Angew. Chem. Int. Ed. Engl.* **1991**, *30*, 80–81.

30 - Gadelle, A.; Defaye, J. Selective halogenation at primary positions of cyclomaltooligosaccharides and a synthesis of per-3,6-anhydro cyclomaltooligosaccharides. *Angew. Chem. Int. Ed. Engl.* **1991**, *30*, 78–80.

31 - Breslow, R.; Hammond, M.; Lauer, M. Selective transamination and optical induction by a beta-cyclodextrin-pyridoxamine artificial enzyme. *J. Am. Chem. Soc.* **1980**, *102*, 421–424.

32 - Brady, B.; Lynam, N.; O'Sullivan, T.; Ahern, C.; Darcy, R. 6A-O-p-toluenesulfonyl – β – cyclodextrin. *Org. Synth.* **2000**, *77*, 220-223.

33 - Baer, H. H.; Vargas-Berenguel, A.; Shu, Y. Y.; Defaye, J.; Gadelle, A.; Gonzalez, F. S. Improved preparation of hexakis(6-deoxy)cyclomalto-hexaose and heptakis(6-deoxy)cyclomaltoheptaose. *Carbohydr. Res.* **1992**, *228*, 307-314.

34 - Uekama K., Otagiri M. Cyclodextrins in drug carrier systems. *Crit. Rev. Ther. Drug Carrier Syst.* **1987**, *3*, 1-40.

35 - Rajewski, R.; Stella, V. J. Pharmaceutical applications of cyclodextrins. 2. In vivo drug delivery. *J. Pharm. Sci.* **1996,** *85*, 1142–1169.

36 - Stella, V. J.; He, Q. Cyclodextrins. *Toxicol. Pathol*. **2008**, *36*, 30–42.

37 - Cyclolab. Approved pharmaceutical products containing cyclodextrins. *Cyclodextrin News*, 2013, 27 (2), 1-13.

38 - Moss, G.P. Nomenclature of tetrapyrroles. *Pure & AppI. Chem*. **1987**, *59*, 779–832.

39 - Steiner, E.; Fowler, P. W. Diamagnetic and paramagnetic ring currents in expanded porphyrins. *Org. Biomol. Chem.* **2004**, *2*, 34–37.

40 - Wijesekera, T. P.; Dolphin, D. Some preparations and properties of porphyrins. *Adv. Exp. Med. Biol.* **1924**, *193*, 229–266.

41 - Kessel, D. Components of hematoporphyrin derivatives and their tumor-localizing capacity components of hematoporphyrin. *Cancer Res.* **1982**, *42*, 1703–1706.

42 - Lipson R. L.; Blades, E.; Olsen, A. The use of a derivative of hematoporphyrin in tumor detection. *J. Natl. Cancer Inst.* **1961**, *26*, 1-11.

43 - Kessel, D.; Thompson, P. Purification and analysis of hematoporphyrin and hematoporphyrin derivative by gel exclusion and reverse-phase chromatography. *Photochem. Photobiol.* **1987**, *46*, 1023-1025.

44 - Monteiro, C. J. P.; Pereira, M. M.; Pinto, S. M. A.; Simões, A. V. C.; Sá, G. F. F.; Arnaut, L. G.; Formosinho, S. J.; Simões, S.; Wyatt, M. F. Synthesis of amphiphilic sulfonamide halogenated porphyrins: MALDI-TOF MS characterisation and evaluation of 1-octanol/water partition coefficient. *Tetrahedron*. **2008**, 64, 5132–5138.

45 - Kadish, K. M.; Smith, M. S.; Guilard, R. The Porphyrin Handbook – Synthesis and Organic Chemistry. *Elsevier*, **2000**.

46 - Adler, A. D.; Longo, F. R.; Finarelli, J. D.; Goldmecher J.; Assour, J.; Korsakoff, L. A simplified synthesis for meso-tetraphenylporphine. *J. Org. Chem.* **1967**, *32*, 476.

47 - Král, V.; Králová, J.; Kaplánek, R.; Bríza, T.; Martásek, P. Quo vadis porphyrin chemistry? *Physiol. Res.* **2006**, *55*, S3–S26.

48 - So, P. T. C.; Dong, C. Y. Fluorescence spectroscopy. ELS, *John Wiley & Sons*, **2002**.

49 - Universidad Autonoma Madrid: Jablonski Diagram - Relaxation mechanism for excited state molecules. http://www.uam.es/docencia/quimcursos/Scimedia/chem-ed/quantum/jablonsk.htm (accessed May 20, 2013).

50 - Josefsen, L. B.; Boyle, R. W. Photodynamic therapy and the development of metal-based photosensitisers. *Met. Based Drugs.* **2008,** *2008 (ID - 276109)*, 1–23.

51 - Anderson, H. L. Building molecular wires from the colours of life: conjugated porphyrin oligomers. *Chem. Commun.* **1999**, *297*, 2323–2330.

52 - Gouterman, M. Spectra of porphyrins. *J. Mol. Spectrosc.* **1961**, *6*, 138–163.

53 - Nemykin, V. N.; Hadt, R. G. Interpretation of the UV-Vis spectra of the meso(ferrocenyl)-containing porphyrins using a TDDFT approach: is Gouterman's classic four-orbital model still in play? *J. Phys. Chem. A.* **2010**, *114*, 12062–12066.

54 - Makarska, M.; Legendziewicz, J.; Radzki, S. Spectroscopic characterisation of the water-soluble cationic porphyrins and their complexes with Cu (II) in various solvents. *J. Alloys Comp.* **2002**, *341*, 233–238.

55 - Cunderlikova, B.; Bjorklund, E. G.; Pettersen, E. O.; Moan, J.; Bjørklund, E. G. pH-dependent spectral properties of HpIX, TPPS, mTHPP and mTHPC. *Photochem. Photobiol.* **2001**, *74*, 246–252.

56 - Braslavsky, S. E. Glossary of terms used in photochemistry. *Pure & Appl. Chem.* **2007**, *79*, 293–465.

57 - Neri, C. R.; Calefi, P. S.; Iamamoto, Y.; Serra, O. A. Luminescent hybrid porphyrino silica obtained by sol gel chemistry. *Mat. Res.* **2002**, *6*, 71–74.

58 - Biesaga, M.; Pyrzyńska, K.; Trojanowicz, M.; Pyrzyn, K. Porphyrins in analytical chemistry. A review. *Talanta* **2000**, *51*, 209-224.

59 - Brown, S.; Shillcock, M. Equilibrium and kinetic studies of the aggregation of porphyrins in aqueous solution. *Biochem. J.* **1976**, *153*, 279–285.

60 - With, T. K.; Pedersen, J. S. Molar absorption coefficients of porphyrin esters in chloroform determined by copper titration. *Biochem. J.* **1977**, *161*, 425–429.

61 - Ribo, J. M.; Crusats, J.; Farrera, J.-A.; Valero, M. L. Aggregation in water solutions of tetrasodium diprotonated meso-tetrakis(4-sulfonatophenyl)-porphyrin. *J. Chem. Soc. Chem. Commun.* **1994**, 681–682.

62 - Cogdell, R. J. Carotenoids in photosynthesis. *Pure & Appl. Chem.***1985**, *57*, 723–728.

63 - Jordan, P.; Fromme, P.; Witt, H. T.; Klukas, O.; Saenger, W.; Krauss, N. Three-dimensional structure of cyanobacterial photosystem I at 2.5 Å resolution. *Nature.* **2001**, *411*, 909–917.

64 - Kiba, T.; Suzuki, H.; Hosokawa, K.; Kobayashi, H.; Baba, S.; Kakuchi, T.; Sato, S. Supramolecular J-aggregate assembly of a covalently linked zinc porphyrin-β-cyclodextrin conjugate in a water/ethanol binary mixture. *J. Phys. Chem. B* **2009**, *113*, 11560–11563.

65 - Micali, N.; Villari, V.; Castriciano, M. A.; Romeo, A.; Scolaro, L. M. From fractal to nanorod porphyrin J-aggregates. Concentration-induced tuning of the aggregate size. *J. Phys. Chem. B.* **2006**, *110*, 8289–8295.

66 - Chauhan, S. M. S.; Kumar, A.; Srinivas, K. A.; Mishra, M. K. Effect of side chain length on the aggregation of amphiphilic 5,10,15-tris (1-methylpyridinium-4-yl)-20-[4-(alkoxy) phenyl] 21H, 23H porphyrin tritosylates. *Indian J. Biochem. Biophys.* **2003**, *40*, 429–438.

67 - Siggel, U.; Binding, U.; Endisch, C.; Komatsu, T.; Tsuchida, E.; Voigt, J.; Fuhrhop, J.-H. Photophysical and photochemical properties of porphyrins Aggregates. *Phys. Chem.* **1996**, *100*, 2070–2075.

68 - Scolaro, M. L.; Castriciano, M.; Romeo, A.; Mazzaglia, A.; Mallamace, F.; Micali, N. Nucleation effects in the aggregation of water-soluble porphyrin aqueous solutions. *Physica A.* **2002**, *304*, 158–169.

69 - Gallagher, W.A.; Elliot, E.B. Ligand binding in porphyrin systems. *Ann. N.Y. Acad. Sci.* **1973**, *206*, 463-482.

70 - White, W.I.; Plane, R.A. A homologous series of water-soluble porphyrins and metalloporphyrins: synthesis, dimerization, protonation and self-complexation. *Bioinorg. Chem.* **1974**, *4*, 21.

71 - Li, X.; Zhang, L.; Mu, J. Formation of new types of porphyrin H- and J-aggregates. *Colloid. Surface A.* **2007,** *311*, 187-190.

72 - D'Urso, A.; Fragalàa, M. E.; Purrello, R. From self-assembly to noncovalent synthesis of programmable porphyrins' arrays in aqueous solution. *Chem. Commun.* **2012**, *48*, 8165–8176.

73 - Fathalla, M.; Neuberger, A.; Li, S-C.; Schmehl, R.; Diebold, U.; Jayawickramajah, J. Straightforward self-Assembly of porphyrin nanowires in water: Harnessing Adamantane/β-Cyclodextrin Interactions. *J. Am. Chem. Soc.* **2010,** *132*, 9966 – 9967.

74 - Ito, S.; Uno, H.; Murashima, T.; Ono, N. Synthesis, properties and crystal structures of rigid porphyrins fused with bicyclo[2.2.2]octene units. *Chem. Commun*. **1999**, 2275–2276.

75 - Gong, X.; Milic, T.; Xu, C.; Batteas, J. D.; Drain, C. M. Preparation and characterisation of porphyrin nanoparticles *J. Am. Chem. Soc.* **2002**, *124*, 14290–14291.

76 - Susana L.H. R.; Gonçalves, A. R.; Pereira, M. M.; Simões, M. M. Q.; Neves, M. G. P. M. S.; Cavaleiro, J. A. S. Epoxidation reactions with hydrogen peroxide activated by a novel heterogeneous metalloporphyrin catalyst. *J. Mol. Catal. A: Chem.* **2006**, *256*, 321 – 323.

77 - Bell, S. R.; Groves, J. T. A highly reactive P450 model compound I. *J. Am. Chem. Soc*. **2009**, *131*, 9640-9641.

78 - Malinski, T.; Taha, Z. Nitric oxide release from a single cell measured in situ by a porphyrinic-based microsensor. *Nature.* **1992**, *358*, 676-678.

79 - Lee S.-K.; Okura I. Optical sensor for oxygen using a porphyrin-doped sol–gel glass. *Analyst*. **1997**, *122*, 81–84.

80 - Kim, Y.; Kim, S.; Lee, W.; Lee, D.; Lee, W. (Korea Advanced Institute of Science and Technology). Metal-porphyrin carbon nanotubes for use in fuel cell electrodes. US Patent 20130030175, Jan. 31, **2013**.

81 - Uttamlal, M., Holmes-Smith A. S. The excitation wavelength dependent fluorescence of porphyrins. *Chem. Phys. Lett.* **2008**, *454*, 223-228.

82 - Allison, R. R.; Downie, G. H.; Cuenca, R.; Hu, X.-H.; Childs, C. J. H.; Sibata, C. H. Photosensitizers in clinical PDT. *Photodiagn. Photodyn.* **2004**, *1*, 27-42.

83 - Agostinis, P.; Berg, K.; Cengel, K. A.; Foster, T. H.; Girotti, A. W.; Gollnick, S. O.; Hahn, S. M.; Hamblin, M. R.; Juzeniene, A.; Kessel, D.; Korbelik, M.; Moan, J.; Mroz, P.; Nowis, D.; Piette, J.; Wilson, B. C.; Golab, J. Photodynamic therapy of cancer: an update. *CA Cancer J Clin.* **2011**, *61*, 250-281.

84 - Kwitniewski, M.; Juzeniene, A.; Ma, L.-W.; Glosnicka, R.; Graczyk, A.; Moan, J. Diamino acid derivatives of PpIX as potential photosensitizers for photodynamic therapy of squamous cell carcinoma and prostate cancer: In vitro studies. *J. Photochem. Photobiol. B. Biol.* **2009**, *94*, 214–222.

85 - Washington Institute of Dermatology Laser Surgery, http://www.skinlaser.com/laser-treatments/photodynamic-therapy-pdt-skin-resurfacing-washington-dc/ (accessed Jun 12, 2013).

86 - Dickinson, B. C.; Chang, C. J. Chemistry and biology of reactive oxygen species in signaling or stress responses. *Nat. Chem. Biol.* **2011**, *7*, 504–511.

87 - Agnez-Lima, L. F.; Melo, J. T. A.; Silva, A. E.; Oliveira, A. H. S.; Timoteo, A. R. S.; Lima-Bessa, K. M.; Martinez, G. R.; Medeiros, M. H. G.; Mascio, P. D.; Galhardo, R. S.; Menck, C. F. M. DNA damage by singlet oxygen and cellular protective mechanisms. *Mutat. Res.* **2012**, *751*, 15–28.

88 - Stenbaek, A.; Jensen, P. E. Redox regulation of chlorophyll biosynthesis. *Phytochemistry*. **2010**, *71*, 853–859.

89 - Buchachenko, A. L. Recent advances in spin chemistry. *Pure Appl. Chem.* **2000**, *72*, 2243–2258.

90 - Quintero, B.; Miranda, M. A. Mechanisms of photosensitization induced by drugs: A general survey. *Ars. Pharmaceutica*. **2000**, *41*, 27-46.

91 - Brown, S. B.; Brown, E. A.; Walker, I. The present and future role of photodynamic therapy in cancer treatment. *Lancet Oncol.* **2004**, *5*, 497–508.

92 - Senge, M. O.; Brandt, J. C. Temoporfin (Foscan®, 5,10,15,20-tetra(m-hydroxyphenyl)chlorin) - a second-generation photosensitizer. *Photochem. Photobiol.* **2011**, *87*, 1240–1296.

93 - Wachowska, M.; Muchowicz, A.; Firczuk, M.; Gabrysiak, M.; Winiarska, M.; Wańczyk, M.; Bojarczuk, K.; Golab, J. Aminolevulinic acid (ALA) as a prodrug in photodynamic therapy of cancer. *Molecules.* **2011**, *16*, 4140–4164.

94 - European Medicine Agency: Foscan®, Temoporfin http://www.ema.europa.eu/ema/index.jsp?curl=pages/medicines/human/medicines/000318/human_med_000801.jsp&mid=WC0b01ac058001d124 (accessed Mar 03, 2014).

95 - Postiglione, I.; Chiaviello, A.; Palumbo, G. Enhancing photodynamyc therapy efficacy by combination therapy: dated, current and oncoming strategies. *Cancers.* **2011**, *3*, 2597–2629.

96 - Mazzaglia, A.; Micali, N.; Monsù, L. Design of photosensitizer / cyclodextrin nanoassemblies : spectroscopy , intracellular delivery and photodamage. *J. Porphyrins Phthalocyanines.* **2010**, *14*, 661–677.

97 - Foley, S., Jones, G., Liuzzi, R., McGarvey, D.J., Perry, M.H., Truscott, T.G. The synthesis and photophysical properties of polyether substituted phthalocyanines of potential use in photodynamic therapy. *J. Chem. Soc. PerkinTrans. 2.* **1997**, *9*, 1725-1730.

98 - Haj-Hosseini, N.; Richter, J.; Andersson-Engels, S.; Wardell, K. Photobleaching behavior of protoporphyrin IX during 5- aminolevulinic acid marked glioblastoma detection. *Proc. SPIE.* **2009**, *7161*, 1–8.

99 - Wainwright, M. Non-porphyrin PS in biomedicine. *Chem. Soc. Rev.* **1996**, *25*, 351–359.

100 - Sternberg, E. D.; Dolphin, D. Porphyrin-based photosensitizers for use in photodynamic therapy. *Tetrahedron.* **1998**, *54*, 4151–4202.

101 - Prasmickaite, L.; Høgset, A.; Selbo, P. K.; Engesæter, B. Ø.; Hellum, M.; Berg, K. Photochemical disruption of endocytic vesicles before delivery of drugs: a new strategy for cancer therapy. *Br. J. Cancer.* **2002**, *86*, 652–657.

102 - U.S. National Institutes of Health, Dose escalating study for amphinex-based PCI of bleomycin, http://clinicaltrials.gov (accessed Mar 03, 2014).

103 - Sykes, R. Towards the magic bullet. *Int. J. Antimicrob. Agents.* **2000**, *14*, 1–12.

104 - Lammers, T.; Hennink, W. E.; Storm, G. Tumour-targeted nanomedicines: principles and practice. *Br. J. Cancer.* **2008**, *99*, 392-397.

105 - Singh, Y.; Palombo, M.; Sinko, P. Recent trends in targeted anticancer prodrug and conjugate design. *Curr. Med. Chem.* **2008**, *18*, 58–61.

106 - Vrignaud, S.; Benoit, J.; Saulnier, P. Strategies for the nanoencapsulation of hydrophilic molecules in polymer-based nanoparticles. *Biomaterials.* **2011**, *32*, 8593–8604.

107 - Clond, M.; Lee, B.-S.; Yu, J. J.; Singer, M. B.; Amano, T.; Lamb, A. W.; Drazin, D.; Kateb, B.; Ley, E. J.; Yu, J. S. Reactive oxygen species-activated nanoprodrug of ibuprofen for targeting traumatic brain injury in mice. *PLoS One.* **2013**, *8*, 1-10, (e61819).

108 - Neuse, E. W. Synthetic polymers as drug-delivery vehicles in medicine. *Met. Based. Drugs.* **2008**, *2008*, 469531.

109 - Fenyvesi, E. Cyclodextrin polymers in the pharmaceutical industry. *J. Incl. Phenom.* **1988**, *6*, 537-545.

110 - Zhang, J.; Ma, P. X. Cyclodextrin-based supramolecular systems for drug delivery: recent progress and future perspective. *Adv. Drug Deliv. Rev.* **2013**, *65*, 1215–12133.

111 - Nielsen, T. T.; Wintgens, V.; Amiel, C.; Wimmer, R.; Larsen, K. L. Facile synthesis of β-cyclodextrin-dextran polymers by click chemistry. *Biomacromolecules*. **2010**, *11*, 1710-1715.

112 - Wintgens, V., Nielsen, T. T., Larsen, K. L.; Amiel, C. Size-controlled nanoassemblies based on cyclodextrin modified dextrans. *Macromol. Biosci.* **2011**, *11*, 1254-1263.

113 - Bohm, I.; Kreth, S. K.; Ritter, H.; Branscheid, R.; Kolb, U. Switchable supramolecular crosslinking of cyclodextrin-modified hyperbranched polyethylenimine via anthraquinone dyes. *Macromolel. Chem. Phys.* **2012**, *213*, 243-248.

114 - Zhu, Y.; Che, L.; He, H.; Jia, Y.; Zhang, J.; Li, X. Highly efficient nanomedicines assembled via polymer–drug multiple interactions: tissue-selective delivery carriers. *J. Control. Release.* **2011**, *152*, 317–324.

115 - Choi, H.S.; Yamashita, A.; Ooya, T.; Yui, N.; Akita, H.; Kogure, K.; Ito, R.; Harashima, H. Sunflower-shaped cyclodextrin - conjugated poly(ε-Lysine) polyplex as a controlled intracellular trafficking device. *ChemBioChem.* **2005**, *11*, 1986–1990.

116 - Kulkarni A.; DeFrees K.; Hyun, S. H.; Thompson D. H. Pendant Polymer: Amino-β-cyclodextrin: siRNA guest : host nanoparticles as efficient vectors for gene silencing. *J. Am. Chem. Soc.* **2012**, *134*, 7596-7599.

117 - Moya-Ortega, M. D.; Alvarez-Lorenzo, C.; Sigurdsson, H. H.; Concheiro, A.; Loftsson, T. Cross-linked hydroxypropyl-β-cyclodextrin and γ-cyclodextrin nanogels for drug delivery: physicochemical and loading/release properties. *Carbohydr. Polym.* **2012**, *87*, 2344–2351.

118 - Díaz-Moscoso, A.; Le Gourriérec, L.; Gomes-García, M.; Benito, J. M.; Balbuena, P.; Ortega-Caballero, F.; Guilloteau, N.; Di Giorgio, C.; Vierling, P.; Defaye, J.; Mellet, C. O.; Fernández, J. M. G. Polycationic amphiphilic cyclodextrins for gene delivery: synthesis and effect of structural modifications on plasmid DNA complex stability, cytotoxicity and gene expression. *Chem. Eur. J.* **2009**, *15*, 12871–12888.

119 - Heidel, J. D.; Schluep, T. Cyclodextrin-containing polymers: versatile platforms of drug delivery materials. *J. Drug. Deliv.* **2012**, *2012*, 1–17.

120 - Loftsson T. Increasing the cyclodextrin complexation of drugs and drug bioavailability through addition of water-soluble polymers. *Pharmazie*. **1998**, *53*, 733-740.

121- Tarimci, N., Celebi, N. Studies on cyclodextrin polymer – the effect of CDP on indomethacin tablet formulation. *Pharmazie*. **1988**, *43*, 323-325.

122 - Fenyvesi, É.; Nagai, T.; Antal, B.; Zsadon, B.; Szejtli, J. Evaluation of cyclodextrin polymer as a disintegrating agent. *J. Inclusion Phenom.***1984**, *2*, 645-654.

123 - Bibby, D. C.; Davies, N. M.; Tucker, I. G. Mechanisms by which cyclodextrins modify drug release from polymeric drug delivery systems. *Int. J. Pharm.* **2000**, *197*, 1–11.

124 - Moya-Ortega, M. D.; Alvarez-Lorenzo, C.; Concheiro, A.; Loftsson, T. Cyclodextrin-based nanogels for pharmaceutical and biomedical applications. *Int. J. Pharm.* **2012**, *428*, 152–163.

125 - Hamilton, A.; Voinnet, O.; Chappell, L.; Baulcombe, D. Two classes of short interfering RNA in RNA silencing. *EMBO J.* **2002**, *21*, 4671–4679.

126 - Kesharwani, P.; Gajbhiye, V.; Jain, N. K. A review of nanocarriers for the delivery of small interfering RNA. *Biomaterials*. **2012**, *33*, 7138–71350.

127 - Davis, M. E. The first targeted delivery of siRNA in humans via a nanoparticle: from concept to clinic. *Mol. Pharm.* **2009**, *6*, 659–668.

128 - U.S. National Institutes of Health: Safety study of CALAA-01 to treat solid tumor cancers. http://www.clinicaltrials.gov/ct2/show/NCT00689065 (accessed Mar 03, 2014).

129 - Cheng, J.; Khin, K. T.; Jensen, G. S.; Liu, A.; Davis, M. E. Synthesis of linear, β-cyclodextrin-based polymers and their camptothecin conjugates. *Bioconjugate Chem.* **2003**, *14*, 1007–1017.

130 - U.S. National Institutes of Health: Study of CRLX101 (Formerly Named IT-101) in the Treatment of Advanced Solid Tumors. http://clinicaltrials.gov/ct2/show/NCT00333502 (accessed Mar 03, 2014).

131 - Kandoth, N.; Vittorino, E.; Sciortino, M. T.; Parisi, T.; Colao, I.; Mazzaglia, A.; Sortino, S. A cyclodextrin-based nanoassembly with bimodal photodynamic action. *Chem. Eur. J.* **2012**, *18*, 1684–1690.

132 - Mezo, G.; Herényi, L.; Habdas, J.; Majer, Z.; Myśliwa-Kurdziel, B.; Tóth, K.; Csík, G. Synthesis and DNA binding of new cationic porphyrin-tetrapeptide conjugates. *Biophys. Chem.* **2011**, *155*, 36–44.

133 - Lei, W.; Xie, J.; Hou, Y.; Jiang, G.; Zhang, H.; Wang, P.; Wang, X.; Zhang, B. Mitochondria-targeting properties and photodynamic activities of porphyrin derivatives bearing cationic pendant. *J. Photochem. Photobiol. B, Biol.* **2010**, *98*, 167–171.

134 - Selvestrel, F.; Moret, F.; Segat, D.; Woodhams, J. H.; Fracasso, G.; Echevarria, I. M. R.; Baù, L.; Rastrelli, F.; Compagnin, C.; Reddi, E.; Fedeli, C.; Papini, E.; Tavano, R.; MacKenzie, A.; Bovis, M.; Yaghini, E.; MacRobert, A. J.; Zanini, S.; Boscaini, A.; Colombatti, M.; Mancin, F. Targeted delivery of photosensitizers: efficacy and selectivity issues revealed by multifunctional ORMOSIL nanovectors in cellular systems. *Nanoscale* **2013**, *5*, 6106–6116.

135 - Puglisi, A.; Purrello, R.; Rizzarelli, E.; Sortino, S.; Vecchio, G. Spectroscopic and self-association behavior of a porphyrin-β-cyclodextrin conjugate. *New J. Chem.* **2007**, *31*, 1499-1506.

136 - Lang, K.; Kral, V.; Kapusta, P.; Kubát, P.; Vasek, P. Photoinduced electron transfer within porphyrin-cyclodextrin conjugates. *Tetrahedron Lett.* **2002**, *43*, 4919–4922.

137 - Králová, J.; Kejík, Z.; Bríza, T.; Poucková, P.; Král, A.; Martásek, P.; Král, V. Porphyrin-cyclodextrin conjugates as a nanosystem for versatile drug delivery and multimodal cancer therapy. *J. Med. Chem.* **2010**, *53*, 128–138.

138 - Breslow, R.; Zhang, X.; Xu, R. Selective catalytic oxidation of substrates that bind to metalloporphyrin enzyme mimics carrying two or four cyclodextrin groups and related metallosalens. *J. Am. Chem. Soc.* **1996**, *118*, 11678–11679.

139 - Silva, J. N.; Silva, A. M. G.; Tomé, J. P.; Ribeiro, A. O.; Domingues, M. R. M.; Cavaleiro, J. A. S.; Silva, A. M. S.; Neves, M. G. P. M. S.; Tomé, A. C.; Serra, O. A.; Bosca, F.; Filipe, P.; Santus, R.; Morlière, P. Photophysical properties of a photocytotoxic fluorinated chlorin conjugated to four beta-cyclodextrins. *Photochem. Photobiol. Sci.* **2008**, *7*, 834–843.

140 - Olliaro, P.; Seiler, J.; Kuesel, A.; Horton, J.; Clark, J. N.; Don, R.; Keiser, J: Potential drug development candidates for human soil-transmitted helminthiases. *PLoS Negl. Trop. Dis.* **2011**, *5*, e1138.

141 - Aggelidou, C.; Theodossiou, T. A; Yannakopoulou, K. Protoporphyrin IX-β-Cyclodextrin Bimodal Conjugate: Nanosized Drug Transporter and Potent Phototoxin. *Photochem. Photobiol*. **2013**, *89*, 1011–1019.

142 - Aggelidou, C.; Theodossiou, T. A.; Mavridis, I.M.; Yannakopoulou, K. 15th International Cyclodextrin Symposium (Vienna), May 9th – 12th, **2010**.

143 - Kano, K.; Fukuda, K.; Wakami, H.; Nishiyabu, R.; Pennsyl, V. Factors influencing self-aggregation tendencies of cationic porphyrins in aqueous solution. *J. Am. Chem. Soc.* **2000**, *122*, 7494–7502.

144 - Fraix, A.; Gonçalves, A. R.; Cardile, V.; Graziano, A. C. E.; Theodossiou, T. A.; Yannakopoulou, K.; Sortino, S. A multifunctional bichromophoric nanoaggregate for fluorescence imaging and simultaneous photogeneration of RNOS and ROS. *Chem. Asian J.* **2013**, *8*, 2634–2641.

145 - Srivastava, R. C., Anand, V. D.; Carper, W. R. A fluorescence study of hematoporphyrin. *Appl. Spectrosc.* **1973**, *27*, 444–449.

146 - Nishiyabu, R.; Kano, K. Double self-inclusion by rotating glucopyranose units in per-O-methylated β-cyclodextrin moieties attached to a porphyrin in aqueous solution. *Eur. J. Org. Chem.* **2004**, *24*, 4985–4988.

147 - Liu, Y.; Shi, J.; Guo, D-S. Novel per-methylated β-cyclodextrin derivatives appended with chromophores as efficient fluorescent sensors for the molecular recognition of bile salts. *J. Org. Chem.* **2007**, *72*, 8227–8234.

148 - Carofiglio, T.; Fomasier, R.; Lucchini, V.; Rosso, C.; Tonellato, U. Very strong binding and mode of complexation with a per-methylated of water-soluble porphyrins with a per-methylated β-cyclodextrin. *Tetrahedron Lett.* **1996**, *37*, 8019–8022.

149 - Kano, K.; Nishiyabu, R.; Asada, T.; Kuroda, Y. Static and dynamic behavior of 2:1 inclusion complexes of cyclodextrins and charged porphyrins in aqueous organic media. *J. Am. Chem. Soc*. **2002**, *124*, 9937–9944.

150 - Xiliang, G.; Shaomin, S.; Chuan, D.; Feng, F.; Wong, M. S. Comparative study on the inclusion behavior between meso-tetrakis(4-N-ethylpyridiniurmyl)-porphyrin and β-cyclodextrin derivatives. *Spectrochim. Acta A.* **2005**, *61*, 413–418.

151 - Tsuchiya, Y.; Shiraki, T.; Matsumoto, T.; Sugikawa, K.; Sada, K.; Yamano, A.; Shinkai, S. Supramolecular dye inclusion single crystals created from 2,3,6-trimethyl-β-cyclodextrin and porphyrins. *Chem. Eur. J.* **2012**, *18*, 456–465.

152 - Kano, K.; Nishiyabu, R.; Doi, R. Novel behavior of *O*-methylated β-cyclodextrins in inclusion of meso-tetraarylporphyrins. *J. Org. Chem.* **2005**, *70*, 3667–3673.

153 - Bonnett, R.; Charlesworth, P.; Djelal, B. D.; Foley, S.; Mcgarvey, D. J.; Truscott, T. G. Photophysical properties of 5,10,15,20-tetrakis(m-hydroxyphenyl)-porphyrin (m-THPP), 5,10,15,20-tetrakis(m-hydroxyphenyl)chlorin (m-THPC) and 5,10,15,20-tetrakis(m-hydroxyphenyl)bacterio-chlorin (m-THPBC): a comparative study. *J. Chem. Soc., Perkin Trans. 2* **1999**, 325–328.

154 - R.F. Pastemack, P.R. Huber, P. Boyd, G. Engasser, L. Francesconi, E. Gibbs, P. Fasella, G. Venturii, L. deC. Hinds, Aggregation of meso-substituted water-soluble porphyrins. *J. Am. Chem. Soc*. **1972**, *94*, 4511-4517.

155 - Long, L.; Jin, J. Y.; Zhang, Y.; Yang, R.; Wang, K. Interactions between protein and porphyrin-containing cyclodextrin supramolecular system: a fluorescent sensing approach for albumin. *Analyst.* **2008**, *133*, 1201–1208.

156 - Kano, K. Porphyrin-cyclodextrin supramolecular complexes as myoglobin model in water. *Colloid. Polym. Sci.* **2008**, *286*, 79–84.

157 - Carofiglio, T.; Fornasier, R.; Lucchini, V.; Simonato, L.; Tonellato, U. Synthesis, characterization, and supramolecular properties of a hydrophilic porphyrin-β-cyclodextrin conjugate. *J. Org. Chem.* **2000**, *65*, 9013–9021.

158 - Venema, F.; Rowan, A. E.; Nolte, R. J. M. Binding of porphyrins in cyclodextrin dimers. *J. Am. Chem. Soc*. **1996**, *118*, 257–258.

159 - Botsi, A.; Yannakopoulou, K.; Hadjoudis, E.; Perly, B. Structural aspects of permethylated cyclodextrins and comparison with their parent oligosaccharides, as derived from unequivocally assigned ^{1}H and ^{13}C NMR spectra in aqueous solutions. *Magn. Res. Chem.* **1996**, *34*, 419–423.

160 - Jung, G.; Wiehler, J.; Gohde, W.; Tittel, J.; Basché, T.; Stepi, B.; Brauchle, C. Confocal microscopy of single molecules of the green fluorescent protein. *Bioimaging*. **1998**, *6*, 54–61.

161 - Perola, E. An Analysis of the binding efficiencies of drugs and their leads in successful drug discovery programs. *J. Med. Chem.* **2010,** *53*, 2986–2997.

162 - Coxon, G. D.; Cooper, C. B.; Gillespie, S. H.; Mchugh, T. D. Strategies and Challenges Involved in the Discovery of New Chemical Entities During Early-Stage Tuberculosis Drug Discovery. *J. Infect. Dis.* **2012**, *205*, S258–S264.

163 - Lindenberg M.; Kopp S.; Dressman JB. Classification of orally administered drugs on the World Health Organization model list of essential medicines according to the biopharmaceutics classification system. *Eur. J. Pharm. Biopharm.* **2004**, *58*, 265-278.

164 - Sosnik, A.; Carcaboso, Á. M.; Chiappetta, D. A. Polymeric nanocarriers: new endeavors for the optimization of the technological aspects of drugs. *Recent Pat. Biomed. Eng.* **2008**, *1*, 43–59.

165 - Fahr, A.; Liu, X. Drug delivery strategies for poorly water-soluble drugs. *Expert Opin. Drug. Deliv*. **2007**, *4*, 403-416.

166 - Cipolla, D. C.; Gonda, I. Formulation technology to repurpose drugs for inhalation delivery. *Drug Discov. Today Ther. Strateg.* **2011**, *8*, 123–130.

167 - Goodsell, D. S. The molecular perspective: tamoxifen and the estrogen receptor. *Oncologist.* **2002**, *7*, 163–164.

168 - Ellen, A.; Katzenellenbogen, J. A.; Long, D. J.; Rorke, E. A.; Katezenellenbogen, B. S. Tamoxifen Antiestrogens. A comparison of the activity, pharmacokinetics, and metabolic activation of the *cis*- and *trans*- isomers of tamoxifen. *J. Steroid Biochem.* **1982**, *16*, 1–13.

169 - Sigma Aldrich: Tamoxifen free base. http://www.sigmaaldrich.com/content/dam/sigma-aldrich/docs/Sigma/Product_Information_Sheet/1/t5648pis.pdf (accessed Jun 12, 2013).

170 - Sigma Aldrich: Tamoxifen Citrate https://www.sigmaaldrich.com/content/dam/sigma-aldrich/docs/Sigma/Product_Information_Sheet/1/t9262pis.pdf (accessed Jun 12, 2013).

171 - Kojima, T.; Onoue, S.; Murase, N.; Katoh, F.; Mano, T; Matsuda, Y. Crystalline form information from multiwell plate salt screening by use of Raman microscopy. *Pharm. Res.* **2006**, *23*, 806-812.

172 - Aggelidou, C.; Theodossiou, T.; Yannakopoulou, K. Protoporphyrin IX-β-cyclodextrin bimodal conjugate: nanosized drug transporter and potent phototoxin. *Photochem. Photobiol.* **2013**, *89*, 1011-1019.

173 - Olofson, R. A., Martz, J. T., Senet, J. P., Piteau, M., Malfroot, T. A new reagent for the selective, high-yield *N*-dealkylation of tertiary-amines - improved syntheses of naltrexone and nalbuphine. *J. Org. Chem*. **1984**, *49*, 2081–2082.

174 - Brown, K.; Heydon, R. T.; Jukes, R.; White, I. N.; Martin, E. Further characterization of the DNA adducts formed in rat liver after the administration of tamoxifen, *N*-desmethyltamoxifen or N, N-didesmethyltamoxifen. *Carcinogenesis.* **1999**, *20*, 2011–2016.

175 - Nelson, D., J., Shagufta, Kumar, R. Characterisation of a tamoxifen-tethered single-walled carbon nanotube conjugate by using NMR spectroscopy. *Anal. Bioanal. Chem.* **2012,** *404*, 771-776.

176 - Jha, A. Unusual synthesis of 1-(4-fluorobenzyl)-N-(1-(1-(4-fluorobenzyl)-6-isopropoxy-1H-benzo[d]imidazol-2-yl)piperidin-4-yl)-6-isopropoxy-1H-benzo[d]imidazol-2-amine. *Arkivoc.* **2006**, *(i)*, 13-20.

177 - Montzka, T. A.; Matiskella, J. D.; Partyka, R. A. 2,2,2-trichloroethyl chloroformate: a general reagent for the demethylation of tertiary methylamines. *Tetrahedron Lett.* **1974,** *14*, 1325-1327.

178 - Dreaden, E. C.; Mwakwari, S. C.; Sodji, Q. H.; Oyelere, A. K.; El-Sayed, M. Tamoxifen-poly(ethylene glycol)-thiol gold nanoparticle conjugates: enhanced potency and selective delivery for breast cancer treatment. *Bioconjugate Chem.* **2009**, *20*, 2247–2253.

179 - Riggs, J. L.; Seiwald, R. J.; Burckhalter, J. H.; Downs, C. M.; Metcalf, T. G. Isothiocyanate compounds as fluorescent labeling agents for imune serum. *Am. J. Pathol.* **1958**, *34*, 1081–1097.

180 - Theodossiou, T. A.; Yannakopoulou, K.; Aggelidou, C.; Hothersall, J. S. Tamoxifen subcellular localization; observation of cell-specific cytotoxicity enhancement by inhibition of mitochondrial ETC complexes I and III. *Photochem. Photobiol.* **2012**, *88*, 1016–1022.

181 - Cho, H. K.; Lone, S.; Kim, D. D.; Choi, J. H.; Choi, S. W.; Cho, J. H.; Kim, J. H.; Cheong, I. W. Synthesis and characterization of fluorescein isothiocyanate (FITC)-labeled PEO–PCL–PEO triblock copolymers for topical delivery. *Polymer*. **2009**, *50*, 2357–2364.

182 - Onishi, H.; Machida, Y. Biodegradation and distribution of water-soluble chitosan in mice *Biomaterials* **1999**, *20*, 175–182.

183 - Bender, D. M.; Bao, J.; Dantzig, A. H.; Diseroad, W. D.; Law, K. L.; Magnus, N.; Peterson, J.; Perkins, E. J.; Pu, Y. J.; Reutzel-Edens, S. M.; Remick, D. M.; Starling, J. J.; Stephenson, G.; Vaid, R. K.; Zhang, D.; McCarthy, J. R. Synthesis, crystallization, and biological evaluation of an orally active prodrug of gemcitabine. *J. Med. Chem.* **2009**, *52*, 6958–6961.

184 - Moysan, E.; Bastiat, G.; Benoit, J.-P. Gemcitabine versus modified gemcitabine: a review of several promising chemical modifications. *Mol. Pharm.* **2013**, *10*, 430–444.

185 - Joullié, M. M.; Lassen, K. M. Evolution of amide bond formation. *Arkivoc.* **2010**, *2010 (viii)*, 189–250.

186 - Eftink, M. R.; Andy, M. L.; Bystrom, K.; Perlmutter, H. D.; Kristol, D. S. Cyclodextrin inclusion complexes: studies of the variation in the size of alicyclic guests. *J. Am. Chem. Soc.* **1989**, *111*, 6765–6772.

187 - Carrazana, J.; Jover, A.; Meijide, F.; Soto, V. H. Complexation of adamantyl compounds by b-cyclodextrin and monoamino derivatives. *J. Phys. Chem. B.* **2005**, *109*, 9719–9726.

188 - Han, S. Recent development of peptide coupling reagents in organic synthesis. *Tetrahedron* **2004**, *60*, 2447–2467.

189 - Al-Warhi, T. I.; Al-Hazimi, H. M. A.; El-Faham, A. Recent development in peptide coupling reagents. *J. Saudi Chem. Soc.* **2011**, *16*, 97-116.

190 - Bender, D. M.; Bao, J.; Dantzig, A. H.; Diseroad, W. D.; Law, K. L.; Magnus, N.; Peterson, J.; Perkins, E. J.; Pu, Y. J.; Reutzel-Edens, S. M.; Remick, D. M.; Starling, J. J.; Stephenson, G.; Vaid, R. K.; Zhang, D.; McCarthy, J. R. Synthesis, crystallization, and biological evaluation of an orally active prodrug of gemcitabine. *J. Med. Chem.* **2009**, *52*, 6958–6961.

191 - Myhren, P. F.; Borretzen, H. B.; Dalen, T. A.; Sandvold, P. M. L. (Norsk Hydro ASA) Gemcitabine Derivatives, *Patent US 6384019 B1*, May 7th, **2002**.

192 - Li, Y.; Chen, X. Sialic acid metabolism and sialyl transferases: natural functions and applications. *Appl. Microbiol. Biotechnol.* **2012**, *94*, 887–905.

193 - Li, J.; Xiao, H.; Li, J.; Zhong, Y. Drug carrier systems based on water-soluble cationic □-cyclodextrin polymers. *Int. J. Pharm.* **2004**, *278*, 329–342.

194 - Mccracken, P. G.; Ferguson, C. G.; Vizitiu, D.; Walkinshaw, C. S.; Wang, Y.; Thatcher, G. R. J. Amino-cyclodextrins as biomimetics: catalysis of the Kemp elimination. *J. Chem. Soc. Perkin Trans. 2* **1999**, 911–912.

195 - Mourtzis, N., Paravatou, M., Mavridis, I. M., Roberts, M. L., Yannakopoulou, K., Synthesis, characterisation and remarkable biological properties of cyclodextrins bearing guanidinoalkylamino and aminoalkylamino groups on their primary side. *Chem. Eur. J.* **2008**, *14*, 4188-4200.

196 - Aggelidou, C., Mavridis, I. M., Yannakopoulou, K. Binding of nucleotides and nucleosides to per-(6-guanidino-6-deoxy)cyclodextrins in solution. *Eur. J. Org. Chem.* **2009**, *14*, 2299-2305.

197 - Del Valle, E. M. M. Cyclodextrins and their uses: a review. *Process Biochem.* **2004**, *39*, 1033–1046.

198 - Messner, M.; Kurkov, S. V; Flavià-Piera, R.; Brewster, M. E.; Loftsson, T. Self-assembly of cyclodextrins: The effect of the guest molecule. *Int. J. Pharm.* **2011**, *408*, 235–247.

199 - Puskás, I.; Szemjonov, A.; Fenyvesi, É.; Malanga, M.; Szente, L. Aspects of determining the molecular weight of cyclodextrin polymers and oligomers by static light scattering. *Carbohydr. Res.* **2013**, *94*, 124–128.

200 - Mirtič, A.; Grdadolnik, J. The structure of poly-L-lysine in different solvents. *Biophys. Chem.* **2013**, *175-176*, 47–53.

201 - Robello, D. R. Chem 421 - Introduction to Polymer Chemistry, http://chem.chem.rochester.edu/~chem421/index.htm, Rochester University, (accessed Feb 16, 2013).

202 - Harwood, L. M.; Moody, C. J. Polymer Chemistry; Oxford University Press, **2004**.

203 - Izunobi, J. U.; Higginbotham, C. L. Polymer molecular weight analysis by ^{1}H NMR spectroscopy. *J. Chem. Educ.* **2011**, *88*, 1098–1104.

204 - Sigma Aldrich: Poly(ethylene glycol) diglycidyl ether http://www.sigmaaldrich.com /catalog/product/aldrich/475696?lang=pt&region=PT (accessed Feb 16th, 2013).

205 - Peng, W.; Liu, P.-Y.; Jiang, N.; Lin, H.-H.; Zhang, G.-L.; Liu, Y.; Yu, X.-Q. Dinuclear macrocyclic polyamine zinc (II) complexes linked with flexible spacers: synthesis, characterization, and DNA cleavage. *Bioorg. Chem.* **2005**, *33*, 374–385.

206 - Chmurski, K.; Defaye, J. An improved synthesis of per-(6-deoxyhalo) cyclodextrins using N-halosuccinimides — triphenylphosphine in dimethylformamide. *Supramol. Chem*. **2000**, *12*, 37–41.

207 - Gadelle, A.; Defaye, J. Selective halogenation at primary positions of cyclomaltooligosaccharides and a synthesis of per-3,6-anhydro cyclomaltooligosaccharides. *Angew. Chem., Int. Ed. Engl*. **1991**, *30*, 78–80.

208 - Yannakopoulou, K.; Mavridis, I. M. (NCSR Demokritos) Per–6-guanidino-, -aminoalkylamino- and –guanidino¬alkylamino-cyclodextrins, methods of their synthesis and their use for the compaction of DNA and intracellular delivery. *Patent EP 05 731 803.2-1214*, April 24th, **2007**.

209 - Petter, R. C.; Salek, J. S.; Sikorski, C. T.; Kumaravel, G.; Lin, F. T. Cooperative binding by aggregated mono-6-(alkylamino)-β-cyclodextrins. *J. Am. Chem. Soc.* **1990,** 112, 3860-3874.

210 - Darcy, R.; O'Keeffe, F.; Schwinté, P. 6-hydroxyalkylamino-6-deoxy-cyclodextrins: towards dendrimeric host-molecules. *J. Inclusion Phenom.* **1996,** 25, 43-46.

211 - Mourtzis, N.; Eliadou, K.; Aggelidou, C.; Sophianopoulou, V.; Mavridis, I. M.; Yannakopoulou, K. Per(6-guanidino-6-deoxy)cyclodextrins: synthesis, characterisation and binding behaviour toward selected small molecules and DNA. *Org. Biomol. Chem.* **2006**, *5*, 125–131.

212 - Inlay, M. A.; Choe, V.; Bharathi, S.; Fernhoff, N. B.; Baker, J. R.; Weissman, I. L.; Choi, S. Ki. Synthesis of a photocaged tamoxifen for light-dependent activation of Cre-ER recombinase-driven gene modification. *Chem. Commun*. **2013**, *49*, 4971-4973.